PROCEEDINGS OF THE ELEVENTH ANNUAL PACIFIC CLIMATE (PACLIM) WORKSHOP

Asilomar, California — April 19-22, 1994

Edited by
Caroline M. Isaacs and Vera L. Tharp

Technical Report 40
of the
Interagency Ecological Program
for the
Sacramento-San Joaquin Estuary

April 1995

Single copies of this report may be obtained without charge from:

California Department of Water Resources
P.O. Box 942836
Sacramento, CA 94236-0001

PROCEEDINGS OF THE ELEVENTH ANNUAL PACIFIC CLIMATE (PACLIM) WORKSHOP

Asilomar, California — April 19-22, 1994

Edited by
Caroline M. Isaacs and Vera L. Tharp

Technical Report 40
of the
Interagency Ecological Program
for the
Sacramento-San Joaquin Estuary

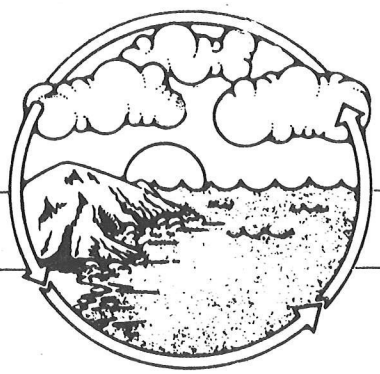

PACLIM

Climate Variability
of the
Eastern North Pacific
and
Western North America

Sponsors

The Eleventh Annual Pacific Climate Workshop was sponsored by:

U.S. GEOLOGICAL SURVEY
Water Resources Division

U.S. GEOLOGICAL SURVEY
Geologic Division

NATIONAL OCEANIC AND ATMOSPHERIC ADMINISTRATION
Paleoclimatology Program

U.S. ENVIRONMENTAL PROTECTION AGENCY
EMAP Program

CALIFORNIA DEPARTMENT OF WATER RESOURCES
Environmental Services Office

SOUTHERN CALIFORNIA EDISON COMPANY

AMERICAN GEOPHYSICAL UNION

NAVAL POSTGRADUATE SCHOOL

NATIONAL SCIENCE FOUNDATION

Publication of this proceedings has been sponsored by the

INTERAGENCY ECOLOGICAL PROGRAM
for the
SACRAMENTO-SAN JOAQUIN ESTUARY

A Cooperative Program of:

California Department of Water Resources
State Water Resources Control Board
U.S. Bureau of Reclamation
U.S. Geological Survey

California Department of Fish and Game
U.S. Fish and Wildlife Service
U.S. Army Corps of Engineers
U.S. Environmental Protection Agency

These proceedings were published by the Interagency Ecological Program for the Sacramento-San Joaquin Estuary (Interagency Program)
in a cooperative effort with the
United States Department of the Interior, Geological Survey, Menlo Park, California.
Information generated by the PACLIM Workshop provides the Interagency Program with a climatological perspective that cannot be obtained from its own studies.
Views and conclusions contained in this publication do not necessarily reflect the opinions of the Interagency Program or its member agencies.

Contents

Sponsors . . . . . *iii*

Authors . . . . . *vii*

Acknowledgments . . . . . *xi*

Statement of Purpose . . . . . *xiii*

Introduction 1
Caroline M. Isaacs

Inter-Decadal Climate Variability in the Southern Hemisphere:
Evidence from Tasmanian Tree Rings over the Past Three Millennia 7
Edward R. Cook, Brendan M. Buckley, and Rosanne D. D'Arrigo

Multivariate Climate Reconstruction for the Last 14,000 Years in
Southernmost South America 21
Vera Markgraf, James W.C. White, Regina A. Figge, and Ray Kenny

Volcanic Activity and Global Change: Probable Short-Term and
Possible Long-Term Linkages 29
David K. Rea and Libby M. Prueher

An Overview of Decadal to Century Time-Scale Variability in the Climate System 35
Thomas F. Stocker

Determining the Role of Linear and Nonlinear Interactions in Records of Climate Change:
Possible Solar Influences in Annual to Century-Scale Records 47
Terri King Hagelberg and Julia Cole

Dynamical Structure in Paleoclimate Data 55
H. Bruce Stewart

Modeling North Pacific Temperature and Pressure Changes from
Coastal Tree-Ring Chronologies 67
Gregory C. Wiles, Rosanne D. D'Arrigo, and Gordon C. Jacoby

Reconstruction of Aridity for the Sierra de la Laguna, Baja California Sur, Mexico 79
Sara Díaz, Laura Arriaga, Cesar Salinas, and Daniel Lluch

South American Streamflow and the Extreme Phases of the Southern Oscillation 85
Thomas C. Piechota, John A. Dracup, Ernesto F. Brown, Tom McMahon, and Francis Chiew

Sea Surface Temperature and Paleo-El Niño Events in
Santa Barbara Basin, AD 1841-1941 93
Arndt Schimmelmann, Meixun Zhao, Gerald G. Kuhn, and Mia J. Tegner

Radiolarian Flux in the Santa Barbara Basin as an Index of Climate Variability. 107
Amy L. Weinheimer and Daniel R. Cayan

High Productivity and Upwelling in the California Current during
Oxygen-Isotope Stage 3: Diatom Evidence 119
Eileen Hemphill-Haley

Neogene through Pleistocene Paleoclimate of the Great Salt Lake Region, Northeastern Great Basin, USA 127
Thomas E. Moutoux and Owen K. Davis

A 139-Year Dendroclimatic Cycle, Cultural/Environmental History, Sunspots, and Longer-Term Cycles 137
Thor Karlstrom

Climatology of the Seasonal Precipitation Maximum in the Western United States 161
Cary J. Mock

Some Effects of Earth's Surface on Winter Jetstream Positions in the Northern Hemisphere and Rainfall Patterns in Northern and Central California 171
Stephen H. Holets

Has the California Drought Returned? 181
Maurice Roos

Late Holocene Environmental Variability in the Upper San Francisco Estuary as Reconstructed from Tidal Marsh Sediments 185
Lisa E. Wells and Michelle Goman

Fijian Coral Reef Damage and Recovery from Cyclone Kina 199
Richard Casey, Annette Ciccateri, and Stewart J. Fallon

Scientific Statistics and Graphics on the Macintosh 207
Stanley L. Grotch

Appendixes

A Agenda 219

B Poster Presentations 225

C Attendees 229

Authors

Laura Arriaga
Centro de Investigaciones
Biológicas del Noroeste
Km 1. Carr San Juan de la Costa
Apdo Postal 128 La Paz 23000
BCS México

Ernesto F. Brown
Escuela de Ingenieria y Cieneras
Universidad de Chile
Auda, Beauchef 850
Santiago, CHILE
Phone 011 56 2 698 2017

Brendan M. Buckley
Institute of Antarctic and
Southern Ocean Studies
University of Tasmania
Hobart, Tasmania 7001

Richard Casey
Ocean Research International
650 Loring Street
San Diego, CA 92109
Phone 619/483-6507

Daniel R. Cayan
Scripps Institution of Oceanography
University of California, San Diego
La Jolla, CA 92093-0224
Phone 619/534-4507
cayan@ucsd.edu

Francis Chiew
Centre for Environmental Applied Hydrology
University of Melbourne
Dept of Civil & Environmental Engineering
Parkville, Victoria
3052 AUSTRALIA
Phone 011 61 3 344 6641

Annette Ciccateri
Ocean Research International
650 Loring Street
San Diego, CA 92109
Phone 619/483-6507

Julia Cole
INSTAAR, Campus Box 450
University of Colorado
Boulder, CO 80309
Phone 303/492-0595 — Fax 303/492-6388
coleje@spot.colorado.edu

Edward R. Cook
Tree Ring Laboratory
Lamont-Doherty Earth Observatory
Palisades, NY 10964

Rosanne D. D'Arrigo
Tree Ring Laboratory
Lamont-Doherty Earth Observatory
Palisades, NY 10964

Owen K. Davis
Department of Geosciences
Gould-Simpson Building
University of Arizona
Tucson, AZ 85721
Phone 602/621-7953

Sara Díaz
Centro de Investigaciones
Biológicas del Noroeste
Km 1. Carr San Juan de la Costa
Apdo Postal 128 La Paz 23000
BCS México

John A. Dracup
University of California, Los Angeles
Civil & Environmental Engineering Department
3066 Engineering I
Los Angeles, CA 90024-1593
Phone 310/206-8612

Stewart J. Fallon
Ocean Research International
650 Loring Street
San Diego, CA 92109
Phone 619/483-6507

Regina A. Figge
INSTAAR
University of Colorado at Boulder
Campus Box 450
Boulder, CO 80309
Phone 303/492-6072 — Fax 303/492-6388
figge_r@cubldr.colorado.edu

Michelle Goman
Department of Geography
University of California, Berkeley
Berkeley, CA 94720-4740

Stanley L. Grotch
Laboratory Associate
Lawrence Livermore National Laboratory
7000 East Avenue
Livermore, California 94550
Phone 510/423-6741 — Fax 510/422-5844

Terri King Hagelberg
University of Rhode Island
Graduate School of Oceanography
Narragansett, RI 02882
Phone 401/792-6662 — Fax 401/792-6709
terrih@gsosun1.gso.uri.edu

Eileen Hemphill-Haley
U.S. Geological Survey
1272 Geological Sciences
University of Oregon
Eugene, OR 97403-1272
Phone 503/346-4582 — Fax 503/346-4692
eileen@octopus.wr.usgs.gov

Stephen H. Holets
Pacific Gas & Electric Co.
77 Beale Street, Room 1651
San Francisco, CA 94177
Phone 415/973-4530 — Fax 415/957-9348
shh2@gcd_ms@gbu_gts_sfgo

Caroline M. Isaacs
U.S. Geological Survey
345 Middlefield Road - MS 999
Menlo Park, CA 94025
Phone 415/354-3014 — Fax 415/354-3224
caroline@octopus.wr.usgs.gov

Gordon C. Jacoby
Tree Ring Laboratory
Lamont-Doherty Earth Observatory
Palisades, NY 10964

Thor Karlstrom
U.S. Geological Survey (Ret)
4811 Brace Point Drive
Seattle, WA 98136
Phone 206/935-7087

Ray Kenny
1560 - 30th Street
Campus Box 450
Boulder, CO 80309-0450

Gerald G. Kuhn
The International Association for the
Physical Sciences of the Oceans
P.O. Box 1161
Del Mar, CA 92014-1161
Phone/Fax 619/942-6163

Daniel Lluch
Centro de Investigaciones
Biológicas del Noroeste
Km 1. Carr San Juan de la Costa
Apdo Postal 128 La Paz 23000
BCS México

Vera Markgraf
1560 - 30th Street
Campus Box 450
Boulder, CO 80309-0450
Phone 303/492-5117 — Fax 303/492-6388
markgraf@spot.colorado.edu

Tom McMahon
Centre for Environmental Applied Hydrology
University of Melbourne
Dept of Civil & Environmental Engineering
Parkville, Victoria
3052 AUSTRALIA
Phone 011 61 3 344 6641

Cary J. Mock
Department of Geology and Geography
University of Massachusetts
Amherst, MA 01003
Phone 413/545-2286 — Fax 413/545-1200

Thomas E. Moutoux
Department of Geosciences
Gould-Simpson Building
University of Arizona
Tucson, AZ 85721
Phone 602/621-7953

Thomas C. Piechota
University of California, Los Angeles
Civil and Environmental Engineering Department
3066 Engineering I
Los Angeles, CA 90024-1593
Phone 310-206-8612

Libby M. Prueher
Department of Geological Sciences
University of Michigan
Ann Arbor, MI 48109-1063
Phone 313/936-0521

David K. Rea
Department of Geological Sciences
University of Michigan
Ann Arbor, MI 48109-1063
Phone 313/936-0521

Maurice Roos
CA Department of Water Resources
P.O. Box 942836
Sacramento, CA 94236-0001
Phone 916/653-8366 — Fax 916/653-8272

Cesar Salinas
Centro de Investigaciones
Biológicas del Noroeste
Km 1. Carr San Juan de la Costa
Apdo Postal 128 La Paz 23000
BCS México

Arndt Schimmelmann
Department of Geological Sciences
Geology 129, Indiana University
1005 East 10th Street
Bloomington, IN 47405-1403
Phone 812/855-7645 — Fax 812/855-7961
aschimme@indiana.edu

H. Bruce Stewart
Brookhaven National Laboratory
Building 490-D
Upton, NY 11973
Phone 516/282-4179 — Fax 516/282-5047
bstewart@bnl.gov

Thomas F. Stocker
Climate and Environmental Physics
Physics Institute, University of Bern
Sidlerstrasse 5
3012 Bern, Switzerland
Phone +41 31 631 44 64 — Fax +41 31 631 44 05
stocker@phil.unibe.ch

Mia J. Tegner
Scripps Institution of Oceanography
University of California, San Diego
La Jolla, CA 92093-0201
Phone 619/534-2059 — Fax 619/534-6500
mtegner@ucsd.edu

Amy Weinheimer
Scripps Institution of Oceanography
University of California, San Diego
La Jolla, CA 92093-0220
Phone 619/534-2049
weinheim@weather.ucsd.edu

Lisa Wells
University of California
Department of Geography
501 Earth Sciences Building
Berkeley, CA 94702
Phone 510/642-1281 — Fax 510/647-3370
lwells@garnet.berkeley.edu

James W.C. White
1560 - 30th Street
Campus Box 450
Boulder, CO 80309-0450

Gregory C. Wiles
Tree Ring Laboratory
Lamont-Doherty Earth Observatory
Palisades, NY 10964
Phone 914/365-8517 — Fax 914/365-3046
e-mail: druidgw@lamont.1deo.columbia.edu

Meixun Zhao
OGU/Chemistry
University of Bristol
Bristol, BS81TS
U.K.

Acknowledgments

The PACLIM workshops are produced by an array of enthusiastic volunteers. For 1994, enormous thanks go to Walt Dean as general workshop chairman and to Lisa Ramirez Bader for exhaustive operational management and oversight. Special thanks also go to Dianne Fox and Ana MacKay for registration (and much other assistance), to Jean Seifert for text processing the program, to Tom Murphree for providing the audiovisual equipment, and to Larry Riddle for the inimitable PACLIM 1994 T-shirts.

Sponsorship and funding for the workshops come from a variety of sources. In addition to the agencies and programs responsible (listed separately), we also thank those who helped in the funding process, including Harry Lins, Dick Poore, Mark Eakin, Dan McKenzie, Jim Young, Fred Spilhaus, Paul Weiss, Randy Brown, and Herman Zimmerman.

For the scientific agenda of the workshop, Dan Cayan deserves our most grateful salute for creating, organizing, and scheduling the main program. Thanks go also to Rob Dunbar, who organized and chaired with me the 1994 Theme Session on "High-Resolution Paleoclimate". The other session chairs and moderators are also gratefully acknowledged — Walt Dean, Dan Cayan, Dave Peterson, and Platt Bradbury. And of course, we thank all our speakers and poster presenters for their contributions and enthusiasm — Stan Grotch, Bob Francis, Dick Casey, Malcolm Hughes, Vera Markgraf, Ed Cook, Julia Cole, Rob Dunbar, Tim Baumgartner, Thomas Stocker, Terri Hagelberg, Dave Rea, Thomas Piechota, M. Filonczuk, Jan Van Wagtendonk, Cary Mock, Mike Dettinger, Stephen Holets, Susan Ustin, Amy Weinheimer, Jim Gardner, Lynn Ingram, Lisa Wells, John McGowan, Don Gautier, Maurice Roos, Dave Meko, Frank Gehrke, Greg Wiles, Mike Moore, Dan Schrag, Thomas Moutoux, Dave Adam, Diana Anderson, Scott Anderson, Platt Bradbury, Dan Cayan, David Clow, Rachael Craig, Peter Dartnell, Walt Dean, Daniel Lluch, Regina Figge, Eileen Hemphill-Haley, Linda Heusser, Jim Ingraham, Thor Karlstrom, Carina Lange, Ken Petersen, Larry Riddle, Gary Sharp, and Jim West. Evening speakers Bruce Stewart and Roger Anderson both deserve special applause, as well as Steven F. Arvizu, President of California State University Monterey Bay (CSUMB), a future partner of PACLIM workshops.

For the 1994 Proceedings volume, enormous thanks go to Vera Tharp for her patience with diverse format types and her incredible expertise with technical editing, graphics, tables, and highly skilled pasting. Invaluable precedents for the 1994 volume were established by the previous editors of the *PACLIM Proceedings* — Dave Peterson (1984-1988) with the able assistance of Lucenia Thomas, Julio Betancourt and Ana MacKay (1989-1990), and Kelly Redmond and Vera Tharp (1991-1993). Special thanks also go to all the authors who contributed.

Caroline M. Isaacs
U.S. Geological Survey
Menlo Park, California

STATEMENT OF PURPOSE
Pacific Climate (PACLIM) Workshops

In 1984, a workshop was held on "Climatic Variability of the Eastern North Pacific and Western North America". From it has emerged an annual series of workshops held at the Asilomar Conference Center, Monterey Peninsula, California. These annual meetings, which involve 80-100 participants, have come to be known as PACLIM (Pacific Climate) Workshops, reflecting broad interests in the climatologies associated with the Pacific Ocean and western Americas in both the northern and southern hemispheres. Participants have included atmospheric scientists, hydrologists, glaciologists, oceanographers, limnologists, and both marine and terrestrial biologists. A major goal of PACLIM is to provide a forum for exploring the insights and perspectives of each of these many disciplines and for understanding the critical linkages between them.

PACLIM arose from growing concern about climate variability and its societal and ecological impacts. Storm frequency, snowpack, droughts and floods, agricultural production, water supply, glacial advances, stream chemistry, sea surface temperature, salmon catch, lake ecosystems, and wildlife habitat are among the many aspects of climate and climatic impacts addressed by PACLIM Workshops. Workshops also address broad concerns about the impact of possible climate change over the next century. From observed changes in the historical record, the conclusion is evident that climate change would have large societal impacts through effects on global ecology, hydrology, geology, and oceanography.

Our ability to predict climate, climate variability, and climate change critically depends on an understanding of global processes. Human impacts are primarily terrestrial in nature, but the major forcing processes are atmospheric and oceanic in origin and transferred through geologic and biologic systems. Our understanding of the global climate system and its relationship to ecosystems in the Eastern Pacific area arises from regional study of its components in the Pacific Ocean and western Americas, where ocean/atmosphere coupling is strongly expressed. Empirical evidence suggests that large-scale climatic fluctuations force large-scale ecosystem response in the California Current and in a very different system, the North Pacific central gyre. With such diverse meteorologic phenomena as the El Niño-Southern Oscillation and shifts in the Aleutian Low and North Pacific High, the Eastern Pacific has tremendous global influences and particularly strong effects on North America. In the western United States, where rainfall is primarily a cool-season phenomenon, year-to-year changes in the activity and tracking of North Pacific winter storms have substantial influence on the hydrological balance. This region is rich in climatic records, both instrumental and proxy. Recent research efforts are beginning to focus on better paleoclimatic reconstructions that will put present-day climatic variability in context and allow better anticipation of future variations and changes.

The PACLIM Workshops address the problem of defining regional coupling of multifold elements, as organized by global phenomena. Because climate expresses itself throughout the natural system, our activity has been, from the beginning, multidisciplinary in scope. The specialized knowledge from different disciplines has brought together climatic records and process measurements to synthesize an understanding of the complete system. Our interdisciplinary group uses diverse time series, measured both directly and through proxy indicators, to study past climatic conditions and current processes in this region. Characterizing and linking the geosphere, biosphere, and hydrosphere in this region provides a scientific analogue and, hence, a basis for understanding similar linkages in other regions, as well as for anticipating the response to future climate variations. Our emphasis in PACLIM is to study the interrelationships among diverse data. To understand these interactive phenomena, we incorporate studies that consider a broad range of topics both physical and biological, time scales from months to millennia, and space scales from single sites to the entire globe.

An overview of the PACLIM Workshops was published in the December 30, 1986, issue of *EOS*.
Proceedings of PACLIM Workshops are published annually by the
California Department of Water Resources as Technical Reports of the
Interagency Ecological Program for the Sacramento-San Joaquin Estuary.
A multi-disciplinary collection of research papers, spawned at least partially by interactions in the initial PACLIM Workshops, was published as *AGU Geophysical Monograph 55* (Peterson, ed., 1989).

Introduction

Caroline M. Isaacs

Nearly 100 participants attended the eleventh annual PACLIM workshop at the Asilomar Conference Center in Pacific Grove, California, on April 19-22, 1994. A one-day theme session of ten 45-minute talks was followed by sessions of 20-minute presentations. In addition, 19 presenters gave 1- to 2-minute introductions to their posters, which were displayed throughout the meeting.

The theme session focused on high-resolution paleoclimate studies, emphasizing records of the last few thousand years, encompassing a pan-Pacific scope, and presenting innovative approaches to analyzing time series. Included were presentations of high-resolution proxy records constructed from tree rings, coral bands, and marine varves. Also discussed were evaluations of solar influences by bispectral analysis, the intriguing connection between climate and volcanism, models of interdecadal climate variability, and potential methods of identifying deterministic chaos in the climate system.

In the first paper of the volume, Edward Cook *et al* present tree-ring records from Tasmania now extending back to 800 BC. Analysis of their warm-season temperature reconstruction indicates that interdecadal variability over the last 3000 years has strong expressions at frequencies with mean periods of 31, 57, 77, and 200 years. Based on singular spectrum analysis, trends from these long-term frequencies are estimated to account for 51% of the anomalous warming in progress over Tasmania for the last 30 years. By extrapolating these low frequency components into the future, the authors forecast a natural cooling trend for the next 30 years, which could mask detection of greenhouse warming in the region.

In the next paper, Vera Markgraf *et al* evaluate the relative importance of temperature and precipitation to major paleoenvironmental changes by comparing pollen and stable isotope ratios in peat in a South American core from Tierra del Fuego spanning the last 14,000 years. Major paleoenvironmental changes at 12700, 9000, 5000, and 4000 YBP (years before present) are concluded to reflect precipitation changes, mainly related to the position and intensity of extratropical stormtracks. High paleoenvironmental variability in late glacial and latest Holocene times, on the other hand, are identified with temperature variability.

David Rea and Libby Prueher review evidence of the link between volcanism and climatic cooling, first noted by Benjamin Franklin following the Laki, Iceland, eruption in 1783. Global cooling lasting 2-5 years and glacial advances lagged 10-15 years after an eruption are well documented, but longer-term links between volcanism and climate have

generally been regarded as speculative. The authors present new evidence from Ocean Drilling Program Leg 145 to the subarctic Pacific of the synchroneity between the abrupt increase in volcanism and the sudden onset of northern hemisphere glaciation at 2.6 Ma (million years ago). Although the requisite changes in atmospheric circulation and CO_2 can be explained by other causes (*eg*, uplift of the Tibetan and American plateaus), the authors point out that the abruptness of glacial onset indicates a threshold phenomenon and suggest that the sudden increase in massive volcanism could have been the critical trigger.

Thomas Stocker examines decadal to century time-scale variability in the climate system, pointing out that high-resolution proxy records exhibit significant power on this scale. Climate modeling has traditionally been based on the concept that observed fluctuations derive from forcings on the same scale, but this paper suggests that fluctuations may be linked to interactions within and between components of the climate system, principally the ocean and atmosphere. Recent models and mechanisms are reviewed. Although concluding that such studies are still in their infancy, the paper discusses new insights into the role of the ocean, the influence of atmosphere-ocean exchange, and the dynamics of marginal seas on internal variability of the climate system.

Nonlinear time series analysis is the focus of Terri Hagelberg and Julie Cole's paper, which examines the relationship between solar forcing and climate change on ENSO (El Niño/Southern Oscillation) scales. Using bispectral and cross-bispectral analysis, the authors compare the annual sunspot cycle 1700-present with instrumental records of sea surface temperature from the central and eastern tropical Pacific, coral proxy data from Indonesia and the Galapagos, and tree-ring proxy data from North American Tree Ring Indices. Results show nonlinear coupling between the 6-year ENSO cycle and 11-year solar cycle that is statistically significant (0.80 level) for at least the past several centuries.

In the next paper, Bruce Stewart suggests that deterministic chaos offers a new paradigm for understanding irregular fluctuations and discusses methods that can test whether paleoclimate proxy data are consistent with a deterministic interpretation. A basic question is whether climate (as contrasted to weather) *has* a dynamical structure; that is to say, is the evolution of climate governed by dynamical laws that, given the present state expressed in terms of annual or seasonal means, determine future conditions? Methods of analysis are illustrated with time series of oxygen isotope ratios from the Quelccaya ice cores 1476-1984 and temperature reconstructions from Fennoscandian trees AD 500-1980.

Gregory Wiles *et al* present the first summer temperature reconstructions from tree-ring chronologies at coastal sites along the Gulf of Alaska and Pacific Northwest. Using both tree-ring widths and maximum latewood density in their analysis by principal components regression techniques and prewhitening to remove persistence in the series, the reconstruction of summer temperatures shows warming in the 1820s and cooling in the

1810s, 1860s, and 1890s for the Gulf of Alaska and cool intervals in the early 1800s and 1880s for the Pacific Northwest. The authors also suggest that ring-width chronologies may provide information on winter temperature and pressure changes in the region.

Turning to paleoclimate data for Mexico, Sarah Diaz *et al* present a pioneering effort to use tree rings to extend instrumental records of aridity in the Sierra de la Laguna Mountains at the southern tip of the Baja California peninsula. Comparison of instrumental and dendrochronology data show that tree-ring width closely correlates with aridity and precipitation but is insignificantly related to temperature. Aridity variations are especially well-reflected in the proxy data at an interdecadal scale. Using a model derived from the period of overlap in the two data sets, they reconstruct aridity for the past two centuries from tree-ring width. Results show: (1) a period of high variability 1810-1890 with generally high aridity interrupted by very low aridity during the mid-1840s, (2) a stable period of intermediate aridity 1900 to the mid-1950s; and (3) a highly variable recent period, with maximum aridity in the early 1970s and minimum aridity in the mid-1960s and mid-1980s.

South American hydrology is the focus of the paper by Thomas Piechota *et al*, who examine the spatial distribution of streamflow response to ENSO events. Using harmonic analysis, these authors identify four coherent regions of strong hydrologic response. In two of these regions (south-central Chile and north-central Chile), anomalously high streamflow occurs during El Niño events. In the other two regions (Guyana and Panama), by contrast, anomalously low streamflow occurs during El Niño events. The authors demonstrate quantified probability distributions for precipitation associated with El Niño and La Niña years at specific stations within each region.

Also focusing on El Niño events is Arndt Schimmelmann *et al's* paleo-reconstruction for the Santa Barbara Basin during 1841-1941, which encompasses the end of the "Little Ice Age". They propose four proxy criteria from the varved sediment record for their reconstructions and compare these with instrumental and historical evidence, concluding that strong El Niño events did not occur during 1841-1870, that three or more events occurred in the short period 1870-1891, perhaps one in 1913, perhaps another in 1926/27, and finally the well-known event of 1941/42. Historical accounts of weather and storms are detailed for 1844-1891, including discussion of weather associated with the eruption of Krakatoa in 1883.

Amy Weinheimer and Daniel Cayan also examined proxy records in varved sediment from the Santa Barbara Basin, focusing on radiolarian assemblages and radiolarian flux rates. For the period 1954-1986, no major assemblage changes were detected, but comparison with instrumental records shows intriguing correlations between radiolarian flux rates and regional California sea surface temperature. High flux rates reflect diminished upwelling and are associated with a positive

Pacific/North American circulation pattern, characterized by a strong North Pacific subtropical High, deep Aleutian Low, and strong high over western Canada-Pacific Northwest.

Examining proxy data in the more distant geologic past, Eileen Hemphill-Haley discusses evidence for more vigorous coastal upwelling and enhanced diatom productivity along the northern California margin 25,000-40,000 YPB. Two cores from the Russian River and Point Arena area are compared with cores from Ocean Drilling Program Site 893A in the Santa Barbara Basin. Changes in mass accumulation rates of organic carbon and total diatoms, as well as contrasting trends between groups within the diatom assemblages, support the idea that upwelling and diatom productivity decreased simultaneously in both areas at the onset of glacial Stage 2, circa 28,000 YBP.

An even longer paleoclimate view is provided by Thomas Moutoux and Owen Davis for the Great Salt Lake region in the northeastern Great Basin. From lacustrine cores spanning the last 8 million years, these authors reconstruct paleotemperatures and paleoprecipitation by comparing paleo pollen assemblages with contemporary assemblages based on a square cord distance dissimilarity function. The most notable result is identification of a widespread and sudden change about 700,000 YBP to a cooler and moister climate, with mean annual temperature estimated as 2°C or more lower than today and precipitation frequently double modern values. Prior to this change, temperatures in the area averaged 1-3°C higher and precipitation 50-100 mm lower than today.

Thor Karlstrom considers evidence of a 139-year climatic cycle, a resonance of maximum tidal force cycles of 3366, 1112, and 556 years. Using a method based on half-cycle smoothing positioned on cycle turning points, the author analyzes dendroclimatic records to conclude that the 139-year cycle is real and regionally robust, reflecting alternations of warm/dry and cool/wet climatic conditions. The method is also illustrated by time series analysis of Egyptian cultural history, sunspot cycle-length, solar tides, tree-ring isotopes, and pollen records.

The next several papers examine climate variability from instrumental records. In the first of these papers, Cary Mock addresses the heterogeneous spatial patterns of seasonal precipitation regimes in the United States west of the Mississippi. To elucidate the scale of various controls, maps of intermonthly precipitation trends are constructed from a dense network of stations including high-elevation sites. While large-scale climate controls (polar jet stream, Pacific subtropical high, subtropical ridge) are important over much of the region, the smaller-scale controls characteristic of mountainous regions (physiography, thermal troughs) contribute significantly to the overall spatial variation of seasonal precipitation maxima. Results have application to forecasting seasonal precipitation anomalies and refining general circulation and high-resolution mesoscale climate models.

Predicting rainfall in the Sierra Nevada Mountain watersheds of California one to two months in advance is the focus of the next paper. Stephen Holets presents an analog model used by Pacific Gas and Electric Company to provide the rainfall outlook, which is based on empirically matching monthly average polar-front jet stream positions in the eastern and central North Pacific with historical jet stream positions. Also discussed are the mean wintertime polar-front jet stream in the northern hemisphere as a whole, and the roles of mountain ranges and land-ocean thermal contrasts in determining its overall structure.

Maurice Roos queries "Has the California Drought Returned?" After 6 years of drought during 1987-1992, the 1993 water year ended the California drought with about 150% of average precipitation and good carryover reservoir capacity. The 1994 water year, however, was again dry, placing California in a "drought watch" mode. The paper distinguishes between hydrological drought and meteorological drought and details consequences for water delivery of current conditions.

A longer view of California hydrology is presented by Lisa Wells and Michelle Goman, who report preliminary results on the history of variations in relative salinity and inundation frequency in tidal marsh sediments of the upper San Francisco estuary over the last 7000 years. Several short-period events have been recognized, including an extreme flood at about 0.5 ka (thousand years ago), several extreme droughts at about 3.0 ka, and increased tidal inundation at about 4.5 ka and 2.2 ka. These preliminary data suggest that both drought and salinity intrusion occurred in the Sacramento/San Joaquin drainage basin even during periods that were generally characterized by much higher freshwater discharge than today.

The sole paper in this volume on large-storm events deals with Cyclone Kina, which struck the Fiji Islands in 1993, causing more than $100 million in damage. Richard Casey *et al* report on an ecological transect made 6 months before the cyclone and contrast the reef condition with results from another transect made a few days after the cyclone. One major impact has been the invasion of opportunistic algae in the inner reef flat. The authors estimate that the reef will take several years — and perhaps up to 30 years — to recover to pre-cyclone conditions.

The final paper in the volume deals with statistical and graphic capabilities of the Macintosh computer, with special application to exploring and illustrating climate datasets (both models and observations). Stanley Grotch discusses recent advances in networking that now permit rapid transfer of large datasets and reviews — from a strictly personal viewpoint — several sophisticated data analysis and graphics packages that are available for the Macintosh. Included in the discussion are basic statistical tools, "linked plots" that highlight selected data, 3-dimensional plots, scripts and macros, interactive graphics, animation, and desktop movie-making. Recommended software sources are also listed.

Inter-Decadal Climate Variability in the Southern Hemisphere: Evidence from Tasmanian Tree Rings over the Past Three Millennia

Edward R. Cook, Brendan M. Buckley, and Rosanne D. D'Arrigo

ABSTRACT: The characterization of inter-decadal climate variability in the Southern Hemisphere is severely constrained by the shortness of the instrumental climate records. To help relieve this constraint, we have developed and analyzed a reconstruction of warm-season (November-April) temperatures from Tasmanian tree rings that now extends back to 800 BC. A detailed analysis of this reconstruction in the time and frequency domains indicates that much of the inter-decadal variability is principally confined to four frequency bands with mean periods of 31, 57, 77, and 200 years. These oscillations are stable and robust with respect to the progressive development and extension of the tree-ring reconstruction back in time. They account for about 12% of the overall variance in annual temperature estimates and 41% of the inter-decadal variance (*ie*, periods >10 years). Using singular spectrum analysis, we estimate the overall inter-decadal temperature signal contributed by these four oscillations and compare its recent behavior to an anomalous warming that has been in progress over Tasmania since about 1965. We find that 51% of the mean anomalous warming can be accounted for by these oscillations. Prediction error filtering is also used to forecast the inter-decadal temperature signal 30 years into the future. In so doing, we show how a future greenhouse warming signal over Tasmania could be masked by these natural oscillations unless they are taken into account.

Introduction

Characterization of inter-decadal climate variability worldwide is constrained by the shortness of the instrumental climate records. This problem is especially acute in the Southern Hemisphere, where such records rarely exceed 100 years in length (Barry 1978). In Tasmania, tree-ring width variations of old-growth Huon pines (*Lagarostrobos franklinii*) provide a means of extending instrumental temperature records back thousands of years. We analyze one such reconstruction of warm-season (November-April) temperatures for Tasmania, which now extends back to 800 BC. As will be shown, there is strong statistical evidence in the time and frequency domains for inter-decadal and century-scale variability of an oscillatory nature. This behavior is stable and robust with respect to the progressive development and extension of the tree-ring reconstruction back in time. Thus, we believe the oscillatory behavior in the series is not a statistical artifact. Rather, it reflects the true dynamics of the ocean/atmosphere system in this sector of the Southern Hemisphere.

In: C.M. Isaacs and V.L. Tharp, Editors. 1995. *Proceedings of the Eleventh Annual Pacific Climate (PACLIM) Workshop, April 19-22, 1994.* Interagency Ecological Program, Technical Report 40. California Department of Water Resources.

Tree-Ring Chronology Development

Tree-ring data used in the temperature reconstruction were collected from a disjunct stand of sub-alpine Huon pine at an elevation of 950 meters on Mount Read, in western Tasmania (Figure 1). The site is called "Lake Johnston" after a small cirque lake about 50-100 meters below the stand. The Huon pine stand is composed of two discrete, adjacent units: one made up solely of living trees and a second area of standing dead trees killed by a fire in 1961. All of the sub-fossil wood used to extend the reconstruction back in time came from the zone of fire-killed trees. Actual wood collections were made over a period of 4 years, with the living trees sampled first. This produced a tree-ring chronology spanning AD 779-1988 (Cook *et al* 1992). Subsequently, standing dead trees were sampled from the fire-killed zone, followed by remnant logs and stumps. The sub-fossil tree rings were exactly cross-dated in time with the living-tree chronology to extend the chronology back in time. Total overlap between the living tree and sub-fossil wood chronologies is 952 years.

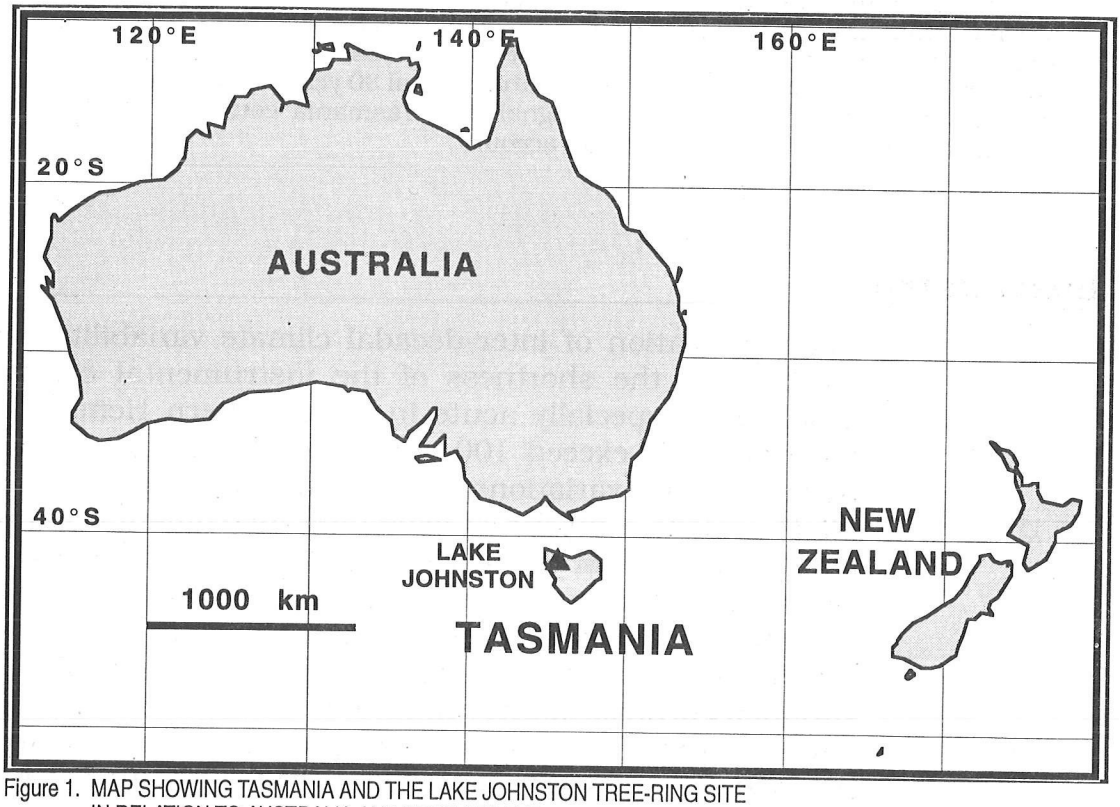

Figure 1. MAP SHOWING TASMANIA AND THE LAKE JOHNSTON TREE-RING SITE IN RELATION TO AUSTRALIA AND NEW ZEALAND

The raw tree-ring measurement series were standardized (Fritts 1976) using very conservative detrending to preserve as much low-frequency variance as possible in the data. In the newest, longest version of the chronology, which now extends back to 800 BC, only linear and negative exponential growth trends were removed from the individual segments. The final site chronologies thus produced for climatic reconstruction

were mean-value functions of all cross-dated and standardized segments available at the time, averaged across years using the biweight robust mean to discount the influence of outliers.

Temperature Reconstructions

The warm-season temperature reconstruction analyzed here was developed in three discrete stages, representing the progressive addition of newly available tree-ring data to the reconstruction and the extension of that series farther back in time. These stages of development are shown in Figure 2. The first reconstruction covers AD 900-1989 and is described in Cook *et al* (1991, 1992). The second reconstruction covers 300 BC-AD 1989 and is described in Cook *et al* (in press). The third reconstruction, which will be analyzed here, covers 800 BC-AD 1991. So, in three independent stages, the length of the warm-season temperature reconstruction was increased from 1089 to 2290 and, finally, to 2792 years.

These progressive extensions also meant the addition of a lot of new tree-ring data throughout the record. Figure 2(d) shows the changing tree-ring sample size over time for each of the three reconstructions. From AD 900 to the present, most of the samples came from living trees. Prior to that date, the tree-ring specimens came from sub-fossil logs and *in situ* stumps at the site. Although the tree-ring samples added to the reconstruction are not spatially independent of those used initially by Cook *et al* (1991,1992) (*ie,* they all came from the same general location above Lake Johnston), they do represent many new trees sampled independently of the living trees.

Spectral analysis (Jenkins and Watts 1968; Marple 1987) of the three series in Figure 2 has revealed the presence of oscillatory behavior that has apparently persisted over the past 2792 years. Cook *et al* (1992) presented both classical Blackman-Tukey and maximum entropy spectra of the shortest record and noted the apparent presence of statistically significant (*a priori* $\alpha<0.05$) peaks with periods around 30, 56, 80, and 180 years. It was speculated that these peaks could have been generated by internal dynamics of the coupled atmosphere/ocean/cryosphere system (*sensu* Stocker and Mysak 1992). However, given the *a posteriori* nature of the spectral analysis, those results had to remain purely speculative. With the extension of the record back to 300 BC, which doubled the original series length, it was possible to test for the longer-term presence of those oscillatory modes and possibly validate their existence. In so doing, Cook *et al* (in press) found that the spectral peaks noted earlier were still present in the longer reconstruction, even when the series was split into two quasi-independent halves and analyzed separately. In this case, the mean periods for the full reconstruction were 31, 56, 79, and 204 years. With this positive result, Cook *et al* (in press) proceeded to characterize the time/domain behavior of these oscillations using singular spectrum analysis (Vautard and Ghil 1989). The extracted wave forms obtained by SSA revealed that these signals were indeed

present throughout the reconstruction and possessed significant amplitude modulation. With the addition of more tree-ring series to the reconstruction and its extension back to 800 BC (Figure 2), we will again make the case for the probable existence of these oscillatory modes and characterize them using SSA.

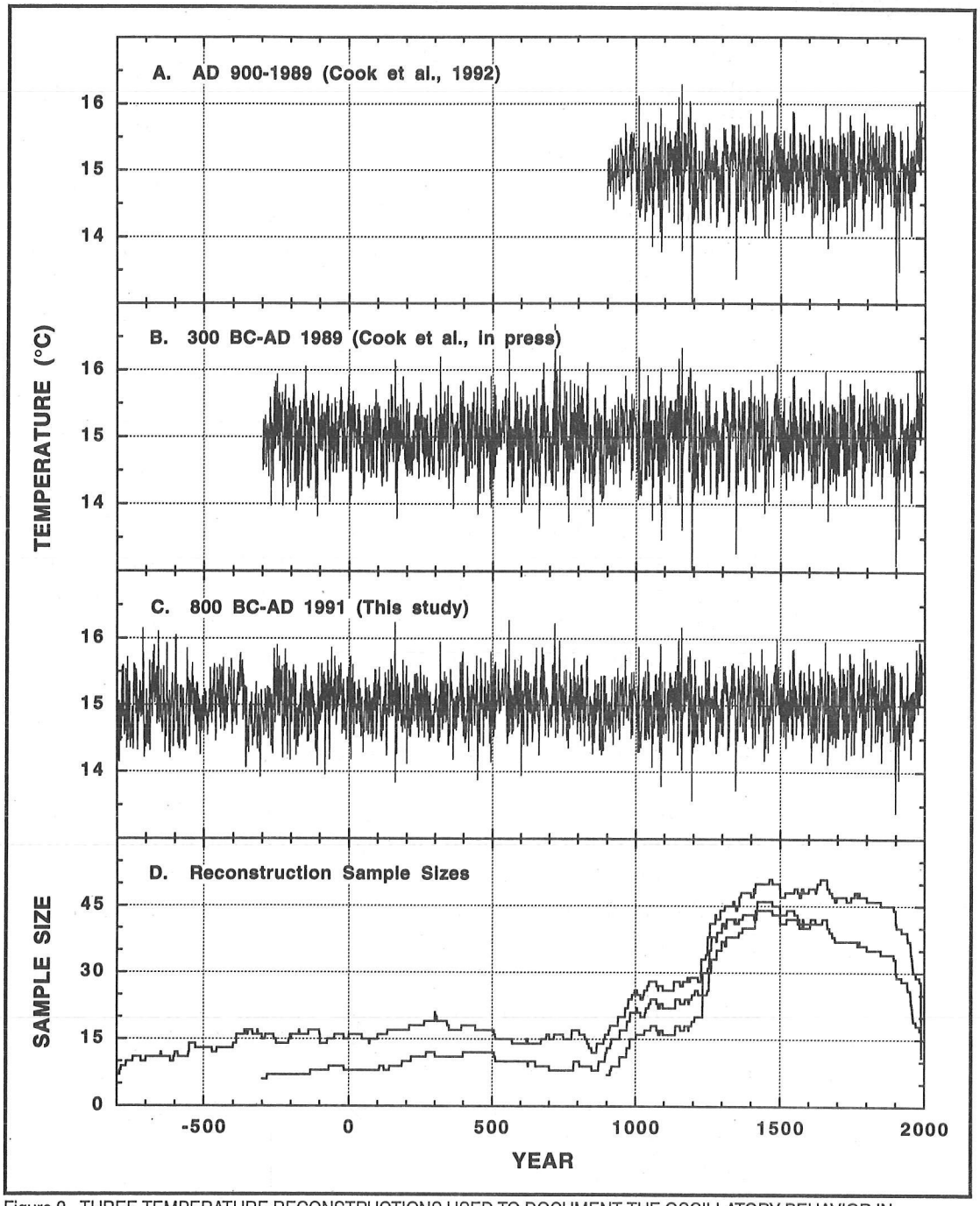

Figure 2. THREE TEMPERATURE RECONSTRUCTIONS USED TO DOCUMENT THE OSCILLATORY BEHAVIOR IN WARM-SEASON TASMANIAN TEMPERATURES
The change in tree-ring sample size is shown to indicate the degree to which new information was added to each successive reconstruction.

Figure 3 shows the power spectra of the three reconstructions developed to date. Each has been computed using identical Blackman-Tukey procedures. The spectral estimates are only shown over frequencies from 0 to 1/10 years, because that is the bandwidth of interest here. Relevant statistics of the power spectra are provided in the figure (*ie*, lags, degrees of freedom, bandwidth). The *a priori* 95% confidence limits are based on a first-order Markov null continuum model (Gilman *et al* 1963). It is arguable that the *a priori* limits are, in fact, correct for testing the spectra in Figure 3 (b-c) because the four spectral peaks being tested were k.

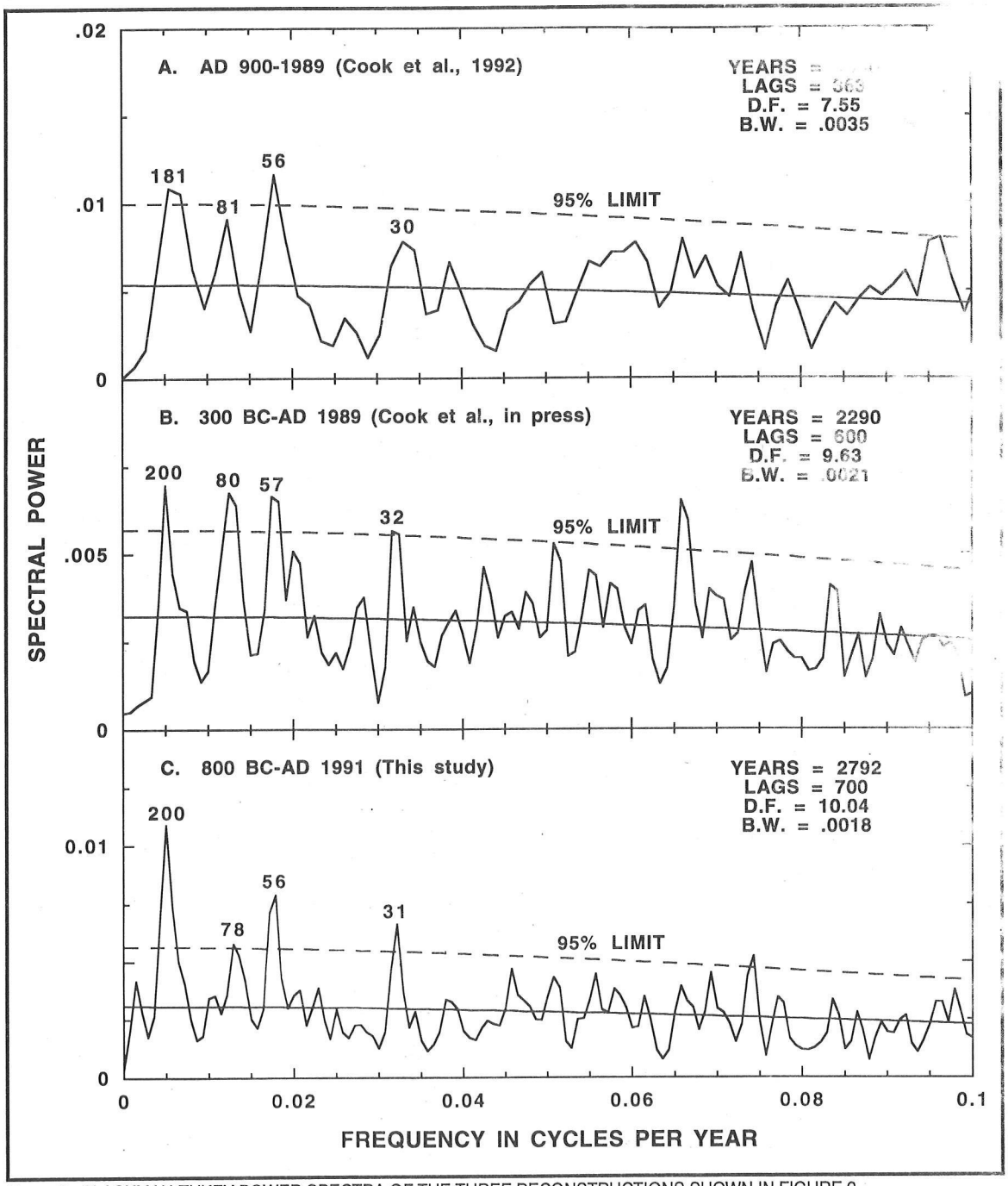

Figure 3. BLACKMAN-TUKEY POWER SPECTRA OF THE THREE RECONSTRUCTIONS SHOWN IN FIGURE 2.
The 95% confidence limits are based on a first-order Markov null continuum model.
The spectra are only shown over the frequency range 0 to 0.10.

in advance. However, the lack of complete independence of the times series analyzed here weakens that argument somewhat.

These spectra basically re-affirm the probable existence of the oscillatory modes reported by Cook *et al* (1992, in press). Each indicates the presence of spectral peaks with periods around 31, 56, 80, and 200 years, although their contributed variances do vary somewhat. In contrast, there is little indication of consistent spectral peaks in the frequency range of 1/28 to 1/10 years that exceed the 95% limits. This suggests that any indicated quasi-periodic behavior in that broad band is either transient or spurious.

Singular Spectrum Analysis

We now take a more detailed look at the oscillations in the Tasmania temperature reconstruction using SSA. The series used for this purpose is that shown in Figure 2(c), which extends back to 800 BC. Singular spectrum analysis is an elegant, data-adaptive method of extracting signals from noise in a time series (Vautard and Ghil 1989; Vautard *et al* 1992). It is based on applying principal components analysis to the autocovariance matrix of the time series. Following Vautard *et al* (1992), we used unbiased estimates of autocovariance for this purpose. The result is a set of eigenvalues (or "singular values") and eigenvectors (or "empirical orthogonal functions") that express particular modes of behavior in the series over time. In particular, periodic behavior is expressed in the eigenvalue trace as a degenerate pair of nearly equal eigenvalues. The corresponding EOFs will behave as even and odd functions, with the latter being in quadrature with the former. When applied to the original time series to extract the oscillatory wave form (or "reconstructed components"; Vautard *et al* 1992), the even and odd EOFs act as digital band-pass filters with data-derived frequency response functions. This is one of the principal strengths of singular spectrum analysis, because it does not impose a potentially incorrect band-limited model on the series as might be the case using classical digital filtering techniques. On the other hand, the reconstructed components produced by SSA might not be physically interpretable beyond a phenomenological level and could, in fact, be transient or totally spurious. The oscillations being investigated here do not appear to be either transient or spurious. However, their physical meanings are still somewhat elusive.

Like all methods of spectral analysis, there is an element of subjectivity and even artwork in applying singular spectrum analysis to noisy time series. Two matters are of particular interest. One is determining the dimension of the signal subspace; *ie,* the number of "true" signals in the time series. Given the link between singular spectrum analysis and principal components analysis, this is equivalent to determining the number of significant eigenvalues in the autocovariance matrix. Monte carlo techniques could be used for this purpose using one of the methods described in Preisendorfer *et al* (1981) if nothing is known about the

signal subspace dimension. Such is not the case here. A related problem, which does not normally exist in PCA, is selecting the optimum embedding dimension for extracting the signals of interest; *ie,* the number of lags used to estimate the autocovariance matrix. Here, the link between SSA and classical Blackman-Tukey spectral analysis is apparent, because the chosen lag window ultimately determines the resolution and stability of spectral estimates in either case.

In our problem here, the number of "true" signals has been defined by previous analyses (Cook *et al* 1992; in press). This means we should expect four pairs of eigenvalues to express the oscillatory behavior associated with the 31-, 56-, 80-, and 200-year modes. In addition, these four periodic components consistently account for most of the band-limited variance in the spectrum at wave-lengths longer than 10 years. Thus, they should be associated with the first eight eigenvalues of the autocovariance matrix if the analysis is restricted to inter-decadal or longer wave-lengths. This is the expected dimension of our signal subspace. The choice of embedding dimension can have an effect on this expectation, however. If it is too small, there will not be sufficient resolution to cleanly separate the oscillatory modes into separate EOF pairs. In this case, the variance associated with the four modes may be condensed into fewer than eight eigenvalues. Conversely, too many lags can lead to something akin to peak splitting, which may cause the variance to be distributed over more than eight eigenvalues.

Because there is no theory for determining the optimum embedding dimension, a form of "window closing" (*sensu* Jenkins and Watts 1968) is usually applied in SSA to search for a range of embedding dimensions where the results do not change very much (Vautard and Ghil 1989; Vautard *et al* 1992). We have used this window closing procedure here, but have adapted it to the individual oscillations, which range from 31 to 200 years. In each case, five embedding dimensions *(M)* were investigated. For the 200-year oscillation, *M* ranged from 300-500 at 50-lag intervals. For the closely spaced 56- and 80-year oscillations, *M* ranged from 200-400 also at 50-lag intervals. For the 31-year oscillation, *M* ranged from 100-200 at 25 lag intervals. Prior to each window closing exercise, we filtered the temperature reconstruction to eliminate higher-frequency variance not associated with the oscillations being modeled. Pre-filtering eliminated some leakage problems apparent in the EOFs, which would have degraded their performance as band-pass filters. However, the EOFs estimated after pre-filtering were always applied to the original, unfiltered reconstruction when estimating the reconstructed components.

Figure 4 shows the reconstructed components using the procedures described above. Component periods were determined by spectral analysis and differ only slightly from the earlier estimates (77 *vs* 80 and 57 *vs* 56 years). Rather than present one reconstructed component per oscillation as the "best" estimate, we have chosen to overlay all five in each case for comparison. In general, the estimated reconstructed

components are not sensitive to the choice of embedding dimension. The biggest differences tend to be during periods of reduced amplitude; *ie*, when the signal-to-noise ratio was lowest. In every case, the reconstructed components show distinct amplitude modulation with a typical range of near zero to 0.1°C. In some cases, the modulation envelope is somewhat regular, the 77-year reconstructed component being the best example. The 31-year reconstructed component also has a tendency for asymmetric, non-linear amplitude modulation, with the rise taking longer than the fall.

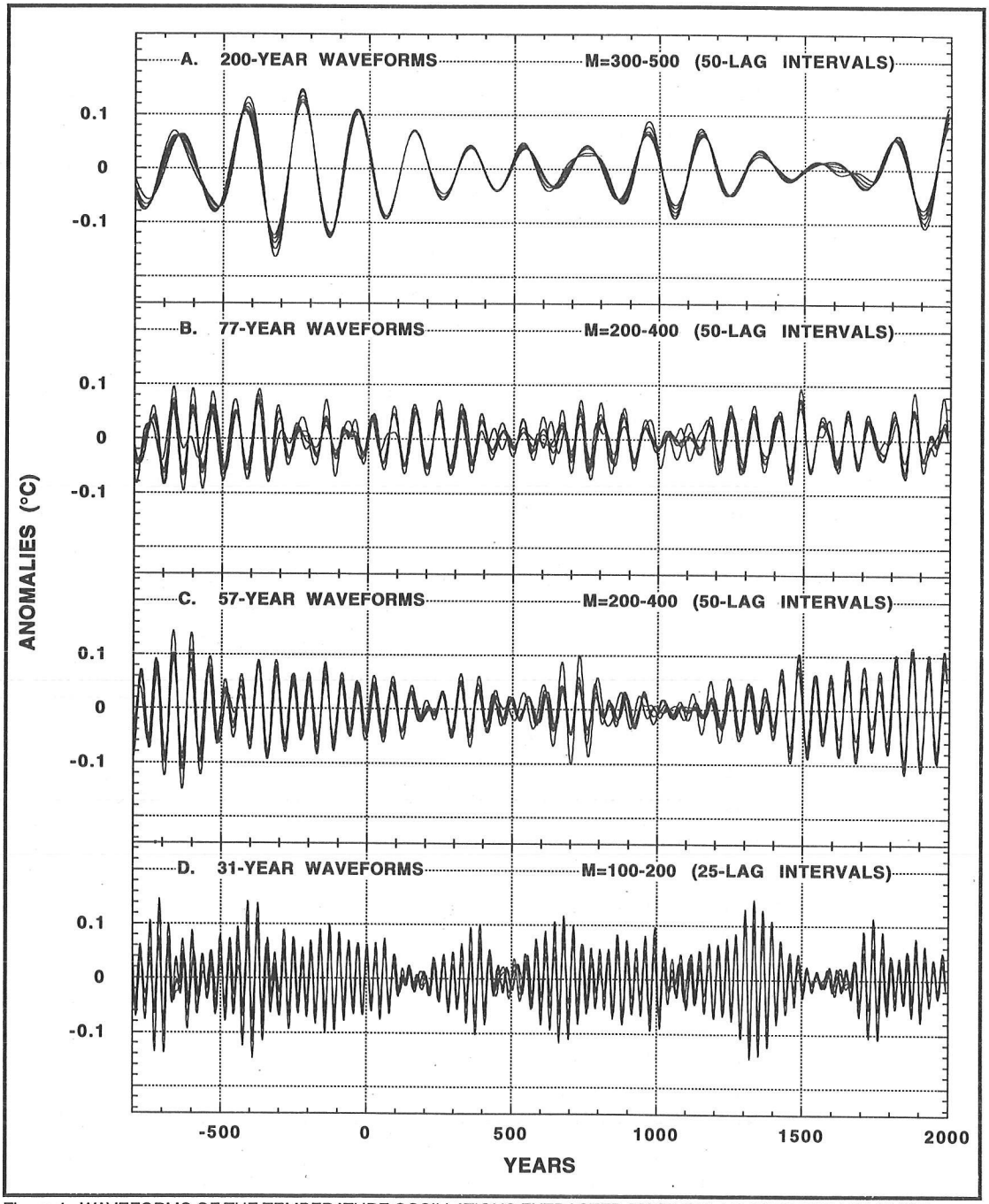

Figure 4. WAVEFORMS OF THE TEMPERATURE OSCILLATIONS EXTRACTED BY SINGULAR SPECTRUM ANALYSIS
Five waveforms per period were estimated and overlaid to indicate the degree to which the chosen embedding dimension affected results.

There is no obvious "best" embedding dimension for selecting the 31-, 57-, 77-, and 200-year reconstructed components to produce a composite temperature signal that expresses the cumulative effect of these inter-decadal oscillations through time. For this reason, we generated all possible combinations of 4-wave form aggregates using the five estimates per oscillation. This resulted in 5^4 or 625 aggregates. We then took the median aggregate as the best estimate of the inter-decadal temperature signal based on the four oscillations. In addition, we used the 2.5 and 97.5 percentiles of the 625 aggregates to generate approximate 95% confidence limits around the median series. These results are shown in Figure 5. From these plots, it is clear that the variance due to the choice of embedding dimensions is quite small relative to the amplitude of the median signal.

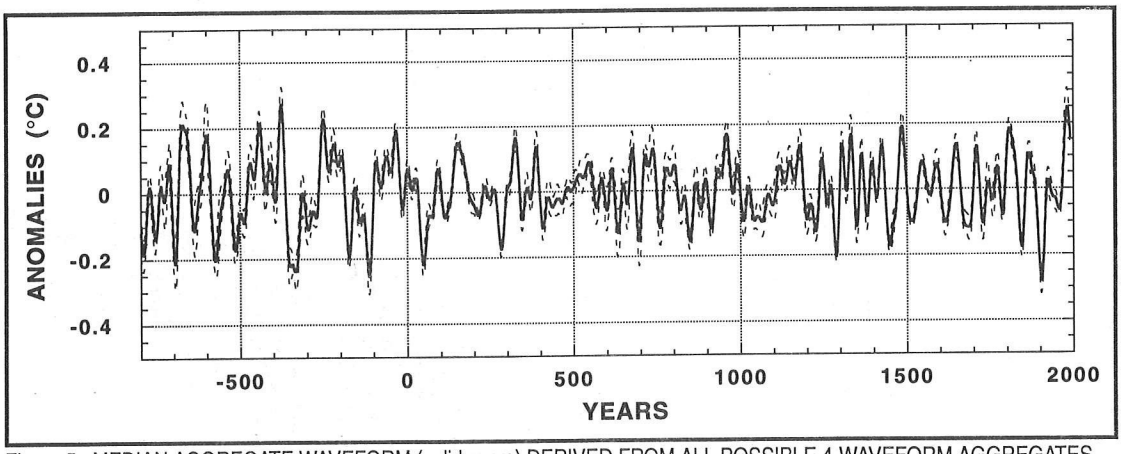

Figure 5. MEDIAN AGGREGATE WAVEFORM (solid curve) DERIVED FROM ALL POSSIBLE 4-WAVEFORM AGGREGATES AVAILABLE FROM FIGURE 4.
The 2.5 and 97.5 percentile limits (dashed curves) from the suite of all possible aggregates are provided as approximate 95% confidence limits.

None of individual oscillations accounts for more than 2 or 3% of the total variance in the original temperature reconstruction, but individual oscillations are much more important when viewed in the context of inter-decadal climate variability alone. Figure 6 shows scatter plots of the median aggregate signal versus the original unfiltered reconstruction and the series after being low-pass filtered to eliminate all variance at periods less than 10 years. The median aggregate has a correlation of 0.35 with the original series; *ie*, it accounts for 12% of the total variance. In contrast, the correlation with the low-pass-filtered series is 0.64, which amounts to 41% of the inter-decadal variance. Thus, in the context of inter-decadal climate variability over Tasmania, these oscillations must be considered highly important contributors.

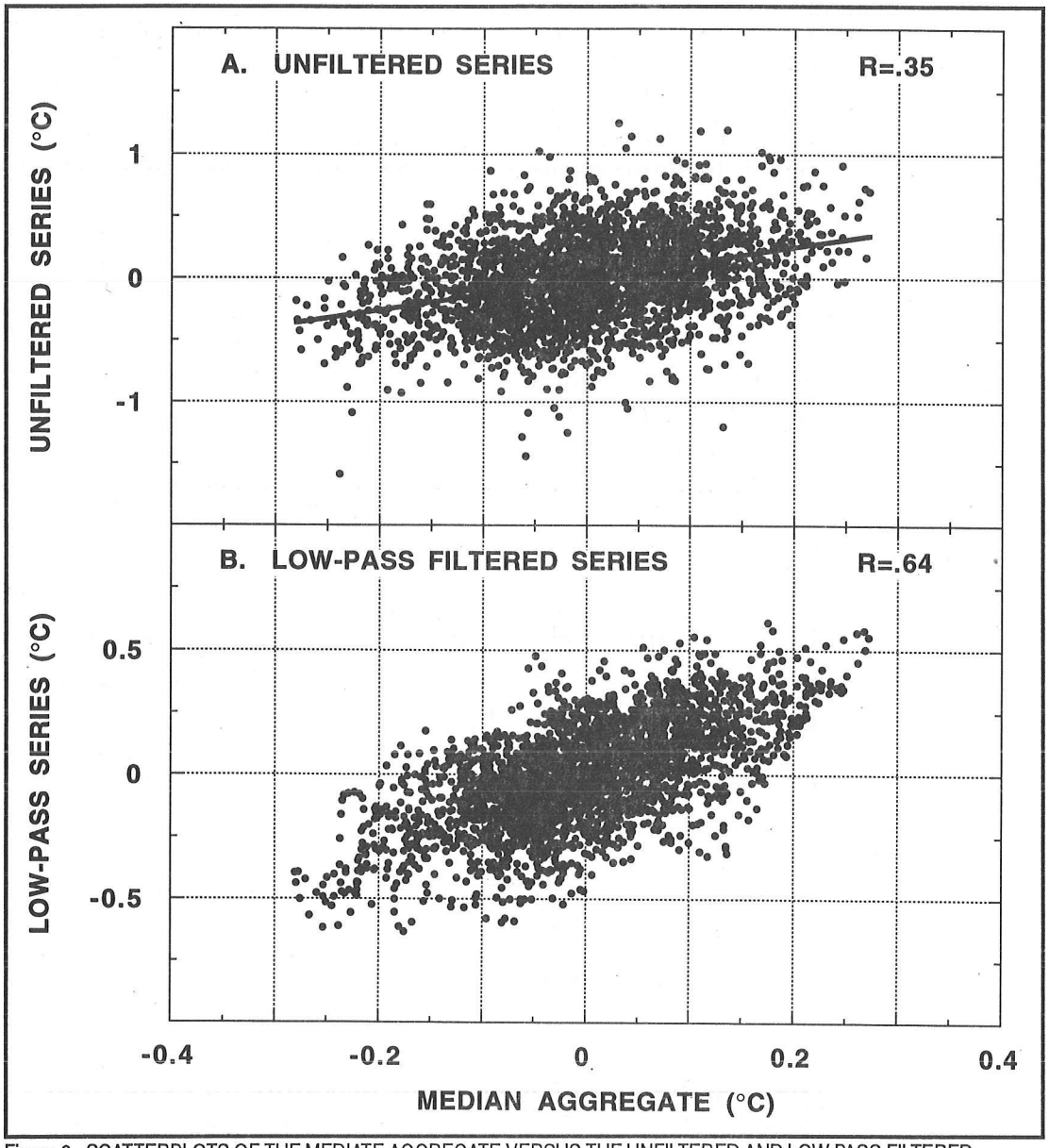

Figure 6. SCATTERPLOTS OF THE MEDIATE AGGREGATE VERSUS THE UNFILTERED AND LOW-PASS FILTERED TEMPERATURE RECONSTRUCTIONS.
Correlations are indicated in the upper righthand corners of the plots.

Temperature Oscillations and Recent Warming over Tasmania

It is instructive now to see how much these oscillations have contributed to recent anomalous warming over Tasmania that was documented by Cook *et al* (1991, 1992). In the AD 900-1989 reconstruction, the 1965-1989 interval was found to be the warmest 25-year period in the 1089-year record. Only when the reconstruction was extended back more than 2000 years was a warmer 25-year period found. In the longest reconstruction, the two warmest 25-year periods are 387-363 BC (0.35±0.046°C) and 1967-1991 (0.33±0.055°C). So while not unique, the

most recent warming is still a rare event that exceeds the long-term mean by 6 standard errors.

With regard to the temperature oscillations being studied here, an obvious question is: "Can they explain the recent warming over Tasmania?" If not, then it could be argued that the climate system is in a new, radiatively altered state due to the buildup of greenhouse gases in the 20th century. Returning to Figure 5, it appears that the oscillations can explain much of the anomalous temperature variability seen in the original reconstruction. The two warmest periods in the median aggregate are the same as before, with peak anomalies of 0.27°C in 376 BC and 0.25°C in 1982.

Figure 7 shows the outer portion of this temperature signal with its 95% limits superimposed on the low-pass filtered reconstruction. The latter highlights the general inter-decadal temperature fluctuations, including the recent warming. For ease of examination, these series are only shown since 1800. It is clear from these plots that the temperature oscillations can cumulatively explain a large fraction of the overall warming since 1967. In terms of mean anomalies, the low-pass-filtered series averages 0.35±0.015°C for 1967-1991, while the mean of the median aggregate is 0.18±0.014°C. So, about 51% of the anomalous warmth can be attributed to the temperature oscillations. This occurred because the individual oscillation anomalies were relatively large, positive, and in phase at this time by chance. However, this comparison may be slightly biased because the 1967-1991 period was used in estimating the EOFs, making the comparison in Figure 7 analogous to results of a fitting exercise. If these data were not used, it is possible that the resulting EOFs would not produce reconstructed components that predict the warming as well. This possibility will be investigated, but it is unlikely to make a large difference. Even withholding all of the 20th century data from estimates of the autocovariances and EOFs would only amount to reducing the series by 3.3% of its total length.

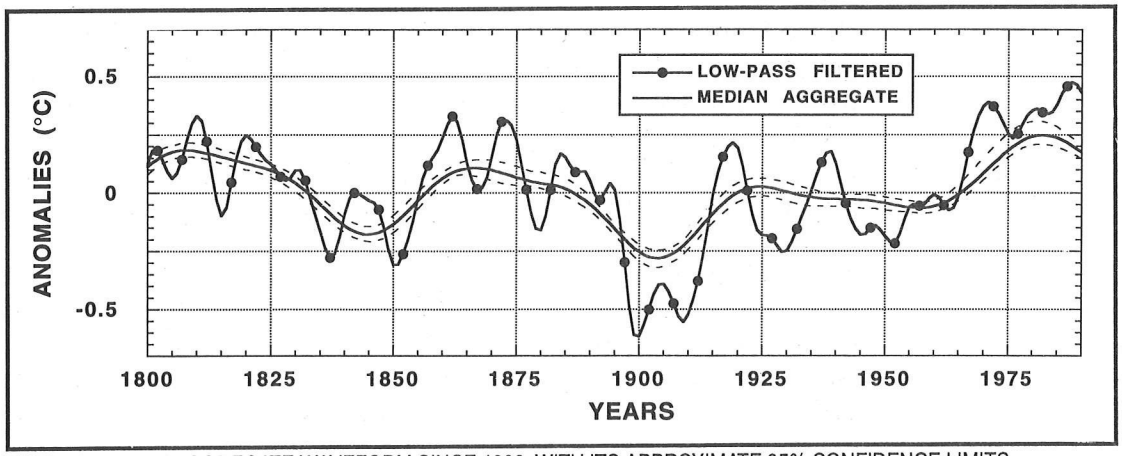

Figure 7. MEDIAN AGGREGATE WAVEFORM SINCE 1800, WITH ITS APPROXIMATE 95% CONFIDENCE LIMITS COMPARED TO THE LOW-PASS FILTERED SERIES
Note the degree to which the aggregate explains much of the inter-decadal warming in the reconstruction since 1965.

Given that the oscillations apparently explain over half of the mean anomalous warming, the median aggregate still systematically underestimates the magnitude of change indicated by the inter-decadal fluctuations. While it is tempting to speculate that greenhouse forcing could be responsible for this residual anomalous warming, systematic under- and over-estimates of inter-decadal temperature change by the median aggregate are as large or larger for similar duration periods in the past. Clearly, there are additional contributors to inter-decadal temperature change over Tasmania, but none seem to be as systematically and persistently effective over the past three millennia as those investigated here.

Implications for Detecting a Greenhouse Warming

The inter-decadal temperature oscillations over Tasmania have the potential to either mimic or mask expected temperature trends due to greenhouse warming. This potential is clearly indicated in Figure 7, where the oscillations collectively explain 51% of the recent anomalous warming. Yet, a closer examination of the median aggregate indicates that it may now be on a down-turn, while the overall inter-decadal temperature trend is stable or rising slightly. Does this mean a divergence is underway that could be reflecting the emergence of greenhouse warming from the natural background variability? It is impossible to say at this time. However, it is possible to describe a reasonable scenario in which the masking effect of the oscillatory modes is factored from expectations of a hypothetical future temperature regime to reveal anomalous warming.

Consider the scenario in which the temperature increase over Tasmania occurred as an abrupt change of state. This is plausible, given the rather rapid and persistent temperature increase that occurred shortly after 1965 in both the instrumental record and the reconstruction (Cook *et al* 1992). Next, suppose this change of state is maintained for the next 30 years (*ie*, no further warming occurs), while at the same time the inter-decadal oscillations continue to operate as they have for the last three millennia. A stable mean maintained over the next 30 years would seem to argue against greenhouse forcing because a warming trend is the first-order (albeit non-unique) expectation, at least on a hemispheric basis. However, maintaining a stable mean would actually require a warming trend from other sources, like greenhouse forcing, to offset a continuing decline by the oscillations in the future.

To see how this might work, the median aggregate was forecast 30 years into the future using a moderate-length prediction error filter estimated by the maximum entropy method (Ulrych and Clayton 1976). The resulting inter-decadal 30-year forecast is shown in Figure 8, along with a simple climatology forecast based on the 1967-1991 mean. The inter-decadal forecast is not sensitive to the prediction error filter length. Varying the order from 200 to 500 produced almost no difference in the forecasts. This is due to the extremely high signal-to-noise ratio in the

median aggregate produced by singular spectrum analysis (cf, Penland *et al* 1991) and the short forecast horizon relative to the lengths of the prediction error filters tested.

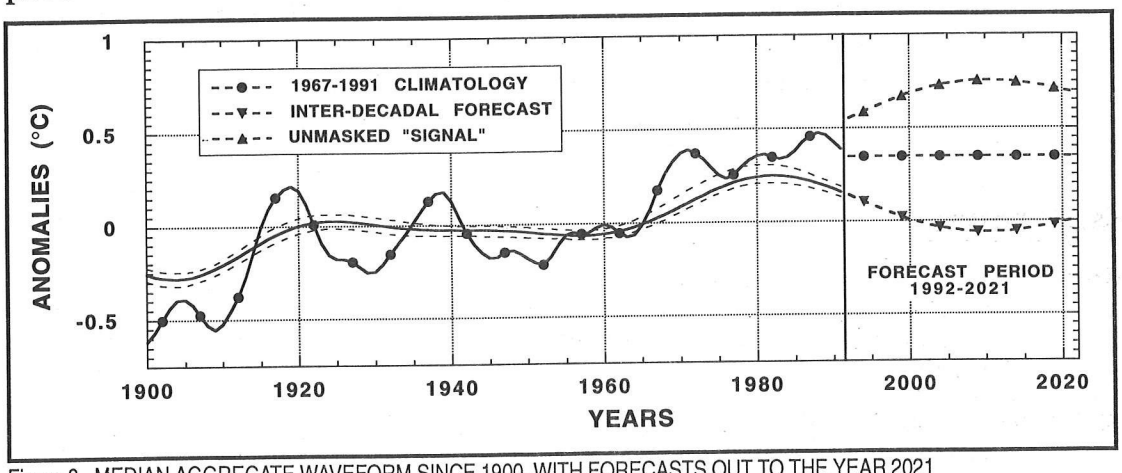

Figure 8. MEDIAN AGGREGATE WAVEFORM SINCE 1900, WITH FORECASTS OUT TO THE YEAR 2021
These are provided to indicate how such inter-decadal, natural variability could mask a future warming trend due to other effects like greenhouse warming. This forecast is compared to a climatology forecast using the mean of the 1967-1991 period, which represents a continuation of the anomalous warmth now affecting Tasmania. If both were to occur in the future, a hidden warming trend indicated by the unmasked "signal" would be required to offset the inter-decadal cooling.

As suspected, the inter-decadal forecast continues to decline from its recent peak in 1982 to a minimum in 2009, after which it begins to climb slowly again. The unmasked hypothetical change is that needed to completely offset the inter-decadal cooling and thus reproduce the climatology forecast. Therefore, it is nothing more than the mirror image of the inter-decadal cooling. The result is an unmasked warming trend. In its unmasked state, this trend would exceed the warmest 25-year period in the reconstruction by a wide margin over the next 30 years. Although rather schematic and strictly hypothetical, this example illustrates how future warming induced by factors not related to the inter-decadal oscillations would have to be substantial just to offset a projected cooling due to this long-term, natural variability.

Conclusions

We have presented a growing body of statistical evidence for the existence of inter-decadal temperature oscillations affecting the climate of Tasmania. This behavior has apparently persisted for almost 3000 years and is an important contributor to past and present temperature change in this sector of the Southern Hemisphere. Although it is always dangerous to extrapolate such results into the future, it is reasonable to expect that these oscillations will continue in more or less the same modes unless a radical change of state occurs in the ocean/atmosphere system. If this behavior continues, then the potential masking effects of these oscillations on a greenhouse warming will need to be considered.

Acknowledgments

We thank Trevor Bird, Mike Peterson, Roger Francey, and Mike Barbetti for field assistance and valuable consultations on Huon pine research in Tasmania. This research is supported by the National Science Foundation, Division of Earth Sciences (Grant EAR 93-10093) and Division of Atmospheric Sciences (Grant ATM 92-12107).

References

Barry, R.G. 1978. Climatic fluctuations during the periods of historical and instrumental record. Pages 150-166 in *Climatic Change and Variability: A Southern Hemisphere Perspective.* A.B. Pittock, L.A. Frakes, D. Jenssen, J.A. Peterson, J.W. Zillman, editors. Cambridge University Press, London.

Cook, E.R., T. Bird, M. Peterson, M. Barbetti, B. Buckley, R. D'Arrigo, R. Francey, P. Tans. 1991. Climatic change in Tasmania inferred from a 1089-year tree-ring chronology of subalpine Huon pine. *Science* 253:1266-1268.

Cook, E.R., T. Bird, M. Peterson, M. Barbetti, B. Buckley, R. D'Arrigo, R. Francey. 1992. Climatic change over the last millennium in Tasmania reconstructed from tree rings. *The Holocene* 2:205-217.

Cook, E.R., B.M. Buckley, R.D. D'Arrigo. In press. Interdecadal temperature oscillations in the southern hemisphere: Evidence from Tasmanian tree rings since 300 BC. In *The Natural Variability of the Climate System on 10-100 Year Time-Scales.* Proceedings of National Academy of Sciences Workshop, Irvine, California, September 21-24, 1992.

Fritts, H.C. 1976. *Tree Rings and Climate.* Academic Press, London.

Gilman, D.L., F.J. Fuglister, and J.M. Mitchell Jr. 1963. On the power spectrum of "red noise". *Journal of the Atmospheric Sciences* 20:182-184.

Jenkins, G.M., and D.G. Watts. 1968. *Spectral Analysis and Its Applications.* Holden-Day, San Francisco.

Marple, S.L. Jr. 1987. *Digital Spectral Analysis with Applications.* Prentice-Hall, New Jersey.

Penland, C., M. Ghil, K.M. Weickmann. 1991. Adaptive filtering and maximum entropy spectra with application to changes in atmospheric angular momentum. *Journal of Geophyiscal Research* 96(D12):22,659-22,671.

Preisendorfer, R.W., F.W. Zwiers, T.P. Barnett. 1981. *Foundations of Principal Components Selection Rules.* SIO Reference Series 81-4, Scripps Institution of Oceanography, La Jolla.

Stocker, T.F., and L.A. Mysak. 1992. Climatic fluctuations on the century time scale: A review of high-resolution proxy data and possible mechanisms. *Climatic Change* 20:227-250.

Ulrych, T.J., and R.W. Clayton. 1976. Time series modeling and maximum entropy. *Physics of the Earth and Planetary Interiors* 12:188-200.

Vautard, R., and M. Ghil. 1989. Singular spectrum analysis in nonlinear dynamics, with applications to paleoclimatic time series. *Physica D* 35:395-424.

Vautard, R., P. Yiou, M. Ghil. 1992. Singular spectrum analysis: A tool kit for short noisy chaotic time series. *Physica D* 58:95-126.

Multivariate Climate Reconstruction for the Last 14,000 Years in Southernmost South America

Vera Markgraf, James W.C. White, Regina A. Figge, Ray Kenny

ABSTRACT: Comparison between past changes in pollen assemblages and stable isotope ratios (deuterium and carbon) analyzed in the same peat core from Tierra del Fuego at latitude 55°S permitted identification of the relative contribution of precipitation versus temperature responsible for the respective change. Major steps in the sequence of paleoenvironmental changes, such as at 12700, 9000, 5000, and 4000 years ago are apparently related only to increase in precipitation, reflecting the latitudinal location and intensity of the westerly storm tracks. On the other hand, high paleoenvironmental variability, which is characteristic for the late-glacial and the latest Holocene, is related to temperature variability, which affects the relative moisture content. Comparison with other paleoenvironmental records suggests that the late-glacial temperature variability is probably related to variability in the extent of Antarctic sea-ice, which in turn appears to be related to the intensity of Atlantic deep-water circulation. Temperature variability during the latest Holocene, on the other hand, is probably related to the dynamics of the El Niño/Southern Oscillation.

Introduction

Late Pleistocene paleoclimate patterns for southern South America are reconstructed from pollen records analyzed from lake and bog sediments recovered between latitudes 40° and 55°S from both sides of the Andes (Markgraf 1991a, 1993a; Villagran 1990, 1993; Heusser 1984; Lumley and Switsur 1993; Ashworth *et al* 1991). Modern environments in this latitudinal band range from warm- to cool-temperate mixed evergreen rain forest to deciduous forest, moorland, steppe and heath, and Andean fjellfield. These major vegetation types reflect the latitudinal and elevational gradients in seasonal precipitation and temperature as well as the rain-shadow effect of the Andes. Cool-temperate rain forests and moorland vegetation on the west coast of southern Chile, for example, receive between 3000 and 5000 millimeters mean annual precipitation, whereas the steppe-forest limit east of the Andes receives less than 600 millimeters. Toward the northern limit of the temperate forests, precipitation occurs primarily in winter; at higher latitudes, precipitation is either aseasonal or has a summer maximum. Seasonality of precipitation is related to the seasonal latitudinal shift of the westerly storm tracks, poleward in summer and equatorward in winter.

This semi-quantitative relationship between vegetation types and climate parameters is the primary source for paleoclimatic interpretation of past changes in vegetation types reconstructed from pollen assemblage changes (Markgraf 1993a). When developing high-resolution paleoclimate histories, however, the lack of a quantitative climate calibration

In: C.M. Isaacs and V.L. Tharp, Editors. 1995. *Proceedings of the Eleventh Annual Pacific Climate (PACLIM) Workshop, April 19-22, 1994.* Interagency Ecological Program, Technical Report 40. California Department of Water Resources.

of pollen assemblages is a handicap (Markgraf 1991b, 1993b). Most critically needed in the attempt to enhance paleoclimate inferences is the ability to quantitatively distinguish between precipitation and temperature parameters. The only earlier pollen/climate transfer function attempt for southern Chile (Heusser and Streeter 1980) yielded unrealistic results, suggesting that the calibration dataset was not adequate. More promising are recent advances using pollen/climate response surface analysis (Anderson and Markgraf 1993). Regression of a spatial network of climate parameters and modern pollen types allows definition of every pollen taxon's climate space, information that can then be used to translate down-core pollen taxa abundances in quantitative climate terms. Ultimately, however, every climate/pollen calibration approach for southern South America will be limited by the limited climate data available.

Another approach to enhance paleoclimatic interpretation is a multi proxy-climate indicator analysis. Recent advances in quantitative paleoclimate interpretation using stable isotopes on organic materials led us to pursue a combined study, analyzing on the same peat core samples pollen, carbon, and deuterium isotopes.

Methods

The core chosen for this multivariate paleoclimate study was recovered from a raised *Sphagnum* peat bog near Estancia Harberton, in the eastern Beagle Channel in Tierra del Fuego, about 50 kilometers east of Ushuaia (latitude 55°S, longitude 67°W). The moss and sedge components of the 10-meter-long peat core are very well preserved. Interpolation between 21 radiocarbon dates (with a basal date of 13600 YBP) suggests a uniform growth rate of 1 centimeter per 15 years. An exception is the interval between 9000 and 10000 (11000) YBP, when fires apparently burnt the bog surface and temporarily changed growth conditions and hence growth rates (Markgraf 1991b, 1993b).

Results

Major times of change according to pollen assemblage changes (Figure 1) date to 12500 YBP when *Empetrum* (Ericaceae) heath was replaced by steppe, to 9000 YBP when *Nothofagus* woodland replaced the steppe, and to 4000 YBP when, after a 1000-year-long heath re-expansion, modern dense *Nothofagus* forests developed.

Results of the carbon isotope analyses on the moss components (*Sphagnum* spp. and *Drepanocladus* s.l.) have been interpreted to reflect changes in the atmospheric content of carbon dioxide (White *et al* 1994; Figge *et al* in press). Three high-amplitude peaks (Figure 1) in the carbon isotope ratios, at 12900, 11600, and 10200 YBP, suggest that there were marked past "pulses" in atmospheric carbon dioxide, which probably

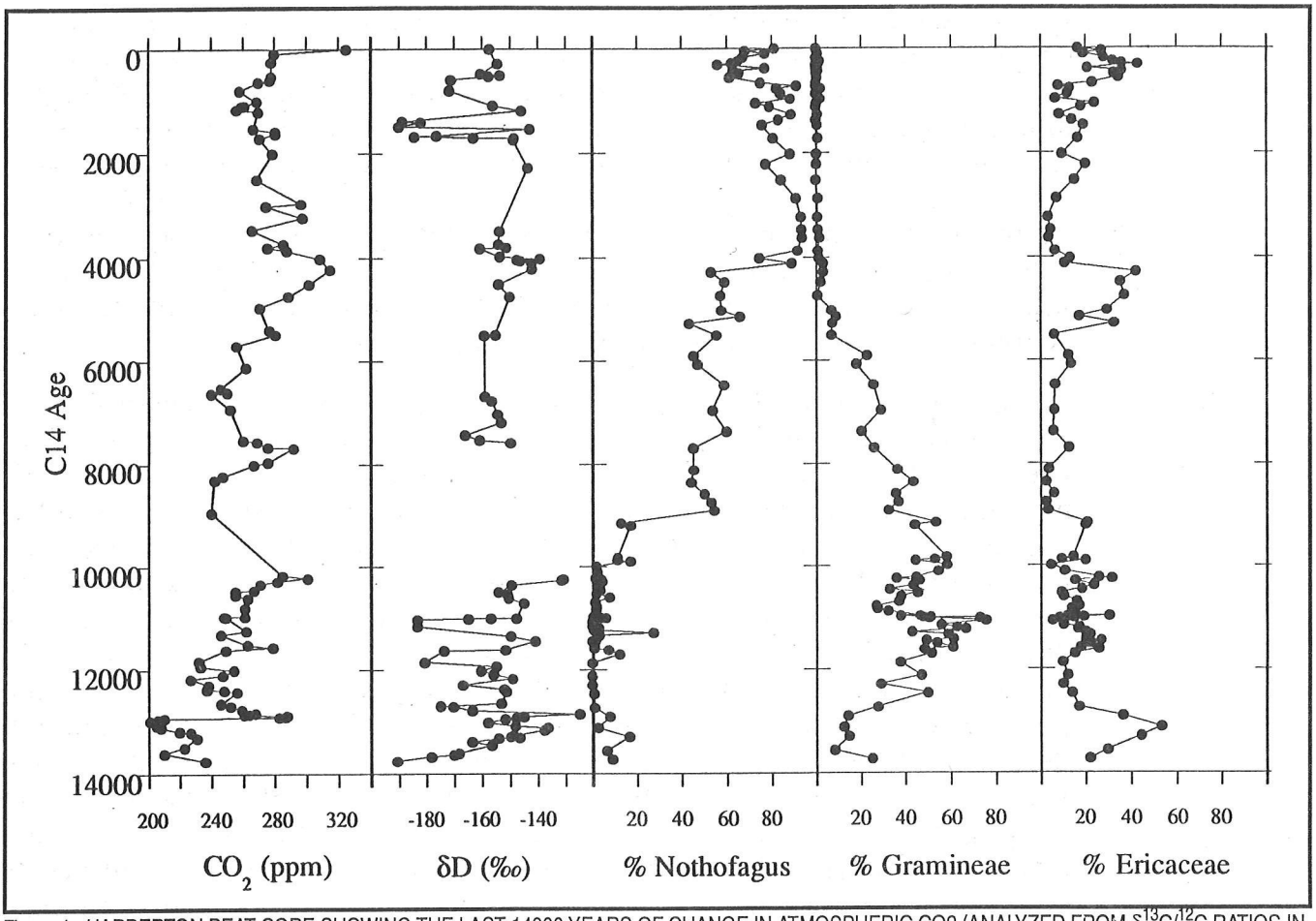

Figure 1. HARBERTON PEAT CORE SHOWING THE LAST 14000 YEARS OF CHANGE IN ATMOSPHERIC CO2 (ANALYZED FROM $\delta^{13}C/^{12}C$ RATIOS IN MOSSES), δD, AND THREE OF THE MAJOR POLEN TAXA: *NOTHOFAGUS* (SOUTHERN BEECH), GRAMINEAE (GRASSES), AND *EMPETRUM* (HEATH).

relate to intervals of deep-ocean degassing events, which in turn relate to changes in intensity of deep-water circulation (Figge and White submitted). Less-rapid and lower-amplitude changes in carbon dioxide also occurred during the Holocene; however, they do not seem related to changes in the thermohaline circulation.

Results from the deuterium analyses are the focus of the following discussion. Ratios between D/H of local precipitation reflect temperature at the site of precipitation (lower temperatures result in more depleted δD values; Dansgaard 1964). δD values of non-exchangeable (C-bound) hydrogen in plant cellulose reflect the δD values of environmental water used by the plant during growth (Epstein *et al* 1976). Thus, δD values from ancient, well-preserved cellulose may provide paleoclimatic information. We have found that the δD values of environmental water in southern South America is indeed strongly controlled by temperature, yielding a δD/temperature gradient of 4‰/°C (White and Kenny in prep).

Several pre-treatment techniques (Brenninkmeijer 1983; White 1983; Coleman *et al* 1982) were tested for efficiency to remove exchangeable

hydrogens from the moss cellulose and hemicellulose; especially the oxygen-bound hydrogens (hydroxyls) are readily exchangeable (Epstein *et al* 1976) and, therefore, need to be removed to obtain a meaningful climate signal. Replicability tests applying different techniques suggest that nitrification procedures proposed by Brenninkmeijer (1983), followed by heating to 200°C under high vacuum, yielded the best results without requiring too much material, which would decrease the temporal resolution of the analyses. The same 1-centimeter samples analyzed for pollen and carbon isotopes were analyzed for deuterium to allow point-by-point correlation between the different paleoclimatic indicators.

The deuterium values in the Harberton record (Figure 1) range from –190 to –130‰, corresponding to a temperature amplitude of more than 10°C. From a value at the base of the record at 14000 YBP of –190‰, deuterium increased rapidly, reaching and exceeding Holocene values of –150‰ between 13500 and 12700 YBP. For the remainder of the late-glacial, variability of the deuterium values is high; values shifted repeatedly and rapidly between –150 and –180‰, which corresponds to temperature shifts of about 3 to 4°C. The duration, especially of the cold intervals, is about 50 years at 12600 YBP, and about 200 years after 11800 YBP, and after 11200 YBP. After a gap related to scarcity of mosses in the sediment, deuterium levels remained relatively stable at –150‰ from 8000 to 4500 YBP. Between 4500 and 4000 YBP, deuterium reached –140‰, representing the relatively warmest temperatures of the Holocene, before returning to early Holocene levels. After 2000 YBP, deuterium variability again increased markedly. Within an interval of 50 years, values jumped from –150 to –190‰, comparable to shifts found during the late-glacial. Using the modern temperature calibration, this implies a temperature decrease of more than 4°C between 2000 and 1700 YBP and between 1000 and 800 YBP.

Comparing changes in the down-core deuterium ratios and pollen assemblages, the former is interpreted to reflect changes in temperature, and the latter interpreted as responding to a combination of temperature and precipitation change, revealing a markedly similar history. Both indicators record high variability during the late-glacial and the latest Holocene and relatively stable climate conditions during the early Holocene. Both indicators follow the same overall pattern of change, and there are no temporal leads or lags between the high amplitude deuterium fluctuations and the proportional shifts of pollen taxa. During the late-glacial, varying proportions of *Empetrum*, Gramineae, and herbaceous taxa represent different types of the late-glacial treeless vegetation in high southern latitudes. During the Holocene, *Nothofagus* enters into the proportional game. This synchroneity of change of the different indicators suggests that either temperature is the leading cause of environmental change in the high southern latitudes or that temperature changes are linked to precipitation changes. A more detailed comparison of deuterium ratios and pollen assemblage changes may help determine which is the case.

The initial rapid deuterium increase culminating between 13500 and 12800 YBP was accompanied by replacement of a species-rich herbaceous steppe pollen assemblage by a depauperate, arid *Empetrum* heath assemblage (Markgraf 1993b). These changes imply that the temperature increase was not compensated by a precipitation increase. The return of Holocene-level deuterium values, which followed a strong but brief interval of more negative values at 12600 YBP, was synchronous with a replacement of *Empetrum* heath by a Gramineae-dominated herbaceous steppe, with substantial amounts of Cyperaceae. This suggests that the temperature increase that followed the brief cold episode must have been accompanied by at least a modest and seasonally evenly distributed precipitation increase, which markedly increased effective moisture. This condition lasted until 11600 YBP, when deuterium values returned again to more negative levels, suggesting another cooling episode. Gramineae apparently responded to the cooling with a slight decrease due to an increase in herbaceous taxa. With the subsequent temperature increase, herbaceous taxa decreased strongly, whereas both *Empetrum* and Gramineae increased. The return of *Empetrum* implies that at that time effective moisture decreased again, probably because precipitation decreased, especially during the warm season. During the final late-glacial cooling episode at 11000 YBP, *Empetrum* decreased and Gramineae increased. This is perhaps best explained in terms of greater moisture availability under cooler conditions. The abrupt, marked decline in Gramineae shortly after that date again occurred at a time of dramatic temperature increase. At the same levels in the core, charcoal amounts increase substantially, and even the bog surface must have burnt, judging from carbonized moss plants (Markgraf 1993b). Thus, the decline in Gramineae is linked indirectly to increased fire frequency as it relates to soil instability as suggested by high levels of herbaceous disturbance indicators, such as ferns, *Gunnera, Acaena, Plantago, etc.*

During the transition interval from late-glacial steppe and steppe/heath vegetation to *Nothofagus* woodland between 10000 and 9000 YBP, mosses are too scarce for deuterium analyses. Continuing high charcoal amounts in the core suggest that fires continued until about 9000 YBP. The burning altered the bog's nutrient balance, which in turn affected microbial activity, decomposition rates, and preservation of the mosses (Markgraf 1993b).

By 8000 YBP, when well preserved mosses are again present, deuterium values are similar to present values. The regional vegetation, however, is less densely forested than today, suggesting greater moisture stress than today, due probably to lower summer precipitation than today (Markgraf 1991a). Of interest is the mid-Holocene warm period, which culminated (according to the deuterium data) between 4500 and 4000 YBP. The pollen data show a marked increase in *Empetrum* between 5000 and 4000 YBP, which suggests a return to substantially more arid conditions than before. As during the late-glacial, the temperature increase was accompanied by a precipitation decrease, especially during the summer.

The mid-Holocene decrease in precipitation affected all the southern temperate forest region, including the wettest moorland regions in the Chilean Channels (Ashworth *et al* 1991), implying that the westerly storm tracks were located equatorward of their modern position. The onset and termination of this mid-Holocene interval occurred in less than 50 years. With the abrupt ending of the warm period at 4000 YBP, the forest became quite dense, suggesting precipitation increased markedly, especially during the warm season.

High variability for both deuterium and pollen characterizes the last 2000 years. The magnitude and frequency of fluctuations of deuterium ratios and pollen proportions at that time equals the late-glacial fluctuations. Twice within less than 200 years, temperatures fluctuated by more than 4°C, reaching minima unequaled since the late-glacial. Another lesser, but longer, temperature decrease occurred after 1000 YBP, which according to the pollen data did not seem to have had much effect on the regional seasonal precipitation pattern. However, the subsequent abrupt temperature increase did again favor expansion of *Empetrum* and increase in fire frequency, suggesting a return to less equable precipitation.

Discussion

High variability in temperature during the late-glacial and the latest Holocene affects regional vegetation composition primarily by altering the effective moisture and fire regimes. Although the paleoclimatic signature during both intervals of high variability is comparable, causes of the variability are different for both time intervals. Intra- and inter-hemispheric correlation of paleoclimate records suggests that the latest Holocene short-term succession of different climate modes and high climate variability is related to El Niño/Southern Oscillation climate anomalies (McGlone *et al* 1992; Markgraf *et al* 1992). During late-glacial times, on the other hand, ENSO apparently did not operate like today, probably because the western tropical Pacific climates were dominated by extended land areas, which greatly altered the downstream climate modes (McGlone *et al* 1992; Markgraf *et al* 1992). Instead, the repeated temperature reversals between 12700 and 11000 YBP most likely reflect short-term changes in Antarctic sea-ice extent. One mechanism for short-term variation in circum-Antarctic sea-ice extent could be related to varying intensity of Atlantic deep-water circulation, which in turn would alter the inter-hemispheric ocean heat transport. High resolution deep-sea records interpreted to document rapid changes in intensity of Atlantic deep-water circulation (Lehman and Keigwin 1992; Charles and Fairbanks 1992) compare well with temperature fluctuations in the Tierra del Fuego record. This mechanism, then, could synchronize paleoclimate change in both hemispheres and could explain similarity between the deuterium data from the peat core from Tierra del Fuego and the Greenland ice core (White and Kenny in prep.).

References

Ashworth, A.C., V. Markgraf, C. Villagran. 1991. Late Quaternary climatic history of the Chilean Channels based on fossil pollen and beetle analyses. *Journal Quaternary Science* 16:279-290.

Anderson, L., and V. Markgraf. 1993. Pollen/climate response surfaces for southern South America: Developing a database for quantitative paleoclimatic reconstruction. Program and Abstracts, *American Association Stratigraphic Palynologist*, 26th Annual Meeting, Baton Rouge. p.5.

Brenninkmeijer, C.A.M. 1983. Deuterium, oxygen-18 and carbon-13 in tree rings and peat deposits in relation to climate. PhD Thesis, University of Groningen.

Charles, C.D., and R.G. Fairbanks. 1992. Evidence from southern ocean sediments for the effect of North Atlantic deep water flux on climate. *Nature* 355:416-419.

Coleman, M.L., T.J. Shepherd, J.J. Durham, J.E. Rouse, G.R. Moore. 1982. Reduction of water with zinc for hydrogen isotope analysis. *Analytical Chemistry* 54:993-995.

Dansgaard, W. 1964. Stable isotopes in precipitation. *Tellus* 16:436-468.

Epstein, S., C.J. Yapp, J.H. Hall. 1976. The determination of the D/H ratio of non-exchangeable hydrogen in cellulose extracted from aquatic and land plants. *Earth and Planetary Science Letters* 30:241-251.

Figge, R.A., J.W.C. White, V. Markgraf, P. Ciais, R. Kenny. In press. A high resolution atmospheric CO_2 record from carbon isotopes in a peat core from Harberton, Argentina. In: *El Cuaternario de America de Sur.* J. Argollo and P. Mougiart, editors. ORSTOM.

Figge, R.A., and J.W.C. White. Submitted. A high resolution Holocene and late glacial atmospheric CO_2 record: Variability tied to changes in thermohaline circulation. *Global Biogeochemical Cycles.*

Heusser, C.J. 1984. Late Quaternary climates of Chile. Pages 59-84 in *Late Cainozoic Palaeoclimates of the Southern Hemisphere.* J.C. Vogel, editor. Balkema, Rotterdam.

Heusser, C.J., and S.S. Streeter. 1980. A temperature and precipitation record of the past 16,000 years in southern Chile. *Quaternary Research* 16:293-321.

Lehman, S.J., and L.D. Keigwin. 1992. Sudden changes in North Atlantic circulation during the last deglaciation. *Nature* 356:757-762.

Lumley, S.H., and R. Switsur. 1993. Late Quaternary chronology of the Taitao Peninsula, southern Chile. *Journal Quaternary Science* 8:161-165.

Markgraf, V. 1991a. Late Pleistocene environmental and climatic evolution in southern South America. *Bamberger Geographische Schriften* 11:271-281.

Markgraf, V. 1991b. Younger Dryas in southern South America? *Boreas* 20:63-69.

Markgraf, V. 1993a. Climatic history of Central and South America since 18,000 yr B.P.: Comparison of pollen records and model simulations. Pages 357-385 in *Global Climates Since the Last Glacial Maximum.* H.E. Wright, Jr., J.E. Kutzbach, T. Webb III, W.F. Ruddiman, F.A. Street-Perrott, P.J. Bartlein, editors. University Minnesota Press.

Markgraf, V. 1993b. Younger Dryas in southernmost South America — revisited. *Quaternary Science Review* 12:352-355.

Markgraf, V., J.R. Dodson, A.P. Kershaw, M.S. McGlone, N. Nicholls. 1992. Evolution of late Pleistocene and Holocene climates in the circum-South Pacific land areas. *Climate Dynamics* 6:193-211.

McGlone, M.S., A.P. Kershaw, V. Markgraf. 1992. El Niño/Southern Oscillation climatic variability in Australasian and South American paleoenvironmental records. Pages 435-462 in *El Niño: Historical and Paleoclimatic Aspects of the Southern Oscillation.* H.F. Diaz and V. Markgraf, editors. Cambridge University Press.

Villagran, C. 1990. Glacial climates and their effects on the history of the vegetation of Chile: A synthesis based on palynological evidence from Isla de Chiloé. *Palaeobotany Palynology* 65:17-24.

Villagran, C. 1993. The Quaternary of the Lake District of Southern Chile. Pages 1-123 in *International Workshop "The Quaternary of Chile"*. Field Guide.

White, J.W.C. 1983. The climatic significance of D/H ratios in white pine in the northeastern U.S. PhD Thesis, Columbia University, New York.

White, J.W.C., P. Ciais, R.A. Figge, R. Kenny, V. Markgraf. 1994. A high-resolution record of atmospheric CO_2 content from carbon isotopes in peat. *Nature 367:153-156.*

White, J.W.C., and R. Kenney. In preparation. Deuterium analysis from a peat core in Tieria del Fuego and its relation to Greenland and Antarctic ice core data.

Volcanic Activity and Global Change: Probable Short-Term and Possible Long-Term Linkages

David K. Rea and Libby M. Prueher

Annual to Decadal Climate Response to Volcanism

Recognition of climatic cooling following large volcanic eruptions is first attributed to observations by Benjamin Franklin following the 1783 Laki, Iceland, eruption (probably the most sulfur-rich in the past 500 years [Palais and Sigurdsson 1989]), which induced an unusually severe winter in 1783-84 (referenced by Lamb 1970 and Chester 1988). H.H. Lamb (*eg*, Lamb 1970) may have been the first modern champion of volcanically-induced climate change.

There was interest through the 1970s in the possible relationship of volcanism to the longer geologic record of climate change (Kennett [1981] provides a good summary), but interest waned toward the end of the decade, probably as a result of the rapidly growing excitement in the demonstrated likelihood of Milankovitch mechanisms to incur climate change at time scales of interest to those studying the late Cenozoic glaciations. Interest in the effects of explosive eruptions on interannual to decadal climate variations remained, however.

In the early 1980s it was realized that the sulfur aerosols were the most important attribute of large eruptions in regard to the ensuing cooling (Rampino and Self 1982; Self and King 1993). Global temperatures decline by 0.2 to 0.3°C for 2 to 5 years after large eruptions (Hoyt 1978; Self *et al* 1981; LaMarche and Hirschboeck 1984; Kelly and Sear 1984). The cooling is not evenly distributed around the earth (Robock and Mao 1992). High latitudes of the Northern Hemisphere cool by as much as several degrees following eruptions, with important consequences to snow/ice retention over the sub-polar summer (Bradley and England 1978; Stommel and Stommel 1983; Vupputuri 1992; Rampino and Self 1992, 1993; Shabbar 1993). Studies of climatic effects incurred by the El Chichon eruption of 1982 were complicated by the large 1982-83 ENSO event (Hofmann 1987), but recent work on the 1991 Pinatubo eruption has resulted in the "first unambiguous, direct measurements of large-scale volcanic forcing" (Minnis *et al* 1993, p. 1411).

Porter (1981, 1986) finds decadal-timescale influences of volcanic activity on glacial advances. He notes a time lag of 10 to 15 years between the response of a glacier terminus (an advance) to the volcanic forcing as indicated by the ice-core acidity signal. Porter (1986) concludes that sulfur-rich aerosols generated by volcanic eruptions are the primary

In: C.M. Isaacs and V.L. Tharp, Editors. 1995. *Proceedings of the Eleventh Annual Pacific Climate (PACLIM) Workshop, April 19-22, 1994.* Interagency Ecological Program, Technical Report 40. California Department of Water Resources.

forcing mechanism of climate on decadal time scales. Lamb (1970) reported that sea ice in high northern latitudes may linger long into the summer for 5 to 10 years after large eruptions. Hammer *et al* (1981) compared the acidity record of a Greenland ice core to northern Europe temperature records back to year 553 and noted the distinct correlation between the acidity level in the Greenland core and cold temperatures. In particular, Hammer *et al* (1981) emphasize that the highest levels of acidity correlate with the two coldest intervals of the Little Ice Age, between 1250-1500 and 1550-1700.

Long-Term Climatic Response to Volcanism

Volcanically-induced cooling on these relatively short time scales seems reasonably well demonstrated. The correlation to longer-term climate change is more speculative. Nearly two decades ago, Kennett and Thunell (1975; see also Stewart 1975) noticed a worldwide increase in the number of ash layers in the late Pliocene and suggested that they may be somehow associated with Northern Hemisphere glaciation. Bray, in a series of papers (1974, 1977, 1979a, 1979b), linked explosive volcanism with both hemispherical and global cooling and glacial advances. A Pacific Basin-wide summary of Neogene and Quaternary volcanism indicated larger eruptive episodes at 0-2 and 14-16 Ma, with lesser events centered near 5 and 10 Ma (Kennett *et al* 1977). Kennett *et al* (1977) suggested that there may be cooling events associated with each maximum.

Several years ago, those studying effects of volcanic eruptions adopted the "nuclear winter" arguments to their use, suggesting significant climatic effects following unusually large eruptions (Stothers *et al* 1989). Rampino and Self (1992, 1993) observed that the 74,000-year-old Toba ash in the northern Indian Ocean, marking one of the largest eruptions in the later Quaternary, occurred at the transition from warm interglacial stage 5a to cold stage 4. They suggested that the rapidity of the stage 5/4 transition was enhanced by the cooling effect of that large eruption. In fact, the observation that this large eruption occurred *after* the beginning of cooling is one argument being made to support the suggestion that ice cap formation *causes* volcanic eruptions. Presumably this is accomplished by unloading the oceans and loading the polar regions with ice. Resulting stress redistribution in the lithosphere then may trigger large eruptions in susceptible regions such as island arcs (Chester 1988; Rampino and Self 1993).

Recent Results from Ocean Drilling in the North Pacific

Recent results of Ocean Drilling Program Leg 145 to the subarctic Pacific (Figure 1) show that it may be appropriate to return to the suggestion of Kennett and Bray and their co-workers that enhanced Pliocene volcanism may be associated in a causal manner with the onset of Northern Hemisphere glaciation at 2.6 Ma. Results of that cruise (Leg 145 Scientific

Party, 1993; Rea, Basov *et al* 1993) show that the late Pliocene beginning of large-scale Northern Hemisphere glaciation, as depicted by the abrupt onset of significant amounts of ice rafting, is intimately associated with the sudden appearance of numerous thick ash layers in the sedimentary section all across the North Pacific (Figure 2). For example, macroscopic description of Core 11H of Hole 882A shows the first thick (5 cm) ash layer

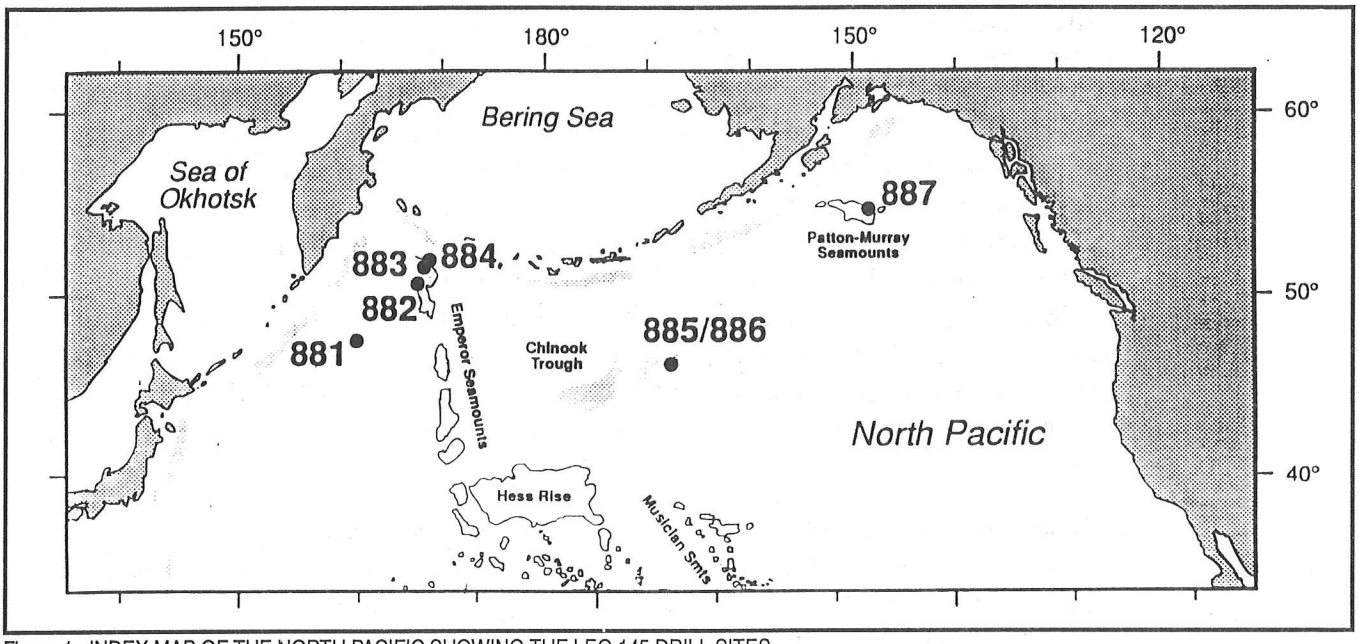

Figure 1. INDEX MAP OF THE NORTH PACIFIC SHOWING THE LEG 145 DRILL SITES

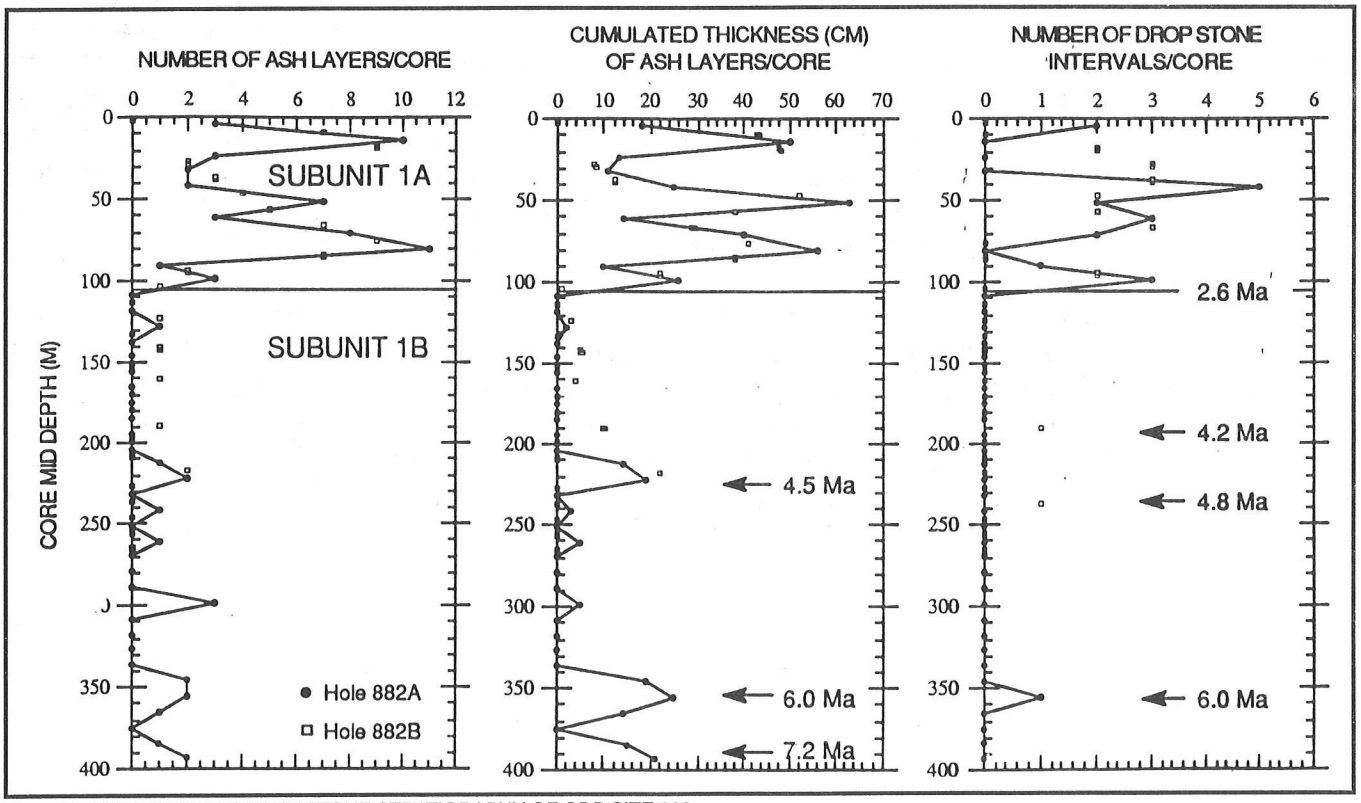

Figure 2. ASH LAYER AND DROPSTONE STRATIGRAPHY OF ODP SITE 882

Lithologic Subunit 1A is a clayey diatom ooze; 1B is a nearly pure diatom ooze. Arrows with ages point to individual ash layers or dropstones. Depth in the sedimentary section of the 2.6 Ma horizon where Northern Hemisphere glaciation begins is denoted by the horizontal line.

at Section 4, 133-138 cm; the Matuyama-Gauss magnetic reversal (at 2.6 Ma) at Section 3, 80 cm; and the first dropstone at Section 1, 88-93 cm, 4.9 meters (60 or 70 kyr) above the first thick ash layer. Similar relationships occur at other northwest Pacific sites and at the Gulf of Alaska Site 887 (Rea, Basov *et al* 1993).

At a distance of about 1000 kilometers downwind from the vent the Toba ash, thought by several authors to be the largest late Quaternary eruptive event (*eg*, Rose and Chesner 1987), is about 10 to 15 centimeters thick (Dehn *et al* 1991). At Site 882 on Detroit Seamount, a paleo-distance of about 1000 kilometers from the Kuril-Kamchatka arc, ODP hydraulic piston cores recovered by the *JOIDES Resolution* contain a dozen ash layers over 10 centimeters thick, and more than 60 distinct ash layers 1 centimeter or greater in thickness in the sequence that begins suddenly at the time of the Matuyama-Gauss magnetic reversal (Rea, Basov *et al* 1993). The suggestion arises that the enormous eruptions of the Kuril-Kamchatka-Aleutian region, which began suddenly at 2.6 Ma, provided the trigger mechanism or threshold phenomenon that rapidly tipped the Northern Hemisphere — already primed for such an event — into an ice age.

Threshold phenomena, geologically sudden responses to gradual changes, have often been called upon to explain the onset of Northern Hemisphere glaciation. One of the earlier ones was the closing of the Isthmus of Panama, resulting in the northerly diversion of warm water in the Gulf Stream. Upon reaching high latitudes, this warmer water served as a moisture source for the growing ice caps (Berger *et al* 1981). The threshold phenomenon now "on the table" is the mid- to late Cenozoic uplift of the Tibetan and American Plateaus. Plateau uplift fulfills the dual function of altering atmospheric circulation in such a way to cool the northern continents and of allowing increased erosion and chemical weathering, resulting in a draw-down of atmospheric CO_2 (Ruddiman and Kutzbach 1989, 1990; Raymo *et al* 1988; Raymo 1991).

This data- and model-based paleoclimatology may well be correct, but amidst the ongoing uplifting, cooling, and chemical weathering, all of which happen on tectonic time scales, Northern Hemisphere glaciation begins abruptly. Hence, there may remain some not yet identified critical threshold phenomenon, possibly the sudden onset of massive volcanism in the western and northern Pacific island arcs.

References

Berger, W.H., E. Vincent, and H.R. Thierstein. 1981. The deep-sea record: Major steps in Cenozoic ocean evolution. Pages 489-504 in *The Deep Sea Drilling Project, A Decade of Progress*, J.E. Warme, R.G. Douglas, and E.L. Winterer, editors. Society of Economic Paleontologists and Mineralogists, Special Publication 32, Tulsa.

Bradley, R.S., and J. England. 1978. Volcanic dust influence on glacier mass balance at high latitudes. *Nature* 271:736-738.

Bray, J.R. 1974. Volcanism and glaciation during the past 40 millennia. *Nature* 252:679-680.

Bray, J.R. 1977. Pleistocene volcanism and glacial initiation. *Science* 197: 251-254.

Bray, J.R. 1979a. Neogene explosive volcanicity, temperature and glaciation. *Nature* 282:603-605.

Bray, J.R. 1979b. Surface albedo increase following massive Pleistocene explosive eruptions in western North America. *Quaternary Research* 12: 204-211.

Chester, D.K. 1988, Volcanoes and climate: recent volcanological perspectives. *Progress in Physical Geography* 12:1-35.

Dehn, J., J.W. Farrell, H.-U. Schmincke. 1991. Neogene tephrochronology from Site 758 on northern Ninetyeast Ridge: Indonesian Arc volcanism of the past 5 Ma. *Proceedings of the Ocean Drilling Program, Scientific Results* 121:273-295.

Hammer, C.U., H.B. Clausen, W. Dansgaard. 1981. Past volcanism and climate revealed by Greenland ice cores. *Journal of Volcanology and Geothermal Research* 11:3-10.

Hofmann, D.J. 1987. Perturbations to the global atmosphere associated with the El Chichon volcanic eruption of 1982. *Reviews of Geophysics* 25:743-759.

Hoyt, D.V. 1978. An explosive volcanic eruption in the Southern Hemisphere in 1928. *Nature* 275:630-632.

Kelly, P.M., and C.B. Sear. 1984. Climatic impact of explosive volcanic eruptions. *Nature* 311:740-743.

Kennett, J.P. 1981. Marine tephrochronology. Pages 1373-1436 in *The Sea, Volume 7, The Oceanic Lithosphere*, C. Emiliani, editor. John Wiley and Sons, New York.

Kennett, J.P., and R.C. Thunell. 1975. Global increase in Quaternary explosive volcanism. *Science* 187:497-503.

Kennett, J.P., A.R. McBirney, R.C. Thunell. 1977. Episodes of Cenozoic volcanism in the circum-Pacific region. *Journal of Volcanology and Geothermal Research* 2:145-163.

LaMarche, V.C. Jr., and K.K. Hirschboeck. 1984. Frost rings in trees as records of major volcanic eruptions. *Nature* 307:121-126.

Lamb. H.H. 1970. Volcanic dust in the atmosphere; with a chronology and assessment of its meteorological significance. *Philosophical Transactions of the Royal Society of London, Series A* 266:425-533.

Leg 145 Scientific Party. 1993. Paleoceanographic record of North Pacific quantified. *EOS* 74:406-411.

Minnis, P., E.F. Harrison, L.L. Stowe, G.G. Gibson, F.M. Denn, D.R. Doeling, W.L. Smith Jr. 1993. Radiative climate forcing by the Mount Pinatubo eruption. *Science* 259:1411-1415.

Palais, J.M., and H. Sigurdsson. 1989. Petrologic evidence of volatile emissions from major historic and pre-historic volcanic eruptions. Pages 31-53 in *Understanding Climate Change*. A. Berger, R.E. Dickinson, J.W. Kidson, editors. American Geophysical Union Geophysical Monograph 52, Washington, DC.

Porter, S.C. 1981. Recent glacier variations and volcanic eruptions. *Nature* 291:139-142.

Porter, S.C. 1986. Pattern and forcing of Northern Hemisphere glacier variations during the last millennium. *Quaternary Research* 26:37-48.

Rampino, M.R., and S. Self. 1982. Historic eruptions of Tambora (1815), Krakatau (1883), and Agung (1963), their stratospheric aerosols, and climatic impact. *Quaternary Research* 18:127-143.

Rampino, M.R., and S. Self. 1992. Volcanic winter and accelerated glaciation following the Toba super-eruption. *Nature* 359:50-52.

Rampino, M.R., and S. Self. 1993. Climate-volcanism feedback and the Toba eruption of 74,000 years ago. *Quaternary Research* 40:269-280.

Raymo, M.E. 1991. Geochemical evidence supporting T.C. Chamberlin's theory of glaciation. *Geology* 19:344-347.

Raymo, M.E., W.F. Ruddiman, P.N. Froelich. 1988. Influence of late Cenozoic mountain building on ocean geochemical cycles. *Geology* 16:649-653.

Rea, D.K., I.A. Basov, *et al.* 1993. *Proceedings of the Ocean Drilling Program: Initial Reports, Vol. 145.* Ocean Drilling Program, College Station, TX. 1040 pp.

Robock, A., and J. Mao. 1992. Winter warming from large volcanic eruptions. *Geophysical Research Letters* 12:2405-2408.

Rose, W.I., and C.A. Chesner. 1987. Dispersal of ash in the great Toba eruption, 75 ka. *Geology* 15:913-917.

Ruddiman, W.F., and J.E. Kutzbach. 1989. Forcing of late Cenozoic Northern Hemisphere climate by plateau uplift in southern Asia and the American west. *Journal of Geophysical Research* 94:18,409-18,427.

Ruddiman, W.F., and J.E. Kutzbach. 1990. Late Cenozoic plateau uplift and climate change. *Transactions of the Royal Society of Edinburgh: Earth Sciences* 81:301-314.

Self, S., and A.J. King. 1993. The 1963 eruption of Gunung Agung and its atmospheric impact. *EOS, 1993 Fall Meeting Supplement,* 105-106.

Self, S., M.R. Rampino, J.J. Barbera. 1981. The possible effect of large 19th and 20th century volcanic eruptions on zonal and hemispheric surface temperatures. *Journal of Volcanology and Geothermal Research* 11:41-60.

Shabbar, A., 1993. Explosive volcanoes ENSOs and the Canadian climate. *EOS, 1993 Fall Meeting Supplement,* 105.

Stewart, R.J. 1975. Late Cainozoic explosive eruptions in the Aleutian and Kuril Island Arcs. *Nature* 258:505-507.

Stommel, H., and E. Stommel. 1983. *Volcano Weather: The Story of 1816, the Year Without a Summer.* Seven Seas Press, Newport, RI.

Stothers, R.B., M.R. Rampino, S. Self, J.A. Wolf. 1989. Volcanic winter? Climatic effects of the largest volcanic eruptions. Pages 3-9 in *Volcanic Hazards.* J.H. Latter, editor. Springer Verlag, Berlin.

Vupputuri, R.K.R. 1992. The Tambora eruption in 1815 provides a test on possible global and chemical perturbations in the past. *Natural Hazards* 5:1-16.

An Overview of Decadal to Century Time-Scale Variability in the Climate System

Thomas F. Stocker

ABSTRACT: Time scales extracted from high-resolution proxy records and observations indicate that the spectrum of climate variability exhibits significant power in the range of decades to centuries superimposed on a red-noise continuum. The classical view of climate variability is based on the concept that observed fluctuations have their origin in periodic forcings on the same time scale. The present sensitivity of the climate system, however, would require strong positive feedback mechanisms to translate the weak forcing signals (such as the variability of solar irradiation) into detectable fluctuations in observed proxy variables. Instead, it is proposed that these fluctuations are linked to interactions within and between the different climate system components. Due to the time scales of interest, these are mainly the ocean and atmosphere. An overview of recent modeling results and the discussion of mechanisms involved show that such interactions internal to the climate system cannot only exhibit the correct time scales but also easily account for the amplitudes observed.

Introduction

Variability is a fundamental property of our climate system. Almost two decades ago, Mitchell (1976) proposed a theoretical framework of climate variability based on a schematic spectrum of climate variations spanning time scales from one hour to the age of the Earth. He distinguishes two types of processes in the climate system: internal stochastic mechanisms and external forcing mechanisms including their resonant amplification of internal modes. The spectrum (Figure 1) thus consists of a series of spectral peaks superimposed on a background continuum. The latter is the consequence of the stochastic aspect of the climate system for which a first-order autoregressive process is a good conceptual model. This red-noise background of the spectrum (*ie,* longer time scales exhibit stronger spectral power) can be seen in observed data from the atmosphere and in ocean and model simulations (Delworth *et al* 1993). Of more interest, due to their predictive potential, are the external mechanisms that produce variability on distinct time scales such as the diurnal and seasonal cycles, the Milankovic cycles, and even slower, tectonic processes.

While this concept is a useful starting point, several important aspects of climate variability are missing. They have been discussed earlier (Bjerknes 1964) but have recently gained attention again. Within each climate system component non-linear processes are operating, and interactions between them are often non-linear too. Therefore, processes in addition to those mentioned above can generate variability. First, *self-sustained oscillations* are due to constant external forcing but owe their characteristic time scale to feedback mechanisms internal to the system.

In: C.M. Isaacs and V.L. Tharp, Editors. 1995. *Proceedings of the Eleventh Annual Pacific Climate (PACLIM) Workshop, April 19-22, 1994.* Interagency Ecological Program, Technical Report 40. California Department of Water Resources.

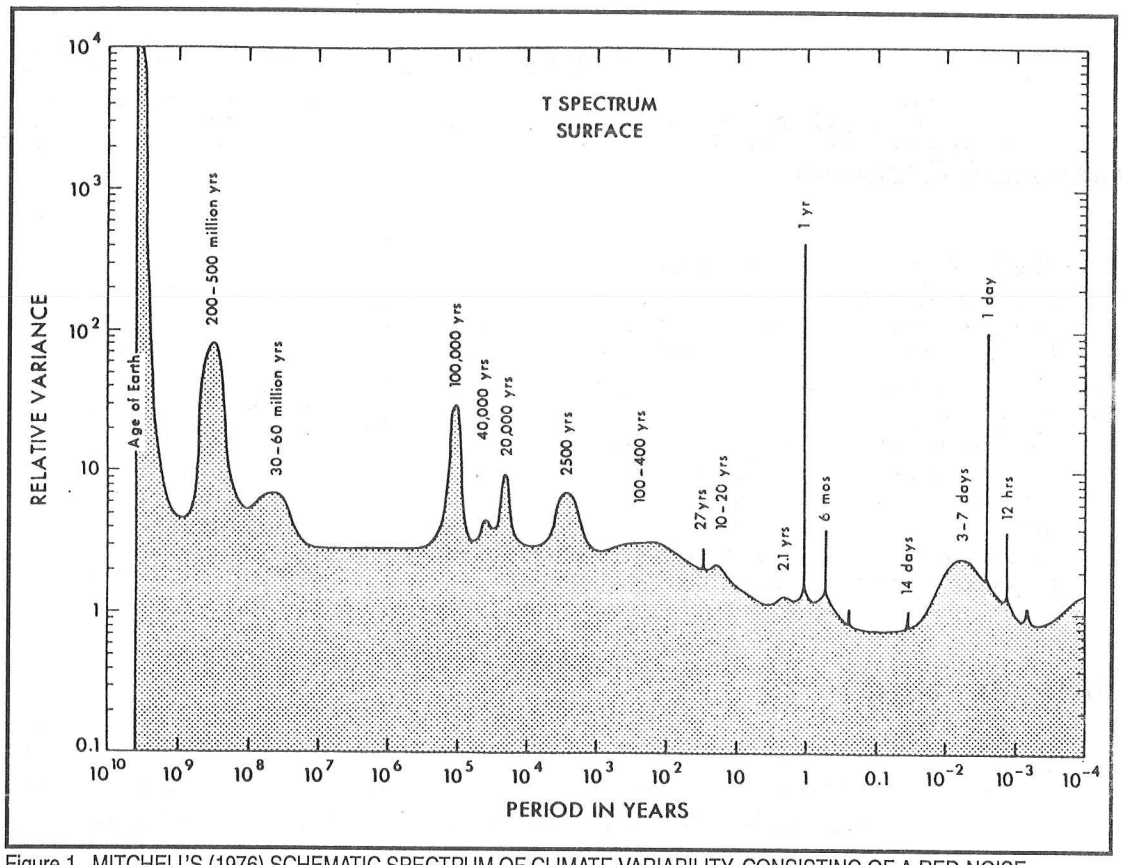

Figure 1. MITCHELL'S (1976) SCHEMATIC SPECTRUM OF CLIMATE VARIABILITY, CONSISTING OF A RED-NOISE BACKGROUND DUE TO STOCHASTIC FLUCTUATIONS AND DISTINCT PEAKS THAT ARE DUE TO VARIOUS EXTERNAL FORCINGS.
Note that no peaks are in the El Niño and decadal to century band.
Source: Peixoto and Oort (1992).

Second, external forcing can generate *modal changes* of the system, *ie*, switches from one equilibrium state to another on a time scale determined by internal mechanisms.

The purpose of this paper is to give an overview of recent results that indicate the importance of these processes on time scales of decades to centuries. Apart from a general interest, this time scale is of particular importance because detection of anthropogenic climate change depends on our knowledge of the time scales and patterns associated with the natural level of variability on the decadal to century time scale. A second purpose is to summarize those mechanisms of interdecadal variability that are quantitatively capable of causing detectable fluctuations. It is not sufficient to find periodic processes in some forcing variables and then postulate enhancing feedback mechanisms. Examples are the various solar cycles such as the sunspot (10-11 years), Hale (22 years), and Gleissberg (84 years) cycles that would require significant positive feedback mechanisms because of the small sensitivity of the climate system to changes in short-wave irradiation (order $0.05\ K/(Wm^{-2})$ instead of $0.5\ K/(Wm^{-2})$ for long-wave radiation).

Direct Observations

Direct observations begin to exhibit large-scale changes in the climate system on the decadal time scale. From the comparison of systematic temperature and salinity measurements of the last 40 years, a distinct warming in depths between 700 and 3000 meters could be identified in the North Atlantic (Roemmich and Wunsch 1984; Levitus 1989). Moreover, Parrilla *et al* (1994) find, superimposed on this warming, zonally alternating regions of cooling at 24°N and attribute this to large-scale decadal variability in the North Atlantic. Distinct spatial patterns of interdecadal variability are also found in North Atlantic sea surface temperatures, and they are linked to pools of anomalously cold or warm water (Kushnir 1994). There is also evidence of long-term variability and even steplike changes in the marginal seas of the Atlantic. Schlosser *et al* (1991) found a significant reduction of ventilation of the deep water in the Greenland Sea on the basis of tracers, while Lazier (1994) shows a notable decrease in salinity in the Labrador Sea.

Interdecadal changes could also be extracted from global data sets of surface air temperatures (Schlesinger and Ramankutty 1994). They found a 70-year cycle in this parameter in various sub-regions of the globe with the largest amplitudes in the North Atlantic and North American regions. Similar decadal-to-century cycles at 24 and 100 years have been found in the longest instrumental temperature record covering 318 years (Stocker and Mysak 1992). They are statistically significant at the 99% level.

Proxy Data

A review of long-term cyclic fluctuations on the century time scale is given in Stocker and Mysak (1992). Cycles of 50 years and longer are abundant in high-resolution proxy records (Figure 2), but rather than a single time scale, a whole range is present. Stuiver (1980) tested the hypothesis whether such cycles found in proxy data could be due to solar variability for which ^{14}C from tree rings was used as a proxy. A statistically significant relationship could not be established.

Briffa *et al* (1992) spectrally analyzed their 1480-year-long tree ring record of Fennoscandia, from which summer temperatures are reconstructed. They found significant power in the band of 30-40 years. The periods are not stable in that they vary by several years depending on the sub-interval considered. This suggests that an internal mechanism may be responsible for these cycles, rather than external forcing on a constant time scale.

It appears from this, that the North Atlantic region is one of the pacemakers of climate variability. However, one should note that only few proxy data come from regions other than Europe or North America, and, therefore, our view may well be biased. This is where models can

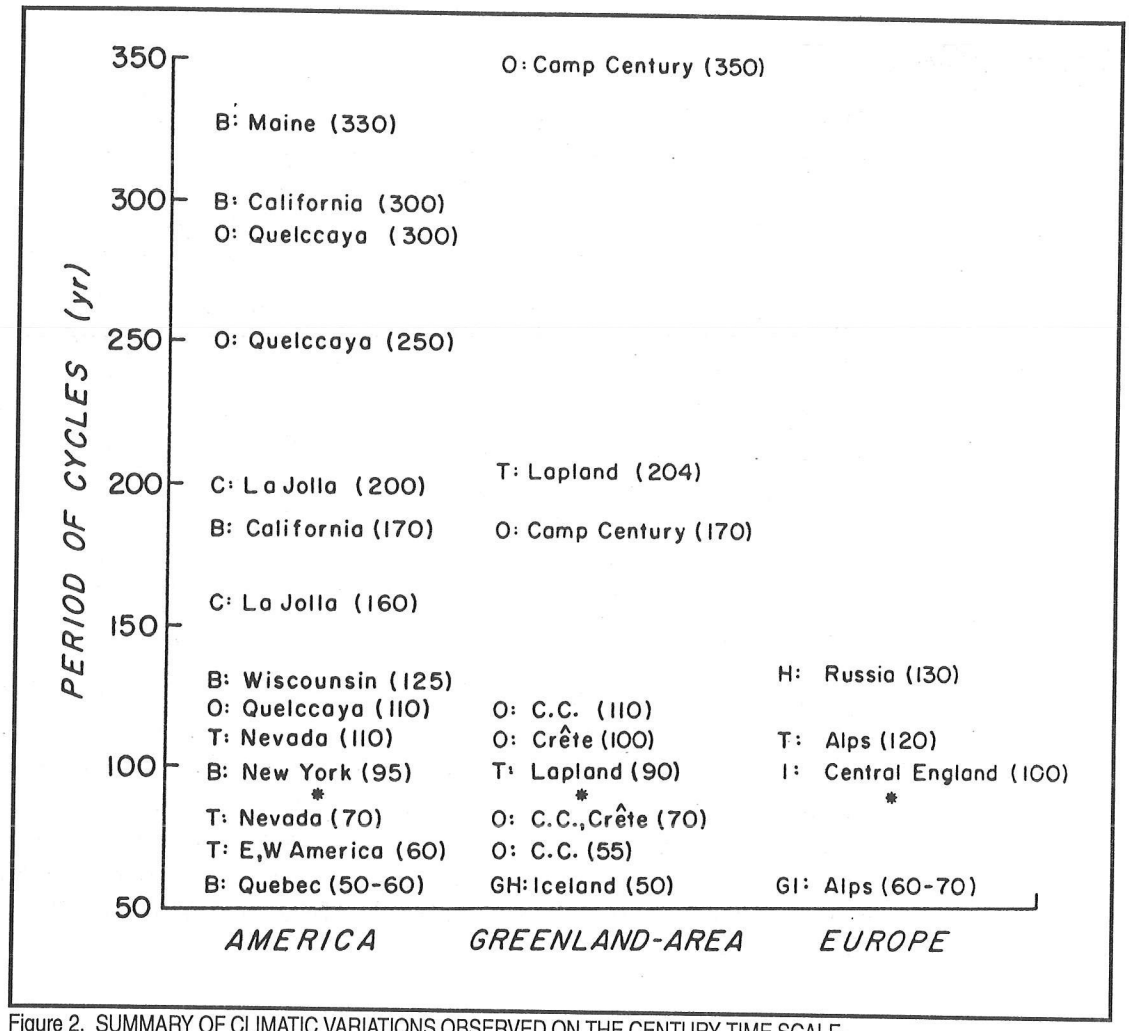

Figure 2. SUMMARY OF CLIMATIC VARIATIONS OBSERVED ON THE CENTURY TIME SCALE.
Findings are spatially and temporally ordered. Capital letters denote evidence in biological (B), radio carbon (C), glaciological (G), historical (H), instrumental (I), oxygen isotope and other ice core parameters (O), and tree ring records (T). The observed cycle period is given in brackets. C.C. denotes the Camp Century $\delta^{18}O$ record, and * indicates the 83-year cycle in marine air and sea surface temperatures of Folland *et al* (1984).
Source: Stocker and Mysak (1992).

provide valuable results in that they may point to mechanisms and locations of variability that have not yet been recorded by suitable proxy data.

Models and Mechanisms

The weakness of the hypothesis of a solar origin of decadal-to-century variability lies in the fact that sensitivity of the climate system to changes in short-wave irradiance is about an order of magnitude smaller than that of the long-wave emission. By monitoring the most recent solar cycle, it was found that solar irradiance changes due to a solar cycle have an amplitude of less than 2 Wm^{-2} (ERBE 1990), which would yield an amplitude of about 0.1 K using the above sensitivity. It is, therefore, important to look for possible alternative explanations and mechanisms of climate variability.

Climate modeling has become an important branch of climate research because only with physically-based models is it possible to *quantitatively* test and verify hypotheses on climate change. Over the last few decades, ocean, atmosphere, and coupled models have achieved sufficient capability of representing the large-scale fields simulated by the model and are in fair agreement with the observations. The next step, then, is to assess these models' capability of simulating natural variability.

Oceanic circulation models have made significant progress by implementing mixed boundary conditions. Sea surface temperature anomalies locally generate heat flux anomalies that operate to remove the SST anomalies within a few weeks. Sea surface salinity anomalies, on the other hand, do not generate local freshwater flux anomalies that could remove sea surface salinity anomalies. They can, therefore, have a longer-lasting impact on the surface buoyancy distribution. Mixed boundary conditions include this important difference between the feedback character of ocean-to-atmosphere heat and freshwater fluxes. The basic mechanism can be understood by a circular convection loop explained by Welander (1986), showing that self-sustained oscillations and different equilibrium states are a consequence of these mixed boundary conditions. However, one should note that ocean models run under these surface conditions often tend to overestimate the sensitivity of models to perturbations of the surface buoyancy balance. This is why other, modified formulations of atmosphere-to-ocean fluxes for ocean models have recently been proposed (Rahmstorf and Willebrand 1995).

Table 1 gives a summary of internal variability found in a number of ocean, atmosphere, and coupled models. The list is not complete, and we focus only on the most robust cycles in these models. The decadal-to-century time scale does, in most cases, include the ocean circulation, in

Table 1
INTERNAL VARIABILITY FOUND IN VARIOUS NUMERICAL MODELS

Ordered according to the time scale.

Model	Period (Years)	Mechanism	Author
3d box OGCM	9	Advection of SSS anomaly, interaction gyre-thermohaline	Weaver and Sarachik (1991)
3d North Atlantic OGCM	20	Labrador Sea, zonal and meridional overturning	Weaver *et al* (1994)
3d, global OGCM	10-40	Labrador Sea, stochastic integrator	Weisse *et al* (1994)
3d global AGCM	5-40	Chaotic nature, subtropical and mid-latitude atmospheric jets	James and James (1992)
3d global A/OGCM	10-20	Advection of T anomalies in the Pacific	Von Storch (1994)
3d global A/OGCM	40-60	West Atlantic gyre anomaly	Delworth *et al* (1993)
2d zonally-averaged OCM	200-300	Large-scale SSS advection	Mysak *et al* (1993)
3d global OGCM	320	Large-scale SSS advection in the Atlantic	Mikolajewicz and Maier-Reimer (1990)
3d box OGCM	400	Interaction between convection and diffusion	Winton (1993)

particular the thermohaline component. Mechanisms are connected with the wind-driven circulation, as well as with the hydrological cycle. Note that long-term variability is also found in atmospheric GCMs, suggesting interesting possibilities of interaction between the atmosphere and the ocean also on decadal time scales.

Gyre-Thermohaline Circulation

Weaver and Sarachik (1991) report self-sustained oscillations in a hemispheric 3-dimensional OGCM under mixed boundary conditions. Formed in the western boundary current, warm and saline anomalies travel eastward and are picked up by the sub-polar gyre, which transports them into the region of deep water formation; this journey takes about 8 to 9 years. There, they influence the basin-scale overturning and so feed back to the surface advection of these anomalies. The role of the structure of the freshwater forcing was also studied with the same model (Weaver *et al* 1993). When precipitation in high latitude cases is increased, internal variability on the decadal (as before) and the interdecadal (15-20 years) time scales is generated. For sufficiently strong forcing sequences of violent overturning and weak deep water formation could be excited. As these are connected to diffusive processes in the ocean interior during the time of reduced ventilation, time scales are on the order of 500 years and are decreasing with increasing amplitude of the stochastic forcing.

Similar oscillations were found by Winton (1993) using a frictional-geostrophic model. Important in these models is the fact that anomalies are advected by the gyre circulation near the surface, which determines the decadal time scale. These oscillations affect the entire water column in the high latitudes by turning on and off deep water formation, and the amplitude of the changes of the meridional heat flux are on the order of 0.2 ± 10^{15} *W*. While these models allow us to isolate and investigate various mechanisms of internal variability, immediate application to the real world is limited because of the simple geometry, surface boundary conditions, and coarse resolution.

SST Anomalies in the Northwest Atlantic

Coupled climate models are also beginning to exhibit natural variability. Delworth *et al* (1993) integrate the GFDL climate model for 600 years and find natural variability whose spectral properties are remarkably similar to observations (Figure 3). Superimposed on a red-noise spectrum, a number of spectral peaks are visible. Interdecadal oscillations of 40-60 years are evident in the maximum meridional overturning in the North Atlantic, reaching amplitudes of about 2 Sv (Figure 4). When thermohaline circulation is weak, decreased advection of lower-latitude warm and saline water into the central regions of the North Atlantic generates a pool of anomalously cold and fresh water. The thermal anomaly dominates and, hence, generates a geostrophically controlled cyclonic circulation at the surface. The western half of this anomalous circulation

enhances the mean northward flow of warm and saline waters in the center of the Atlantic, which are part of the large-scale conveyer belt circulation. The strengthened conveyer then carries more saline and warm low-latitude waters into the region and eventually creates an anomalous warm pool with its associated anti-cyclonic circulation. The latter weakens the mean flow again, and the cycle is closed.

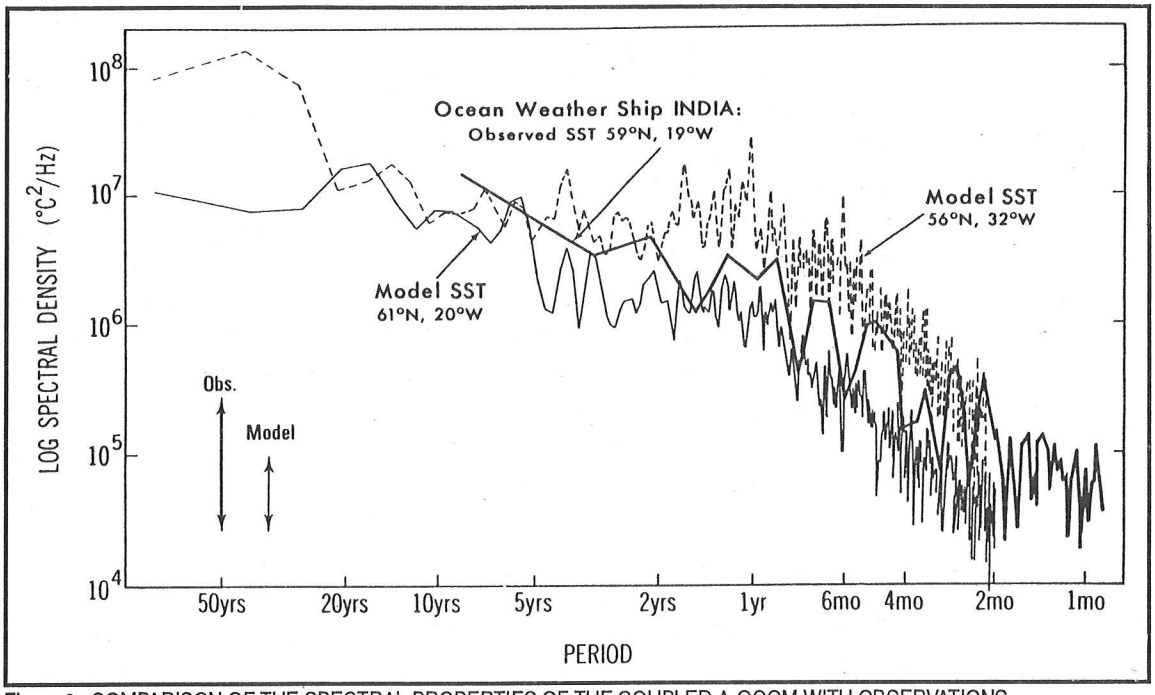

Figure 3. COMPARISON OF THE SPECTRAL PROPERTIES OF THE COUPLED A-OGCM WITH OBSERVATIONS
Source: Delworth *et al* (1993).

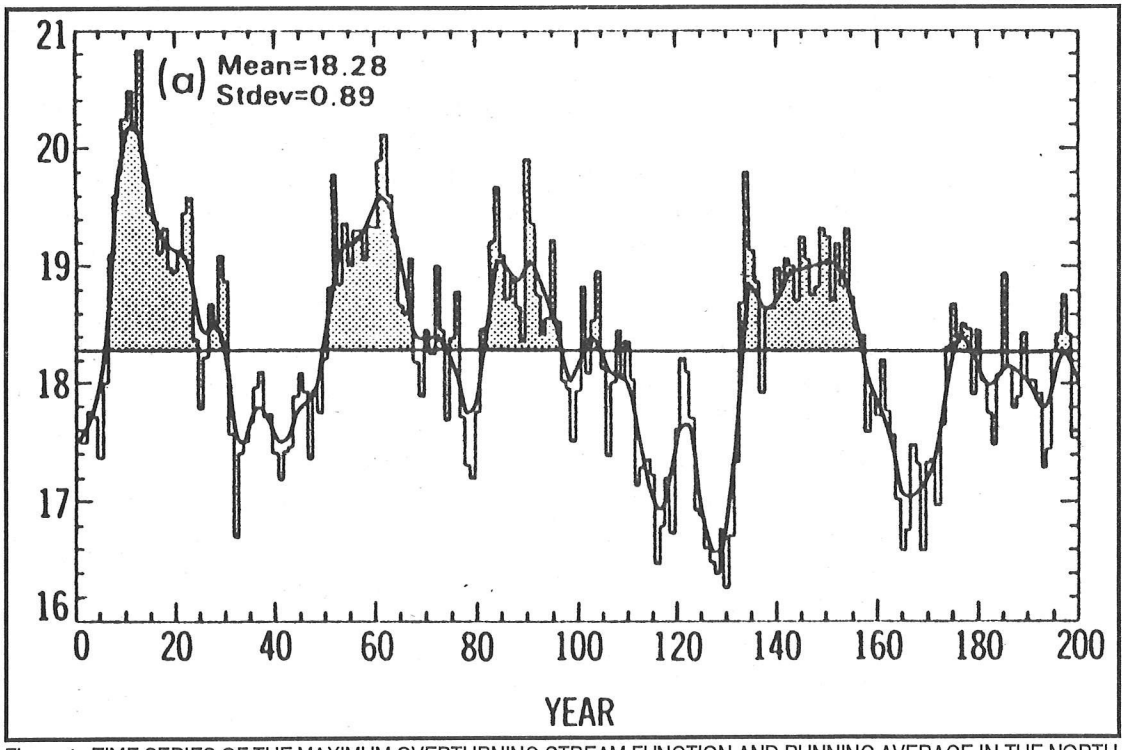

Figure 4. TIME SERIES OF THE MAXIMUM OVERTURNING STREAM FUNCTION AND RUNNING AVERAGE IN THE NORTH ATLANTIC FOR THE FIRST 200 YEARS OF THE 600-YEAR INTEGRATION OF A COUPLED A-OGCM
Source: Delworth *et al* (1993).

The oscillation is distinctly irregular, a common feature of nonlinear dynamical systems. Although the first 200 years of the integration show a quasi-periodic cycle of 40-50 years, the periods are longer in the following 400 years. It seems that some preconditioning of the ocean at a particular location is required and that the fluctuation itself may remove or add to it. It is intriguing that a similar instability of interdecadal cycles was found in the proxy records (Briffa *et al* 1992).

There are still limitations of such models. To achieve a stable climate consistent with the observations, spatially-dependent flux corrections have to be applied. Although these corrections do not impose a time scale on the model, they act as an additional forcing, which in a nonlinear system could generate additional variability. Also, the region where the oscillation is observed (northwest Atlantic) is one of the areas of large flux correction (Manabe and Stouffer 1988). On the other hand, the model does suggest a deterministic mechanism with time scales and amplitudes similar to those of proxy records and also indicates the focal regions of oscillatory activity. Moreover, the spatial patterns and depth structures of temperature and salinity in the ocean and sea level pressure can be directly compared to observations.

Marginal Seas

Recent modeling results indicate that marginal seas are potentially important pacemakers for self-sustained variability of the ocean circulation. Weaver *et al* (1994) found oscillations of about 20 years in the Labrador Sea of their model. The mechanism is linked to an interaction between the meridional (and zonal) pressure gradients and the geostrophically controlled zonal (and meridional) overturning in the Labrador Sea. In contrast to the mechanism discussed in the previous section, this variability is dependent on neither the surface freshwater budget nor on the wind-driven gyral circulation. While the resolution of this model in the most important area is very low (only 3 tracer grid points), it is encouraging to note that SST anomalies are very similar to those reported by Kushnir (1994) based on observations.

A complementary study with a global model was done by Weisse *et al* (1994). A stochastic freshwater flux perturbation excites century- (320 years) and decadal-scale oscillations. The latter are localized in the Labrador Sea area and have periods in the range of 10-40 years, but the mechanism is distinctly different from that above. The relatively isolated marginal sea integrates the stochastic freshwater flux perturbations and sends salinity anomalies into the North Atlantic on a time scale of about 10-40 years. This time scale is determined by the flushing time of the upper 250 meters of the basin, since the stratification is quite stable. Once the perturbations arrive in the North Atlantic, where the stratification between 50°N and 60°N is weak, they strongly influence the deep water formation rates and create the observed variability.

It is apparent that these two mechanisms are distinctly different. In the first study, the Labrador Sea itself generates the variability by changing rates of local deep water formation; in the other case, the same region merely appears as a storage of perturbations that act outside the basin. An increased resolution and, with it, a better representation of the water masses in the Labrador Sea will increase our understanding of its role in controlling the natural variability in the North Atlantic region.

Basin-Scale Thermohaline Circulation

Basin-scale variations of the Atlantic meridional overturning and, hence, meridional heat flux have time scales of typically 200 to 300 years. The Hamburg global OGCM was run under mixed boundary conditions including a stochastic freshwater flux perturbation. Large fluctuations with a time scale of 320 years are found in the mass transport through Drake Passage and the meridional heat flux and overturning in the North Atlantic. Amplitudes would be large enough to be detected in paleoclimatic archives. The heat budget in the Southern Ocean shows peak-to-peak amplitudes of up to 3 ± 10^{15} *W*; these are not regular cycles but, rather, appear as events. The mechanism of these successions of events is associated with the long residence time of sea surface salinity anomalies. The random flux perturbations create local salinity anomalies that are advected northward by the near-surface circulation in the Atlantic. Depending on the spatial structure of the freshwater fluxes, they are enhanced or removed before they reach the deep water formation area in the high-latitude Atlantic. If they are enhanced, they accelerate meridional overturning and so decrease the exposure time of subsequent sea surface salinity anomalies. Anomalies can be traced along the entire path of overturning.

Mysak *et al* (1993) used a zonally-averaged one-basin ocean circulation model and found oscillations with time scales between 200 and 300 years over a wide range of parameters (Figures 5 and 6). In contrast to the previous model, salinity anomalies could not be traced around a complete loop of the circulation but became well mixed once in the deep ocean. This indicates that these cycles are primarily due to an interaction between the detailed spatial structure of the surface freshwater flux and the strength of the thermohaline overturning that determines the preferred time scale.

Other Mechanisms

In the previous section, mainly oceanic processes related to the Atlantic have been discussed. However, there are also recent model results of interdecadal cycles in the Pacific and in the atmosphere alone. In their atmospheric circulation model, James and James (1992) found variability on time scales of 10 to 40 years and associated them with changes in the structure of the subtropical and mid-latitude jets.

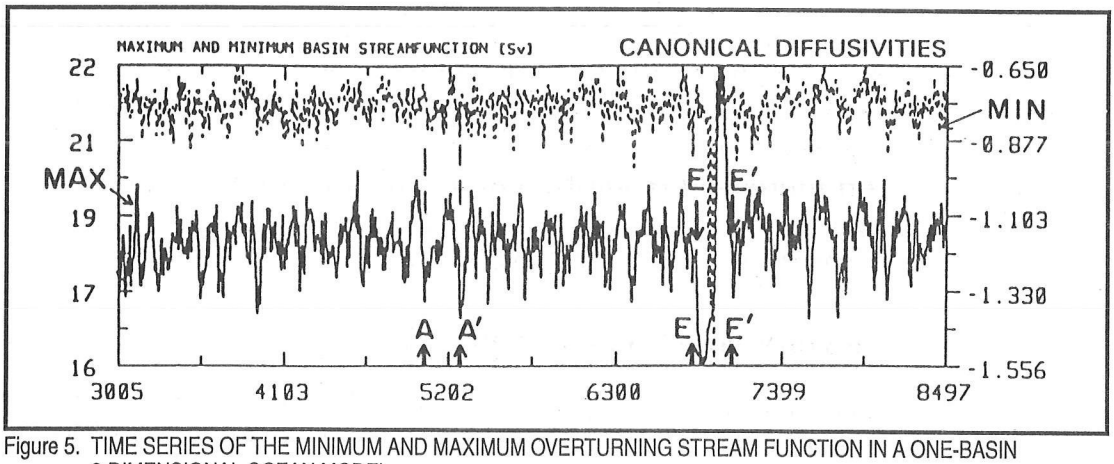

Figure 5. TIME SERIES OF THE MINIMUM AND MAXIMUM OVERTURNING STREAM FUNCTION IN A ONE-BASIN 2-DIMENSIONAL OCEAN MODEL
Source: Mysak *et al* (1993).

Von Storch (1994), on the other hand, uses a coupled A/OGCM and identifies two types of low-frequency variability. The atmospheric fluctuations are essentially red noise, and there appears to be an out-of-phase relationship between the stratosphere and the troposphere. In the ocean, there is an irregular cycle of about 17 years located in the Pacific Ocean. In contrast to ocean models and most models in Table 1, no distinct variability is found in the Atlantic Basin.

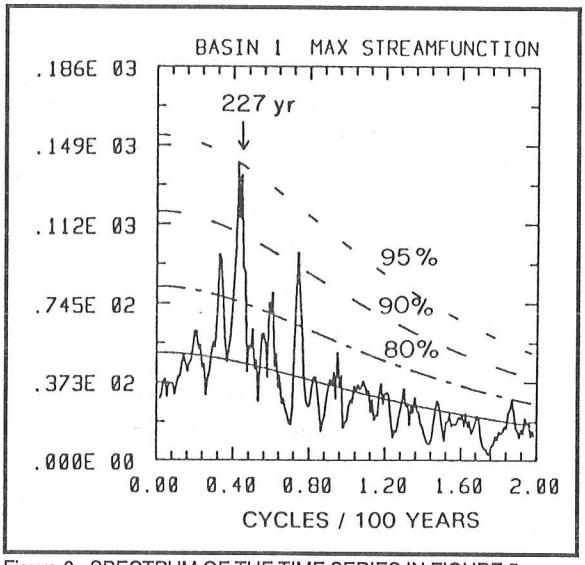

Figure 6. SPECTRUM OF THE TIME SERIES IN FIGURE 5. Significant power is found on the century time scale.
Source: Mysak *et al* (1993).

Conclusions

The study and quantitative understanding of internal variability in the climate system is only at its beginning. Focal regions where internal variability is enhanced or generated have been identified and preliminary results have shed light on a palette of mechanisms. However, we are still at the stage where each model produces its characteristic fluctuations with the associated time scales. Important results have been found as to the role of the ocean, the influence of atmosphere/ocean exchange fluxes, and the dynamics in marginal seas, but a consistent quantitative theory on climatic cycles is still missing. Further work is urgently needed. We need to improve formulation of surface exchange processes (boundary conditions), especially in the ocean-only models, and the resolution must be increased to better represent marginal but important regions of the ocean basins.

References

Bjerknes, J. 1964. Atlantic air-sea interaction. *Adv. Geophys.* 10:1-82.

Briffa, K.R., and seven others. 1992. Fennoscandian summers from AD 500: Temperature changes on short and long timescales. *Clim. Dyn.*, 7:111-119.

Delworth, T., S. Manabe, R.J. Stouffer. 1993. Interdecadal variations of the thermohaline circulation in a coupled ocean-atmosphere model. *J. Climate* 6:1993-2011.

ERBE. 1990. Earth Radiation Budget Experiment, *EOS* 71:297—305.

Folland, C.K., D.E. Parker, F.E. Kates. 1984. Worldwide marine temperature fluctuations 1856-1981. *Nature* 310:670-673.

James, I.N., and P.M. James. 1992. Spatial structure of ultra-low frequency variability of the flow in a simple atmospheric circulation model. *Q. J. Roy. Met. Soc.* 118:1211-1233.

Kushnir, J. 1994. Interdecadal variations in North Atlantic sea surface temperature and associated atmospheric conditions. *J. Climate* 7:141-157.

Lazier, J.R.N. (in press, 1994). The salinity decrease in the Labrador Sea over the past thirty years. In *Natural Climate Variability on Decade-to Century Time Scales.* National Research Council.

Levitus, S. 1989. Interpentadal variability of temperature and salinity in the deep North Atlantic, 1970-1974 versus 1955-1959. *J. Geophys. Res.* 94:16125-16131.

Manabe, S., and R.J. Stouffer. 1988. Two stable equilibria of a coupled ocean-atmosphere model. *J. Climate* 1:841-866.

Mikolajewicz, U., and E. Maier-Reimer. 1990. Internal secular variability in an ocean general circulation model. *Clim. Dyn.* 2:63-90.

Mitchell, J.M. 1976. An overview of climatic variability and its causal mechanisms. *Quat. Res.* 6:481-493.

Mysak, L.A., T.F. Stocker, F. Huang. 1993. Century-scale variability in a randomly forced, two-dimensional thermohaline ocean circulation model. *Clim. Dyn.* 8:103-116.

Parrilla, G., A. Lavin, H. Bryden, M. Garcia, R. Millard. 1994. Rising temperatures in the subtropical North Atlantic Ocean over the past 35 years. *Nature* 369:48-51.

Peixoto, J.P., and A.H. Oort. *Physics of Climate.* American Institute of Physics. 520 pp.

Rahmstorf, S., and J. Willebrand. 1995. The role of temperature feedback in stabilizing the thermohaline circulation. *J Phys Oceanogr.* In press.

Roemmich, D., and C. Wunsch. 1984. Apparent changes in the climatic state of the deep North Atlantic. *Nature* 307:447-450.

Schlesinger, M.E., and N. Ramankutty. 1994. An oscillation in the global climate system of period 65-70 years. *Nature* 367:723-726.

Schlosser, P., G. Bönisch, M. Rhein, R. Bayer. 1991. Reduction of deepwater formation in the Greenland Sea during the 1980s: Evidence from tracer data. *Science* 251:1054-1056.

Stocker, T.F. 1994. The variable ocean. *Nature* 367:221-222.

Stocker, T.F., and L.A. Mysak. 1992. Climatic fluctuations on the century time scale: A review of high-resolution proxy data and possible mechanisms. *Clim. Change* 20:227-250.

Stuiver, M. 1980. Solar variability and climatic change during the current millennium. *Nature* 286:868-871.

Von Storch, J. 1994. Interdecadal variability in a global coupled model. *Tellus* 46A:419-432.

Weaver, A.J., and E.S. Sarachik. 1991. Evidence for decadal variability in an ocean general circulation model: An advective mechanism. *Atm.-Ocean* 29:197-231.

Weaver, A.J., J. Marotzke, P.F. Cummins, E.S. Sarachik. 1993. Stability and variability of the thermohaline circulation. *J. Phys. Oceanogr.* 23:39-60.

Weaver, A.J., S.M. Aura, P.G. Myers. 1994. Interdecadal variability in an idealized model of the North Atlantic. *J. Geophys. Res.* 99:12423-12441.

Weisse, R., U. Mikolajewicz, E. Maier-Reimer. 1994. Decadal variability of the North Atlantic in an ocean general circulation model. *J. Geophys. Res.* 99:12411-12421.

Welander, P. 1986. Thermohaline effects in the ocean circulation and related simple models. Pages 163-200 in *Large-Scale Transport Processes in Oceans and Atmosphere.* J. Willebrand and D.L.T. Anderson (editors). NATO ASI, C190.

Winton, M. 1993. Deep decoupling oscillation of the oceanic thermohaline circulation. Pages 417-432 in *Ice in the Climate System. W.R. Peltier (editor). NATO ASI I 12.*

Determining the Role of Linear and Nonlinear Interactions in Records of Climate Change: Possible Solar Influences in Annual to Century-Scale Records

Terri King Hagelberg and Julia Cole

Abstract: Time series analysis methods have traditionally helped in identifying the role of various forcing mechanisms in influencing climate change. A challenge to understanding decadal and century-scale climate change has been that the linkages between climate changes and potential forcing mechanisms such as solar variability are often uncertain. However, most studies have focused on the role of climate forcing and climate response within a strictly linear framework. Nonlinear time series analysis procedures provide the opportunity to analyze the role of climate forcing and climate responses between different time scales of climate change. An example is provided by the possible nonlinear response of paleo-ENSO-scale climate changes as identified from coral records to forcing by the solar cycle at longer time scales.

Introduction

Taking a nonlinear time series approach to the study of annual to century-scale climate change allows one to objectively determine the extent of interactions between centennial, decadal, and interannual scales of climate change. In this study, such an approach is taken to identify the possible role of solar variations in forcing climate on interannual time scales. In particular, we focus on ENSO-scale climate variations and potential forcing mechanisms. Rather than focusing only on observations of linear statistical relationships between solar variability and climate, the objective is to determine whether there is now observational evidence for nonlinear interactions between solar variability at 11-year scales and climate variability at 6 years, which lies in the ENSO band.

A large number of studies have regarded ENSO dynamics as coupled oscillating systems. This has been well documented in reference to the phase locking of ENSO with the annual cycle and seasonal variability. With this in mind, it is not unusual to expect that in the ENSO band of climate change, interactions, or "teleconnections" between seasonal, annual, and interannual time scales are significant. It is just as conceivable that interactions between these time scales and longer time scales of climate change may be significant. Although it is unclear how ENSO's primary oscillations might translate into longer-term cycles, abundant evidence suggests that these longer-term cycles exist (Diaz and Markgraf 1992).

In: C.M. Isaacs and V.L. Tharp, Editors. 1995. *Proceedings of the Eleventh Annual Pacific Climate (PACLIM) Workshop, April 19-22, 1994.* Interagency Ecological Program, Technical Report 40. California Department of Water Resources.

If we can empirically determine from existing data that the relative amplitude of ENSO events systematically increases and/or decreases over time, then this raises the possibility that ENSO is modulated by some other process. This, in turn, implies a longer-term forcing mechanism. The possibility of a link between ENSO variability and solar variations has been raised many times over the years. However, conclusive data have been scant. The role of solar variations and ENSO in forcing long-term decadal-scale climate changes has been referred to as "long-term ENSO" changes by Anderson *et al* (1992), who suggested that long-term changes in the amplitude and frequency of ENSO over the scale of decades might be related to solar forcing and changes in mid-latitude tropospheric winds associated with changes in solar variability.

If ENSO teleconnections are to be confidently related to solar variability, two fundamental items must be in place. First, one must determine a quantitative association between solar/geomagnetic changes and ENSO. Second, to evaluate the role of potential forcing mechanisms, paleo-ENSO proxy records having annual resolution that can be compared to records of solar variability over many decades and even centuries are required. We deal with each of these points separately. Regarding the first item, there have been over 1000 referenced studies of solar variations and climate responses (McCormac 1982). However, most studies have focused on correlations and not mechanisms, inviting the criticism that if one searches long enough for a correlation, eventually one will occur by random chance (*eg*, Pittock 1978).

Of the whole of the solar variability/climate change literature, two basic categories of potential quantitative mechanisms arise whereby solar variability impacts climate. The first category can be termed "direct" hypotheses, whereby changes in solar luminosity and total irradiance changes due to solar dynamics are significant enough to affect climate. A recent example of this hypothesis was set forth by Nesme-Ribes *et al* (1993). The second category can be termed "indirect" hypotheses. These theories hold that geomagnetic disturbances associated with solar activity are sufficient to impact atmospheric UV flux, and that this flux affects stratospheric and tropospheric planetary waves. Thus, although the irradiance change is slight, changes in the UV band significantly affect stratospheric zonal and thermal winds, thus affecting tropospheric zonal winds and eventually climate on the earth's surface.

Data, Methods, and Results

The second item stated above that is required to relate ENSO changes to solar variations is adequate data series. paleo-ENSO proxy time series that are high enough resolution (subannual resolution) and yet long enough (at least 100 years) to determine linkages have only recently been available. Because such records are now available, we can focus on quantifying these relationships. There are several ways to represent solar variability, including such proxies as solar cycle length (Friis-Christensen

and Lassen 1991). In this study, we have used as a proxy for solar variations the annual sunspot record from 1700 A.D. to present. We make use of four ENSO proxy datasets, summarized below. The time series for each proxy is shown in Figure 1.

Data Sets Used in This Study

Type	Record Length	Citation
1. Solar Variability		
Annual Sunspot record	1700 – 1993	
2. ENSO		
Tropical Pacific sea surface temperature	1828 – 1977	Wright 1989
Tarawa Coral $\delta^{18}O$	1894 – 1989	Cole *et al* 1993
Urvina Bay Coral $\delta^{18}O$	1607 – 1981	Dunbar *et al* 1994
Tree Ring Index EOF1	1828 – 1965	NATRD

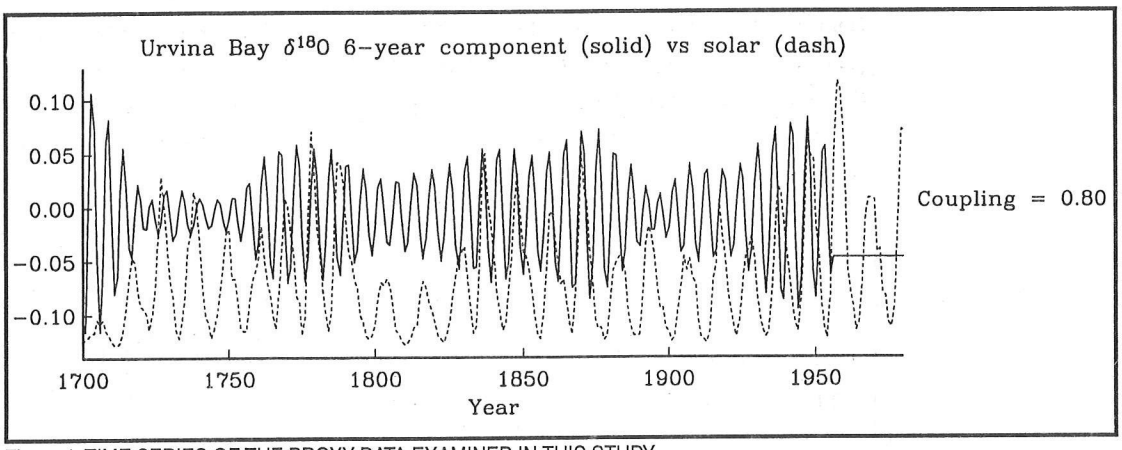

Figure 1. TIME SERIES OF THE PROXY DATA EXAMINED IN THIS STUDY.

The first ENSO proxy is an instrumental record of sea surface temperature from the central and eastern tropical Pacific (Wright 1989). The remainder of the ENSO indicators are geological proxy data. Coral $\delta^{18}O$ from Tarawa Atoll (Cole *et al* 1993) record the location and intensity of the Indonesian low. The $\delta^{18}O$ variations in the corals at this location are mainly driven by sea water salinity responses to precipitation, with high rainfall (ENSO) correlated with more depleted $\delta^{18}O$. Coral $\delta^{18}O$ from Urvina Bay, Galapagos (Dunbar *et al* 1994) primarily record sea surface temperature variations from that region, as deduced from the high correlation to instrumental sea surface temperature variations, and low salinity variations at that location. The index for tree-ring variations was computed as the first Principal Component (or EOF, Empirical Orthogonal Function) of North American Tree Ring Indices (data were provided by the NATR Database, Boulder, CO). All available site chronologies (611 total) from the United States/Canada and Central America (Mexico) were combined into a single dataset and gridded. After screening out chronologies with a low number of sites, a weighted time series calculated for each 100-by-100 kilometer grid box containing tree ring chronologies to obtain a composite chronology for each grid box. Principal Component Analysis (also called EOF analysis) was used to determine spatially and temporally coherent modes of variability. The first mode explained 26% of the

variance in the entire dataset. Loadings were concentrated mainly in the southwestern United States and Mexico. Judging from comparisons with other tree ring studies, this mode should mainly indicate precipitation.

Analyses of these proxy time series can be subdivided into linear and nonlinear analyses. The focus of this study is frequency domain relationships. The linear analyses can be summarized by spectral and cross spectral analyses. The frequency distribution of variance of the proxy time series is indicated by Figure 2. The ENSO signature is primarily recorded in the 310 year band, as noted in several (*eg*, Trenberth and Shea 1987; Barnett 1989; Rasmusson and Wallace 1983). The Wright sea surface temperature indices indicate a dominance in the 6-year band. The ENSO proxy time series show significant concentrations of variance in both the "ENSO band", from 3 to 7 years, as well as in the "solar band", from 11 to 22 years. This low-frequency component was documented in previous studies from corals (Cole *et al* 1993), which demonstrated an evolution in the low-frequency component. Similarly, Dunbar *et al* (1994) made the observation that the 11- and 22-year cycles are similar in amplitude to solar variations.

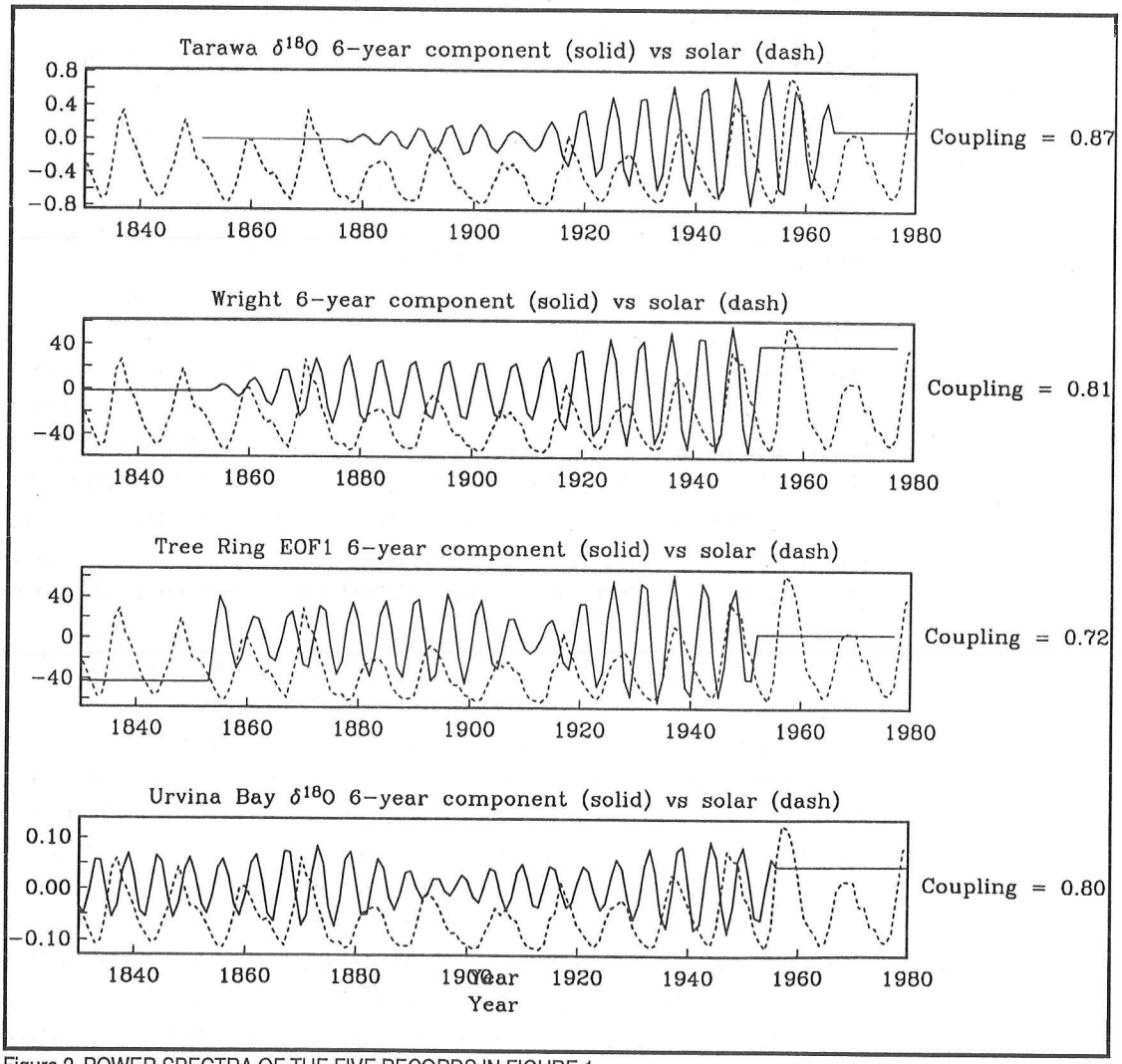

Figure 2. POWER SPECTRA OF THE FIVE RECORDS IN FIGURE 1, INDICATING SIGNIFICANT CONCENTRATIONS OF VARIANCE.

Coherences, or frequency domain cross-correlations, are summarized in Table 1 for the 11-year band and the 6-year band. Note the high correlation between ENSO indices in the 6-year band (because there is no power in the 6-year band for solar variations, the solar index was not used here). In the 11-year band, although correlations between the ENSO proxy data are significant, there is low coherence between solar variations and the proxy data with the exception of the Urvina coral $\delta^{18}O$, consistent with the observation made by Dunbar *et al* (1994).

Table 1
SUMMARY OF COHERENCE

Significant (0.90 level) coherences noted in boldface.

11-Year Band

	Solar	Wright SST	Tree Ring
Solar	1.0		
Wright SST	0.24	1.0	
Tree Rings	0.42	0.19	1.0
Tarawa $\delta^{18}O$	0.41	**0.85**	**0.65**
Urvina Bay $\delta^{18}O$	**0.74**	0.18	0.49

6-Year Band

	Wright SST	Tree Ring
Wright SST	1.0	**0.94**
Tarawa $\delta^{18}O$	**0.95**	**0.93**
Urvina Bay $\delta^{18}O$	**0.75**	0.61
Tree Rings	**0.94**	1.0

The nonlinear relationships between the ENSO proxy data and solar variations are examined using the methods of higher order spectra. Applications of bi-spectral and cross-bispectral analyses to paleoclimate series have been described previously by Hagelberg *et al* (1991, 1994). Briefly, the cross-bispectrum yields a quantity similar to coherence, cross-bicoherence, which is simply a third order correlation coefficient, calculated and normalized in the frequency domain. Just as coherence is a correlation coefficient between two time series, calculated and normalized in the frequency domain, cross-bicoherence is the third order correlation coefficient between two cycles in one time series and its harmonic in a second time series. In other words, we are examining the coupling between the 11-year cycle in the solar records and the 6-year cycle in the data (which is equal to the first harmonic).

Results of the cross-bispectral analysis are summarized in Table 2 for the 11-year (solar) / 6-year (proxy) nonlinear interactions. A strong coupling, or cross-bicoherence, indicates that the 6-year cycle in the proxy data is nonlinearly coupled to solar variations at 11 years. Indeed, the relationship is statistically significant (0.80 level) for each of the records. This result quantitatively supports the hypothesis that the relationship between solar variability and ENSO variations is not a fortuitous one, as a significant phase coupling persists over hundreds of years.

Table 2
SUMMARY OF
CROSS BICOHERENCE FOR THE
11-YEAR (SOLAR) / 6-YEAR (ENSO)
NONLINEAR COUPLING

	Solar (11-Year)
Tree Rings (6-year)	0.72
Wright SST (6-year)	0.81
Tarawa $\delta^{18}O$ (6-year)	0.87
Urvina Bay $\delta^{18}O$ (6-year)	0.80

It is convenient to display this phase coupling between 11-year solar variations and the harmonic 6-year variations in the time domain. This is done by comparing the bandpass filtered records. Figure 3 shows the 6-year component of the ENSO proxy records compared to the 11-year component of the solar record for 1840 to 1965 only. Although the time series are short, there is evidence for phase locking and the amplitudes of the cycles are relatively similar, with high-amplitude 6-year cycles corresponding to high-amplitude 11-year cycles. Before 1920, the amplitude patterns are ambiguous, however. This result is similar to previous results by Barnett (1989), in which the Quasi-Biennial Oscillation appeared modulated by the solar cycle but only since 1920. Only one paleo-ENSO dataset, the Urvina Bay $\delta^{18}O$, has a long enough record length to test the solar/ENSO relationship back to the 1700s. Figure 4 indicates that the amplitude relationship appears to hold up from 1750 to present, with high-amplitude 6-year cycles corresponding to high-amplitude solar variability. Thus, the relationship does appear to hold for time intervals other than the past 70 years.

Conclusions

Coupled oscillations in the ENSO system appear to exist on decadal scales as well as annual and biennial scales. These oscillations may be related to solar variations at 11-year time scales. Cross spectra and third order spectra are useful in quantifying the strength of this linear and nonlinear coupling. There is quantitative evidence for the response of the climate system in the ENSO band to solar forcing over the past several centuries. ENSO proxy records are significantly phase-coupled to changes in the 11-year solar cycle. Future work requires determining a physical linkage between the mechanisms whereby solar variability affects climate and the ENSO system.

References

Anderson, R.Y. 1992. Long-term changes in the frequency of occurrence of El Niño events. Pages 193-200 in *El Niño: Historical and Paleoclimatic Aspects of the Southern Oscillation.* H.F. Diaz and V. Markgraf, editors. Cambridge University Press, NY.

Barnett, T.P. 1989. A solar-ocean relation: fact or fiction? *Geophysical Research Letters* 16:03806.

Cole, J.E., R.G. Fairbanks, G.T. Shen. 1993. Recent variability in the Southern Oscillation: isotopic results from a Tarawa Atoll coral. *Science* 260: 669683.

Diaz, H.F., and V. Markgraf. 1992. *El Niño: Historical and Paleoclimatic Aspects of the Southern Oscillation.* Cambridge University Press, NY.

Dunbar, R.B., G.M. Wellington, M.W. Colgan, P.W. Glynn. 1994. Eastern Pacific sea surface temperature since 1600 A.D.: The $\delta^{18}O$ record of climate variability in Galapagos corals. *Paleoceanography.*

Friis-Christensen, E., and K. Lassen. 1991. Length of the solar cycle: An indicator of solar activity closely associated with climate. *Science* 254:698700.

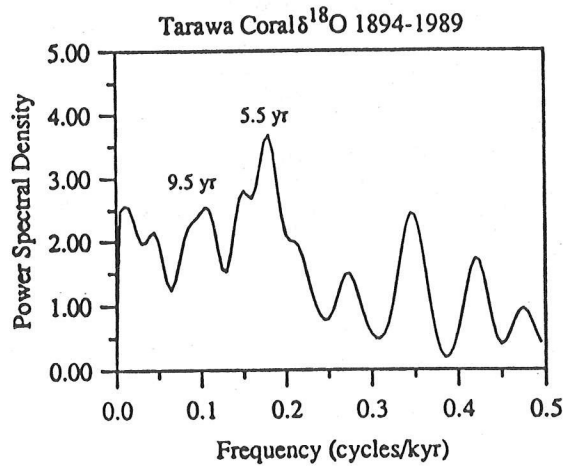

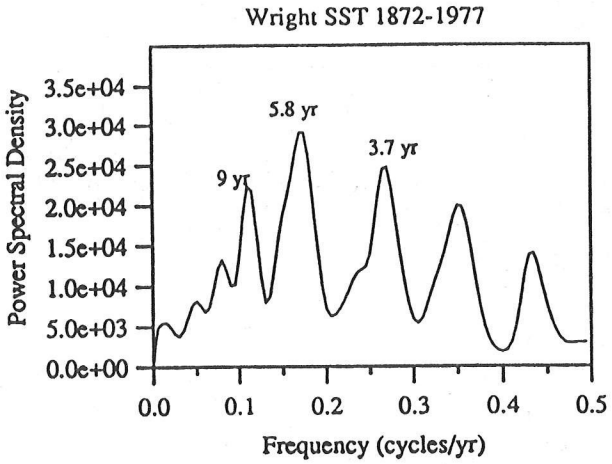

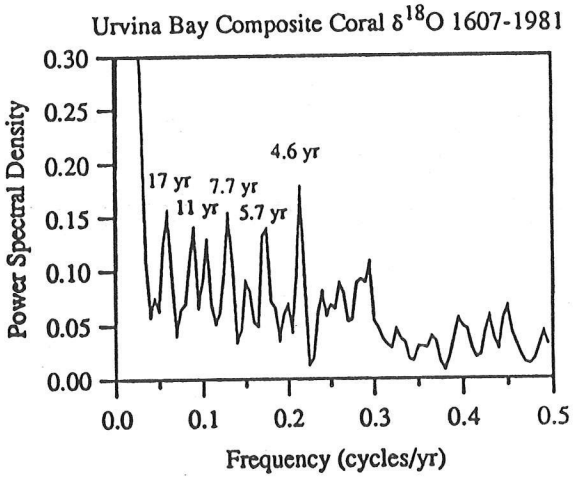

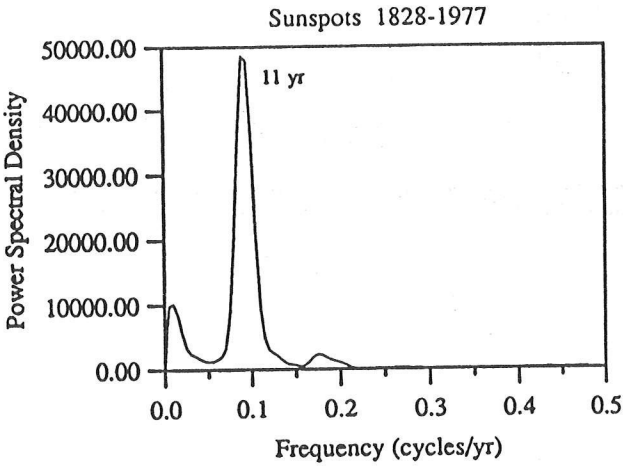

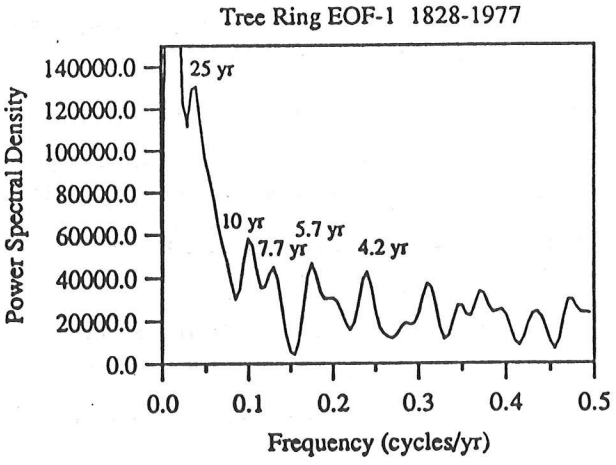

Figure 3. 6-YEAR COMPONENT OF THE ENSO PROXY RECORDS COMPARED TO THE 11-YEAR COMPONENT OF THE SOLAR RECORD FOR 1840 TO 1965 ONLY.

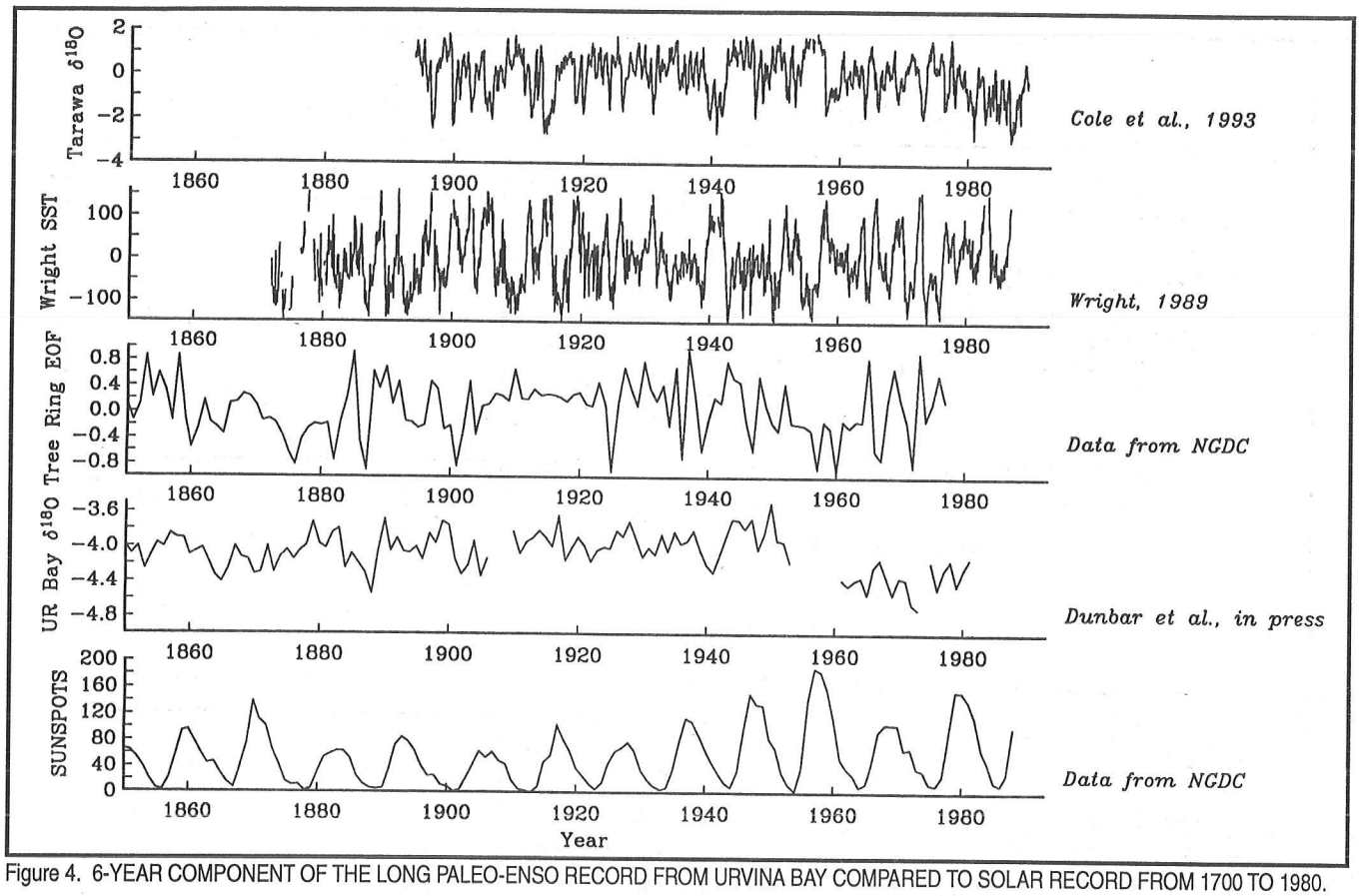

Figure 4. 6-YEAR COMPONENT OF THE LONG PALEO-ENSO RECORD FROM URVINA BAY COMPARED TO SOLAR RECORD FROM 1700 TO 1980.

Hagelberg, T.K., G. Bond, P. deMenocal. 1994. Milankovitch band forcing of sub-Milankovitch climate variability during the Pleistocene. *Paleoceanography* 9: 545558.

Hagelberg, T.K., N.G. Pisias, S. Elgar, 1991. Linear and nonlinear couplings between orbital forcing and the marine $\delta^{18}O$ record during the late Neogene. *Paleoceanography* 6:729746.

McCormac, B. 1982. *Weather and Climate Responses to Solar Variations.* Colorado Assoc. Univ. Press.

Nesme-Ribes, E., E.N. Ferreira, R. Sadourny, H. LeTreut, Z.X. Li. 1993. Solar dynamics and its impact on solar irradiance and the terrestrial climate. *Journal of Geophysical Research* 98:18,92318,935.

Pittock, A.B. 1978. A critical look at long term sun-weather relationships. *Reviews of Geophysics and Space Physics* 16:400420.

Rasmusson, E.M., and J.M. Wallace. 1983. Meteorological aspects of the El Niño/Southern Oscillation. *Science* 222: 11951202.

Trenberth, K.E., and D.J. Shea. 1987. On the evolution of the Southern Oscillation. *Monthly Weather Review* 115:30783096.

Wright, P.B. 1989. Homogenized long-period Southern Oscillation indices. *International Journal Climate* 9:3354.

Dynamical Structure in Paleoclimate Data

H. Bruce Stewart

ABSTRACT: Deterministic chaos in dynamical systems offers a new paradigm for understanding irregular fluctuations. The theory of chaotic dynamical systems includes methods that can test whether any given set of time series data, such as paleoclimate proxy data, are consistent with a deterministic interpretation. Paleoclimate data with annual resolution and absolute dating provide multiple channels of concurrent time series; these multiple time series can be treated as potential phase space coordinates to test whether interannual climate variability is deterministic. Dynamical structure tests which take advantage of such multichannel data are proposed and illustrated by application to a simple synthetic model of chaos, and to two paleoclimate proxy data series.

The Notion of Dynamical Structure

The emergence of the chaos paradigm of dynamical systems theory raises the possibility that some of the irregular oscillations observed in the natural world may be explainable as the workings of deterministic dynamics. Moreover, there is reason to hope that the deterministic rules governing the behavior of even large and complex natural systems may be expressed in terms of just a handful of active modes of oscillation, which can be fully described using a small number of state variables.

A deterministic dynamical system requires a state space or phase space whose coordinates are the state variables $x_1, x_2, \ldots, x_n$; these variables describe the state of the system at any instant of time, and the functions $x_1(t), x_2(t), \ldots, x_n(t)$ describe the system evolution over time. In addition, a dynamical system possesses a dynamical rule that specifies completely and unambiguously for each state $X=\{x_1, x_2, \ldots, x_n\}$ the immediate future trend of evolution; that is, the rule uses $X(t)$ at time t to determine X a short time interval into the future (Abraham and Shaw 1992; Thompson and Stewart 1986).

For many systems, there is a natural discrete unit of time, such as a day or a year. The evolution is described by a sequence of X_i with index i indicating time, that is, $X_i = X(t_i)$. The dynamical rule is then conveniently expressed as an iterated function:

$$X_{i+1} = F(X_i)$$

where F is a vector function with vector arguments. The evolution begins from an appropriate initial condition:

$$X_0 = \{x_1(t_0), x_2(t_0), \ldots x_n(t_0)\}$$

In: C.M. Isaacs and V.L. Tharp, Editors. 1995. *Proceedings of the Eleventh Annual Pacific Climate (PACLIM) Workshop, April 19-22, 1994.* Interagency Ecological Program, Technical Report 40. California Department of Water Resources.

In other systems, it is natural to consider time flowing as a continuum, so that the dynamical rule is a differential equation:

$$dX/dt = \dot{X} = F(X)$$

that is,

$$\dot{x}_1 = f_1(x_1, x_2, \ldots, x_n)$$

$$\dot{x}_2 = f_2(x_1, x_2, \ldots, x_n)$$

$$\dot{x}_n = f_n(x_1, x_2, \ldots, x_n)$$

The evolution of the system from an initial state:

$$X_0 = \{x_1(t=0), x_2(t=0), \ldots, x_n(t=0)\}$$

forward in time is the solution $X(t) = \{x_1(t), x_2(t), \ldots, x_n(t)\}$ of this initial value problem. The evolution from an initial state — a point in phase space — traces out a smooth trajectory in phase space, provided the functions $f_1, f_2, \ldots, f_n$ are continuous functions. That is, the magnitude of the difference $|F(X_1) - F(X_2)|$ should be small whenever $|X_1 - X_2|$ is sufficiently small. Here $|\cdot|$ indicates a distance (for example, Euclidean distance) in phase space.

In discrete time systems governed by an iterated function, the trajectory is usually not smooth, but F should still be continuous in X.

In physical problems, such as mechanical or electrical systems, an appropriate phase space is usually apparent from the form of the laws of motion. For example, mechanical problems require a position and a velocity for each mechanical degree of freedom (Abraham and Shaw 1992). However, in other cases it may be a difficult task to choose an economical set of state variables, that is, a reasonably small number of coordinates that still retain the essential property of the dynamical rule: that knowing the instantaneous state $X = \{x_1, x_2, \ldots, x_n\}$ is sufficient to specify the immediate future trend of evolution is a completely deterministic way and without ambiguity. In spite of this difficulty, recent successes like the characterization of the historical fluctuations in the level of the Great Salt Lake using a 4-dimensional state space (Abarbanel 1995) show that it is possible. More particularly, it is possible to determine an appropriate state space or phase space by analyzing an observed time series, without recourse to a model based on physical laws.

Low-dimensional long-term behavior can occur in complex natural systems whose phase space would seem to be of very high dimension. Dissipation, which exists in most natural systems, causes volumes of ensembles in phase space to contract as time advances; this is the equivalent of Liouville's theorem for energy-conserving systems (Thompson and Stewart 1986, p. 221). In many cases, dissipation acts even more

strongly, reducing the long-term fluctuations to a subset of dimension much smaller than the number of phase space dimensions suggested by the laws of motion. This is not a theorem, but a commonly observed phenomenon.

If the long-term dynamics of a system have a low-dimensional description, then one may hope that a moderately long observed trajectory will come near to every state possible for the long-term dynamics; that is, it comes near every point in the attractor. If the dynamical rule $F(X)$ is a continuous function, then it will be possible to make good short-term forecasts by identifying dynamical analogs in past observed behavior (Lorenz 1969).

Most of the methods for detecting dynamical structure begin with the modest assumption that only one time series of a single state variable has been recorded. From a single time series, additional phase space coordinates can be reconstructed using a procedure known as timedelay embedding (Packard *et al* 1980). An excellent review of these methods has recently appeared (Abarbanel *et al* 1993). Here we consider a situation in which two or more concurrent time series of different variables are available for analysis.

The growing body of paleoclimate proxy data with annual resolution makes it possible to consider whether year-to-year climatic fluctuations can be described by a deterministic dynamical rule, in the sense stated above, by examining observed data. Furthermore, the absolute dating of annual resolution data means that the concurrence of two or more independent time series can be established. This concurrence is an essential prerequisite for asking whether such multichannel data represent phase space coordinates for a possible deterministic dynamical rule.

Identifying Dynamical Structure from Time Series

The hallmark of chaos is that evolutions from two nearby states in phase space will gradually diverge from each other as time progresses. In mathematical terms, the system is sensitive to initial conditions. An error or perturbation introduced at any time will grow over time, typically at a geometric rate; this makes long-term forecasting impossible. Given a moderately long time series of all n phase space coordinates, this gradual divergence can be verified by finding good dynamical analogies, that is, pairs of widely separated times in the observed record when the two system states were near each other in phase space. These good dynamical analogies are manifestations of recurrence.

Let us consider data $X(t_i)$ from a continuous time evolution sampled discretely at equally spaced times $t = t_i$, $i = 1, 2, \ldots, N$. For each t_i, the best dynamical analogy for $X(t_i)$ involves its nearest neighbor in phase space. Let us say that this nearest neighbor occurs at time $t = t_{N(i)}$; in determining $N(i)$ we exclude times near t_i so that the analogy belongs to distinct parts of the trajectory and represents a true recurrence.

For each such analogy, the rate of divergence over j steps forward in time can be measured in terms of the local spreading ratio:

$$S(i, j) = \infty X(t_{N(i)+j}) - X(t_{i+j}) \infty / \infty X(t_{N(j)}) - X(t_i) \infty$$

An important mathematical fact about this spreading ratio is that (roughly speaking) for large values of j, the equivalent rate $(1/j) \ln S(i, j)$ tends to a limit that is independent of i and independent of the particular choice of coordinates; in other words, the limit is an invariant quantity. The limiting value is called the largest Lyapunov exponent, denoted λ_1. Sometimes base 2 logarithms are used, so that λ_1 is an inverse doubling time for uncertainties or perturbations. There is, in fact, a spectrum of limiting rates or Lyapunov exponents; only the largest, λ_1, is manifested in the long-term spreading of two typical nearby trajectories. The criterion for chaos is $\lambda_1 > 0$ (Abarbanel *et al* 1993).

In the mathematical definition of Lyapunov exponents, it is assumed that the initial separation at $j = 0$ is infinitesimal, so that even for large j the separation is not too large. When dealing with a finite sample of observed data, this is of course not true, so it may not be practical to consider j large enough to obtain a true invariant quantity. Instead, one may examine the local divergence rate:

$$s(i, j) = (1/j) \ln S(i, j)$$

and its average:

$$\bar{s}(j) = (1/i) \sum_i s(i,j)$$

Although these are not invariant quantities, and they do depend on the choice of coordinates, it is still possible to obtain from them useful information about possible dynamical structure.

A Prototype Example

To illustrate how this can be accomplished, we first consider synthetic data generated by numerical solution of a simple system of three firstorder ordinary differential equations

$$\dot{x} = -y-z$$

$$\dot{y} = x+0.36y$$

$$\dot{z} = 0.4+z(x-4.5)$$

This system was devised by Roessler (1976) to give an example of the simplest possible chaotic attractor, the folded band. Any trajectory of this system will, after an initial transient, settle onto a coherent 3-dimensional structure. Within this coherent structure, nearby states exhibit gradual divergence over time.

A typical trajectory on this attractor is illustrated in Figure 1, which shows the coordinates x, y, and z plotted as three time series above, and in phase portraits. The upper left phase portrait shows an orthogonal projection of the three coordinates with the z-axis tilted at 45 degrees, while the lower left shows a projection along the z-axis onto the (x, y) plane. On the right is a different trajectory to be discussed below.

On the average, separations are roughly doubled for each circuit around this attractor; sampling at about 60 discrete time steps per circuit, we expect λ_1 to be about (1/60) ln 2, or roughly 0.011.

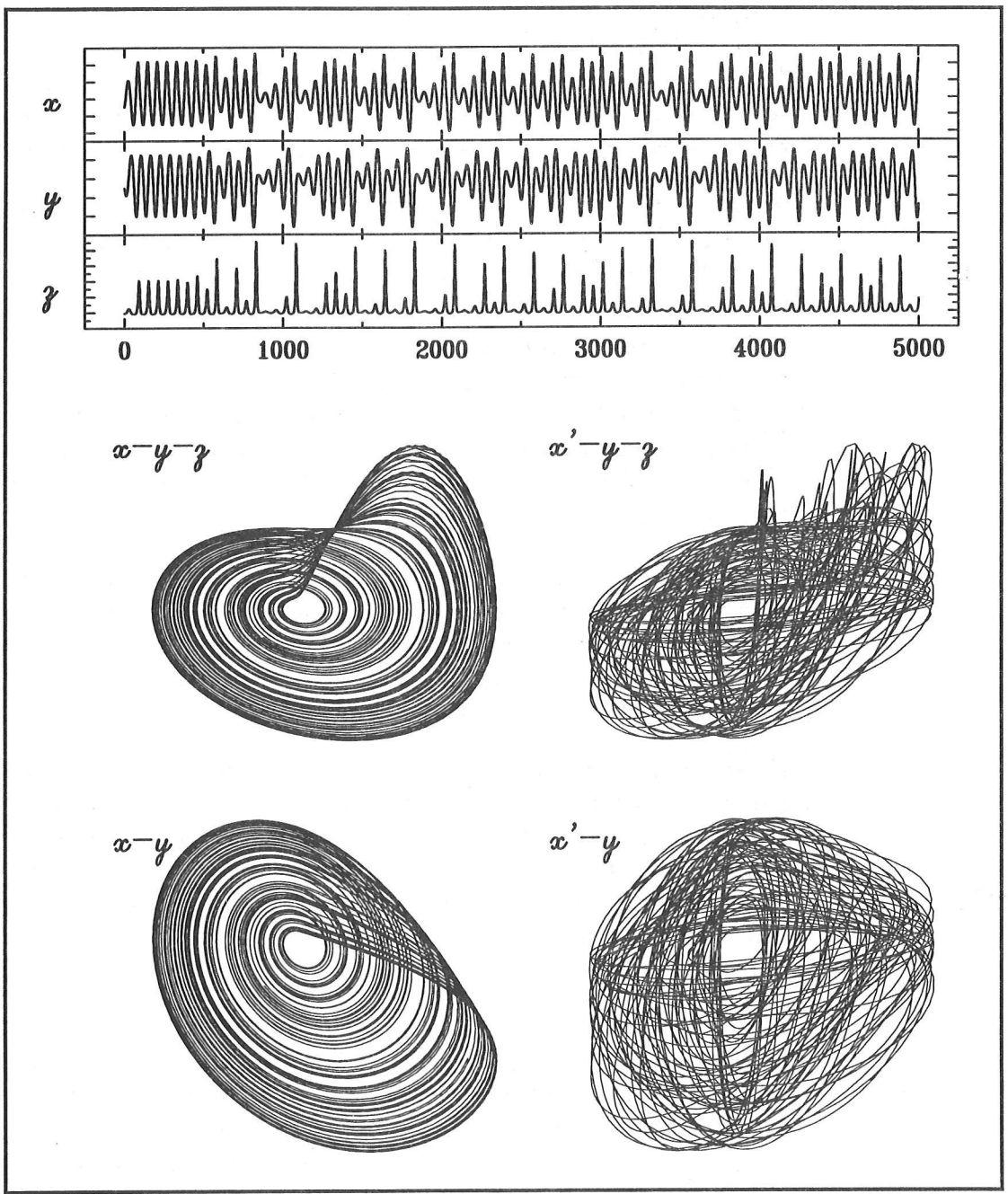

Figure 1. TIME SERIES AND PHASE SPACE PROJECTIONS OF A TRAJECTORY OF ROESSLER'S EQUATIONS AND PHASE PROJECTIONS OF A TRAJECTORY OBTAINED BY SUBSTITUTING SURROGATE CHANNEL DATA x FOR x.

Suppose we are given a 3-channel time series $x(t_i)$, $y(t_i)$, $z(t_i)$; we wish to determine, from the data themselves and without knowing their origin in Roessler's equations, whether they were generated by a deterministic rule. One method of diagnosis consists of computing the average local divergence rate $\bar{s}(j)$ and comparing it with the divergence rate computed from a surrogate data set. By surrogate, we mean data that from their appearance as time series could plausibly have come from the same source but that have in fact been arranged or manipulated so that they lack dynamical structure.

Surrogate data sets have been used for this type of diagnosis using time-delay embeddings, where only a single variable has been observed and recorded (*eg*, Theiler *et al* 1992; Takens 1993). Here we are considering multichannel data, so it makes sense to look at surrogate data in which only one channel has been replaced by a plausible substitute, with other channels unchanged. We then speak of a surrogate channel of data.

A simple method of generating surrogate channels is to divide the original multichannel data set into halves. We denote the first half of the data, $i = 1, 2, \ldots, N/2$ by $x(t_i)$, $y(t_i)$, $z(t_i)$, and the second half, for $i = N/2, N/2+1, \ldots, N$, is displaced in time to $i = 1, 2, \ldots, N/2$ and denoted by $x'(t_i)$, $y'(t_i)$, $z'(t_i)$. Now x' has dynamical structure when taken with y' and z', but its structure is, time step for time step, unrelated to the structure of y and z. Nearest neighbors identified using coordinates $x'(t_i)$, $y(t_i)$, $z(t_i)$ will not be true dynamical analogies, and can be expected to diverge rapidly. Thus the value of $\bar{s}(j)$ for the surrogate data $x'(t_i)$, $y(t_i)$, $z(t_i)$ will be much larger than for the original.

On the other hand, if the original data $x(t_i)$, $y(t_i)$, $z(t_i)$ came not from a dynamical system but from random behavior, then the spreading rate should be large for both the original and the surrogate data. Since we do not know *a priori* what is a large spreading rate, the comparison with surrogate data is essential.

Examples of average local divergence rates $\bar{s}(j)$ for true trajectories of Roessler's equations and with surrogate channels are given in Table 1. Two disjoint segments each 5000 steps in length were extracted from a longer trajectory. The two segments were spliced into a single 6-channel data set to facilitate surrogate substitutions. Various embeddings and surrogate substitutions were tried, with two cases each to give a crude estimate of the variance due to finite sampling of the attractor.

Case 1 is the complete natural embedding of the first segment with coordinates $x(t_i)$, $y(t_i)$, $z(t_i)$, and case 2 is the complete natural embedding of the second segment with coordinates $x'(t_i)$, $y'(t_i)$, $z'(t_i)$. In both cases the average local divergence rate $\bar{s}(j)$ depends on j, the number of steps forward. For $j = 1$, the average rate is smaller than the expected long-term value of 0.011, and the variance due to finite sampling is relatively large.

Table 1
AVERAGE LOCAL DIVERGENCE RATE $\bar{s}(j)$ FOR TRIAL EMBEDDINGS OF THE ROESSLER BAND ATTRACTOR IN TWO AND THREE DIMENSIONS

5000-Point Trajectories Samples 60x per Turn

		Average Local Divergence Rate						
Case	Coordinates	j = 1	j = 2	j = 4	j = 8	j = 16	j = 32	j = 64
1	x-y-z	0.001	0.012	0.018	0.018	0.016	0.013	0.011
2		0.010	0.016	0.020	0.018	0.015	0.012	0.011
3	x'-y-z	0.796	0.655	0.471	0.302	0.166	0.059	0.036
4		0.819	0.664	0.475	0.303	0.165	0.056	0.036
5	x-y-z'	0.201	0.175	0.144	0.110	0.080	0.040	0.017
6		0.209	0.189	0.158	0.122	0.086	0.041	0.019
7	x-y	0.392	0.248	0.149	0.086	0.052	0.030	0.020
8		0.363	0.233	0.142	0.083	0.051	0.030	0.020
9	x'-y	2.479	1.575	0.952	0.549	0.294	0.107	0.065
10		2.738	1.706	1.019	0.583	0.308	0.111	0.068

For increasing j, the variance due to sampling decreases; $\bar{s}(j)$ increases to a maximum near $j = 4$ and then decreases to the expected long-term value at $j = 64$.

Cases 3 and 4 are the results of surrogate substitution in the x coordinate. In case 3, $x'(t_i)$ was substituted for $x(t_i)$ in the first trajectory segment; in case 4 the opposite was done. Since the trajectories $x'(t_i)$, $y(t_i)$, $z(t_i)$ and $x(t_i)$, $y'(t_i)$, $z'(t_i)$ are, of course, not trajectories of a dynamical system, it is an abuse of terminology to speak of local Lyapunov exponents. Nevertheless, computing the average local divergence rates as in cases 1 and 2, we find a large increase in magnitude. If we were presented with data of unknown origin, such an effect would be evidence for the significance of the x coordinate in the dynamical structure of the trajectory.

Note that the effect of the surrogate channel upon the local divergence rates is greatest for $j = 1$, and becomes less pronounced as j increases. When trajectory self-crossing inconsistent with dynamical structure occurs, the largest separations occur in the near term. Thus, when using surrogates to test for dynamical structure, the short-term divergence rates provide better diagnosis than the long-term rates, even though the short-term rates are not invariant quantities.

Cases 5 and 6 are likewise obtained by surrogate substitution, this time for the z coordinate. Again the importance of this coordinate in the dynamical structure is confirmed, although it is somewhat less significant than the x coordinate.

Cases 7 through 10 relate to the detection of dynamical structure using an incomplete set of phase space coordinates. Only x and y are used as trial phase space coordinates; we therefore do not expect the divergences, even for large j, to approach the true Lyapunov exponent λ_1 in the 3-dimensional phase space. Nevertheless, when a surrogate channel is substituted (in cases 9 and 10) for the x coordinate in the partial x, y embedding, the effect on local divergence rates is unmistakable.

This suggests that it may be possible, using surrogate channel substitution, to detect dynamical structure in multichannel time series data, even if there are not enough data channels to fully embed the attractor; that is, there are not enough phase space coordinates to correctly identify good dynamical analogies.

Of course this prototype example of chaos only suggests what may happen with more complicated chaotic attractors in higher-dimensional phase space. The use of surrogate channels and local divergence rates has recently been tested on another model, a very low-order moist general circulation model devised by Lorenz (1984), which is equivalent to a system of 27 ordinary differential equations. Applying multichannel time series analysis to simulations of this model confirmed that surrogate channel substitution and diagnosis from short-term divergence rates can be used to detect dynamical structure in incomplete embeddings (Stewart 1994).

A Paleoclimate Example

We now describe an example of how such methods might be applied to paleoclimate data. Here we must, at least for the present, abandon thought of any specific model that would describe dynamical structure of climate. Of course there are dynamical models of climate evolution, but the differential equations model the evolution in steps of hours or days, and nearby trajectories diverge in weeks or, at most, months. Here we pose a different question: Is the evolution of climate governed by dynamical laws, known or unknown, that determine the state one or a few years forward given the present state, expressed in terms of annual or seasonal means?

We emphasize that we know of no persuasive argument that climate has such a dynamical structure (on yearly time scales) at all. In fact, the rate of divergence of weather conditions seems (at least superficially) to make this dynamical structure of climate an unlikely hypothesis. Nevertheless, it is not ruled out. If true, or even partly true, it would be of great

consequence. As just one example, it might permit earlier detection of a greenhouse signal manifested as a departure in (or from) dynamical structure. In any case, we are simply posing this as a hypothesis, to be tested using multichannel time series analysis.

For our example, we shall use two paleoclimate proxy data series of very different origin. For a more thorough study, additional data series should be included. One series used here is the annual oxygen isotope ratio in cores from the Quelccaya ice cap in Peru published by Thompson and Mosley-Thompson (1989), extending from 1476 to 1984. The other series is a tree-ring index developed by Briffa *et al* (1992) from Fennoscandian trees, extending from A.D. 500 to 1980, and kindly furnished to the author by Professor Briffa. These two data series were treated as possible phase space coordinates for dynamical structure, if it exists. The notion underlying this choice is that these two proxies would represent different and complementary modes or degrees of freedom of a hypothesized dynamical structure. Of course any climatological insight that would bear on the suitability of these or other data series as reflecting the state of the climate should be considered (*eg*, Cole *et al* 1993). For present illustrational purposes, we take these two series to represent the state of the art.

These two data series are analyzed on two time scales. First, we test for dynamical structure on the yearly time scale. Both data series exhibit large fluctuations from year to year; for this reason, a smooth evolution on yearly time scales, as with differential equations, is not an appropriate hypothesis, and instead we must suppose a system in which time passes in discrete units, as in the iterated function $X_{i+1} = F(X_i)$. Second, we test for dynamical structure on multiyear time scales, taking running means to smooth the data; this gives somewhat less ragged trajectories, which might correspond to a differential equation model. The numerical evaluation of local divergence rates is essentially the same in both cases, with one small difference: with the smoothed data we determine nearest neighbors by interpolating between successive data points; with the raw yearly data, there is no interpolation.

In the previous example of synthetic data from a simulation, there was little harm in generating surrogates by cutting a long trajectory into two disjoint segments: small sample size was not a problem, as the simulation can always be extended. However, with limited and precious paleoclimate data, cutting the time series in half would seem extravagant. One would prefer to test the full length of available data against surrogates of equal length.

Another means of generating surrogate channels is by randomization of the given data. Substituting data from a random number generator is too crude. We want our surrogates to lack dynamical structure but be able to pass superficially for the real data. One algorithm for achieving this is

the following: take the complex Fourier transform of the data, then randomize the phases of the complex coefficients $a(\omega)$ in the frequency domain. In order that the inverse transform yield a real time series, the phases must be randomized under the constraint that $a(\omega) = a^*(-\omega)$. The inverse transform of data randomized in this manner will be a surrogate having the same power spectrum as the original data, but with any dynamical structure removed.

This is the procedure we adopt for generating surrogates for both the ice core and the tree ring data. It is not the only — or necessarily the best — procedure; see Theiler *et al* (1992), Takens (1993), and Kennel and Isabelle (1992) for further discussion.

Figure 2 shows local divergence rates $\bar{s}(j)$ for a 2-dimensional trajectory whose coordinates are the Quelccaya oxygen isotope ratio and the Fennoscandian tree ring index; the values of are indicated by dots and connected with solid lines. Also shown are the divergence rates for three surrogate substitutes for each coordinate, plotted as broken lines. In the upper plot, surrogates are substituted for the tree ring data. The values of $\bar{s}(j)$ for surrogates fall very slightly above the values for the data at $j = 1$ and $j = 2$; we can easily imagine that with more than three surrogate substitutions, their range would include the $\bar{s}(j)$ of the original data. For larger j, the $\bar{s}(j)$ for the data lie within the range for the three surrogates. In the lower plot, surrogates are substituted for the ice core data; all the $\bar{s}(j)$ for the original data are within the ranges for the surrogates. We conclude that these tests show no evidence of dynamical structure in the data on yearly time scales.

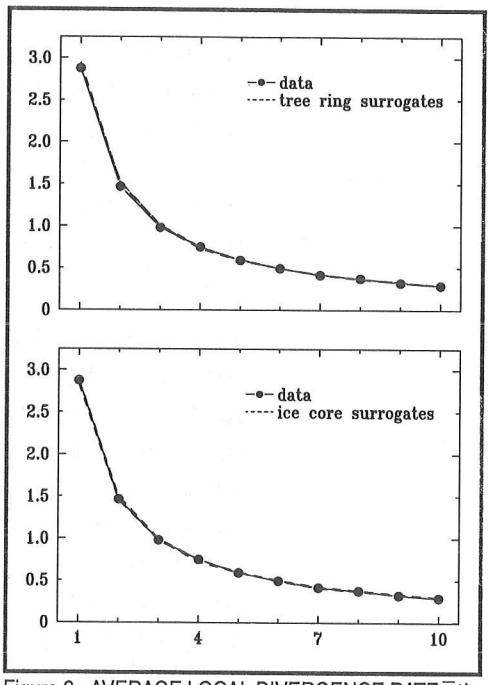

Figure 2. AVERAGE LOCAL DIVERGENCE RATE $\bar{s}(j)$ OF A PALEOCLIMATE PROXY DATA TRAJECTORY FROM 1476-1980
Coordinates are oxygen isotope ratio from Quelccaya ice core and Fennoscandian tree ring index.
Above, paleoclimate trajector and three trajectories with surrogate tree ring data.
Below, paleoclimate trajectory and three trajectories with surrogate ice core data.

The same two time series were then smoothed and retested for local divergence on multiyear time scales. Seven-year running means were used, based on the presence of a strong 14-year component in spectrum of the ice core data. We also used 11- and 13-year running means. When generating surrogates for smoothed data, we randomize phases of the raw data and then smooth, rather than randomizing smoothed data; this is in accord with the recommendation of Prichard (1994) to randomize before filtering. Typical results for the 7-year running means are shown in Figure 3, again using three surrogate substitutes for each channel. The divergence rates for the data again fall within or are very close to the range for the surrogates. We conclude that there is also no evidence for dynamic structure in the data on multiyear timescales.

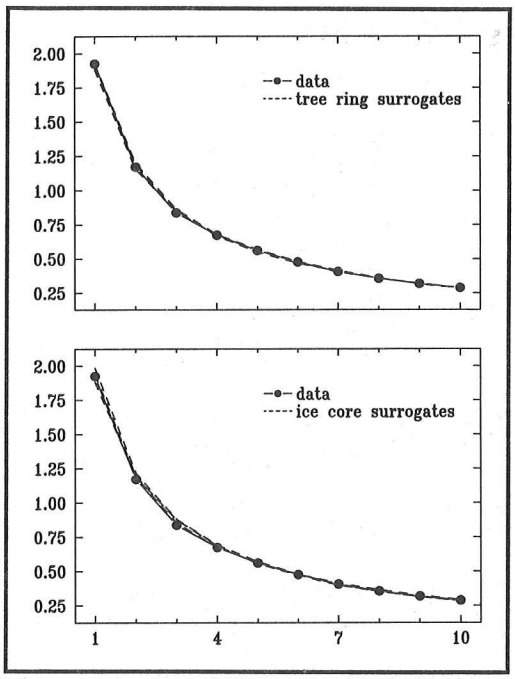

Figure 3. AVERAGE LOCAL DIVERGENCE RATE $\bar{s}(j)$ OF A PALEOCLIMATE PROXY DATA TRAJECTORY FROM 1476-1980, SMOOTHED BY TAKING 7-YEAR RUNNING MEANS OF OXYGEN ISOTOPE RATIO AND FENNOSCANDIAN TREE RING INDEX
Above, paleoclimate trajector and three trajectories with smoothed surrogate tree ring data.
Below, paleoclimate trajectory and three trajectories with smoothed surrogate ice core data.

The development and application of dynamical systems approaches to time series analysis is still in its infancy. In due course, with deeper insight into climate and perhaps some serendipity, these multichannel methods should achieve successes with climate data comparable to the recent success analyzing single time series (Abarbanel 1995).

Acknowledgment

The author is indebted to Henry Abarbanel, Keith Briffa, and Caroline Isaacs for stimulating discussions. This work was supported by the CHAMMP initiative of the Office of Health and Environmental Research, U.S. Department of Energy under Contract DE-AC02-76CH00016.

References

Abarbanel, H.D.I. 1995. *Analysis of Observed Chaotic Data.* To be published by Springer-Verlag, New York.

Abarbanel, H.D.I., R. Brown, J.J. Sidorowich, L.Sh.T. Tsimring. 1993. The analysis of observed chaotic data in physical systems. *Reviews of Modern Physics* 65:1331-1392.

Abraham, R.H., and C.D. Shaw. 1992. *Dynamics: the Geometry of Behavior.* Addison-Wesley, Redwood City, CA. 642 pp.

Briffa, K.R., P.D. Jones, T.S. Bartholin, D. Eckstein, F.H. Schweingruber, W. Karlen, P. Zetterberg. 1992. Fennoscandian summers from AD 500: Temperature changes on short and long timescales. *Climate Dynamics* 7:111-119.

Cole, J.E., D. Rind, R.G. Fairbanks. 1993. Isotopic responses to interannual climate variability simulated by an atmospheric general circulation model. *Quaternary Science Reviews* 12:387-406.

Kennel, M.B., and S. Isabelle. 1992. Method to distinguish possible chaos from colored noise and to determine embedding parameters. *Physical Review A* 46:3111-3118.

Lorenz, E.N. 1969. Atmospheric predictability as revealed by naturally occurring analogues. *Journal of the Atmospheric Sciences* 26:636-646.

Lorenz, E.N. 1984. Formulation of a low-order model of a moist general circulation. *Journal of the Atmospheric Sciences* 41:1933-1945.

Packard, N.H., J.P. Crutchfield, J.D. Farmer, R.S. Shaw. 1980. Geometry from a time series. *Physical Review Letters* 45:712-716.

Prichard, D. 1994. The correlation dimension of differenced data. *Physics Letters A* 191:245-250.

Roessler, O.E. 1976. An equation for continuous chaos. *Physics Letters A* 57:397-398.

Stewart, H.B. 1994. Dynamical structure of a low-order moist atmospheric circulation model. To appear in *Physics and Chemistry of Fluids: Chaos and Turbulence*, M.G. Velarde, editor.

Takens, F. 1993. Detecting nonlinearities in stationary time series. *International Journal of Bifurcation and Chaos* 3:241-256.

Theiler, J., S. Eubank, A. Longtin, B. Galdrikian, J.D. Farmer. 1994. Testing for nonlinearity in time series: the method of surrogate data. *Physica D* 58:77-94.

Thompson, J.M.T., and H.B. Stewart, 1986. *Nonlinear Dynamics and Chaos.* John Wiley and Sons, Chichester, 376 pp.

Thompson, L.G., and E. Mosley-Thompson. 1989. One-half millenia of tropical climate variability as recorded in the stratigraphy of the Quelccaya ice cap, Peru. Pages 15-31 in *Aspects of Climate Variability in the Pacific and the Western Americas.* D.H. Peterson, editor. Geophysical Monograph 55, American Geophysical Union, Washington, DC.

Modeling North Pacific Temperature and Pressure Changes from Coastal Tree-Ring Chronologies

Gregory C. Wiles, Rosanne D. D'Arrigo, and Gordon C. Jacoby

ABSTRACT: Climate modeling using coastal tree-ring chronologies has yielded the first summer temperature reconstructions for coastal stations along the Gulf of Alaska and the Pacific Northwest. These land temperature reconstructions are strongly correlated with nearby sea surface temperatures, indicating large-scale ocean-atmospheric influences. Significant progress has also been made in modeling winter land temperatures and sea surface temperatures from coastal and shipboard stations. In addition to temperature, the pressure variability center over the central North Pacific Ocean (PAC), which is related to the strength and location of the Aleutian Low pressure system, could be extended using coastal tree rings.

Introduction

Temperature and pressure fluctuations in the Northeastern Pacific sector are important for understanding global climate and its prediction (Cayan 1980; Namias *et al* 1988; Trenberth and Hurrell 1994) as well as for their impact on major fishery resources (Mysak 1986; Francis and Sibley 1991). Few physical or biological time series from the Gulf of Alaska and the Pacific Northwest extend over more than several decades, an insufficient interval to evaluate long-term climate variability (Roden 1989). Coastal tree-ring width and density records provide some of the best proxies for year-to-year climate change and can extend existing records by several centuries or more. Tree-rings from coastal and near coastal sites along the Northeastern Pacific are influenced by and can be used to reconstruct large-scale oceanic and atmospheric temperature changes (Blasing and Fritts 1975, 1976; Xiangding and Lough 1987).

Whereas a relatively dense network of tree-ring records for climatic reconstruction exists for western North American interior forest sites (Chapter 1, Cook and Kairiukstis 1990), few studies have used coastal trees to reconstruct oceanic and climatic variations for the Northeastern Pacific sector. Climatic conditions along coastal regions can differ considerably from those at interior sites. How climate changes in these transitional zones between the continental and oceanic environment is crucial for understanding Earth's climate system. Goals of this paper are:

- To analyze the climate signal in Northeastern Pacific ring-width and maximum latewood density chronologies.
- To present summer temperature reconstructions and evaluate the linkages between sea surface and land temperatures as recorded in tree rings.
- To examine the winter climate signal in the tree-ring time series.

In: C.M. Isaacs and V.L. Tharp, Editors. 1995. *Proceedings of the Eleventh Annual Pacific Climate (PACLIM) Workshop, April 19-22, 1994.* Interagency Ecological Program, Technical Report 40. California Department of Water Resources.

Previous Dendroclimatic Studies in the Northeastern Pacific Sector

Previous researchers have used tree-ring chronologies from western North America to model temperature and pressure variations in the North Pacific sector (Blasing and Fritts 1975, 1976; Douglas 1980). For example, Blasing and Fritts (1975) identified 10 patterns of summer tree growth from 21 ring-width chronologies in western Canada and interior and Arctic Alaska. No coastal chronologies were included in these analyses. A more extensive network of 49 ring-width chronologies in western North America was employed to reconstruct winter climatic anomalies for the North Pacific sector and western North America (Blasing and Fritts 1976). Reconstruction of Pacific sea level pressure variations was the subject of a study by Xiangding and Lough (1987), who estimated summer sea level pressure using tree-ring chronologies from North America combined with documentary records of precipitation from China.

Tree-ring chronologies from near-coastal and interior regions have been used in various temperature reconstructions for the Northeastern Pacific sector. Graumlich and Brubaker (1986) reconstructed mean annual temperatures for Longmire, Washington, from a set of ring-width chronologies in the Cascade Range. More recently, Schweingruber *et al* (1993) presented new tree-ring chronologies from a major sampling transect across North America. Analysis of this dataset by Briffa *et al* (1992) included growing season temperature reconstructions for the Alaska-Yukon region and the Pacific Northwest. Using only chronologies from coastal and near-coastal sites, Buckley *et al* (1992) investigated the temperature and precipitation response of tree-ring records from the Pacific Northwest. In this study, density chronologies were found to be more sensitive indicators of year-to-year temperature variations than the companion ring-width series. Additionally, links between the tree-ring records and sea surface temperatures and sea level pressure suggested that the chronologies had the potential to reconstruct large-scale atmospheric phenomena such as changes in the Aleutian Low pressure system. Their tree-ring dataset included some of the same tree-ring chronologies presented in this analysis. This paper uses an approach similar to that of Buckley *et al* (1992), employing climatically sensitive chronologies to reconstruct coastal climate variations for regions in the Northeastern Pacific sector.

Tree-Ring and Meteorological Data

New tree-ring data from the Gulf of Alaska, together with existing collections from British Columbia, Alaska, Washington, and California, make up the primary database for modeling studies in coastal regions of the Northeastern Pacific (Figure 1; Table 1). Maximum latewood density chronologies for Alaska, Washington, and Vancouver Island were processed in Switzerland by F. Schweingruber at the Swiss Federal Institute of Forestry Research as part of a collection of 69 tree-ring sites sampled in northern North America during 1984 and 1989 (Schweingruber *et al*,

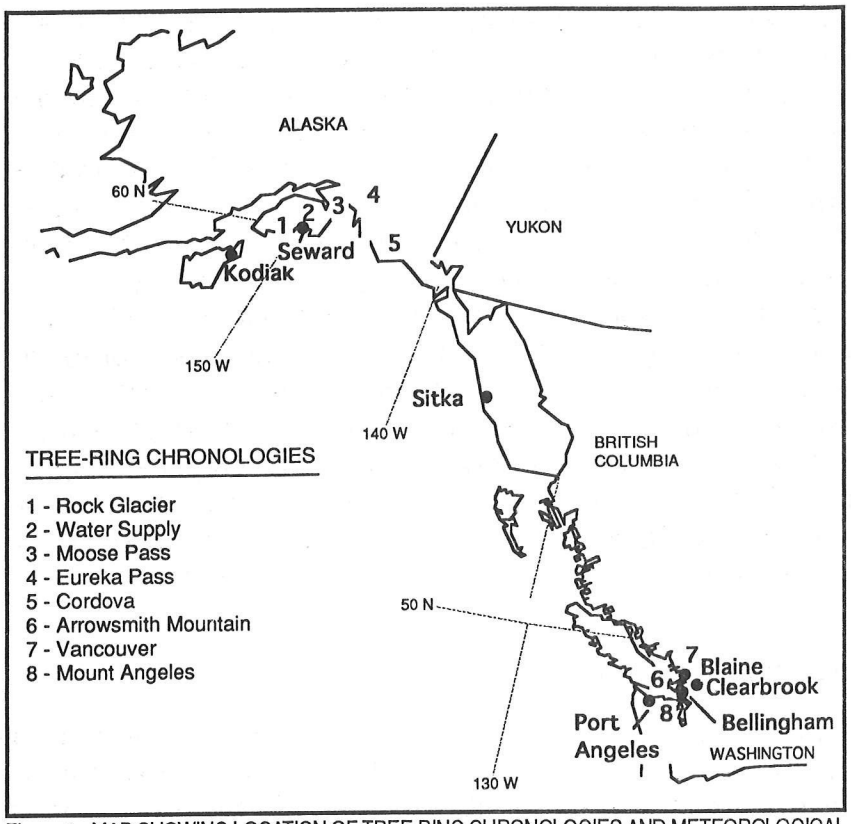

Figure 1. MAP SHOWING LOCATION OF TREE-RING CHRONOLOGIES AND METEOROLOGICAL STATIONS USED IN SUMMER TEMPERATURE RECONSTRUCTIONS FOR THE GULF OF ALASKA AND THE PACIFIC NORTHWEST

1993). Final chronologies were developed from their raw data at the Tree Ring Laboratory of Lamont-Doherty Earth Observatory, using standard dendrochronological techniques (Fritts 1976; Cook and Kairiukstis 1990). Additional chronologies were obtained through the International Tree-Ring Database of the University of Arizona.

Table 1
TREE-RING SITES USED IN MODELING NORTHEAST PACIFIC CLIMATE.

Tree Ring Site	Species	Interval	Elevation (meters)	Latitude / Longitude
ALASKA				
Cordova (CV)	TSME	1192-1992	428	61°20' N / 145°40' W
Eureka Summit (ES)	PCGL	1654-1983	960	61°50' N / 147°20' W
Moose Pass (MP)	PCSI	1732-1983	100	61°20' N / 149°35' W
Nichawak Mountain (NK)	PCSI	1762-1992	320	60°15' N / 144°00' W
Rock Glacier (RGL)	TSME	1530-1991	420	61°04' N / 148°00' W
Water Supply (WS)	TSME	1727-1989	305	61°05' N / 149°36' W
CALIFORNIA				
Snow White Ridge (SNO)	PIPO	1557-1980	1731	38°08' N / 120°03' W
NEVADA				
Pete's Summit (PSU)	PIMO	1439-1982	2347	39°11' N / 116°47' W
WASHINGTON				
Arrowsmith Mountain (ARW)	TSME	1629-1983	1020	49°09' N / 125°14' W
Frying Pan Creek (FPC)	PSME	1286-1980	1170	46°53' N / 121°37' W
Mount Angeles (ANG)	PSME	1750-1983	1360	47°58' N / 123°26' W
Vancouver (VAN)	TSME	1413-1983	1110	49°20' N / 123°20' W

PCGL = *Picea glauca*
PCSI = *Picea sitchensis*
PIMO = *Pinus cembroides*
PIPO = *Pinus ponderosa*
PSME = *Pseudotsuga menziesii*
TSME = *Tsuga mertensiana*

Individual average monthly temperature series for meteorological stations at Sitka, Seward, and Kodiak, along the Gulf of Alaska, and from the coastal stations of Blaine, Bellingham, Clearbrook, and Port Angeles, all in northwestern Washington, were obtained from the Historical Climate Network. Regional average temperature series for the last 80 years were computed for the Gulf of Alaska (GOA) and for Washington stations in the Pacific Northwest (PNW). In addition to the land temperature series, a 5°X5° monthly sea surface temperature dataset for the Northeast Pacific (1947 to 1990) was obtained from Dr. Dan Cayan of Scripps Institution of Oceanography. Tree-ring data were also compared with the PAC teleconnection index series of Rogers (1990). The PAC index is the North-Central Pacific low-frequency variability pattern that is related to the strength of the Aleutian Low pressure system. A strong low is associated with a high index value and a weaker low with a smaller index value. Sea surface temperatures recorded at the coastal station of Amphitrite Point, British Columbia, were provided by D. Ware.

Summer Temperature Reconstructions

The temperature signal in the tree-ring time series was evaluated by simple correlations between the series and the 17-month dendroclimatic year (June of the previous year through October of the growth year; Figure 2) of the regional average temperature series from PNW and GOA. The GOA ring-width data correlated positively with all months; strongest correlations were for the growing season, March through September. Density chronologies along the gulf showed a negative relationship with previous July through November mean temperatures and a positive correlation with temperatures from March through September. Chronologies of maximum latewood density from Washington State are also positively correlated with temperature during April through September. Based on these results, we decided to use the tree-ring data to model temperatures averaged over the April-September season.

Principal components regression techniques (Chapter 4, Cook and Kairiukstis 1990) were employed to reconstruct summer temperatures. Tree-ring data for the current year (t) were used to predict summer temperatures. The GOA model is based on three ring-width time series and two maximum latewood density chronologies, which have a similar response to growing season temperatures (Figure 2a, b). The PNW model uses the three latewood density chronologies (Figure 2c). Both the tree-ring and temperature data were prewhitened prior to modeling to remove the persistence in the series (Box and Jenkins 1970). In each case, most of the variance was explained in the first eigenvector, and only the first eigenvector of the principal component analysis was retained for regression.

Model verification was performed by halving each temperature series, with each half verified using the calibration of the other. For the PNW

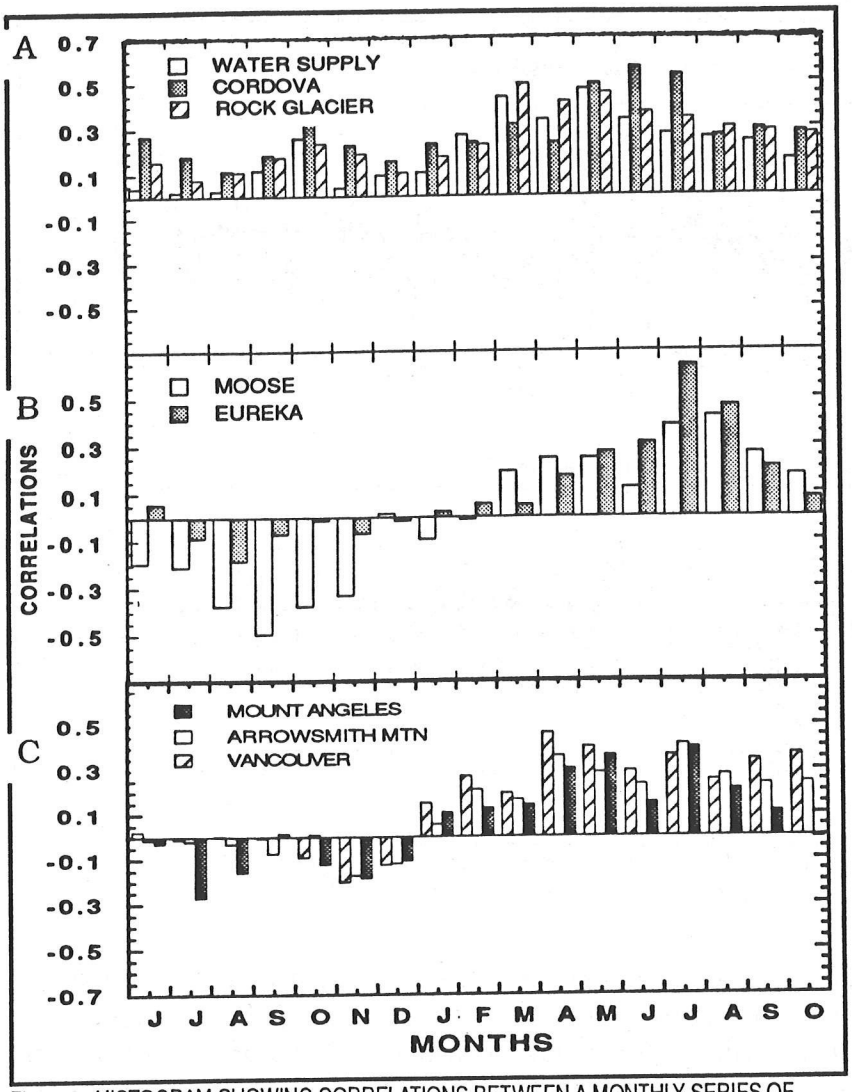

Figure 2. HISTOGRAM SHOWING CORRELATIONS BETWEEN A MONTHLY SERIES OF REGIONAL AVERAGE TEMPERATURES AND: (A) RING WIDTH SERIES, (B) TREE-RING DENSITY CHRONOLOGIES FROM THE GULF OF ALASKA, AND (C) DENSITY CHRONOLOGIES FROM NORTHWEST WASHINGTON

reconstruction, about 39% of the variance for 1905 to 1983 is explained after adjusting for degrees of freedom lost in regression (ar^2). When the period 1905-1944 was used in calibration and the verification was 1945-1983, the adjusted variance explained was 31%, with a reduction of error (RE) of 0.33 and a Spearman correlation of 0.56. The reduction of error is a method of test significance (Gordon and LeDuc 1981) where any value above zero indicates significant predictive success. When the calibration (1945-1983) and verification (1905-1944) intervals were reversed, the variance explained was 46%, with an RE of 0.47 and a Spearman correlation of 0.64.

Somewhat better results were obtained for the Gulf of Alaska model, with 47% of the variance explained for the full period of 1909 to 1983. The calibration interval of 1909 to 1945 yielded an adjusted r-square of 0.40, an RE of 0.42, and a Spearman correlation coefficient of 0.51 for the later verification period. When these intervals were reversed, 56% of the temperature variance was explained, with an RE of 0.56 and a Spearman coefficient of 0.70. Figure 3 presents the two well-verified, summer temperature reconstructions for the Gulf of Alaska and the Pacific Northwest.

No summer temperature reconstructions have been available for the Gulf of Alaska prior to current study. Some features of the Yukon and Alaska regional summer temperature reconstruction (Briffa *et al* 1992) are consistent with the GOA reconstruction, including warming in the 1820s and cooling in the 1810s, 1860s, and 1890s (Figure 3a). They identified the summer of 1810 as the coldest over their Alaska -Yukon study region, as was found in our record of GOA summer temperatures. Historical 19th century temperature data for Sitka, Alaska (compiled by Roden [1989]), are consistent with the GOA temperature reconstruction, with extended cold periods during 1857-1863 and warm intervals during 1864-1870.

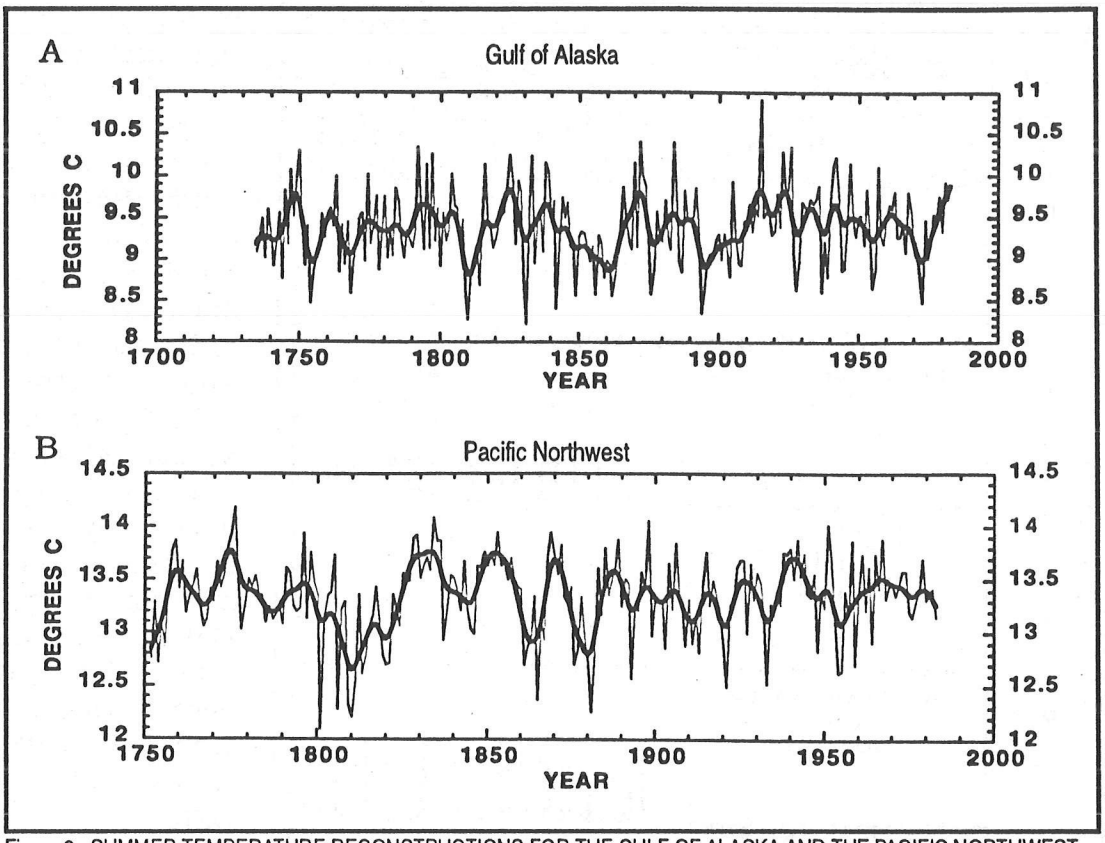

Figure 3. SUMMER TEMPERATURE RECONSTRUCTIONS FOR THE GULF OF ALASKA AND THE PACIFIC NORTHWEST
Smoothed reconstructions lines represent a 10-year cubic smoothing spline (Cook and Peters 1981).

The mean annual temperature reconstruction for Longmire, Washington, based on ring-width data from high elevations (Graumlich and Brubaker 1986) shows cool intervals in the early 1800s and the 1880s, consistent with the PNW reconstruction. However, the Graumlich and Brubaker reconstruction exhibits warming in the latter part of the 20th century; the coastal PNW series does not show this change (Figure 3b).

The density chronologies used in the summer temperature reconstruction of Briffa *et al* (1992) for the Pacific Northwest and British Columbia (their BCPNW) include the three density chronologies used in our PNW reconstruction. As expected, most primary features in the two reconstructions are similar. However, the cool interval centered around 1860 AD is not apparent in the Briffa *et al* (1992) reconstruction. This cool period is a significant interval in the coastal reconstruction and is also noted as a major cool interval from coastal temperature time series (Roden 1989).

The good correspondence with independent historical data from coastal temperature instrumental records and the broad agreement with published reconstructions based on tree-ring data suggest that the two summer temperature reconstructions are reliable records of temperature change along the Pacific Northeastern coastal areas.

Tree Growth and Sea Surface Temperatures

The next step in the analyses was to explore links between tree growth, land surface temperatures, and sea surface temperatures. Land surface and sea surface temperature records from the Gulf of Alaska are strongly correlated for April through September, with the strongest correlations at 55°N latitude, 150°W longitude (Figure 4). PCA scores from the five tree-ring chronologies show a similar correlation pattern, with the strongest correlation also at 55°N, 150°W (Figure 5).

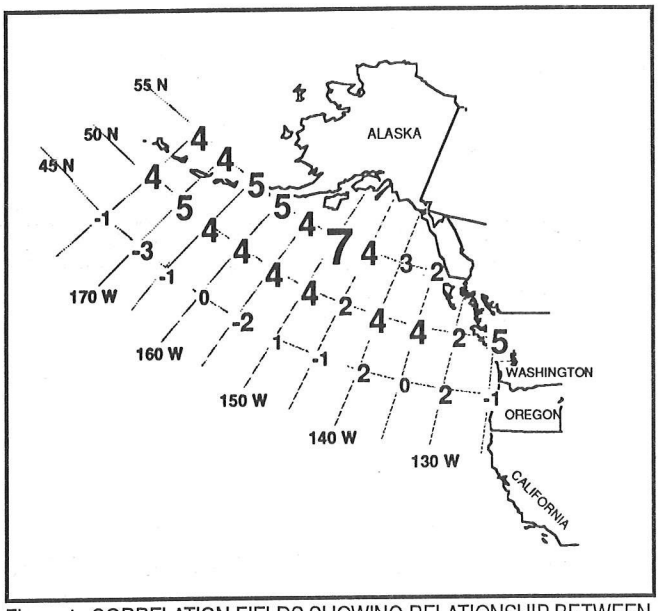

Figure 4. CORRELATION FIELDS SHOWING RELATIONSHIP BETWEEN LAND TEMPERATURE AND SEA SURFACE TEMPERATURE FOR THE GULF OF ALASKA

Magnitude of Correlation:				
	0	.00 - .09	4	.40 - .49
	1	.10 - .19	5	.50 - .59
	2	.20 - .29	6	.60 - .69
	3	.30 - .39	7	.70 - .79

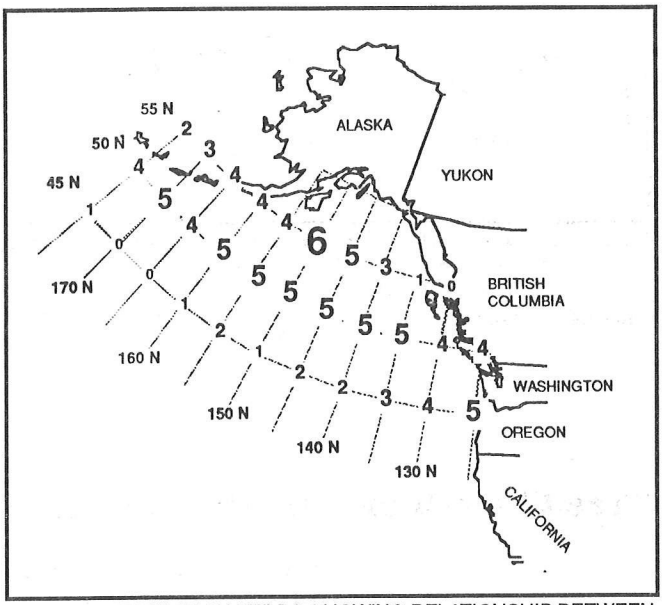

Figure 5. CORRELATION FIELDS SHOWING RELATIONSHIP BETWEEN TREE RING PCA SCORES AND SEA SURFACE TEMPERATURE FOR THE GULF OF ALASKA

Magnitude of Correlation:				
	0	.00 - .09	4	.40 - .49
	1	.10 - .19	5	.50 - .59
	2	.20 - .29	6	.60 - .69
	3	.30 - .39	7	.70 - .79

The average land temperature record from northwestern Washington is highly correlated with sea surface temperatures from offshore British Columbia to southern California (Figure 6). The PNW temperature reconstruction correlates most strongly with sea surface temperature at 45°N latitude and 135°W longitude, with correlations dropping off dramatically away from this point (Figure 7). These linkages of tree growth, land temperatures, and sea surface temperatures suggest that tree growth is strongly affected by and provides information about nearby ocean temperatures.

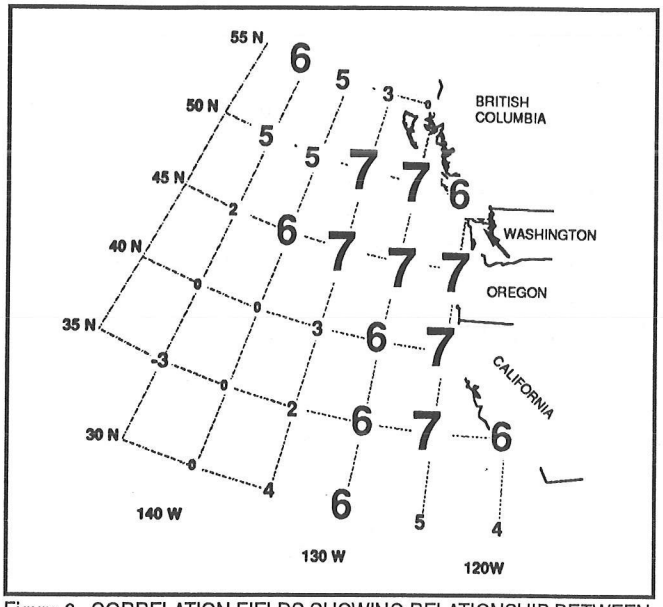

Figure 6. CORRELATION FIELDS SHOWING RELATIONSHIP BETWEEN LAND TEMPERATURE AND SEA SURFACE TEMPERATURE FOR THE PACIFIC NORTHWEST

Magnitude of Correlation:				
	0	.00 - .09	4	.40 - .49
	1	.10 - .19	5	.50 - .59
	2	.20 - .29	6	.60 - .69
	3	.30 - .39	7	.70 - .79

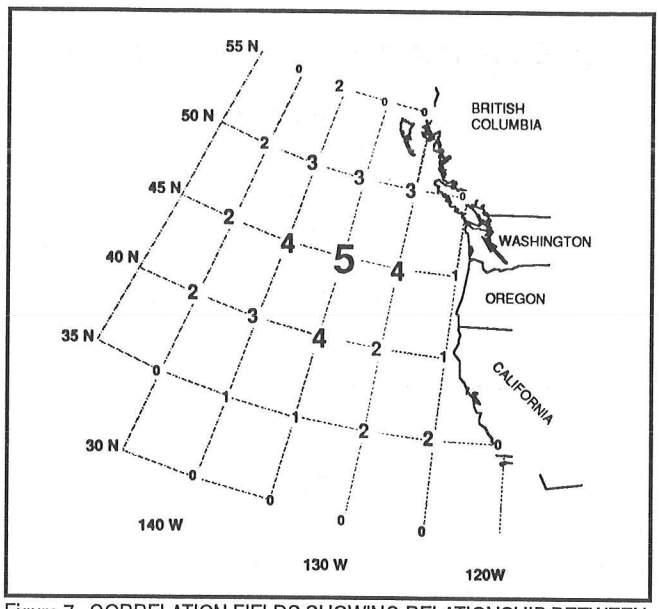

Figure 7. CORRELATION FIELDS SHOWING RELATIONSHIP BETWEEN TREE RING PCA SCORES AND SEA SURFACE TEMPERATURE FOR THE PACIFIC NORTHWEST

Magnitude of Correlation:				
	0	.00 - .09	4	.40 - .49
	1	.10 - .19	5	.50 - .59
	2	.20 - .29	6	.60 - .69
	3	.30 - .39	7	.70 - .79

Tree Growth and Winter Climate

Chronologies used to model winter temperature at the Amphitrite Point lighthouse shore station were ring-width time series from northern California (SNO), Washington State (FPC), Vancouver Island (ANG), and the Gulf of Alaska (NK). Tree-ring widths show a strong positive correlation with winter temperatures (Figure 8). Both the average winter (December-February) temperature series and the tree-ring data were prewhitened prior to PCA regression. The four ring-width chronologies together explain 41% of the variance in winter temperature for the full 44-year calibration period (Figure 9).

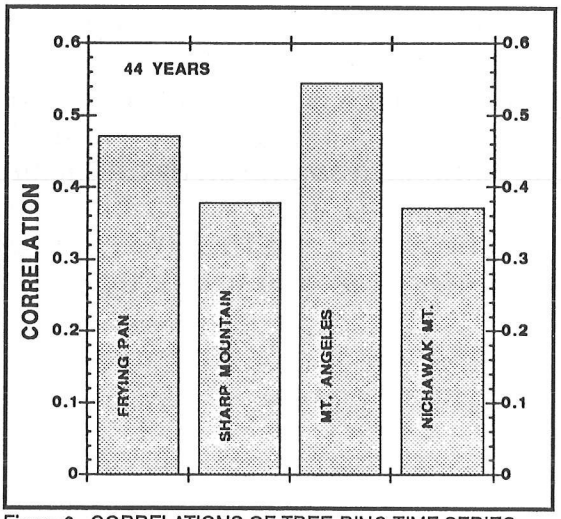

Figure 8. CORRELATIONS OF TREE-RING TIME SERIES AND 44 YEARS OF OBSERVED WINTER SEA SURFACE TEMPERATURE FROM AMPHITRITE POINT, VANCOUVER ISLAND

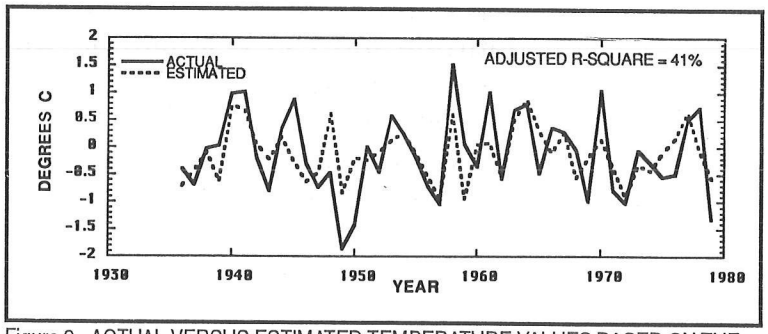

Figure 9. ACTUAL VERSUS ESTIMATED TEMPERATURE VALUES BASED ON THE FOUR CHRONOLOGIES IN FIGURE 8.

Ring-width data are also strongly correlated with shipboard winter sea surface temperatures. The Frying Pan Creek ring-width chronology (Table 1; Graumlich 1985), included in the analysis above, shows strong correlations with winter sea surface temperatures, with the center of correlation just off the northwest Washington coast at 50°N latitude and 130°W longitude (Figure 10).

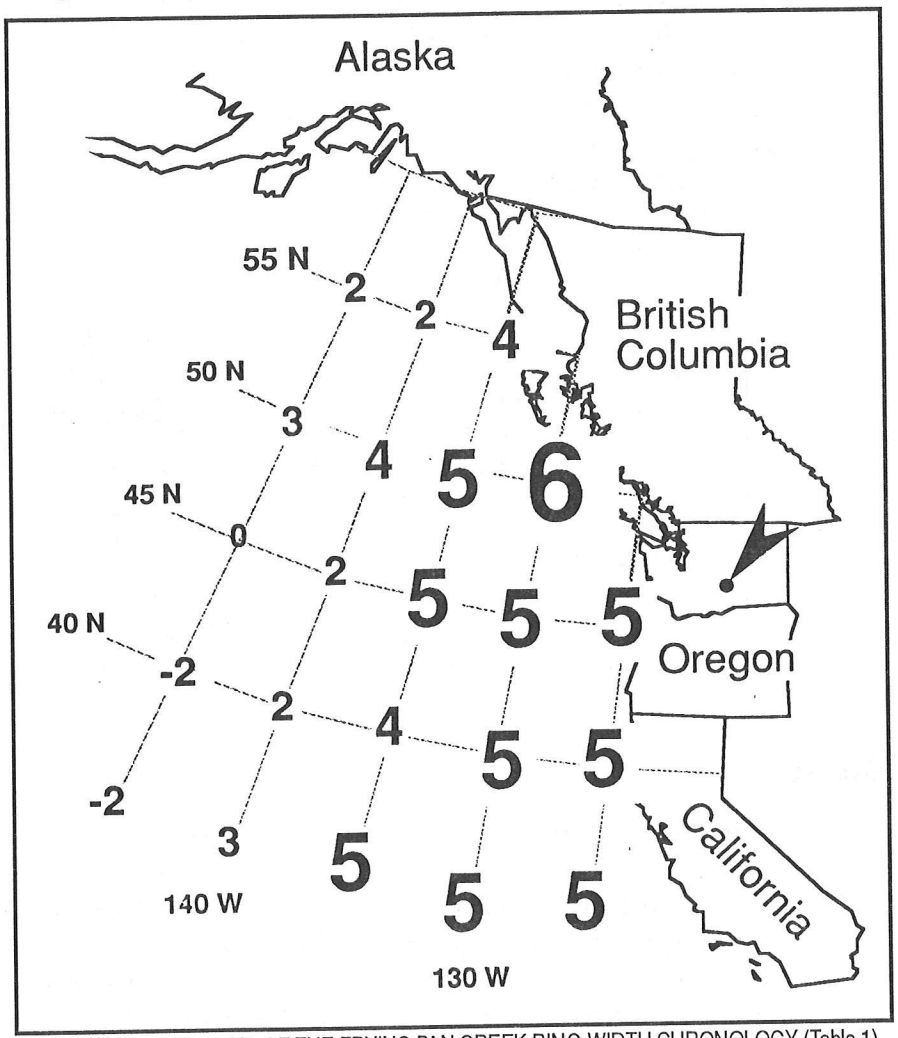

Figure 10. CORRELATIONS OF THE FRYING PAN CREEK RING-WIDTH CHRONOLOGY (Table 1) AND WINTER SEA SURFACE TEMPERATURE VALUES

Magnitude of Correlation:				
	0	.00 - .09	4	.40 - .49
	1	.10 - .19	5	.50 - .59
	2	.20 - .29	6	.60 - .69
	3	.30 - .39	7	.70 - .79

In addition to the potential of tree-ring data in coastal regions for reconstructing temperature changes, pressure variability is also recorded in the tree-ring record. The Aleutian Low is a major feature influencing circulation in the Northeast Pacific, especially during the winter (Namias *et al* 1988; Emery and Hamilton 1985). Modeling the Aleutian Low with tree rings using the Aleutian Low index was explored by Buckley *et al* (1992). Here we compare three ring-width chronologies with the PAC index of Rogers (1990). A strong Aleutian Low (higher PAC index) is associated with a near-shore climate influenced by warm subtropical water. During times of weaker lows (lower PAC index), cooler waters

dominate as northward flow of warmer waters is inhibited. The strength of this low pressure system is most pronounced during winter and spring. Thus the climatic link between trees and pressure variations is that warmer temperatures are associated with a strong Aleutian Low that is, in turn, favorable for tree growth.

The average of winter and spring (December-May) PAC values were used in modeling. In correlations for the RGL Alaskan chronology (0.45) and the California series (SNO, 0.39), the PAC is negatively correlated with the Nevada chronology (PTS, –0.36). After prewhitening, these three chronologies together explain 38% of the variance in the PAC for an 81-year calibration period (Figure 11).

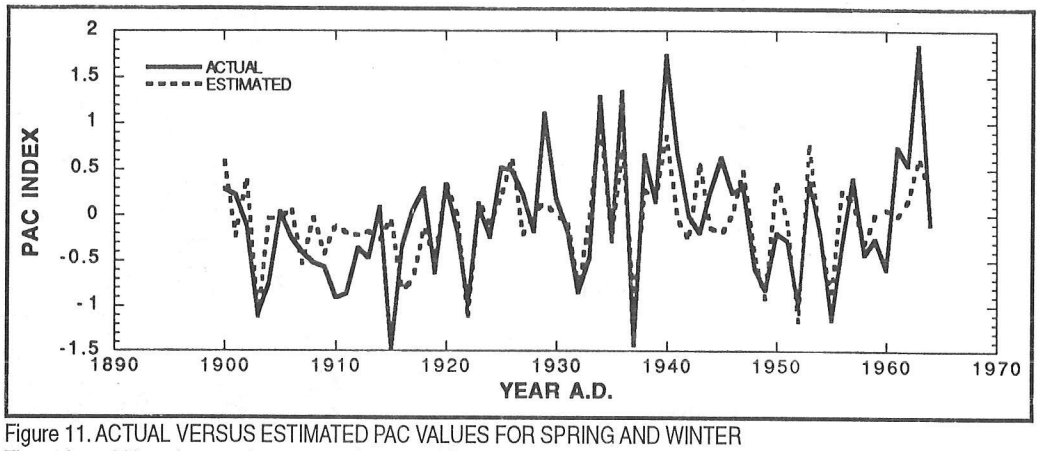

Figure 11. ACTUAL VERSUS ESTIMATED PAC VALUES FOR SPRING AND WINTER
Three ring-width series together account for 38% of the variance over the 81-year calibration period.

Conclusions

Summer temperature reconstructions presented here are the first temperature series from the Pacific Northeast sector that are based only on coastal and near-coastal tree-ring sites. These well-verified models based on ring-width and maximum latewood density chronologies provided the strongest records of temperature change in our analyses. In addition to the tree rings as a record of land temperature change, tree ring comparisons with sea surface temperatures suggest that tree growth variations reflect oceanic as well as atmospheric conditions.

Ring-width chronologies from the Northeast Pacific can provide information related to winter temperature and pressure change in the region. Updating existing chronologies and adding new chronologies could lead to rigorous reconstruction of land temperatures as well as sea surface temperatures from coastal stations (such as Amphitrite Point) in addition to sea surface temperature records from ship observations.

The relationship between tree growth and sea level pressure variability patterns such as the PAC suggests that tree rings can potentially extend the record of sea level pressure changes in the Northeast Pacific. Continued sampling in subarctic coastal areas will yield greater coverage for improved pressure reconstructions.

Acknowledgments

The National Science Foundation's Division of Polar Programs Grant DPP-8922696 to P.E. Calkin supported research that provided Alaskan ring-width chronologies. National Science Foundation, Division of Atmospheric Sciences Grants ATM89-15353 and ATM94-06732 to G.C. Jacoby and R.D. D'Arrigo and a Lamont-Doherty Post-Doctoral Fellowship to G. Wiles are gratefully acknowledged.

References

Blasing, T.J., and H.C. Fritts. 1975. Past climate of Alaska and northwestern Canada as reconstructed from tree-rings. Pages 48-58 in *Climate of the Arctic.* G. Weller and A.A. Bowling, editors. 24th Alaska Science Conference, Geophysical Institute, University of Alaska at Fairbanks.

Blasing, T.J., and H.C. Fritts. 1976. Reconstructing past climatic anomalies in the North Pacific and western North America from tree-ring data. *Quaternary Research* 5:563-579.

Box, G.E.P., and G.M. Jenkins. 1970. *Time Series Analysis: Forecasting and Control.* Holden-Day, San Franscisco.

Briffa, K.R., P.D. Jones, F.H. Schweingruber. 1992. Tree-ring reconstructions of summer temperature patterns across western North America since 1600. *Journal of Climate* 5:735-754.

Buckley, B.M., R.D. D'Arrigo, G.C. Jacoby. 1992. Tree-ring records as indicators of air-sea interaction in the northeast Pacific sector. Pages 35-45 in *Proceedings of the Eighth Annual Pacific Climate (PACLIM) Workshop, March 10-13, 1991.* K.T. Redmond, editor. California Department of Water Resources, Interagency Ecological Studies Program Technical Report 31.

Cayan, D.R. 1980. Large-scale relationships between sea surface temperature and surface air temperature. *Monthly Weather Review* 108:1293-1301.

Chelton, D.B., and R.E. Davis. 1982. Monthly sea-level variability along the west coast of North America. *Journal of Physical Oceanography* 12:757-784.

Cook, E.R., and L.A. Kairiukstis. 1990. *Methods of Dendrochronology.* Kluwer Academic Publishing, Dordrecht. 394 pp.

Cook, E.R., and K. Peters. 1981. The smoothing spline: a new approach to standardizing forest interior tree-ring width series for dendroclimatic studies. *Tree-Ring Bulletin* 41:45-54.

Douglas, A.V. 1980. *Geophysical Estimates of Sea Surface Temperatures Off Western North America since 1671.* CALCOFI Report 21:102-112.

Douglas, A.V., D.R. Cayan, J. Namias. 1982. Large-scale changes in North Pacific and North American weather patterns in recent decades. *Monthly Weather Review* 110:1851-1862.

Emery, W.J., and K. Hamilton. 1985. Atmospheric forcing of interannual variability in the northeast Pacific Ocean, connections with El Niño. *Journal of Geophysical Research* 90:857-868.

Francis, R.C. 1992. Climate change and salmonid production in the North Pacific Ocean. Pages 33-43 in *Proceedings of the Ninth Annual Pacific Climate (PACLIM) Workshop.* K.T. Redmond and V.L. Tharp, editors. California Department of Water Resources, Interagency Ecological Studies Program Technical Report 34.

Francis, R.C., and T.H. Sibley. 1991. Climate change and fisheries: What are the real issues? *The Northwest Environmental Journal* 7:295-307.

Fritts, H.C. 1976. *Tree Rings and Climate.* Academic Press, New York. 567 pp.

Gordon, G.A., and S.K. LeDuc. 1981. *Verification Statistics for Regression Models*. Seventh Conference on Probability and Statistics in Atmospheric Sciences, Monterey, CA, USA.

Graumlich, L. 1985. *Long-Term Records of Temperature and Precipitation in the Pacific Northwest Derived from Tree Rings*. PhD Thesis, University of Washington. 198 pp.

Mysak, L.A. 1986. El Niño, interannual variability and fisheries in the northeast Pacific Ocean. *Canadian Journal of Fisheries and Aquatic Sciences* 43:464-497.

Namias, H.J., Y. Xiaojun, D.R. Cayan. 1988. Persistence of North Pacific sea surface temperature and atmospheric flow patterns. *Journal of Climate* 1:682-703.

Roden, G.I. 1989. Analysis and interpretation of long-term climatic variability along the west coast of North America. Pages 93-111 in *Aspects of Climate Variability in the Pacific and the Western Americas*. D.H. Peterson, editor. Geophysical Monograph 55, American Geophysical Union, Washington DC.

Rogers, J.C. 1990. Patterns of low-frequency monthly sea level pressure variability (1899-1986) and associated wave cyclone frequencies. *Journal of Climate* 3:1364-1379.

Schweingruber, F.H., K.R. Briffa, P. Nolger. 1993. A tree-ring densitometric transect from Alaska to Labrador: Comparison of ring-width and maximum-latewood-density chronologies in the conifer belt of northern North America. *International Journal of Biometeorology* 37:151-169.

Ware, D.M. 1991. Climate, predators, and prey: Behavior of a linked oscillating system. Pages 279-291 in *Long-Term Variability of Pelagic Fish Populations and Their Environment*. T. Kawalski, editor. Pergamon Press, Tokyo.

Xiangding, W., and J.M. Lough. 1987. Estimating north Pacific summer sea-level pressure back to 1600 using proxy climate records from China and North America. *Advances in Atmospheric Sciences* 4:74-84.

Reconstruction of Aridity for the Sierra de la Laguna, Baja California Sur, Mexico

Sara Díaz, Laura Arriaga, Cesar Salinas, and Daniel Lluch

Introduction

A well-documented history of past climatic conditions is needed to understand and resolve some ecological problems, but the existing climatological records are too short to detect long-term climatic variability and changes. Some trees, such as pines, produce annual tree rings with different widths depending on prevailing environmental conditions, such as climate. Tree-ring analysis of long-lived trees can be used to estimate past variations in climate.

The principal aim of this study is to reconstruct aridity for the southern portion of the Baja California Peninsula, by means of dendroclimatologic techniques.

The study was carried out in the Sierra de la Laguna, a mountain range in the southern part of the Baja California Peninsula (Figure 1). The altitudinal range of the Sierra de la Laguna shows marked climatic differences, as well as life forms, different from the rest of the state. At higher altitudes are the only oak-pine woodlands of the state where an endemic conifer, *Pinus lagunae*, grows. This species was the subject of the present study.

Methodology

Within the Sierra de la Laguna oak-pine forest, 80 pines were selected to obtain two increment cores from each tree with a standard increment borer. Dendrochronology procedures and techniques for analyzing radial growth in trees included the following steps:

- Increment core samples were cross-dated by the skeleton plot to synchronize variations in ring width of the different trees and assign them to the correct time sequence.
- Ring widths were measured on a sliding-stage micrometer. Measurements were transformed to growth indices by fitting curves to the series and dividing the ring widths by the values of the fitted curves.
- A master dendrochronology time series was created by simply averaging the core indices with a computer program (Holmes 1992).

In: C.M. Isaacs and V.L. Tharp, Editors. 1995. *Proceedings of the Eleventh Annual Pacific Climate (PACLIM) Workshop, April 19-22, 1994.* Interagency Ecological Program, Technical Report 40. California Department of Water Resources.

The regional instrumental climatic series was obtained from Díaz *et al* (1994). They based the analysis on climatologic recordings of total monthly rainfall and monthly mean temperatures of stations in low and middle altitudes of the Sierra de la Laguna, at an average of 451 meters above sea level. The aridity index was calculated from these data using Martonne's (1926) formula. In addition, from the climatologic data of Díaz *et al* (1994), we constructed annual instrumental rainfall and temperature time series.

Dendrochronologic and aridity data were compared over a period of time called the "calibration period". With the resulting model, aridity was reconstructed from dendrochronologic data for the pre-instrumental period.

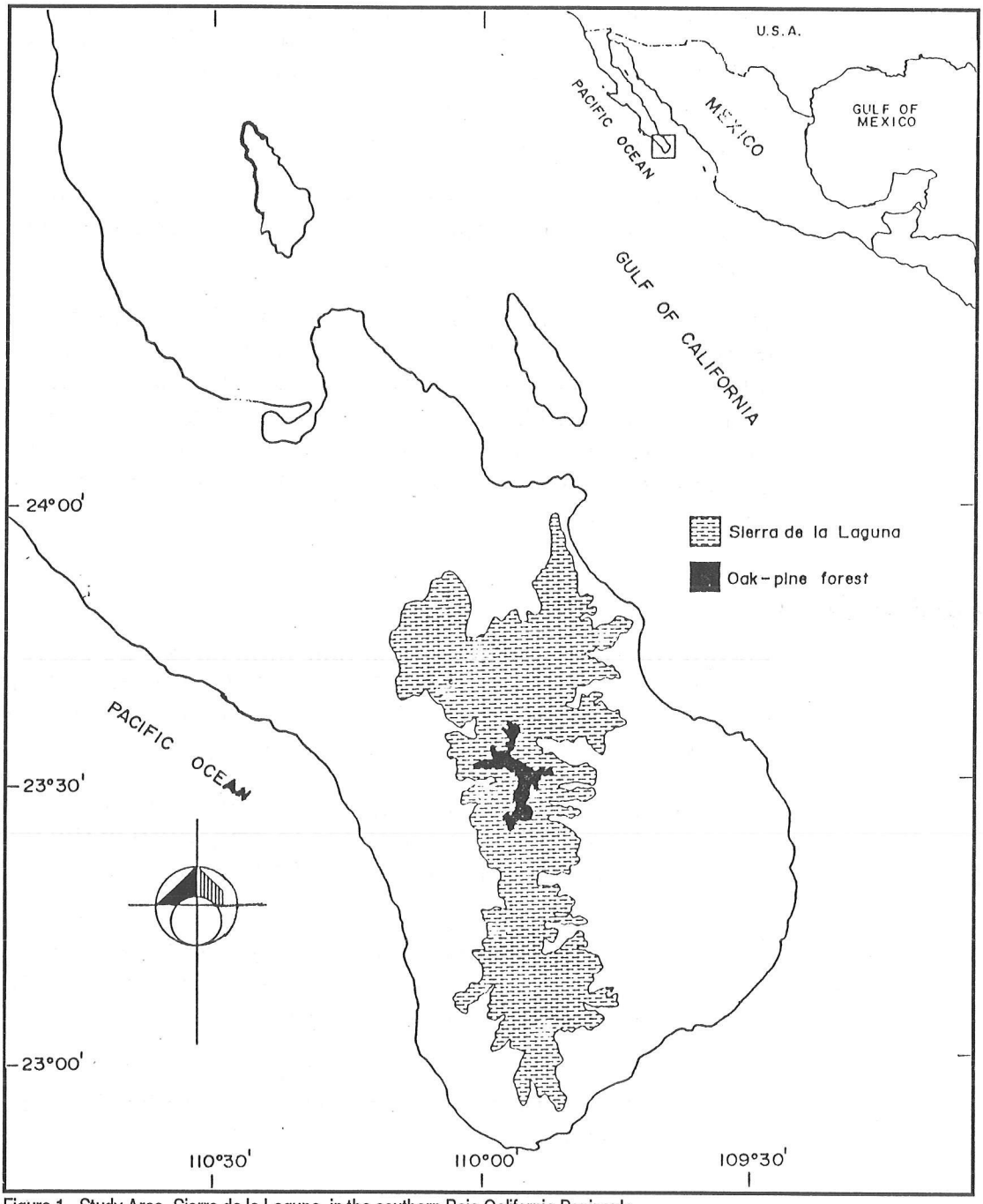

Figure 1. Study Area, Sierra de la Laguna, in the southern Baja California Peninsula.

Results and Discussion

For the calibration period, the dendrochronology time series and estimated rainfall and temperature time series were used to search for possible relationships between tree growth and meteorological variables. Since linear regression models were to be used, series were first tested for normality. For the aridity series, the five upper outliers deviated significantly from the general fitted normal distribution (Figure 2). These values were replaced with their corresponding five terms unweighted moving averages. No other transformation of data was done.

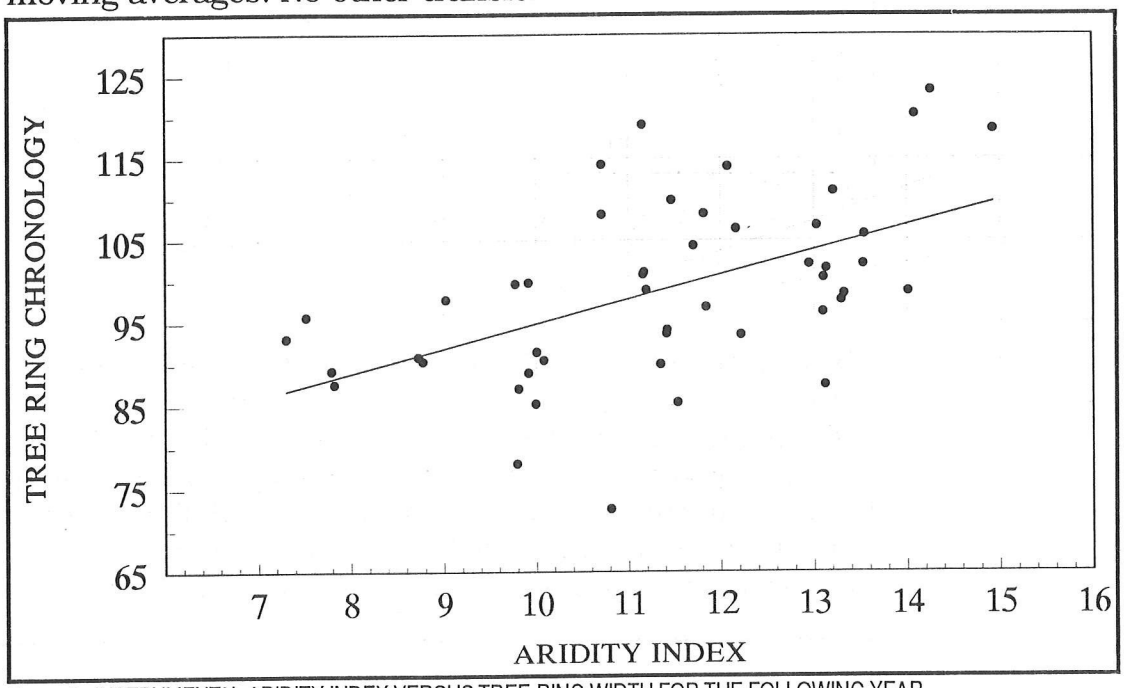

Figure 2. INSTRUMENTAL ARIDITY INDEX VERSUS TREE-RING WIDTH FOR THE FOLLOWING YEAR
The equation for the best-fit regression line is Y = 2.988X + 65; r = 0.523 (**).

Single and multiple regression between dendrochronology (dependent variable) and temperature, precipitation, and aridity for the previous year (independent variables) were tested. Only precipitation and aridity (r=0.523) were significantly correlated with the dendrochronology. However, multiple correlation showed that the two variables were highly redundant (r=0.524). The regression coefficient (beta) for precipitation was not significant under the multiple linear regression model. Thus, simple linear regression between aridity and dendrochronology was selected for the reconstruction.

Since the applied regression model assumes a linear relationship between normally distributed variables, standardized residuals were tested for these assumptions using normal probability plots (residuals *vs* expected normal value). No indications were found of severe violations to the model assumptions. In addition, we plotted residuals *vs* deleted residuals (*ie*, the residual for a particular value when regression is performed without that value; Figure 3). Regression was not seriously biased by outliers, since there is not a great difference between residual and deleted residual for any value.

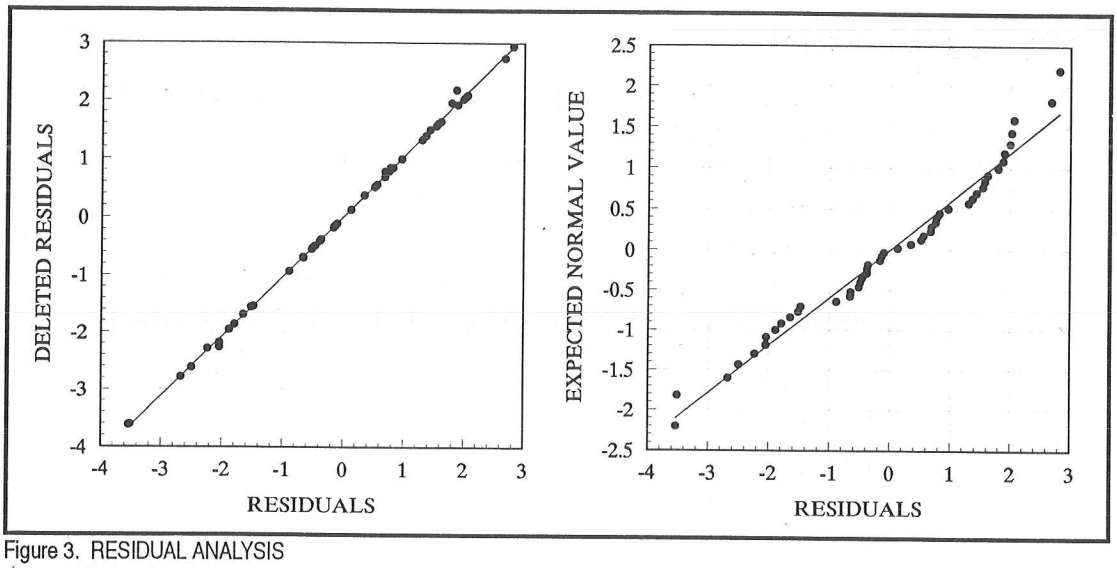

Figure 3. RESIDUAL ANALYSIS
Left: Residuals versus Deleted Residuals: Regression is not seriously biased by outliers.
Right: Normal Probability of Residuals: The assumption of a linear relationship between variables and the normal underlying distributions seems reasonable.

The aridity index was calculated from the regression equation, and these values were compared to the actual aridity index values. For 1940 to 1989 (Figure 4), the dendrochronology/aridity relationship was not very close. However, aridity reconstruction at an interdecadal scale is promising. The upward trend between the mid-1940s and the early 1960s, the downward trend up to 1970, the upward trend up to 1983, and the downward trend up to 1989 are all evident in both series.

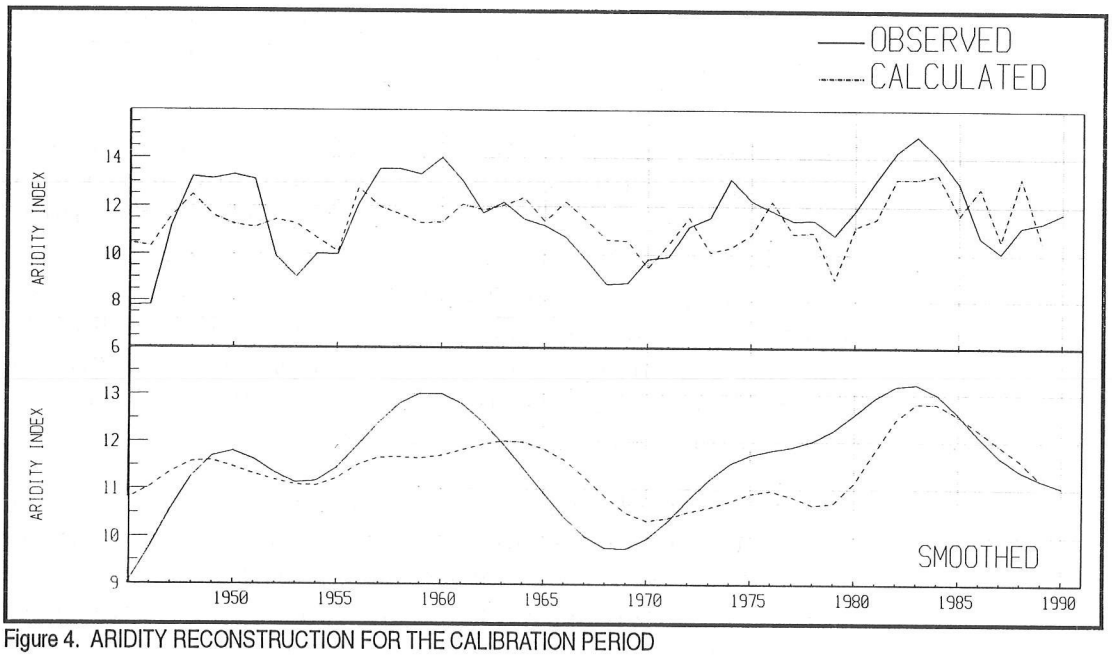

Figure 4. ARIDITY RECONSTRUCTION FOR THE CALIBRATION PERIOD

The aridity reconstruction series shows some interesting features:

- From 1810 to 1890, a period of high variability and high aridity occurred, interrupted by a few years of very low aridity during the mid-1840s.
- From 1900 to the mid-1950s, there was a remarkably stable period of intermediate aridity.
- Recent years have been highly variable, with minimum aridity in the mid-1960s, a maximum during the early 1970s, and another minimum during the mid-1980s.

Conclusions

Dendrochronology does not correlate highly with aridity at an interannual scale. Possible reasons include:

- There are no long precipitation/temperature records for the woodland area, so nearby meteorological stations had to be used. These stations are at much lower altitude than the woodland area.
- Although water availability should be a limiting factor on tree growth, the biological response to interannual variability in aridity may be "filtered" if physiological compensation is to be expected. If so, dendrochronology may reflect sustained trends much better than interannual variations, as observed.
- Dendrochronology is much more closely correlated with aridity at an interdecadal scale. Accordingly, we reconstructed aridity for the last two centuries based on dendrochronology data (Figure 5).
- Recent-year trends for the reconstructed aridity are also present in the meteorological records for nearby areas. It is concluded that the species *Pinus lagunae* is sensitive to climatic changes.

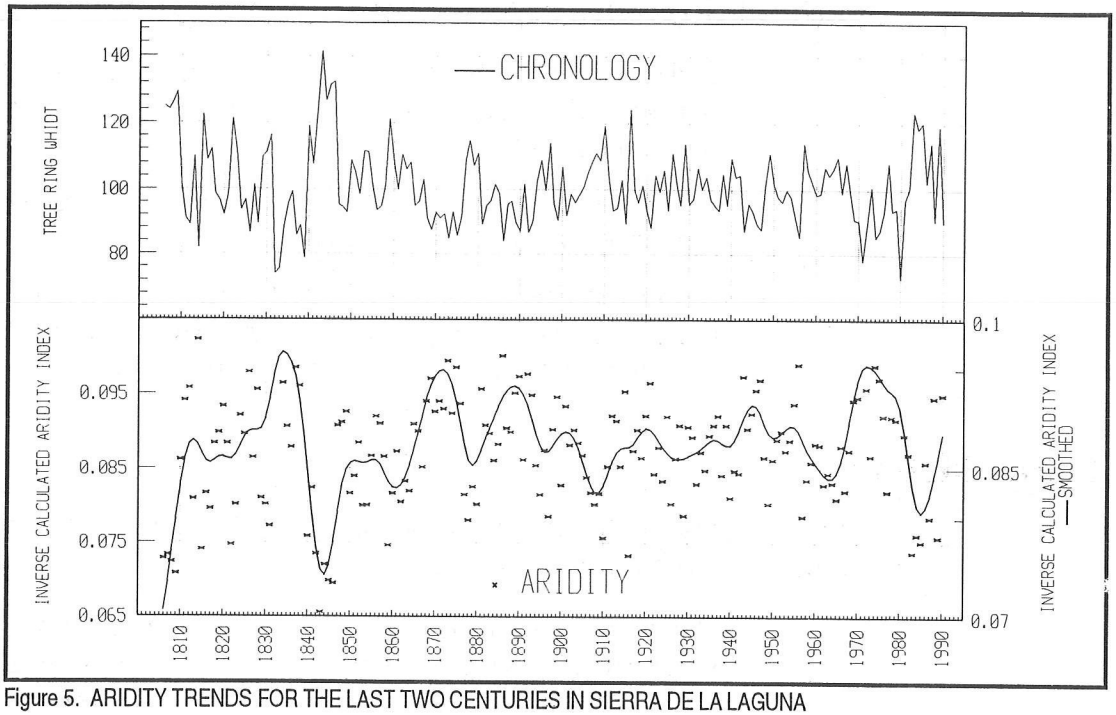

Figure 5. ARIDITY TRENDS FOR THE LAST TWO CENTURIES IN SIERRA DE LA LAGUNA

References

Díaz, C.S., C. Salinas-Zavala, L. Arriaga. 1994. An interannual aridity series for the Sierra de la Laguna, BCS, México. *Mountain Research and Development.* 14(2):137-146.

Holmes, R.L. 1992. *Dendrochronology Program Library.* Tree-Ring Research. University of Arizona.

Martone, E. 1926. Areísme et indice d'aridity. *Competes Rendus de L'Acad. des. Sci. Paris.* 182:1395-1398.

South American Streamflow and the Extreme Phases of the Southern Oscillation

Thomas C. Piechota, John A. Dracup, Ernesto F. Brown,
Tom McMahon, and Francis Chiew

Introduction

This study investigates the extent of the affect of the El Niño/Southern Oscillation on South American streamflow. The response of South American precipitation and temperature to the extreme phases of ENSO (El Niño and La Niña events) is well documented (*eg*, Ropelewski and Halpert 1987, Rogers 1988, Kiladis and Diaz 1989, Tapley and Waylen 1990); but the response of South American hydrology has been barely studied (Waylen and Caviedes 1990, Mechoso and Iribarren 1992). Such paucity of research contrasts sharply with that available on the response of North American streamflow to ENSO events (*eg*, Kahya and Dracup 1993, Cayan and Webb 1993, Redmond and Koch 1991).

This present study is based on a hydrologic study by Kahya and Dracup (1993) of North America streamflow and, with their techniques, examines South American streamflow. A schematic of our research approach is presented in Figure 1. In South America, regions with a coherent response to ENSO are identified, and by computing and analyzing the shift

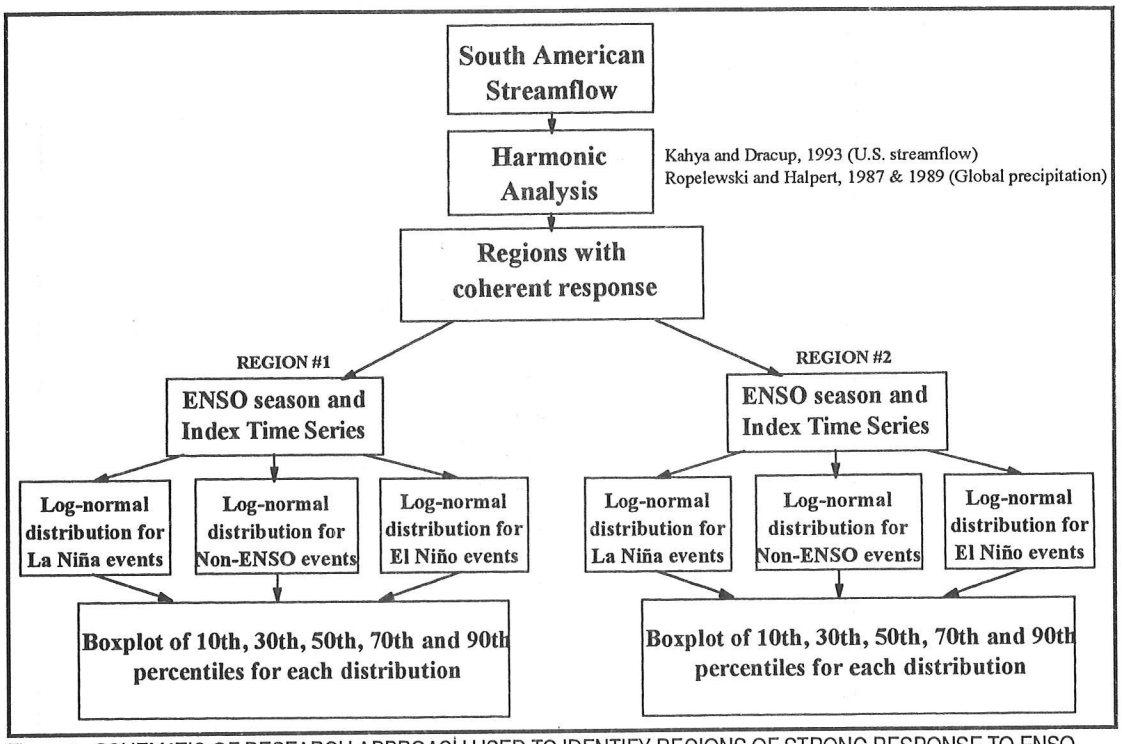

Figure 1. SCHEMATIC OF RESEARCH APPROACH USED TO IDENTIFY REGIONS OF STRONG RESPONSE TO ENSO

In: C.M. Isaacs and V.L. Tharp, Editors. 1995. *Proceedings of the Eleventh Annual Pacific Climate (PACLIM) Workshop, April 19-22, 1994.* Interagency Ecological Program, Technical Report 40. California Department of Water Resources.

in the probability distribution for La Niña, non-ENSO, and El Niño events, we are able to represent and chart the South American streamflow anomalies.

Data

The impetus for this research was a University of California Pacific Rim Workshop held at UCLA in December 1993. At this workshop, hydrologists from several Pacific Rim countries gathered to study the influence of ENSO on Pacific Rim streamflow. Each participant brought streamflow data collected from his region, which augmented the global runoff dataset of McMahon *et al* (1992), the database for this study.

Data on 95 streamflow stations in South America and Panama were compiled (Figure 2). These data represent monthly runoff volumes with records of varying lengths, although most cover periods of 30 to 40 years. The La Niña and El Niño years are based on definitions presented in Ropelewski and Halpert (1989) and Rasmusson and Carpenter (1983).

Figure 2. GEOGRAPHIC DISTRIBUTION OF THE 95 STREAMFLOW STATIONS
Data for each station consist of monthly runoff volumes.

Harmonic Analysis

Using harmonic analysis, we examined the tendency for a streamflow anomaly to occur biennially during ENSO events. We explain this biennial occurrence as the response of streamflow to ENSO events as they move from positive to negative (above or below the norm), or vice versa, within a 2-year period. Two notable studies have incorporated this biennial tendency into their methods for examining the forcings of ENSO: Ropelewski and Halpert (1987) and Kahya and Dracup (1993).

Our research proceeded as follows. First, original records are transformed into percentiles based on a log-normal distribution for each month at each station. With this transformation, all streamflow records having a different original mean and variance are put into an equal basis. A 2-year period is chosen to represent a lifetime period for the ENSO event.

Using common conventions, the ENSO year is designated by (0), the year before is (-), and the year after is (+). A 24-month percentile composite, based on the ENSO episodes, is then established for each individual station. The first harmonic extracted from such a composite is represented as a harmonic vector, which is mapped, identifying core regions of spatially coherent streamflow responses to the ENSO forcing. The amplitude and phase of a harmonic vector refer to the respective strength and time of the response. The statistical significance of the harmonic amplitude and phase is assigned by use of Schuster's test for an autocorrelated series. The degree of significance of each station, or the probability that the first harmonic representation of the El Niño composite is produced by chance, is measured by Schuster's quantitative test of significance. Within each region, the vectorial coherence is found by computing the ratio of the vector mean to the scalar mean. The concept of coherence is defined and discussed in Kahya and Dracup (1993).

Figure 3 presents the first harmonic vectors for the 95 streamflow stations. Regions that have similar phase and amplitude (*ie*, areas showing vectors with similar length and pointing in the same direction) are identified for further analysis. Four regions are identified: North-Central Chile (NCH); South-Central Chile (SCH); Guyana (GUY); and Panama (PAN).

Within each of these regions, the normalized streamflow is aggregated to form a 36-month composite, with the middle 12 months still representing the ENSO year. The aggregate composite then identifies a season with a persistent streamflow anomaly; that is, a season in which the streamflow index is consistently above or below the 50th percentile value. Figure 4 is the aggregate composite for the SCH region. In this composite, a consistent negative (dry) anomaly in the latter part of year (–) is followed by a positive (wet) anomaly in the latter part of year (0).

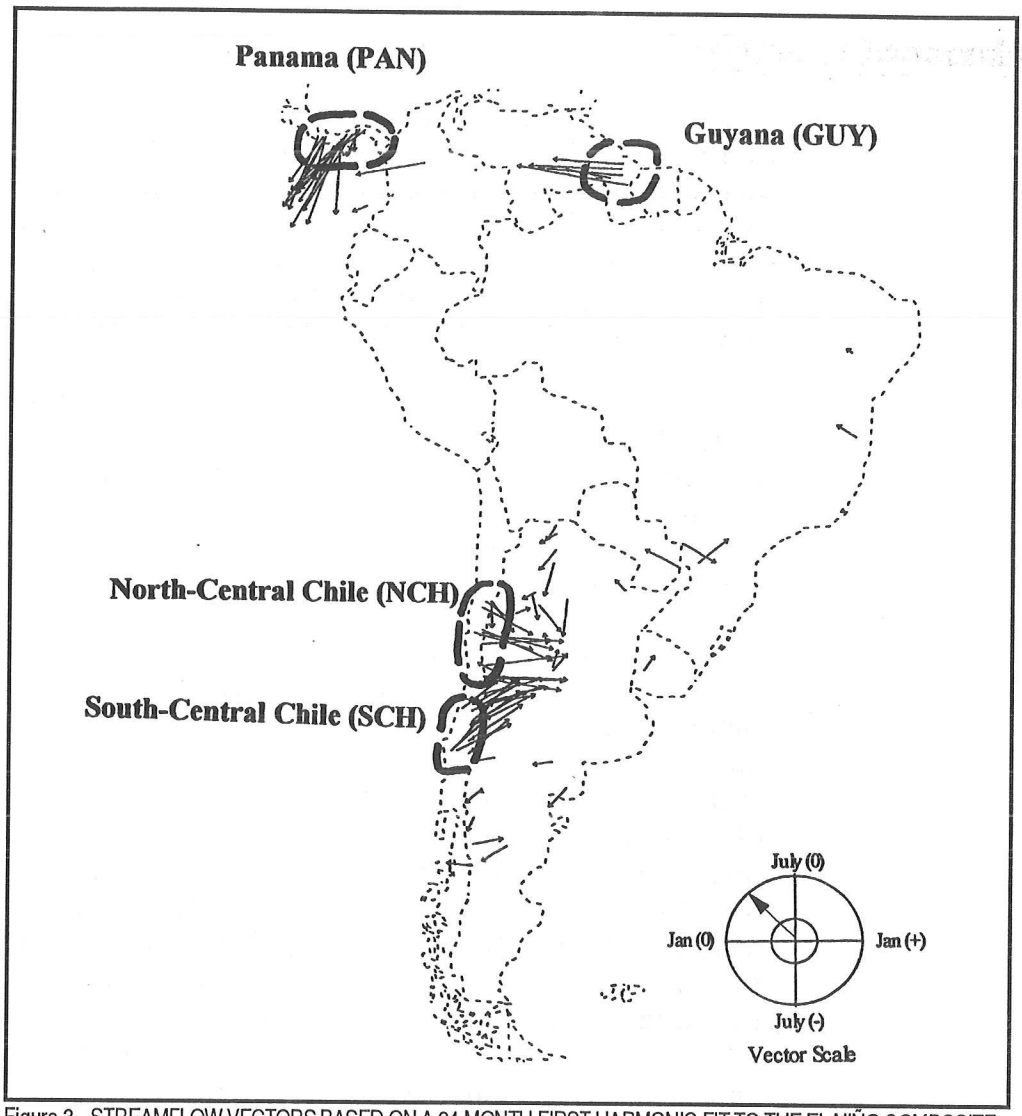

Figure 3. STREAMFLOW VECTORS BASED ON A 24-MONTH FIRST HARMONIC FIT TO THE EL NIÑO COMPOSITE
Vector orientation is represented by the harmonic dial. Regions with a coherence value greater than 0.80 are outlined.

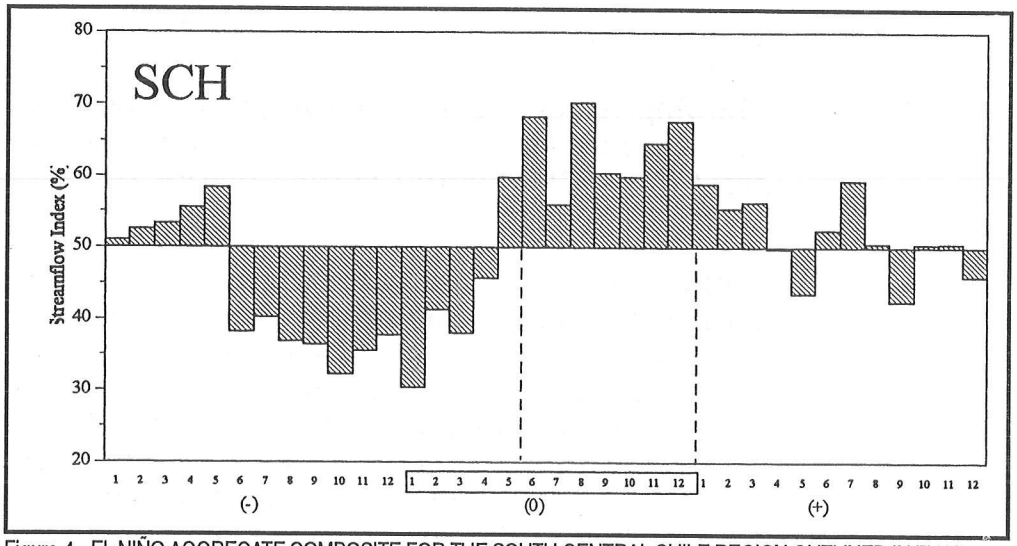

Figure 4. EL NIÑO AGGREGATE COMPOSITE FOR THE SOUTH-CENTRAL CHILE REGION OUTLINED IN FIGURE 3.
The 36-month composite starts at Jan(–) and ends at Dec(+). Dashed lines identify the season that has a consistent anomaly, above or below the mean.

The second anomaly in the 36-month composite is identified as the El Niño season. Using this season, an index time series is formed to observe the consistency of the response in relation to the entire time series (Figure 5). Eight of the nine El Niño events, as identified by the dark bars, are associated with a wet streamflow anomaly in the SCH region. Three of the largest streamflow anomalies occurred during El Niño years. This represents a strong relationship between ENSO and extreme streamflow events. A summary of the results for each region is provided in Table 1.

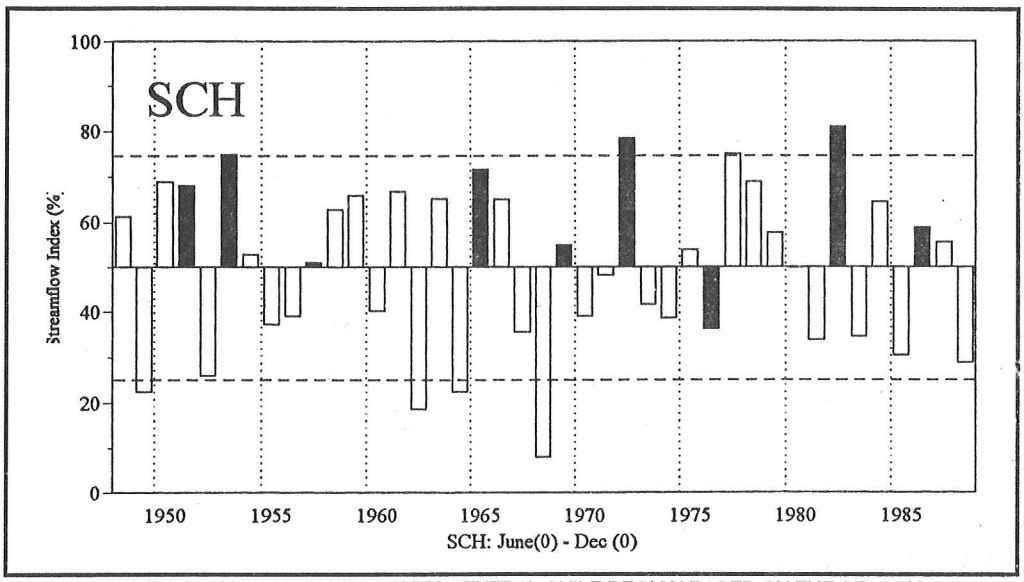

Figure 5. INDEX TIME SERIES FOR THE SOUTH-CENTRAL CHILE REGION BASED ON THE SEASON DETECTED IN FIGURE 4.
El Niño years are represented by dark bars. Horizontal dashed lines represent the upper (90%) and lower (10%) limits of the distribution based on the ranked data.

Table 1
PROPERTIES OF THE FOUR REGIONS IDENTIFIED USING HARMONIC ANALYSIS

(0) refers to the El Niño year; (+) refers to the following year.

Candidate Region	Number of Stations	Degree of Significance DOS <0.15	El Niño Signal	El Niño Season	Consistency
Panama (PAN)	23	16	Dry	Apr(0)-Dec(0)	4 of 5
Guyana (GUY)	5	5	Dry	Aug(0)-Mar(+)	5 of 6
South-Central Chile (SCH)	19	19	Wet	Jun(0)-Dec(0)	8 of 9
North-Central Chile (NCH)	13	13	Wet	Dec(0)-Jul(+)	6 of 9

Seasonal Cycle

In assessing the impact of ENSO, timing of the maximum anomaly in relation to the annual cycle is also important. Does the anomaly occur during the normal wet or dry period? This is answered by plotting the normal annual cycle along with the corresponding annual cycle that occurs during El Niño and La Niña events (Figure 6). For the SCH region, the annual cycle is enhanced during the El Niño events at the time of

maximum runoff (July-September). Conversely, the annual cycle is depressed at the time of maximum runoff during La Niña events. Finally, normal conditions prevail in the year following the El Niño event.

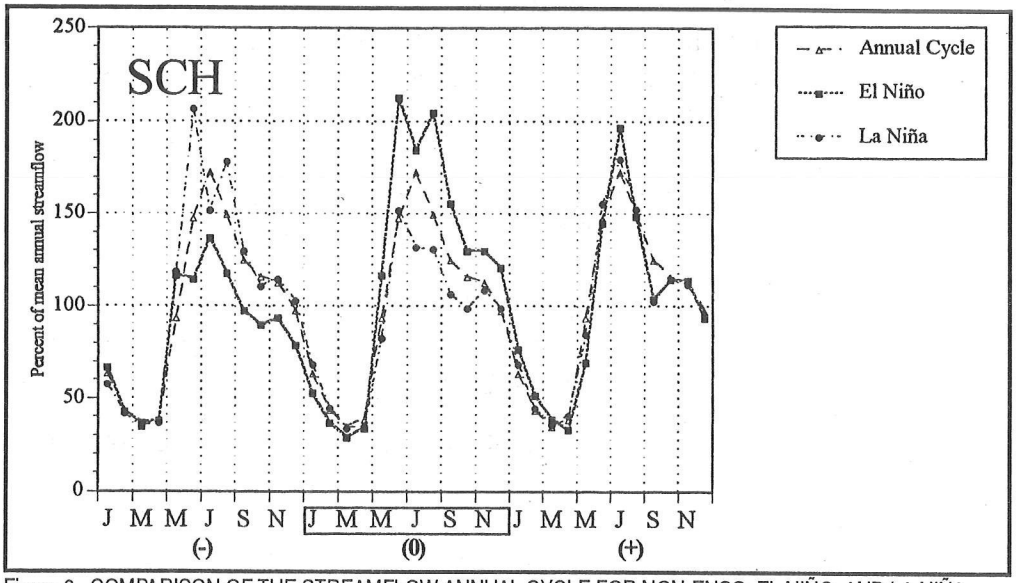

Figure 6. COMPARISON OF THE STREAMFLOW ANNUAL CYCLE FOR NON-ENSO, EL NIÑO, AND LA NIÑA CONDITIONS IN THE SOUTH-CENTRAL CHILE REGION.
Values are a percentage of mean annual streamflow.

Shift in the Probability Distributions

After each region has been identified through harmonic analysis, it is quantified for the ENSO signal by computing the expected streamflow value based on the percentile anomaly. Because of the variability of the strength of ENSO events and the inherent variability in streamflow, computed results may be misleading. The ENSO signal may be more usefully measured by the shift in the probability distribution of streamflow during La Niña, non-ENSO, and El Niño events. The shift is made by breaking our original streamflow data into three sub-sets corresponding to the different conditions in the tropical Pacific. The shift in the probability distribution can be observed by computing the 10th, 30th, 50th, 70th, and 90th percentiles for each sub-set and by presenting the values in a boxplot. Figure 7 displays the shift in the probability distribution for streamflow stations in three of the four regions. This method of analysis is similar to that used in the study by Halpert and Ropelewski (1994); that study quantified the impact of ENSO on regions identified throughout the world in their earlier study (Ropelewski and Halpert 1987).

We offer one interpretation for the shift of the Rio Maule Armerilla, located in the SCH region (Figure 7): the median (50th percentile) streamflow during El Niño years is shifted to the 75th percentile of the non-ENSO distribution. This means there is a 75% probability that the Rio Maule Armerilla will receive non-ENSO median runoff during El Niño years. Conversely, the median during La Niña years is shifted to the 30th percentile of the non-ENSO distribution. Only 30% probability exists that

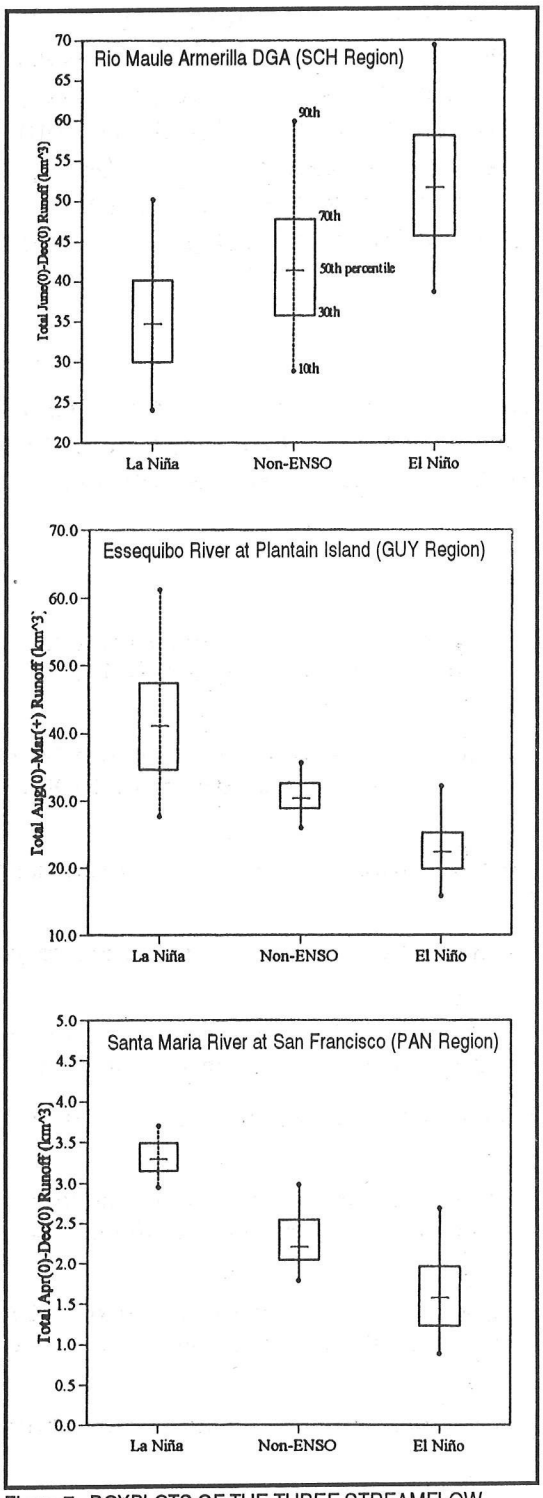

Figure 7. BOXPLOTS OF THE THREE STREAMFLOW DISTRIBUTIONS FOR LA NIÑA, NON-ENSO, AND EL NIÑO YEARS AT RIO MAULE ARMERILLA, ESSEQUIBO RIVER, AND SANTA MARIA RIVER
Short horizontal line inside box represents the 50th percentile.
Top of box represents the 70th percentile.
Bottom of box represents the 30th percentile.
Top of line represents the 90th percentile.
Bottom of line represents the 10th percentile.

the Rio Maule Armerilla will receive non-ENSO median runoff during La Niña years.

The GUY and PAN regions have shifts opposite those of the two Chilean regions (Figure 7). The opposite shift reflects the dry anomaly present during El Niño. The shift is large for the Santa Maria River, in the PAN region. The median value during El Niño years is shifted to the 10th percentile of the non-ENSO distribution. This represents a 10% probability that the Santa Maria River will receive non-ENSO median runoff during El Niño years. The Essequibo River, in the GUY region, has the median value shifted below the 10th percentile of the non-ENSO distribution during El Niño years. The probability of the Essequibo River receiving non-ENSO median runoff during El Niño years is less than 10%.

Conclusions

The response of South American streamflow to extreme phases of the ENSO is observed by using harmonic analysis to identify regions of coherent response. Four regions are identified as having a strong response: SCH, NCH, GUY, and PAN. In two Chilean regions (SCH and NCH) a wet streamflow anomaly occurs during El Niño events. In the GUY and PAN regions, which represent northern South America, a dry streamflow anomaly occurs during El Niño events. This streamflow anomaly coincides with the shift in the probability distribution for the extreme phases of ENSO and non-ENSO conditions.

These results are similar to those of Ropelewski and Halpert (1987), who used precipitation data to identify northeastern South America and Central America as regions with a coherent response to ENSO. Their northeastern South American region has an El Niño season of Jul(0) to Mar(+). This is similar to our GUY region, which has a Aug(0) to Mar(+) season. Our PAN region, with a season of Apr(0) to Dec(0), is similar to their Central America region, which has a Jul(0) to Oct(0) season. Although the area of western South America was not well represented by Ropelewski and Halpert (1987), the study presented here has sufficient data on Chile to identify it also as a coherent region.

The scant availability of data representing all of South America limits this study. The four regions identified here may not be the only areas of South America with a strong response to ENSO; nonetheless, our results are an excellent starting point for exploring the influence of ENSO on South American hydrology. When sufficient data are available covering Brazil, Columbia, Venezuela, Ecuador, Peru, and Bolivia, yet other regions of coherent response to ENSO forcings may be located within South America.

Acknowledgments

This work and the Pacific Rim Workshop (UCLA 1993) are supported by the University of California Pacific Rim Research Center under award MC930526A. The authors thank Mariam Reed for editing this paper.

References

Cayan, D.R., and R.H. Webb. 1993. El Niño/Southern Oscillation and streamflow in the United States. Pages 29-68 in *El Niño: Historical and Paleoclimatic Aspects of the Southern Oscillation*. H.F. Diaz and V. Markgraf, editors. Cambridge University Press.

Halpert, M.S., and C.F. Ropelewski. 1994. Quantifying SO-precipitation relationships. Pages 33-36 in *Proceedings of the 18th Annual Climate Diagnostics Workshop*. U.S. Government Printing Office, Washington, DC.

Kahya, E., and J.A. Dracup. 1993. U.S. streamflow patterns in relation to the El Niño/Southern Oscillation. *Water Resources Research* 29(8):2491-2503.

Kiladis, G.N., and H.F. Diaz. 1989. Global climatic anomalies associated with extremes in the Southern Oscillation. *Journal of Climate* 2:1069-1090.

McMahon, T.A., B.L. Finlayson, A.T. Haines, R. Srikanthan. 1992. *Global Runoff — Continental Comparisons of Annual Flows and Peak Discharges*. Catena Paperback, Cremlingen-Destedt.

Mechoso, C.R., and G.P. Iribarren. 1992. Streamflow in southeastern South America and the Southern Oscillation. *Journal of Climate* 6:1535-1539.

Rasmusson E.M., and T.H. Carpenter. 1983. The relationship between eastern equatorial Pacific sea surface temperatures and rainfall over India and Sri Lanka. *Monthly Weather Review* 111:517-528.

Redmond, K.T., and R.W. Koch. 1991. Surface climate and streamflow variability in the western United States and their relationship to large-scale circulation indices. *Water Resources Research* 27(9):2381-2399.

Rogers, J.C. 1988. Precipitation variability over the Caribbean and tropical Americas associated with the Southern Oscillation. *Journal of Climate* 1:172-182.

Ropelewski, C.F., and M.S. Halpert. 1987. Global and regional scale precipitation patterns associated with the El Niño/Southern Oscillation. *Monthly Weather Review* 115:1606-1626.

Ropelewski, C.F., and M.S. Halpert. 1989. Precipitation patterns associated with the high index phase of the Southern Oscillation. *Journal of Climate* 2:268-284.

Tapley, T.D., and P.R. Waylen. 1990. Spatial variability of annual precipitation and ENSO events in western Peru. *Hydrological Sciences* 35(4):429-446.

Waylen, P.R., and C.N. Caviedes. 1990. Annual and seasonal fluctuations of precipitation and streamflow in the Aconcagus River Basin, Chile. *Journal of Hydrology* 120:79-102.

Sea Surface Temperature and Paleo-El Niño Events in Santa Barbara Basin, AD 1841-1941

Arndt Schimmelmann, Meixun Zhao, Gerald G. Kuhn, Mia J. Tegner

Introduction

Like pages of a "natural coastal diary", successive layers of anoxic varved sediment in the central Santa Barbara Basin have been used by paleoceanographers to reconstruct aspects of past coastal climate. This report focuses on the end of the "Little Ice Age" (15th to 19th century) and on the beginning of this century, a period known to encompass extreme climatic excursions and weather events in the Santa Barbara Basin (Dayton and Tegner 1990; Schimmelmann *et al* 1992) and other parts of Southern California (Kuhn and Shepard 1984). El Niño events are known to disrupt Southern California's coastal ecosystems (Dayton and Tegner 1990) and to cause anomalous weather conditions (Enfield 1989), but El Niño events in Southern California before 1990 have been largely undocumented.

A collective assessment of several independent geochemical parameters is necessary to achieve trustworthy paleo-El Niño reconstructions, because any individual geochemical parameter is responsive to environmental and climatic events in addition to El Niño. Our reconstructions of paleo-El Niño events employ four independently determined geochemical parameters.

- Some of the most valuable data for assessment of global climate change are time series of prehistoric sea surface temperature reconstructed from relative abundances of long-chain alkenone molecules, commonly expressed by the U^K_{37} index, that are preserved in dated ocean sediments (Brassell *et al* 1986; McCaffrey *et al* 1990; Eglinton *et al* 1992; Brassell 1993; Zhao *et al* 1993). An inherent limitation of this method is its seasonal bias toward bloom periods of the alkenone-producing marine algae. Kennedy and Brassell (1992) successfully used alkenone abundances to correlate increases in sea surface temperature in Santa Barbara Basin with El Niño events for much of the 20th century. This report includes the downcore continuation of their work with about annual resolution, to the AD 1830 level, 65 centimeters below the sea floor.

- The stable isotope ratio of total organic carbon (TOC) as an indicator for El Niño events was documented by Schimmelmann and Tegner (1991). Following the onset of an El Niño event in the Santa Barbara

In: C.M. Isaacs and V.L. Tharp, Editors. 1995. *Proceedings of the Eleventh Annual Pacific Climate (PACLIM) Workshop, April 19-22, 1994.* Interagency Ecological Program, Technical Report 40. California Department of Water Resources.

Basin, physical and biological stress on the locally abundant kelp forests liberates large amounts of ^{13}C-enriched kelp biomass. The carbon isotopic signal permeates through the ecosystem and becomes incorporated in the sedimentary TOC of the accumulating varve. However, reconstruction of El Niño events based on carbon stable isotopes is not fully reliable. Carbon isotope responses may be caused by ecological/climatic events unrelated to El Niño events, and kelp forests may not have been abundant in the Santa Barbara Basin at certain time intervals.

- Concentrations of sedimentary components in the Santa Barbara Basin can be converted into fluxes by taking into account the annual varve thickness or annual sedimentation rate. Detailed measurements of the content of total organic carbon in Santa Barbara Basin sediment yield a carbon burial flux that expresses the annual amount of organic carbon delivered to and preserved in the sediment per unit area of ocean floor. The TOC burial flux is independent from dilution by terrigenous lithogenic debris but should be sensitive to large fluctuations of marine productivity. El Niño conditions are characterized by low productivity. The calculated carbon burial is highly variable from one sample (=sediment interval) to another and strongly depends on the chronology. For example, the TOC burial flux of a sample encompassing 8 months of sedimentation would be decreased by 25% if a 10-month time span were adopted. In the process of dating, the cross-correlation between the X-radiographically determined varve boundaries versus the actual sample boundaries bears an uncertainty of a few months. We, therefore, report our TOC burial flux as a 5-point running mean. Accordingly, a rapidly decreasing flux may also be compatible with El Niño conditions.

- Sediment layers deposited during times of cool sea surface temperature frequently contain more water than adjacent layers relating to warmer periods. Cold water conditions are generally associated with increased upwelling, high productivity, and a large flux of porous biogenic material to the accumulating varve. At the same time, the abundant supply of organic carbon to the benthic environment reduces the oxygen content of sub-sill bottom waters and permits the filamentous *Beggiatoa* spp. bacterial mat to flourish at the sediment/water interface. As a result, the accumulating varve is more water-rich in comparison to a varve that accumulated during times of higher sea surface temperature and reduced upwelling. The impact of El Niño conditions on the benthic environment causes a decrease of the water content in the accumulating sediment, sometimes quite abruptly.

We demonstrate that the combined, critically assessed, geochemical evidence is in agreement with historical evidence of weather and El Niño conditions off Southern California.

Materials and Methods

Box cores were recovered from the deep center of the Santa Barbara Basin in 1987 and 1988. The sediment was sampled with about annual resolution and dated using varve-counts and correlation of varve thickness versus dendrochronological data (Schimmelmann *et al* 1990, 1992). Samples used in this study do not include thin gray "turbidites" or flood deposits (Lange *et al*, in press). Weighing of samples before and after freeze-drying permitted calculation of the water content in wet sediment. Samples were stored freeze-dried until aliquots were analyzed for total organic carbon and its carbon stable isotope ratio (Schimmelmann and Tegner 1991). The burial flux of organic carbon was calculated as a running mean over five samples. The determination of alkenone abundances is described by Parry (1993). A few of the sediment samples did not provide the required 0.2 to 0.3 gram of freeze-dried sediment. Sea surface temperature was calculated from the U^{K}_{37} index using Prahl and Wakeham's (1987) equation: $SST\ (°C) = (U^{K}_{37} - 0.039)/0.034$. Analytical precision of alkenone-based sea surface temperature is about $\lceil 0.3°C$.

Accuracy and Relevancy of Cross-Correlations

The high temporal resolution of the various time series displayed in Figures 1 to 3 invites close cross-correlation. We caution, however, that there are several sources of uncertainty. The accuracy of dating of the Santa Barbara Basin sediment is estimated to be $\lceil 1$ year in the 20th century and $\lceil 2$ years at the 1840 level (Schimmelmann *et al* 1992). Stratigraphic sample boundaries do not coincide with varve boundaries, although the sampling resolution is about annual. This may critically dampen the amplitude of geochemical signals. For example, the warm season will be under-represented in a sample encompassing 15 months of material from fall to winter, whereas the adjacent samples tend to over-represent warm seasons.

Instrumental sea surface temperature time series compiled from ship of opportunity data off the west coast of North America (Barnett 1984) tend to deviate from local nearshore time series such as the Scripps Institution of Oceanography (San Diego) pier measurements. The difference in our example in Figure 1 is most obvious for much of the 1980s. Given the strong correlation among shore stations in Southern California for low frequency events (*eg*, El Niño events; List and Koh 1976), the Scripps pier sea surface temperature record may be more appropriate for comparison with Santa Barbara Basin data.

Historical data are not exempt from criticism. Quinn and Neal's (1992) famous compilation of historical South American strong El Niño years is depicted in our figures by vertical shading. However, propagation of warm waters to the Northern Hemisphere and the Santa Barbara Basin may require many months. Actual timing, duration, and severity of possible

El Niño repercussions on Southern California's coast remain largely uncertain for the 19th century. South American historical El Niño events, even those confirmed by South American instrumental records, may in some cases bear no relevance for the Santa Barbara Basin; the case of the "missing El Niño" of 1972 in the Santa Barbara Basin, when sea surface temperature was actually dropping below normal, reminds us that the South American El Niño record does not reliably predict El Niño occurrences in the Santa Barbara Basin. Figure 1 compares the well-documented South American strong El Niño events of the 20th century with records of sea surface temperature, TOC burial flux, and sediment water content in Santa Barbara Basin sediment. Only five of nine strong El Niño events are clearly and unambiguously recognizable in the shown instrumental West Coast and Scripps pier sea surface temperature records, namely around 1918, 1926, 1941, 1958-59, and 1983-84. Quinn and Neal's (1992) historical record was recently criticized by Ortlieb and Macharé (1993). The revision of the AD 1578 to 1891 Peruvian paleo-El Niño record proposes that there were no strong El Niño

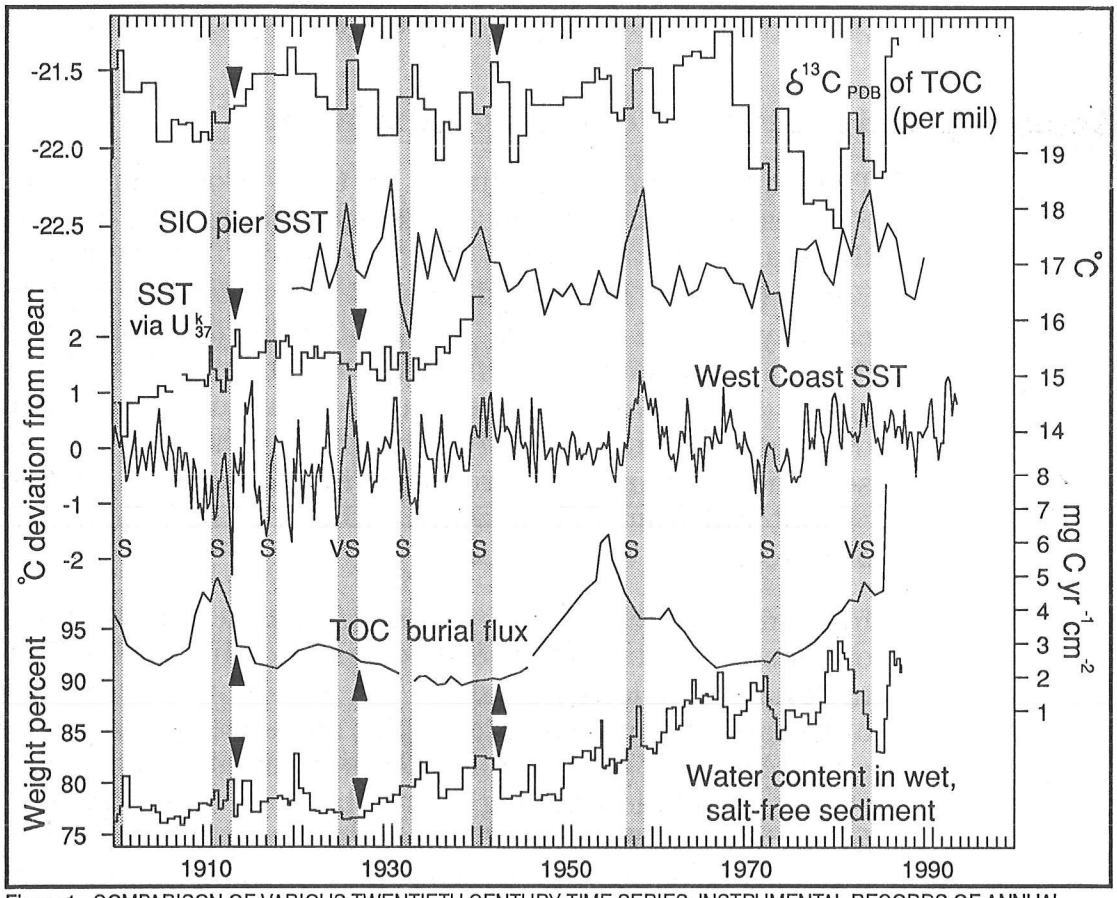

Figure 1. COMPARISON OF VARIOUS TWENTIETH CENTURY TIME SERIES: INSTRUMENTAL RECORDS OF ANNUAL MEAN SEA SURFACE TEMPERATURE FROM THE PIER OF SCRIPPS INSTITUTION OF OCEANOGRAPHY AND A SEASONAL MEAN SEA SURFACE TEMPERATURE FOR THE WEST COAST BASED ON SHIP OF OPPORTUNITY MEASUREMENTS (Barnett 1984)

SIO pier temperatures and the alkenone-derived SST are on an absolute scale; West Coast SST is plotted as deviation from the mean. Santa Barbara Basin sediment yielded time series of geochemically reconstructed SST, of the sediment water content, and of the burial flux of total organic carbon expressed as a running mean over five samples.
Vertical shaded bars indicate historical strong (S) and very strong (VS) El Niño events reported for South America by Quinn and Neal (1992). Filled triangles indicate geochemically-confirmed El Niño events during 1900 to 1942.

events off Peru during 1829 to 1870, followed by a cluster of events in 1871, 1877-78, 1884, and 1891 (see asterisks in Figure 2).

With these uncertainties in mind, the reader is encouraged to visually shift Santa Barbara Basin sediment-based time series relative to instrumental and historical data by a few years to test hypothetical correlation patterns.

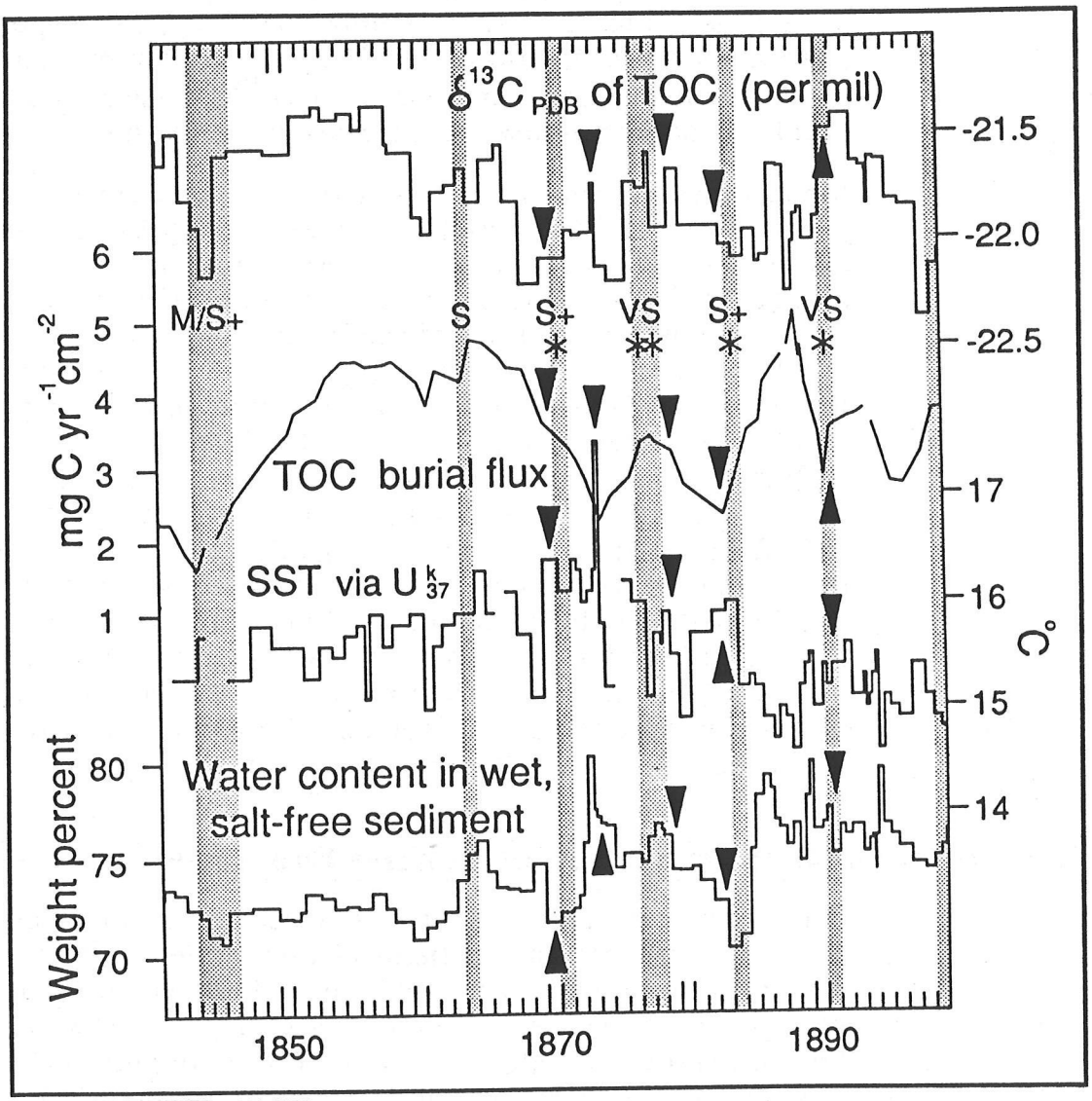

Figure 2. TIME SERIES, 1841-1899
From top to bottom: Carbon stable isotope ratio of total organic carbon in δ-notation (in per mil, *vs* PDB standard); TOC burial flux; alkenone-based sea surface temperature; sediment water content (see Figure 1 caption for more information).
Quinn and Neal's (1992) historical El Niño events include medium/strong (M/S+) and strong "S+" events.
Asterisks indicate Peruvian El Niño years of the 19th century that are confirmed by Ortlieb and Macharé (1993).
Filled triangles indicate geochemically-confirmed El Niño events during 1899 to 1942.

Time Series of the 20th Century

Instrumental records are mostly limited to the 20th century, for which we have also the most accurately dated sediments and some of the most detailed geochemical time series (Figure 1). The combined data can serve to test our working hypotheses within a calibration time interval. Specifically for the detection of paleo-El Niño events, we need to formulate several conditions that indicate the connection of a particular sediment layer to an El Niño event. Exemplary geochemical responses to El Niño conditions would be: dramatically decreasing or very low water content and TOC burial flux, an increase in the $\delta^{13}C$ value of total organic carbon, and high alkenone-based sea surface temperature.

Inspection of the four geochemical time series confirms that no individual parameter is El Niño-specific or records every El Niño event. The short alkenone-based sea surface temperature record in Figure 1 shows low amplitude fluctuations between 1910 and 1935, until it reproduces the late 1930s warming trend of the "West Coast SST" shipboard data and finally peaks into the 1940-41 El Niño event. The longer time series of Kennedy and Brassell (1992) shows more convincingly that alkenone-based sea surface temperature in the Santa Barbara Basin correlates with instrumental sea surface temperature. The long time series of the TOC burial flux in Figure 1 shows a consistent pattern in response to El Niño events; the amount of organic carbon being delivered to and buried in the sediment appears to have decreased or remained low during and immediately following an El Niño event. The exception of the 1982-1984 event, where an apparent massive increase of organic carbon is seen for 1985, is due to the proximity of the organic-rich bacterial mat and the abundance of undecomposed organic matter near the sediment surface in 1987 when the box core was retrieved.

Geochemical Reconstruction of El Niño Events, AD 1841-1941

Our attempt to reconstruct a 101-year El Niño record in the Santa Barbara Basin using geochemical time series is based on a matrix of year-by-year individual assessments of four geochemical parameters. All four geochemical assessments rank evenly in our statistical approach. Low or decreasing water content, $\delta^{13}C$ enrichment, high alkenone-based sea surface temperature, and low or decreasing TOC burial flux are judged as:

- +2 (strong positive evidence for El Niño conditions),
- +1 (moderate positive evidence),
- 0 (neutral),
- −1 (moderate negative evidence),
- −2 (strong negative evidence).

The sum of the four assessments for each year yields a subjective numerical estimate of the probability for El Niño conditions in the Santa

Barbara Basin, ranging from +8 (El Niño) to -6 (no El Niño). Of the 101 years 1841 to 1941, only 7 years rank between +4 and +8: 1870 (+6), 1873 (+8), 1879 (+6), 1883 (+5), 1891 (+6), 1913 (+5), and 1927 (+4). In addition, 1942 ranks +5 in absence of sea surface temperature data. The geochemical responses linking these 8 years to El Niño conditions are marked with filled triangles in Figures 1 and 2.

Ortlieb and Macharé's (1993) revised list of Peruvian paleo-El Niño events (asterisks in Figure 2) corresponds with El Niño conditions in the Santa Barbara Basin as inferred from our geochemical data; the Santa Barbara Basin sediment features no strong geochemical indication for El Niño events between 1841 and 1869-70 and a subsequent dense cluster of El Niño events between 1870 and 1891 (Figure 2). A precise dating of El Niño events in the Santa Barbara Basin and the exact correlation with Peruvian El Niño events is not warranted on this basis, however, due to the inherent uncertainty of our stratigraphic time scale by up to 2 years in the 19th century and due to the lag between El Niño in South America and El Niño in the Santa Barbara Basin.

Comparison with California Historical Accounts, 1844-1891

The validity of geochemical reconstructions of El Niño events can be tested against historical accounts of weather and weather-related events. Storms and unusual precipitation patterns can be useful, albeit unspecific indicators for El Niño conditions in Southern California. El Niño conditions in California can be associated with unusually heavy rainfall or can be rain free, depending on the position of the high and low pressure systems. Severe storms, associated shipwrecks, and flooding are frequently documented in the history of Santa Barbara County (Mason 1961; Schimmelmann and Tegner 1992) as well as in San Diego County (Kuhn and Shepard 1984). Table 1 is a chronological listing of a variety of unusual and extreme historical events, together with citations. Mason's (1961) history of Santa Barbara and Ventura counties as a major source of information was compiled in the mid-1880s. Although its coverage appears to be biased in favor of the 1870s and early 1880s, its factual reliability is corroborated by cross-references from other historical sources such as biographies, diaries, and travel reports. A detailed reference list of relevant historical sources is given by Schimmelman and Tegner (1992), also pertaining to weather events discussed below.

The preponderance of the historical record suggests the absence of strong El Niño events in the Santa Barbara Basin from the 1840s until 1872. This revises our earlier view of winter storms indicating an El Niño occurrence around 1846-1848 (Schimmelmann and Tegner 1992). The area experienced severe storms and several shipwrecks between 1846 and 1848, but storms unrelated to El Niño had been common in the 1820s and 1830s (references given in Schimmelmann and Tegner 1992). The lack of contemporary reports on flooding in the Santa Barbara area and other parts of California make an El Niño association of the 1846-

Table 1
HISTORICAL EXTREME WEATHER AND WEATHER-RELATED EVENTS IN SOUTHERN CALIFORNIA 1870s-1890s, WITH EMPHASIS ON SANTA BARBARA COUNTY AND PERIODS CONTAINING SOUTH AMERICAN EL NIÑO EVENTS

"EN" = Event most likely related to El Niño conditions; "–" = Event indicating absence of El Niño conditions.

1872-73	–	Steamers anchored "near the kelp" (Mason 1961, p. 260).
1873	EN	Severe storm at Santa Barbara on February 1 (Mason 1961, p. 467).
1873	EN	Considerable rain in August in Ventura, near Santa Barbara. Severe rain in Los Angeles. "It was called the "tail end" of the Sonora rains, as rain was falling in Mexico at that time." (Mason 1961, p. 458).
1877	EN	San Buenaventura wharf wrecked in March by severe storm; two schooners and one steamer wrecked (Mason 1961, p. 370).
1877	EN	"Hot wind for several hours [on August 25]. Thermometer reaching 100°." (Mason 1961, p. 469).
1877	EN	Southeaster storm at San Buenaventura wharf on October 23, extreme wave event. Excerpt from *San Buenaventura Free Press*: "Monday evening, October 23, 1876, Charles Bartlett and Walter Perkins took a walk down the wharf to look at the breakers, and saw them. Finally Mr. Bartlett observed three tremendous rollers, larger than any yet seen, approaching, and fearful of consequences, the two took to their heels. When two-thirds up the wharf the first roller struck it, 200 feet behind them, making a breach, and as it advanced shoreward the piles went down before it as grain before a reaper." (Mason 1961, p. 370).
1877	EN	"Fierce storm at Santa Barbara, injuring wharves [on November 16]." (Mason 1961, p. 469).
1878	EN	"Heavy storm and high winds [on January 14], breaking up the old wharf at Santa Barbara, and carrying a portion through the new one, near the shore line." (Mason 1961, p. 469).
1878	EN	Storm [on January 19] wrecks the schooner *Reliance* on the rocks near Goleta (Mason 1961, pp. 223, 469). "Wednesday, February 19, 1878, a terrific rainstorm at Santa Cruz Island raised the creek ten feet, so that it completely washed away the old Indian burying-ground, leaving not a trace behind. Rocks weighing two or three tons were carried along the stream." (Mason 1961, pp. 256, 469).
1878	EN	"Large portion of Point Sal Wharf destroyed [on November 15] by a storm." (Mason 1961, p. 469).
1878	EN	Southeaster and cyclone in Santa Barbara on December 31. Excerpt from the *Press*, January 4, 1879: "The severest [storm] that Santa Barbara has ever experienced." (Mason 1961, pp. 225, 226). "On February 1, 1879, snow fell on the mountains [near Ventura] and remained several hours." (Mason 1961, p. 458).
1879	EN	"Extreme local rain" in Santa Barbara on December 21. (Mason 1961, p. 270).
1879	EN	"Lompoc wharf damaged by a severe storm [on December 31]" (Mason 1961, p. 470).
1880	EN?	April 23, *San Diego Union*: "The worst storm [wind and rain] in San Diego County since 1861." August 19, *San Diego Union*: "Nearly 2 inches of rain in San Diego.... The worst storm in the history of San Diego."
1880	EN?	"Tornado near Goleta [on March 8], uprooting trees and leveling buildings." (Mason 1961, p. 470).
1884	EN?	February-April, southeaster storms bring heaviest rain recorded in San Diego County (*San Diego Union*, February 2, 3, 5, 7, 8, 12, 16, 19, 23; March 3, 28; April 2, 12, 15. Reviewed by Kuhn and Shepard 1984).
1887	–	In spring 1887 the naturalist J.W. Fewkes sailed across the Santa Barbara Basin, observing abundant kelp beds off Santa Barbara "...about three hundred yards from the shore. This zone imparts a highly characteristic appearance to the coast of many parts of Southern California." (Fewkes 1889, p. 212).
1891	EN	Severe storms in Southern California during summer and fall, with indication for unusual warming of ocean waters (Pyke 1975).

1848 storms unlikely. The following years until 1872 appear to have been uneventful in the Santa Barbara area. The mentioning of steamers anchoring "near the kelp" beds in late 1872 indicates no severe storms had destroyed the local kelp forests until winter 1872/73.

A well-documented, extremely unusual occurrence of the warm-water crustaceans *Pleuroncodes planiceps* was reported for March 1859 in Monterey, hundreds of miles north of the species' present range (Hubbs 1948). These crustaceans undoubtedly took advantage of temporarily elevated sea surface temperature and unusual warm currents, but we cannot cite any supporting historical evidence such as Peruvian El Niño events or contemporaneous California weather events. There may be a tenuous connection with the extreme precipitation of 1861/62 ("Noachian Deluge") that entailed bankruptcy of the State of California. The very high sea surface temperature off Southern California in 1931, one year before the 1932 South American El Niño event, demonstrates that some sea surface temperature maxima off California are unrelated to El Niño conditions.

The year 1873 brought to the Santa Barbara area a severe storm in February and considerable rain in August. Severe rain was reported in Los Angeles. Summer rain in Southern California is a rare occurrence that suggests the influence of El Niño in 1873. This El Niño is likely related to the 1871 Peruvian El Niño event.

In early 1877, local wharfs and ships were damaged by "storms". Spectacular damage due to high winds and waves in October 1877 and January 1878 was followed by enormous rainfall in February 1878 on Santa Cruz Island. Reports for winter 1878/79 include rare snowfall, "extreme local rain", severe storms, and even a damaging cyclone in Santa Barbara. The overall severity and clustering of the unusual occurrences advocate El Niño conditions in the Santa Barbara Basin, probably related to the 1877/78 Peruvian El Niño event.

In August 1883, Krakatoa erupted and weather patterns changed abruptly throughout the United States and western Europe. Southern California's climate changed temporarily from semiarid to subtropical, with unusually heavy rainfall through June (Kuhn and Shepard 1984). The rapid climatic response following the eruption bears the signature of fast atmospheric propagation rather than via ocean currents. The heavy rains of 1884 in Southern California in the wake of the eruption are well documented, for example, in San Diego and Los Angeles. We suggest that the postulated South American El Niño event of 1884 and its possible oceanographic repercussions on the Santa Barbara Basin may be related to, or even caused by, the Krakatoa eruption. The immediate physical impact on the Santa Barbara Basin may have been small, though; a naturalist observed the large abundance of kelp forests in the Santa Barbara Basin in spring 1887 (Fewkes 1889). This may be interpreted as evidence that no severely destructive storm-and-wave events had occurred in the area for a few years prior to 1887.

Interestingly, the alkenone-based sea surface temperature declined sharply in 1884 (following the eruption of Krakatoa, according to our varve stratigraphy) and did not return to 1883 values until the late 1930s. In his detailed study of historical abundance patterns of fish along the Pacific Coast, in close comparison with historical sea surface temperature and air temperature records, Hubbs (1948, 1960) concluded that "the 1850 and 1860 decades appear to have been in a prolonged warm [SST] period." Some warmwater fauna "seems to have persisted [off Southern California] through the 1870's until 1880". The cooling of sea surface temperature in the latter part of the 19th century was best documented off San Diego, whereas "the region of San Francisco ≤ indicates a relatively stable fauna throughout the last hundred years."

Hubbs (1948) demonstrates that the San Diego air temperature record and the Scripps pier sea surface temperature record are closely correlated. He then uses the 19th century San Diego annual mean air temperature record as evidence for cooling of sea surface temperature, but at the same time cautions about possible artifacts in the early instrumental air temperature record until 1871. Figure 3 compares the early San Diego annual mean air temperature record with our alkenone-based sea surface temperature record from the Santa Barbara Basin. The reader is reminded that the uncertainty of the sea surface temperature chronology discourages year-to-year correlation. Both records agree in their lower-than-average temperatures during the decades around the turn of the century. Both temperature records rebound to strongly above-average values in the late 1930s.

There is abundant historical evidence that El Niño conditions were present off Southern California around 1891 (Pyke 1975).

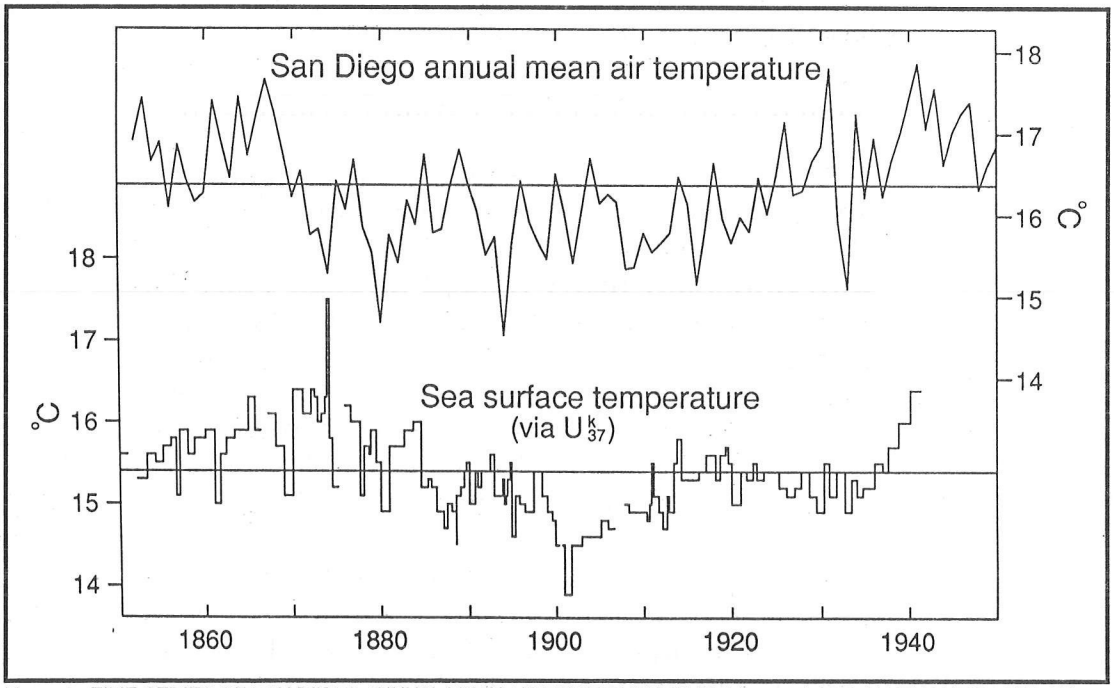

Figure 3. TIME SERIES OF SAN DIEGO ANNUAL MEAN AIR TEMPERATURE (Hubbs 1948) AND ALKENONE-BASED SEA SURFACE TEMPERATURE RECONSTRUCTED FROM SANTA BARBARA BASIN SEDIMENT

The 1871-1880 Instrumental Air Temperature Time Series

The monthly means and extremes of air temperature in Santa Barbara for 1871-1880 are reported in Mason (1961, p. 457). We note that the quality of the monthly mean temperature data may be questionable, because in some cases our recalculated annual mean temperatures did deviate from the values offered by the original table. Nevertheless, the original annual mean temperature data show positive excursions for 1872, 1877, and 1879 (Table 2). Mason's (1961) reported matrix of monthly maximum temperatures shows the most dense clusters of high temperatures in 1872 (May-December) and 1878/79 (December-June; Table 2), in excellent agreement with the suggested South American El Niño events of 1871 and 1877/78.

Table 2
INSTRUMENTAL RECORD OF AIR TEMPERATURES IN SANTA BARBARA, 1871-1880
(Mason 1961, p. 457)

Annual mean temperature is converted from the last column of the original data table.
Shading indicates temperatures of at least 1.9 degrees above 1871-1880 means of the monthly maximum temperatures.
All temperatures are in degrees Celsius.

	Monthly maximum temperature													
year	jan	feb	mar	apr	may	jun	jul	aug	sep	oct	nov	dec	mean	annual mean temp.
1880	21.1	17.2	20.0	20.6	27.8	23.9	23.9	25.0	29.4	27.2	25.0	21.1	23.5	14.25
1879	20.0	26.1	31.7	28.3	33.3	36.1	26.7	29.4	30.0	32.2	25.0	22.8	28.5	16.36
1878	19.4	20.6	20.6	25.0	25.0	24.4	26.7	28.9	34.4	28.9	24.4	24.4	25.2	15.97
1877	28.3	26.1	24.4	22.8	23.9	38.9	30.6	27.8	30.0	25.0	27.8	23.3	27.4	16.94
1876	22.8	21.7	23.3	30.0	26.7	28.9	28.9	28.3	28.3	29.4	27.2	23.9	26.6	16.19
1875	22.8	25.0	24.4	30.0	35.0	26.7	28.9	32.2	28.3	22.2	25.6	20.6	26.8	16.22
1874	21.1	20.6	21.1	25.6	25.6	27.8	30.0	31.1	28.3	22.2	25.6	20.6	25.0	16.22
1873	24.4	19.4	24.4	26.7	25.6	26.7	30.0	27.8	28.3	27.8	27.8	20.0	25.7	16.06
1872	22.2	22.8	23.3	23.9	34.4	37.8	27.8	35.6	28.3	31.1	27.2	26.1	28.4	16.63
1871	24.4	20.0	23.9	28.3	28.9	26.1	31.7	36.7	31.1	37.8	26.7	22.2	28.1	16.15
	Means of the monthly maximum temperatures, 1871-1880													
	22.7	21.9	23.7	26.1	28.6	29.7	28.5	30.3	29.7	28.4	26.2	22.5		

Conclusions

The combined diagnostic use of four independently determined geochemical El Niño indicators in laminated Santa Barbara Basin sediment permits the reconstruction of paleo-El Niño events. In agreement with instrumental and historical evidence, apparently no strong El Niño events occurred in the Santa Barbara Basin between 1841 and about 1870. A rapid succession of strong El Niño events occurred from about 1870 to 1891. Historic sources advocate El Niño events in the Santa

Barbara Basin for 1873, 1878/79, and 1891. The year 1884, one year after the eruption of Krakatoa, was characterized by abnormal weather, but the oceanographic link to simultaneous South American El Niño in 1884 is uncertain. Subsequent El Niño conditions may have been present in the Santa Barbara Basin around 1913 and 1926/27, followed by the well-known event of 1941/42.

Acknowledgments

Funding was provided in part by National Science Foundation grant OCE-9301438, by the Western Regional Center of the National Institute for Global Environmental Change (WESTGEC) grant 92-007, by NATO Collaborative Research Grant 930391, and by National Oceanic and Atmospheric Administration grant NA16RC0083-01.

References

Barnett, T.P. 1984. Long term trends in surface temperature over the oceans. *Monthly Weather Review* 112:303-312.

Brassell, S.C. 1993. Applications of biomarkers for delineating marine paleoclimatic fluctuations during the Quaternary. Pages 699-728 in *Organic Geochemistry*. M.H. Engel and S.A. Macko, editors. Plenum, NY.

Brassell, S.C., G. Eglinton, I. Marlowe, M. Sarnthein, U. Pflaumann. 1986. Molecular stratigraphy: A new tool for climatic assessment. *Nature* 320:129-133.

Dayton, P.K., and M.J. Tegner. 1990. Bottoms below troubled waters: Benthic impacts of the 1982-1984 El Niño in the temperate zone. Pages 433-472 in *Ecological Consequences of the 1982-84 El Niño to Marine Life*. P.W. Glynn, editor. Elsevier Oceanography Series No. 52, Amsterdam.

Eglinton, G., S.A. Bradshaw, A. Rosell, M. Sarnthein, U. Pflaumann, R. Tiedemann. 1992. Molecular record of secular sea surface temperature changes on 100-year timescales for glacial terminations I, II, and IV. *Nature* 356:423-426.

Ellison, W.H. (editor). 1937. *The Life and Adventures of George Nidever [1802-1883]*. University of California Press, Berkeley, 128 pp.

Enfield, D.B. 1989. El Niño, past and present. *Rev. Geophys.* 27:159-187.

Fewkes J.W. 1889. Across the Santa Barbara Channel. *The American Naturalist* 23:211-217 and 387-394.

Hubbs, C.L. 1948. Changes in the fish fauna of western North America correlated with changes in ocean temperatures. *Journal of Marine Research* 8:459-482.

Hubbs, C.L. 1960. Quaternary paleoclimatology of the Pacific Coast of North America. *California Cooperative Oceanic Fisheries Investigations (CalCOFI) Report* 7:105-110.

Kennedy, J.A., and S.C. Brassell. 1992. Molecular records of twentieth century El Niño events in laminated sediments from the Santa Barbara basin. *Nature* 357:62-64.

Kuhn, G.G., and F.P. Shepard. 1984. *Sea Cliffs, Beaches, and Coastal Valleys of San Diego County: Some Amazing Histories and Some Horrifying Implications*. University of California Press, Berkeley. 193 pp.

List, E.J., and R.C.Y. Koh. 1976. Variations in coastal temperature on the southern and central California Coast. *Journal of Geophysical Research* 81:1971-1979.

Lange, C.B., A. Schimmelmann, M.K. Yasuda, W.H. Berger (in press). Paleoclimatic significance of marine varves off southern California. In *Southern California Climate: Trends and Extremes of the Past 2000 Years*. P. Wigand and M. Rose, editors. Desert Research Institute, Reno, NV.

Mason, J.D. (editor). 1961. *Reproduction of Thompson and West's History of Santa Barbara and Ventura Counties*. Howell-North, Berkeley, CA. 477 pp.

McCaffrey, M.A., J.W. Farrington, D.J. Repeta. 1990. The organic geochemistry of Peru margin surface sediments: I. A comparison of the C_{37} alkenone and historical El Niño records. *Geochimica et Cosmochimica Acta* 54:1671-1682.

Ortlieb, L., and J. Macharé. 1993. Former El Niño events: Records from western South America. *Global and Planetary Change* 7:181-202.

Parry, A.T. 1992. *Automation of the* U^K_{37} *method*. MS Thesis, School of Chemistry, University of Bristol, England, 64 pp.

Prahl, F.G., and S.G. Wakeham. 1987. Calibration of unsaturation patterns in long-chain ketone compositions for paleotemperature assessment. *Nature* 320:367-369.

Pyke, C.B. 1975. *Some Aspects of the Influence of Abnormal Eastern Equatorial Pacific Ocean Surface Temperature upon Weather Patterns in the Southwestern United States*. PhD Dissertation, University of California, Los Angeles. 99 pp.

Quinn, W.H., and V.T. Neal. 1992. The historical record of El Niño events. Pages 623-648 in *Climate Since A.D. 1500*. R.S. Bradley and P.D. Jones, editors. Routledge, London.

Schimmelmann, A., and M. Kastner. 1993. Evolutionary changes over the last 1000 years of reduced sulfur phases and organic carbon in varved sediments of the Santa Barbara Basin, California. *Geochimica et Cosmochimica Acta* 57:67-78.

Schimmelmann, A., C.B. Lange, W.H. Berger. 1990. Climatically controlled marker layers in Santa Barbara Basin sediments, and fine-scale core-to-core correlation. *Limnology and Oceanography* 35: 165-173.

Schimmelmann, A., C.B. Lange, W.H. Berger, A. Simon, S.K. Burke, R.B. Dunbar. 1992. Extreme climatic conditions recorded in Santa Barbara Basin laminated sediments: The 1835-1840 Macoma Event. *Marine Geology* 106:279-299.

Schimmelmann, A., and M.J. Tegner. 1991. Historical oceanographic events reflected in $^{13}C/^{12}C$ ratio of total organic carbon in laminated Santa Barbara Basin sediment. *Global Biogeochemical Cycles* 5:173-188.

Schimmelmann, A., and M.J. Tegner. 1992. Historical evidence of abrupt coastal climatic change in Southern California, 1790-1880. Pages 47-56 in *Proceedings of the Eighth Annual Pacific Climate (PACLIM) Workshop, March 10-13, 1991*. K.T. Redmond, editor. California Department of Water Resources, Interagency Ecological Studies Program Technical Report 31.

Zhao, M., A. Rosell, G. Eglinton. 1993. Comparison of two U^K_{37}-sea surface temperature records for the last climatic cycle at ODP Site 658 from the sub-tropical Northeast Atlantic. *Palaeogeography, Palaeoclimatology, Palaeoecology* 103:57-65.

Radiolarian Flux in the Santa Barbara Basin as an Index of Climate Variability

Amy L. Weinheimer and Daniel R. Cayan

ABSTRACT: Annual radiolarian flux (1954-1986) extrapolated from varved Santa Barbara Basin sediments was compared to instrumental data to examine the effect of interannual climate variability. Paleo-reconstructions over large geographic areas or 10^3 years and longer typically rely on changes in species composition to signal environment or climate shifts. In the relatively short period studied, climate fluctuations were insufficient to significantly alter the assemblage, but there was considerable variability in the total flux of radiolarians. This variability, greatest on 5- to 25-year time scales, appears to be linked to regional climate variability. Total flux correlates to regional California sea surface temperature and the composite of sea level pressure over the Northern Hemisphere for years of high radiolarian flux resembles positive PNA circulation.

Background

The effort to understand and model interdecadal to centennial-scale climate variability relies on development of high resolution climate proxies that extend farther back in time than the 100-year instrumental record. Such proxies are contained in sedimentary and other natural records (tree rings, corals, ice cores); however, high resolution records are relatively rare. Of the marine sedimentary records, that in the Santa Barbara Basin in the Southern California borderland is particularly useful for climate studies. Seasonal deposition in the basin is preserved in annual layers composed of couplets (varves) (Koide *et al* 1972) allowing for annual to subseasonal analysis. Additionally, the basin lies in the path of the California Current, whose properties are closely tied to climate (Norton *et al* 1985). Present-day teleconnections suggest that climate variability at Santa Barbara Basin is a sensitive indicator of broader-scale climate variability over the North Pacific/North American sector (Figure 1a, b).

Several microfossil records from Santa Barbara Basin have been used in climatic reconstructions (Kling 1977; Lange *et al* 1990; Baumgartner *et al* 1989; Weinheimer *et al* 1986). For example, at a resolution of 25 years Pisias (1978, 1979) used changes in radiolarian assemblages to reconstruct sea surface temperatures and dynamic heights for the past 8,000 years. These assemblages shifted synchronously with initiation of alpine glacial advances, on the order of 10^2-10^3 years. Annual geochemical and paleontological data from several Santa Barbara Basin cores spanning 50-200 years relate to deposition of varved and non-varved sections of the sediment and are considered to reflect climatic fluctuations (Schimmelmann *et al* 1992). Previous studies on annual time scales indicate that diatoms (Lange *et al* 1990) and fish scales (Baumgartner *et al* 1989) in the varves contain yearly-decadal variations indicative of some facets

In: C.M. Isaacs and V.L. Tharp, Editors. 1995. *Proceedings of the Eleventh Annual Pacific Climate (PACLIM) Workshop, April 19-22, 1994.* Interagency Ecological Program, Technical Report 40. California Department of Water Resources.

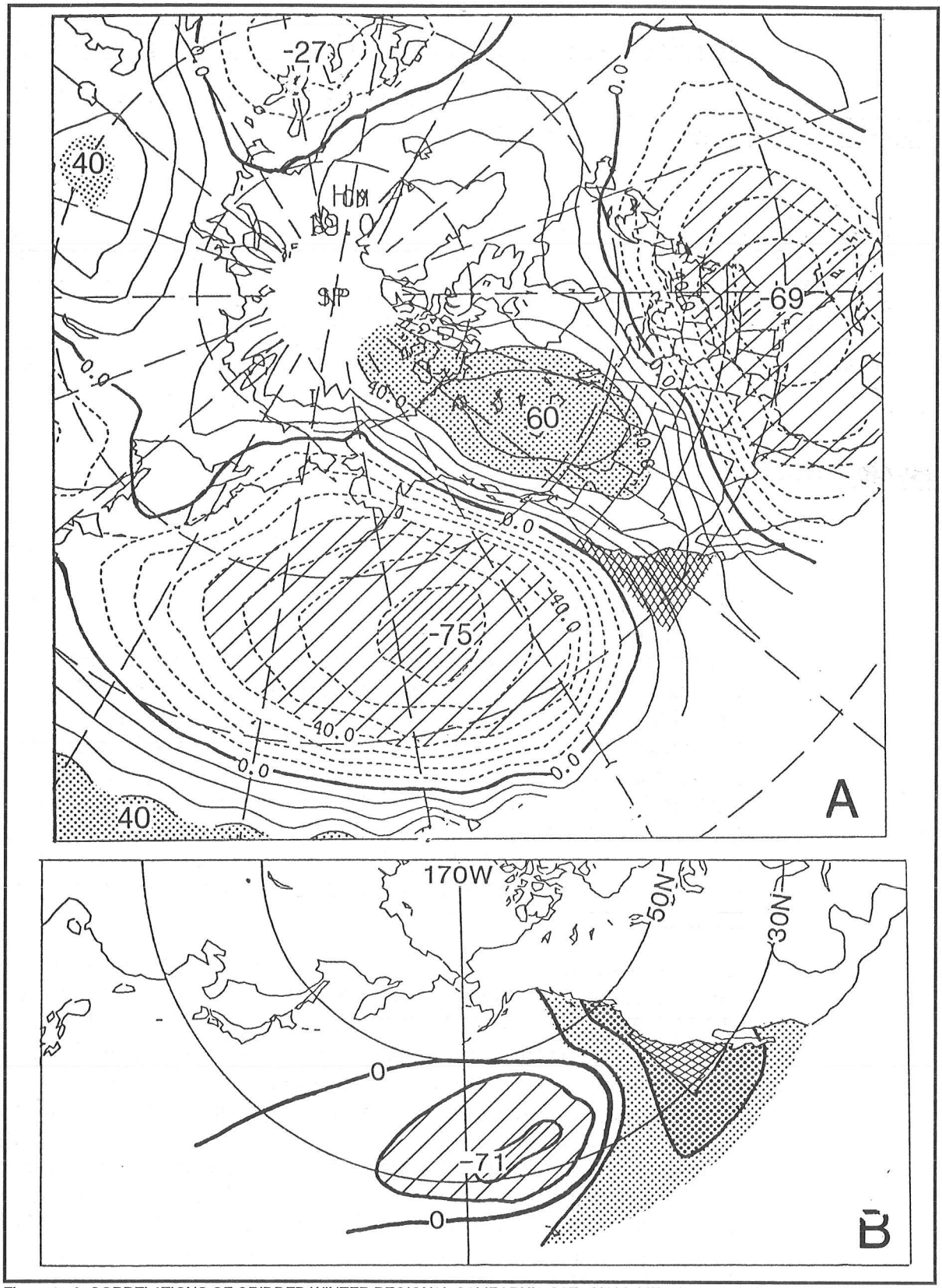

Figure 1. A. CORRELATIONS OF GRIDDED WINTER REGIONAL CALIFORNIA SST ANOMALIES (hatchured box) AGAINST 5° LATITUDE BY 10° LONGITUDE WINTER 700-MB HEIGHT ANOMALIES OVER THE NORTHERN HEMISPHERE.
B. CORRELATIONS (x 100) OF THE SAME SST ANOMALIES (hatchured box) AGAINST GRIDDED NORTH PACIFIC WINTER SST ANOMALIES.
Note the centers of action resulting from spatial coherence of sea surface temperature and pressure anomalies, as well as teleconnections over the North Pacific and North America.

of short-period climate variations. Also, radiolarian total and environmental group fluxes correspond to variability in the California Current, with higher fluxes during warm conditions (Weinheimer *et al* 1986). Even at much higher temporal resolution, on the order of weeks to months, available from sediment traps, variability in relative radiolarian species abundances has been related to seasonality of California Current flow (Welling *et al* 1992). The existence of interannual radiolarian fluctuations and their potential utility as climate proxies on a yearly scale warrants investigation of radiolarian flux in relation to interdecadal climate variability.

The period studied, 1954-1986, includes several climatic events that might be expected to affect radiolarian flux to Santa Barbara Basin. For instance, two major El Niños (1958-59 and 1983-84) and several smaller El Niños occurred during these years. Also, a major shift in Pacific climate occurred in the mid-1970s, affecting many systems (Ebbesmeyer *et al* 1991). These 30+ years seemed to contain enough interannual to interdecadal climate variability to further calibrate relative radiolarian species distributions as well as the total radiolarian flux against the instrumental record.

Methods

Sediment collected with a Soutar boxcore was retrieved from the center of Santa Barbara Basin at 580 meters depth. Thin slabs (1-2 centimeters thick) of the sediment were x-rayed, and contact prints of these were used to develop a chronology of the varves. The varves were dated independently by three investigators by counting the varves down from the top and comparing the varves to other previously dated cores. The three chronologies were within 1+/- years of each other. Varves dated 1954-1986 were individually sampled. These 33 samples were treated with hydrogen peroxide solution and hydrochloric acid, then sieved over a 45 μm screen. Quantitative slides of the larger than 45 μm fraction were counted for radiolarians (about 300 specimens per sample). All specimens were identified to the lowest possible taxonomic unit. Annual fluxes ($no.cm^{-2}yr^{-1}$) were extrapolated from the counts and surface area of the core. Potential error in subsampling of the varves was reduced by using 3-year averages of the fluxes.

Instrumental sea surface temperature data from six 5-degree squares along the California coast (Namias *et al* 1988) were averaged for an annual regional sea surface temperature time series. The salinity data are annual averages from La Jolla, California. The sea surface temperature and salinity data were smoothed with a 3-year running average. These two data sets were chosen over the CalCOFI data set for their continuity and frequency of observations.

Radiolarian Time Series

To estimate the effect of El Niño on the radiolarian flux, the annual total flux (no.cm^{-2}yr^{-1}) to the Santa Barbara Basin for El Niño and non-El Niño years can be compared (Figure 2a). The resulting time series does not show a consistent response to the El Niño events, though from previous work on a slightly different size fraction and time scale, there is some evidence for increased radiolarian flux during very strong El Niños (Casey *et al* 1989). A striking feature of the total radiolarian flux time series is its low-frequency signal.

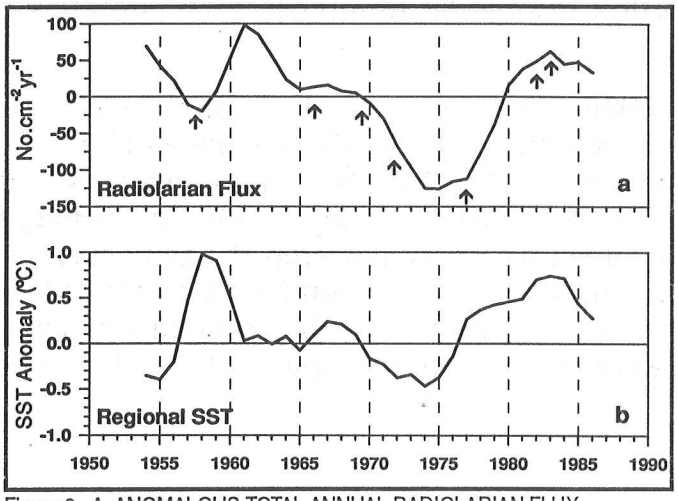

Figure 2. A. ANOMALOUS TOTAL ANNUAL RADIOLARIAN FLUX, 1954-1986, FROM SANTA BARBARA BASIN SEDIMENT.
B. ANOMALOUS REGIONAL ANNUAL SEA SURFACE TEMPERATURE (hatchured box, Figure 1).
Arrows indicate El Niño years. Both are 3-year running averages of annual anomalies.

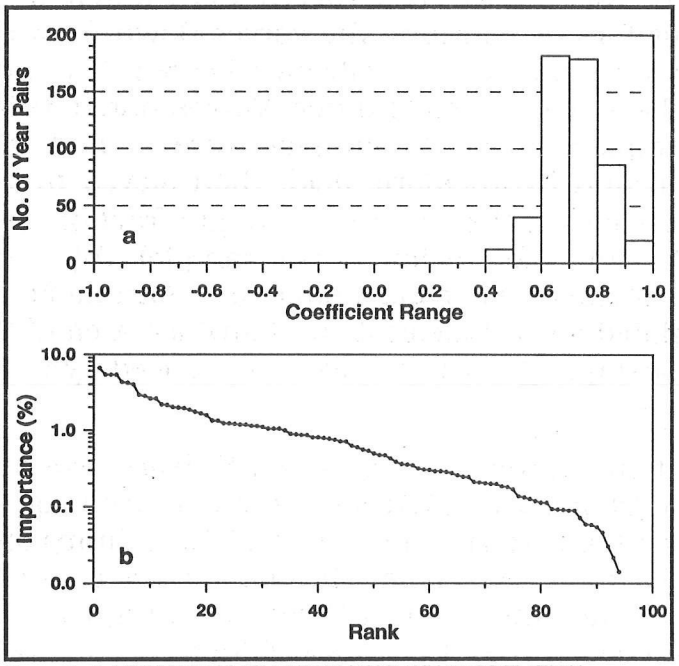

Figure 3. A. HISTOGRAM OF SPEARMAN RANK CORRELATION COEFFICIENTS OF SPECIES RANK COMPARISONS FOR ALL YEAR PAIRS, 1954-1986.
B. SPECIES IMPORTANCE AS MEASURED BY PERCENT OF TOTAL FLUX OVER ALL YEARS.

The flux of radiolarian tests into Santa Barbara Basin sediments is made up of species with different environmental preferences, so it is possible that their cumulative flux may reflect a regional climate influence. Time series of individual species flux were constructed to determine whether any species responded strongly to environmental conditions. These time series were quite similar to each other and to that of the total flux. To confirm and quantify this observation, the Spearman rank correlation coefficients for all possible pairs of years were calculated (Figure 3a). Spearman rank coefficients measure the similarity of relative abundance of pairs of variables (species). McGowan and Walker (1985) found that relative abundances of copepod species from the North Pacific were similar in tows taken within a province but showed significant differences between provinces. The generally high correlation coefficients for the Santa Barbara Basin radiolarians imply that the assemblage represents a population from one province. This is an interesting result, considering the heterogeneous nature of the California Current system and the occurrence of events such as the extraordinary 1982-83 El Niño.

Another important characteristic of the Santa Barbara Basin sediment's radiolarian assemblage is the stability over time of the cumulative distribution of species. Summing the species' relative

abundance for all years and ranking them generates a log normal distribution (Figure 3b), with 13 species accounting for 50% of the cumulative distribution. The high coefficients, together with the log normal distribution, suggest that a few species consistently dominate the assemblage, few are rare, and many have intermediate abundances. This type of distribution characterizes species abundances in other single provinces (McGowan and Walker 1985; Hubbell 1979). The stable log normal species distribution implies that the radiolarian assemblage represents a single environment. The climate variability over the 3-decade study period apparently is not sufficient to significantly change the radiolarian assemblage, as it was over the past 8,000 years (Pisias 1979).

Comparison to Regional Sea Surface Temperature

Radiolarian flux during 1954-1986 to Santa Barbara Basin varies at a frequency similar to the 5- to 10-year periods that characterize the California Current (Chelton *et al* 1982). The state of the California Current, as represented by dynamic height and temperature data from the California Cooperative Fisheries Investigations (CalCOFI), has been related to sea surface temperature with low temperatures during strong southward transport and high temperatures with weak southward transport (Chelton *et al* 1982). Although the CalCOFI data set is the most complete of its kind, there are critical gaps, especially in the 1970s. Consequently, we use sea surface temperature determined from routine weather observations (ships and buoys, primarily; Namias *et al* 1988) as a proxy for California Current flow.

Interestingly, the radiolarian and sea surface temperature time series (Figure 2b) closely resemble each other, but with poorer fit at the beginning of the record (1954-1970, r=-0.30) than afterward (1970-1986, r=0.81). If the radiolarian time series is lagged 2 years with respect to sea surface temperature, the correlations improve (r=0.69 and 0.96, respectively). The correlation of sea surface temperature and radiolarian flux over the entire study period (r=0.49 at zero and 0.84 at 2-year lags) suggests that the two are related. If this connection is real, the relationship may be direct (*ie,* radiolarian flux is forced by temperature fluctuations) or it may be indirect (*ie,* both respond similarly to some common overall force). However, the offset of the flux and sea surface temperature in the first half of the record is large enough to warrant further investigation. A potential cause could be inaccuracies in dating the core, whereby if one or two years were not identified in the core, a given varve would appear to occur later (closer to the core top) and, hence, would lag its corresponding climatic match. We tried to avoid this type of error by having the core dated independently by three investigators, but it is possible that the same mistake is made repeatedly in dating the core.

Alternatively, a shift around 1970 in the biological response to external forcing relative to the sea surface temperature response could also produce the observed offset. For example, the mechanism(s) producing

positively proportional sea surface temperature and flux (as in the later half of the time series) may be different to that creating the first half of the record when sea surface temperature and flux are not as well correlated. If this were the case, we could expect the physical mechanism forcing the sea surface temperature record to affect other physical aspects of the environment (*ie*, salinity).

In the region off California in the California Current system, the average salinity (1950-1978) decreases offshore and increases with depth; temperature increases offshore and decreases with depth; both increase southward along shore (Lynn *et al* 1982). (To the west of the California Current, in the North Pacific gyre, salinity increases to the west.) Consequently, under typical conditions, an increase in temperature should coincide with a decrease in salinity (in the area between the coast and the offshore salinity minimum of the California Current) and vice versa. Exceptions would perhaps include especially strong northward flow (El Niño) when an increase in temperature could be accompanied by an increase in salinity and, possibly, unusually strong southward flow with lower temperature and salinity.

Correlations and visual interpretations of scatter plots of the regional sea surface temperature and La Jolla salinity for the periods before and after 1970 (Figure 4a, b) show that temperature and salinity tend to vary inversely, and that there may have been a shift in the regime around 1970. Perhaps the higher correlation between sea surface temperature and salinity for 1970-1986 (r=-0.66) than 1954-1969 (r=-0.19) is evidence of a shift in the environment.

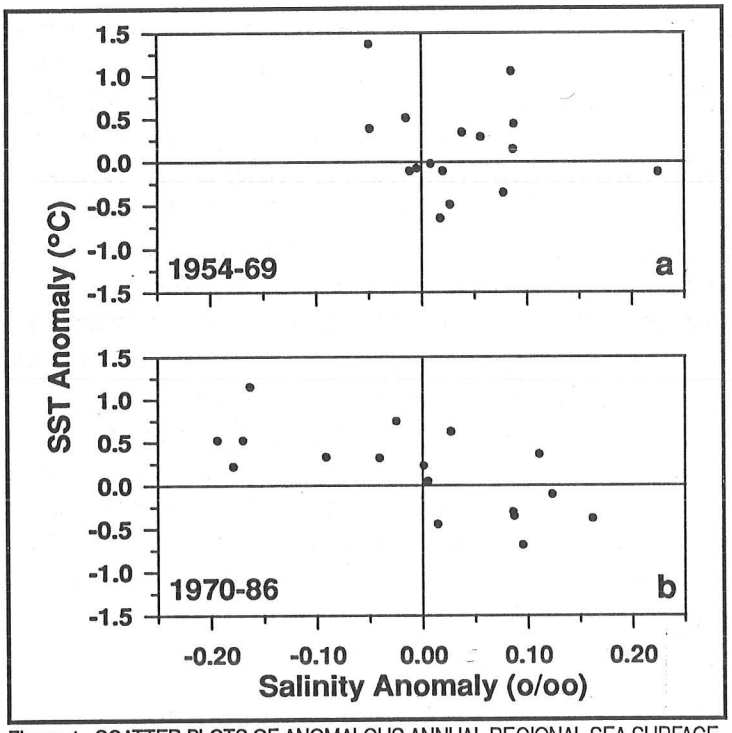

Figure 4. SCATTER PLOTS OF ANOMALOUS ANNUAL REGIONAL SEA SURFACE TEMPERATURE AND LA JOLLA SALINITY, 1954-1969 (A) AND 1970-1986 (B).

Although total radiolarian flux lags sea surface temperature, the possibility of the flux reflecting sea surface temperature still exists. If the radiolarian flux truly reflects sea surface temperature, what mechanism(s) produces this relationship and why is it apparently different from relationships linking sea surface temperature to other plankton groups? For example, low diatom (Lange *et al* 1990), foraminifera (Thunell and Sautter 1992), and zooplankton (Chelton *et al* 1982) abundances off California are associated with high sea surface temperature. Radiolarians differ from these groups in that they are relatively small heterotrophs (20-200 µm), omnivorous, and accept very small prey, including diatoms (Anderson 1983). Diatom cell size has been

found to be related to nutrient distribution; generally decreasing in size with diminished nutrient concentration and patchiness (Turpin and Harrison 1980; Harrison and Turpin 1982; Harris 1986). It is conceivable that small heterotrophs are similarly adapted to low nutrient environments, characterized by less patchiness and small primary producers that would provide suitable prey. In the California Current system off northern California, Hood *et al* (1990, 1991) found small diatoms (<10 μm) predominant in the relatively warmer, lower salinity water, and less patchy chlorophyll *a* distribution seaward of colder, higher salinity water with larger, chain forming diatoms and patchier chlorophyll *a* distribution. The character of warmer water in the California Current system, lying seaward of upwelled waters, resembles an environment in which small heterotrophs such as radiolarians could thrive.

A possible hydrographic mechanism generating warm sea surface temperature and corresponding high radiolarian flux can be described as follows. Cooler sea surface temperature off the California coast occurs with enhanced southward transport and consequent upwelling. Conversely, warm sea surface temperature occurs when these transport mechanisms relax. This interpretation is consistent with the inverse relationship of coastal temperature and salinity observed. Considering that radiolarian density has been found to be low in water upwelled in the California Current system and to increase offshore (Gowing and Coale 1989), increased upwelling associated with offshore transport of upwelled water (Hood *et al* 1990), incorporates more radiolarian-poor, cool, high-salinity water into the California Current system; whereas, diminished upwelling associated with onshore movement of the California Current brings radiolarian-rich, warmer, low-salinity water into Santa Barbara Basin.

Such a scenario of strong southerly flow with offshore transport of upwelled water in contrast to diminished southerly flow with onshore movement of the California Current can explain the observed relationships between sea surface temperature, salinity, and radiolarian flux. During periods of upwelling, cold, high-salinity water with low radiolarian content is incorporated into the California Current system via filaments and eddies (Hood *et al* 1990). As southward transport and upwelling decrease, the California Current moves inshore and brings warm, low-salinity water with high radiolarian content into Santa Barbara Basin.

Radiolarian Flux-Regional Climate Relationship

The correlation of radiolarian flux to regional sea surface temperature fluctuations suggests that the flux is related to large-scale atmospheric circulation. One indicator of circulation in the region is sea level pressure over the North Pacific and western North America sector. A predominant mode of variability in sea level pressure over the North Pacific consists of two clusters of anomalies that are out of phase with each other; one along the west coast and the other over the central North Pacific (Figure 1a).

The seasonal sea surface temperature anomaly exhibits a similar pattern (Davis 1976) (Figure 1b). The circulation pattern characterized by a strengthened North Pacific subtropical high, deepened Aleutian low, and strengthened high over western Canada-Pacific Northwest is referred to as positive Pacific/North American pattern (PNA) (Wallace and Gutzler 1981). A regional effect of positive PNA is warmer temperatures off the California coast, possibly resulting from an increase in warm water entering from the south and west and diminished input of cool subarctic water from the north (Norton *et al* 1985).

The composite winter sea level pressure anomaly over the Northern Hemisphere for the 12 years of highest radiolarian flux (Figure 5) exhibits a well-developed Aleutian low and a high pressure center over the Pacific Northwest. This pattern of sea level pressure resembles the deep Aleutian low phase of PNA circulation suggesting that the PNA can be extracted from radiolarian data.

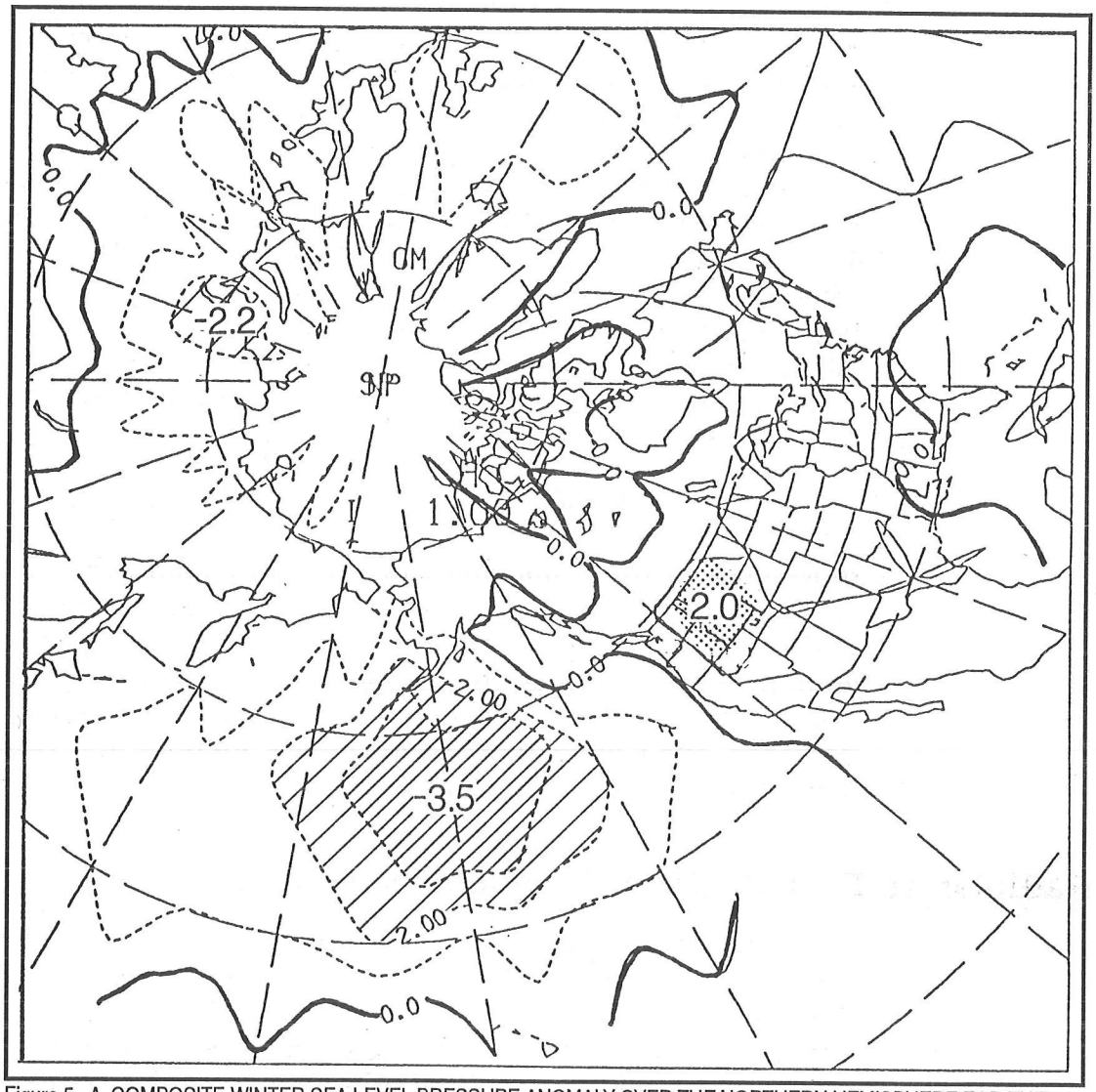

Figure 5. A. COMPOSITE WINTER SEA LEVEL PRESSURE ANOMALY OVER THE NORTHERN HEMISPHERE FOR THE 12 YEARS OF HIGHEST RADIOLARIAN FLUX, 1954-1986.
The deep Aleutian low over the North Pacific and high pressure center over the Pacific Northwest resembles positive PNA circulation.

The negative mode of PNA, typified by an Aleutian high and lows where highs exist in the positive PNA, is associated with cool temperatures along the California coast. Cross-correlations of the total radiolarian flux and sea level pressure do not generate this phase of PNA.

Conclusions

The radiolarian assemblage preserved in Santa Barbara Basin sediment exhibits an organization resembling that of other plankton groups within single provinces. A Spearman rank correlation indicates that the climate variability during 1954-1986 was large enough to slightly alter the mix of dominance within this province, but this is less than would be expected if there were an alternation of multiple assemblages from surrounding provinces. Apparently, the Spearman rank analysis is not sensitive to potential, but more subtle, changes due to interannual-decadal scale environmental change. Because none of the species consistently becomes rarer through time, it is likely that post-deposition alteration of the assemblage is negligible.

Comparison of radiolarian flux with environmental variables suggests that flux is related to sea surface temperature and salinity in the California Current system. These time series closely resemble each other, varying at a low-frequency decadal scale. However, there are some differences between the period before about 1970 and afterward. For instance, the radiolarian record is offset from sea surface temperature and the inverse relationship between annual coastal sea surface temperature and salinity is less well defined before 1970 than in the years following. Correlation between radiolarian flux and sea surface temperature peaks at flux lagging sea surface temperature by 2 years, which is perplexing because of the short radiolarian life cycle and their rapid sinking rates. The lag may reflect a biological response to environmental conditions before 1970 that differed from those after 1970, though an error in the chronology may also contribute to the lag. Inspection of radiolarian environmental group and individual species fluxes may reveal finer-scale variability relating to the apparent change around 1970, which may help in understanding the 1970 transition. Further, different cores will be sampled to test whether the chronology and the shift in response are consistent.

The association between increased total radiolarian flux and increased temperature may be explained by considering radiolarian environmental adaptations and their horizontal and vertical distributions. Radiolarians are adapted to environments with small primary producers and reduced patchiness, as occurs in the warmer water of the California Current system (Hood *et al* 1991). Additionally, the distribution of radiolarian abundance and temperature increase offshore, while salinity decreases; onshore-offshore shifts of the California Current system would lead to increased radiolarian abundance with increased temperature and

decreased coastal salinity. This is consistent with the atmospheric circulation composite, which shows that a positive PNA-type circulation corresponds to high radiolarian flux and high sea surface temperatures along the California coast.

Initial analysis of the recent 30+ year portion of the available Santa Barbara Basin radiolarian record indicates that regional-basin scale variability of yearly climate can be retrieved from this time series. To verify and further elucidate this relationship, a time series spanning the instrumental record (about the last 100 years) must be developed and tested to determine whether the relationship of the radiolarian flux to sea surface temperature and sea level pressure presented here are maintained. If this test is successful, then a much longer (at least 2000-year) Santa Barbara Basin record can be exploited.

Acknowledgments

Thanks to L. Riddle for graphics, W. Riedel and A. Sanfilippo for laboratory space, T. Baumgartner, A. Soutar, and R. Casey for core material. This work was supported in part by NSF grant ATM 94-06510.

Bibliography

Anderson, O.R. 1983. *Radiolaria.* Springer-Verlag, New York, 355 pp.

Baumgartner, T.R., J. Michaelsen, L.G. Thompson, G.T. Shen, A. Soutar, R.E. Casey. 1989. The recording of interannual climatic change by high-resolution natural systems: tree-rings, coral bands, glacial ice layers and marine varves. Pages 1-14 in *Aspects of Climate Variability in the Pacific and the Western Americas.* D.H. Peterson, editor. Geophysical Monograph 55, American Geophysical Union, Washington, D.C.

Casey, R.E., A.L. Weinheimer, C.O. Nelson. 1989. California El Niños and related changes of the California Current system from recent and fossil radiolarian records. Pages 85-92 in *Aspects of Climate Variability in the Pacific and the Western Americas.* D.H. Peterson, editor. Geophysical Monograph 55, American Geophysical Union, Washington, D.C.

Chelton, D.B., P.A. Bernal, J.A. McGowan. 1982. Large-scale interannual physical and biological interaction in the California Current. *Journal of Marine Research* 40(4):1095-1125.

Davis, R. 1976. Predictability of sea surface temperature and sea level pressure anomalies over the North Pacific Ocean. *Journal of Physical Oceanography* 6:249-266.

Ebbesmeyer, C.D., D.R. Cayan, D.R. McLain, F.H. Nichols, D.H. Peterson, K.T. Redmond, 1991. 1976 step in the Pacific climate: Forty environmental changes between 196875 and 197784. Pages 115-126 in *Proceedings of the Seventh Annual Pacific Climate (PACLIM) Workshop.* J.L. Betancourt and V.L. Tharp, editors. Asilomar, California, April 1990.

Gowing, M.M., and S.L. Coale. 1989. Fluxes of living radiolarians and their skeletons along a northeast Pacific transect from coastal upwelling to open ocean waters. *Deep-Sea Research* 36(4): 561-576.

Harris, G.P. 1986. *Phytoplankton ecology: structure, function and fluctuation.* Chapman and Hall, New York, 384 pp.

Harrison, P.J., and D.H. Turpin. 1982. The manipulation of physical, chemical and biological factors to select species from natural phytoplankton communities. Pages 275-289 in *Marine Mesocosms.* G.D. Grice and M.R. Reeve, editors. Springer, New York.

Hood, R.R., M.R. Abbott, A. Huyer, P.M. Kosro. 1990. Surface patterns in temperature, flow, phytoplankton biomass and species composition in the coastal transition zone off Northern California. *Journal of Geophysical Research* 95(C10):18,081-18,094.

Hood, R.R., M.R. Abbott, A. Huyer. 1991. Phytoplankton and photosynthetic light response in the coastal transition zone off Northern California in June 1987. *Journal of Geophysical Research* 96(C8):14,769-14,780.

Hubbell, S.P. 1979. Tree dispersion, abundance, and diversity in a tropical dry forest. *Science* 203:1299-1309.

Kling, S.A. 1977. Local and regional imprints on radiolarian assemblages from California coastal basin sediments. *Marine Micropaleontology* 2(3):207-221.

Koide, M.A., A. Soutar, E.D. Goldberg. 1972. Marine geochronology with 210Pb. *Earth and Planetary Science Letters* 14:442446.

Lange, C.B., S.K. Burke, W.H. Berger. 1990. Biological production off southern California is linked to climate change. *Climatic Change* 16:319-329.

Lynn, R.J., K.A. Bliss, L.E. Eber. 1982. Vertical and horizontal distributions of seasonal mean temperature, salinity, sigma-t, stability, dynamic height, oxygen, and oxygen saturation in the California Current, 1950-1978. *CalCOFI Atlas 30,* State of California Marine Resources Commission, La Jolla, 513 pp.

McGowan, J.A., and P.A. Walker. 1985. Dominance and diversity maintenance in an oceanic ecosystem. *Ecological Monographs* 55(1):103-118.

Namias, J., X. Yuan, D.R. Cayan. 1988. Persistence of North Pacific sea surface temperature and atmospheric flow patterns. *Journal of Climate* 1:682-703.

Norton, J., D. McLain, R. Brainard, D. Husby. 1985. The 198283 El Niño event off Baja and Alta California and its ocean climate context. Pages 44-72 in *El Niño North: Niño Effects in the Eastern Subarctic Pacific Ocean.* W.S. Wooster and D.L. Fluharty, editors. Washington Sea Grant Program.

Pisias, N.G. 1978. Paleoceanography of the Santa Barbara Basin during the last 8000 years. *Quaternary Research* 10:366-384.

Pisias, N.G. 1979. Model for Paleoceanographic reconstructions of the California Current during the last 8000 years. *Quaternary Research* 11:373-386.

Schimmelmann, A., C.B. Lange, W.H. Berger, A. Simon, S.K. Burke, R.B. Dunbar. 1992. Extreme climatic conditions recorded in Santa Barbara Basin laminated sediments: the 1835-1840 *Macoma* event. *Marine Geology* 106:279-299.

Thunell, R., and L.R. Sautter. 1992. Planktonic foraminiferal faunal and stable isotopic indices of upwelling: a sediment trap study in the San Pedro Basin, Southern California Bight. Pages 77-91 in *Upwelling Systems: Evolution Since the Early Miocene.* C.P. Summerhayes, W.L. Prell, and K.C. Emeis, editors. Geological Society Special Publication No. 64, London, England.

Turpin, D.H., and P.J. Harrison. 1980. Cell size manipulation in natural marine, planktonic, diatom communities. *Canadian Journal of Fisheries and Aquatic Sciences* 37:1193-1195.

Wallace, J.M., and D.S. Gutzler. 1981. Teleconnections in the geopotential height field during the Northern Hemisphere winter. *Monthly Weather Review* 109:784-812.

Weinheimer, A.L., T.L. Carson, C.R. Wigley, R.E. Casey. 1986. Radiolarian responses to recent and Neogene California el Niño and anti-el Niño events. *Palaeogeography, Palaeoclimatology, Palaeoecology* 53:325.

Welling, L.A., N.G. Pisias, A.K. Roelofs. 1992. Radiolarian microfauna in the northern California Current system: indicators of multiple processes controlling productivity. Pages 177-195 in *Upwelling Systems: Evolution Since the Early Miocene.* C.P. Summerhayes, W.L. Prell, K.C. Emeis, editors. Geological Society Special Publication No. 64, London, England.

High Productivity and Upwelling in the California Current during Oxygen-Isotope Stage 3: Diatom Evidence

Eileen Hemphill-Haley

Evidence for vigorous coastal upwelling and enhanced diatom productivity during the latter part of Oxygen-Isotope Stage 3 (OIS-3) is suggested by changes in diatom assemblages in laminated sediment from the northern California margin and in bioturbated and laminated sediment from Santa Barbara Basin. These conditions require strong along-shore or off-shore wind stress off California preceding the onset of global glacial conditions.

Upwelling-driven productivity during late OIS-3 resulted in a suboxic oxygen-minimum zone and episodic preservation of laminated deposits along at least 85 kilometers of the continental slope off California (Hemphill-Haley and Gardner 1994). Comparison of organic carbon (C_{org}), biogenic silica ($\%Si_{opal}$), and diatom assemblages from laminated deposits in two gravity cores reflect the influences of a strong upwelling center off Point Arena that persisted during late OIS-3 (Hemphill-Haley *et al*, in review). Gravity core TT197-G330 was collected off Point Arena near 39°N, and gravity core L13-81-117 was collected 85 kilometers to the south, off of the Russian River (Figure 1). Both cores contain finely laminated deposits of late OIS-3 age (Figure 2).

C_{org} in laminated sediment is comparable for both cores, and ranges from about 1.0-2.0% (Figure 3). However, $\%Si_{opal}$ is greater in laminated sediment in the Russian River core (2.0-5.0%) than in the Point Arena core (<%2.0). Higher $\%Si_{opal}$ in the Russian River core is the result of greater overall concentration of diatom frustules compared to the Point Arena core, as supported visually by strewn slide analysis.

Striking differences in dominant diatom taxa exist between the two cores, in addition to differences in diatom concentration. In the Point Arena core, well-preserved laminated deposits of late OIS-3 age contain low relative abundances of planktonic diatoms and *Chaetoceros* spp. resting spores and valves, but high relative abundances of reworked freshwater diatoms and the heavily silicified (and easily reworked) taxa *Stephanopyxis* spp. (Figure 4a). In contrast, laminated deposits of OIS-3 age in the Russian River core contain abundant planktonic diatoms and *Chaetoceros* resting spores and valves (Figure 4b). Excellent preservation of rare planktonic species in laminated deposits of the Point Arena core strongly suggests that the differences in diatom assemblages between the two cores is not an artifact of preservation.

In: C.M. Isaacs and V.L. Tharp, Editors. 1995. *Proceedings of the Eleventh Annual Pacific Climate (PACLIM) Workshop, April 19-22, 1994.* Interagency Ecological Program, Technical Report 40. California Department of Water Resources.

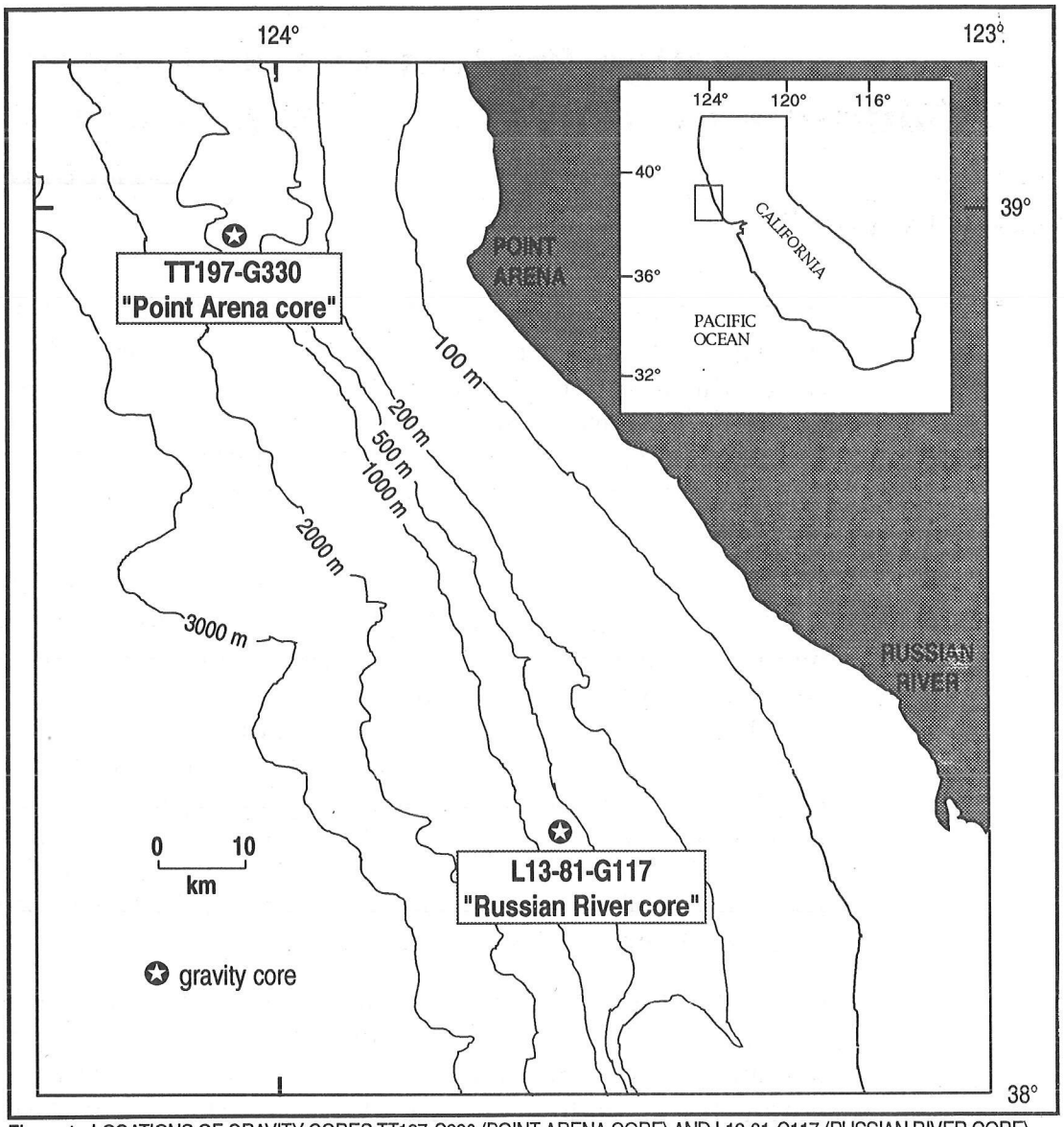

Figure 1. LOCATIONS OF GRAVITY CORES TT197-G330 (POINT ARENA CORE) AND L13-81-G117 (RUSSIAN RIVER CORE)

Modern coastal upwelling is prevalent along the northern California coast, but is particularly vigorous at the coastal promontory of Point Arena, where some of the highest seaward- and southward-directed surface water velocities have been recorded during the spring/summer upwelling season (Huyer 1983). The contrasting diatom thanatocoenoses between the Point Arena and Russian River cores, therefore, may be the result of one of the cores being located beneath a vigorous upwelling center sustained by exceptionally strong equatorward or off-shore winds during late OIS-3. The high surface water velocities would have restricted flux of planktonic diatoms from surface waters to the sea floor at Point Arena, whereas "downstream" of the upwelling center, off the Russian River, lower surface water velocities would have permitted the accumulation of high numbers of *Chaetoceros* spp. and other planktonic diatoms in low-oxygen slope deposits. Diatom analyses for a series of additional gravity and piston cores indicate that strong upwelling, high diatom

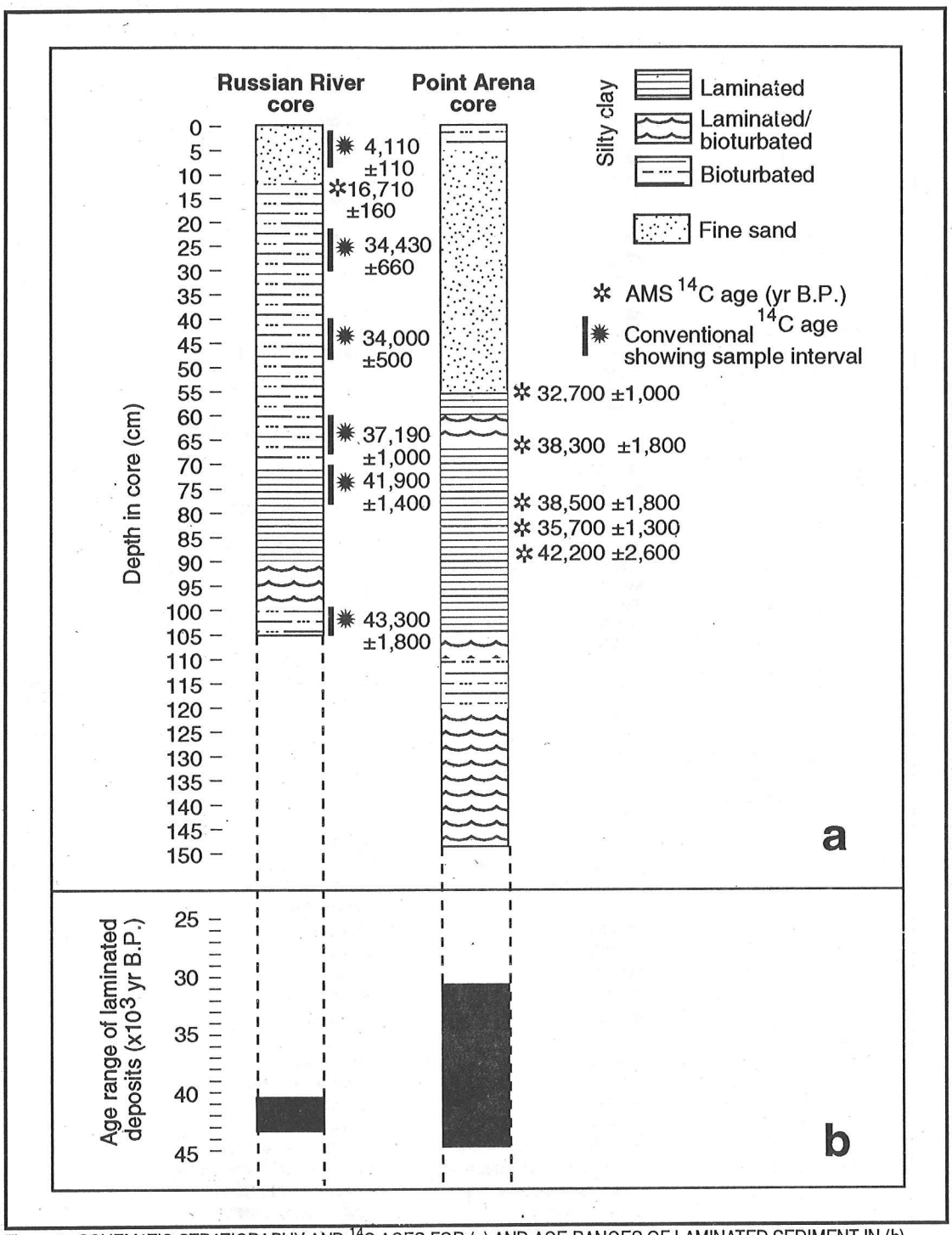

Figure 2. SCHEMATIC STRATIGRAPHY AND ^{14}C AGES FOR (a) AND AGE RANGES OF LAMINATED SEDIMENT IN (b) THE POINT ARENA AND RUSSIAN RIVER CORES

productivity, and accumulation of laminated deposits on the northern California slope, as well as the restricted flux of planktonic species off Point Arena, are characteristic of late OIS-3 (Gardner *et al* 1988; Hemphill-Haley 1993; Hemphill-Haley and Gardner 1994). The data, therefore, suggest that the coastal wind stress and upwelling that episodically persisted off northern California during late OIS-3 exceeded that of glacial OIS-2 or the Holocene.

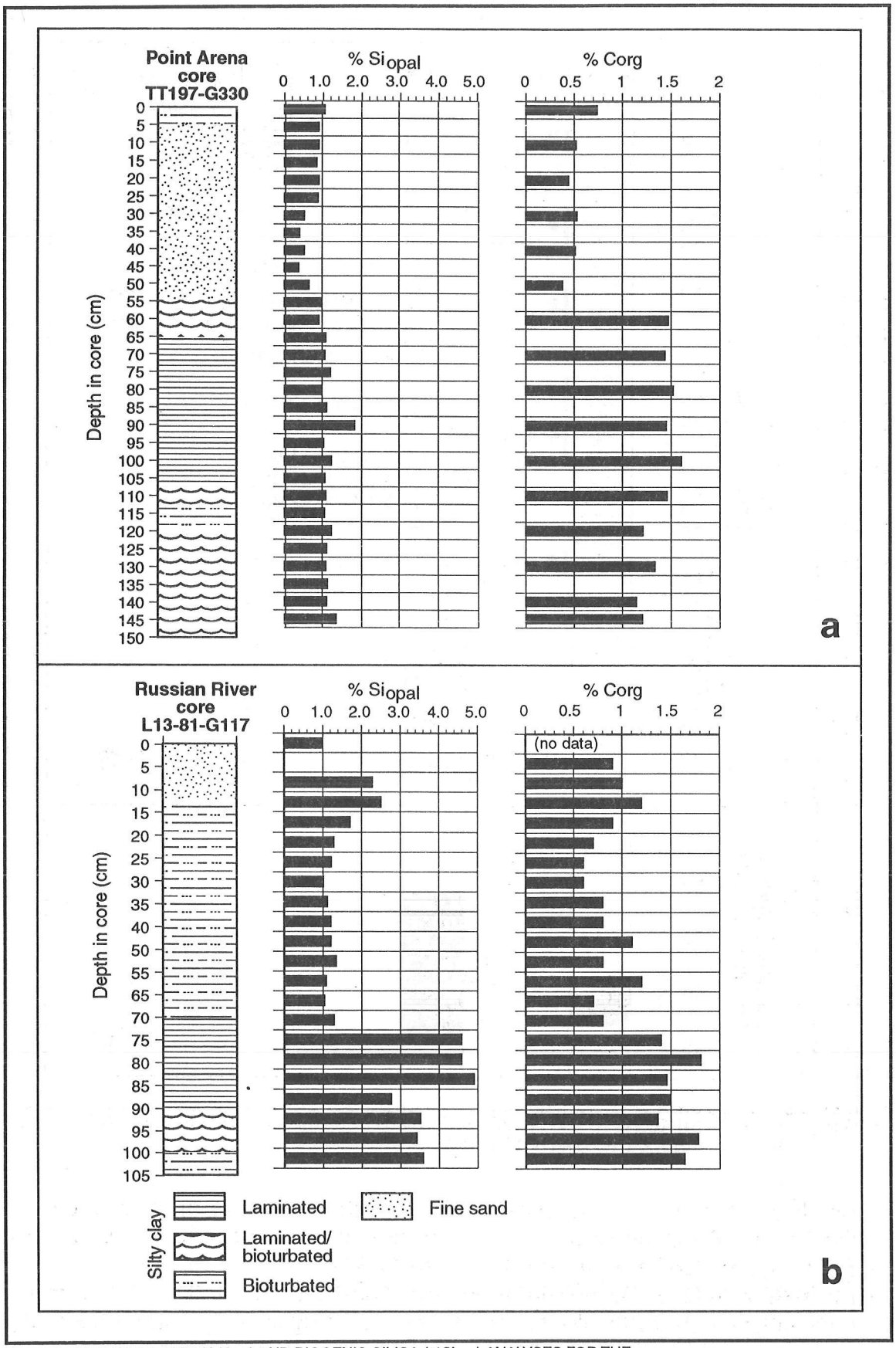

Figure 3. ORGANIC CARBON (C_{org}) AND BIOGENIC SILICA ($\%Si_{opal}$) ANALYSES FOR THE POINT ARENA (a) AND RUSSIAN RIVER (b) CORES

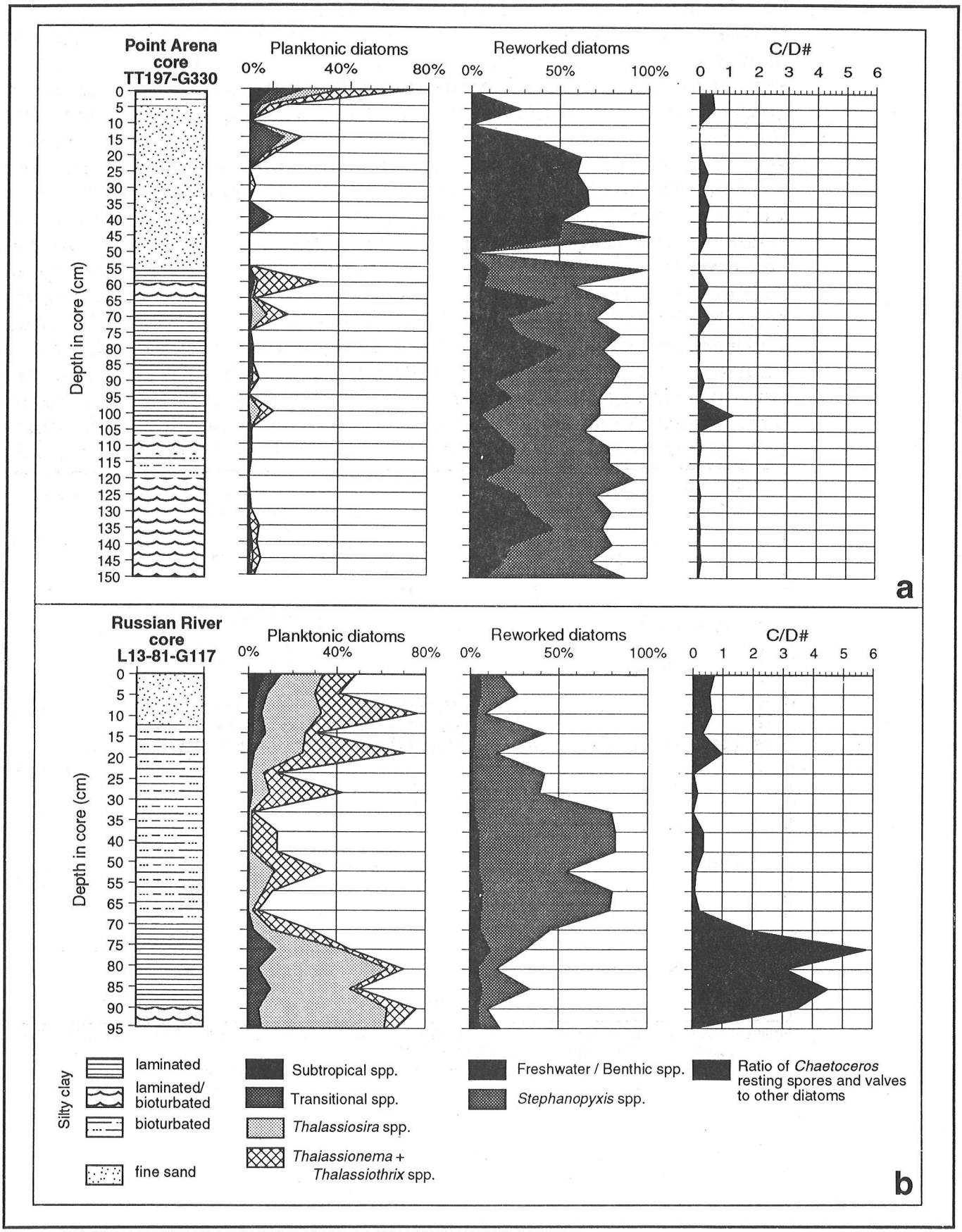

Figure 4. DIATOM ANALYSES FOR THE POINT ARENA (a) AND RUSSIAN RIVER (b)CORES
C/D# is the ratio of *Chaetoceros* spp. resting spores and valves to all other diatoms.

OIS-3 deposits between about 46,000 and 28,000 years ago in Santa Barbara Basin consist of short alternating intervals of laminated and bioturbated sediment. This is in contrast to thoroughly bioturbated deposits of OIS-2 and is evidence for rapid fluctuations in bottom-water oxygen (Kennett *et al* 1994). Diatoms of late OIS-3 age in Santa Barbara Basin sediments are overwhelmingly dominated by the spring/summer upwelling group, *Chaetoceros* spp., in both laminated and bioturbated intervals (Figures 5, 6a). Mass accumulation rates (MARs, in g/(cm^2*kyr) for total diatoms (dominantly *Chaetoceros* spp.) show a consistent decrease from 46,000 to 28,000 years ago, suggesting a decrease in overall productivity over time (Figure 5). Differences in MARs for the same diatom taxa (*Chaetoceros* spp., *Thalassionema* spp., and *Stephanopyxis* spp.) in adjacent laminated and bioturbated samples are most likely due to poorer preservation in most bioturbated intervals (Figure 6). However, comparison of MARs for the upwelling group, *Chaetoceros* spp., and the non-upwelling group, *Thalassionema* spp. (Reimers *et al* 1990), in laminated intervals indicates different trends for the two groups. Other than a sharp increase at about 33,000 years ago, MARs in laminated intervals

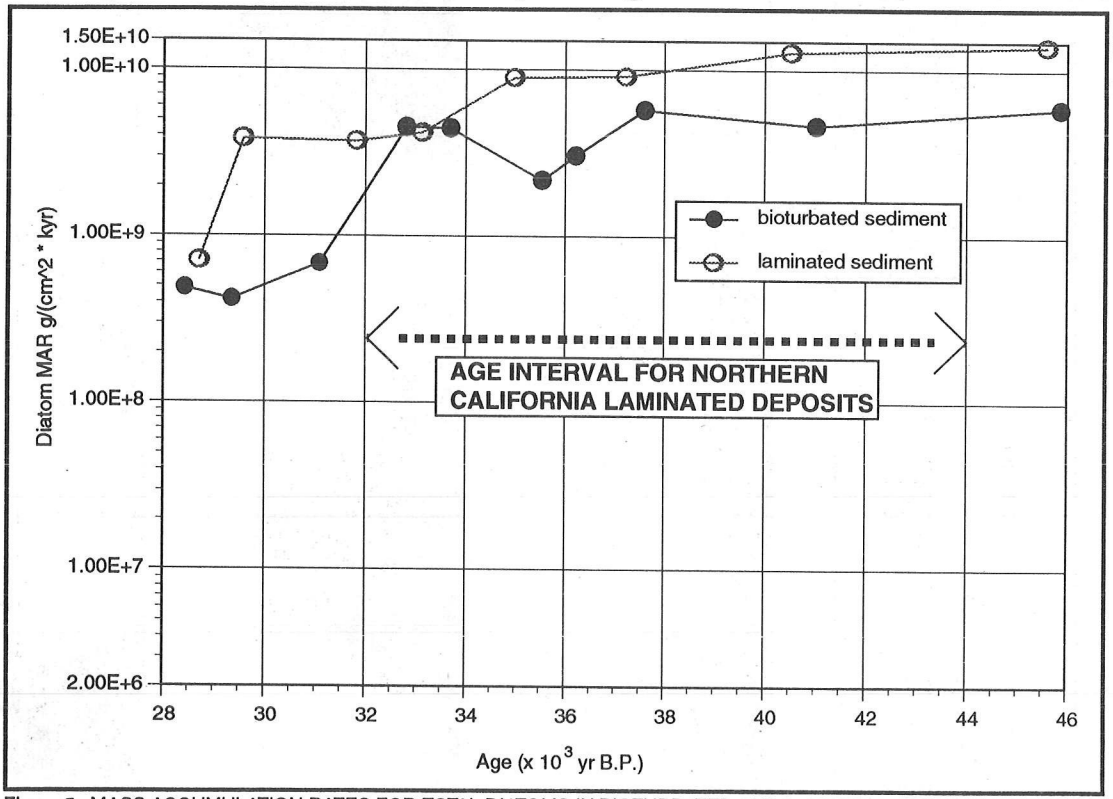

Figure 5. MASS ACCUMULATION RATES FOR TOTAL DIATOMS IN BIOTURBATED AND LAMINATED INTERVALS OF LATE OIS-3 AGE AT SANTA BARBARA BASIN ODP SITE 893A
Arrow brackets the range of ages for laminated sediment in the Point Arena and Russian River cores.

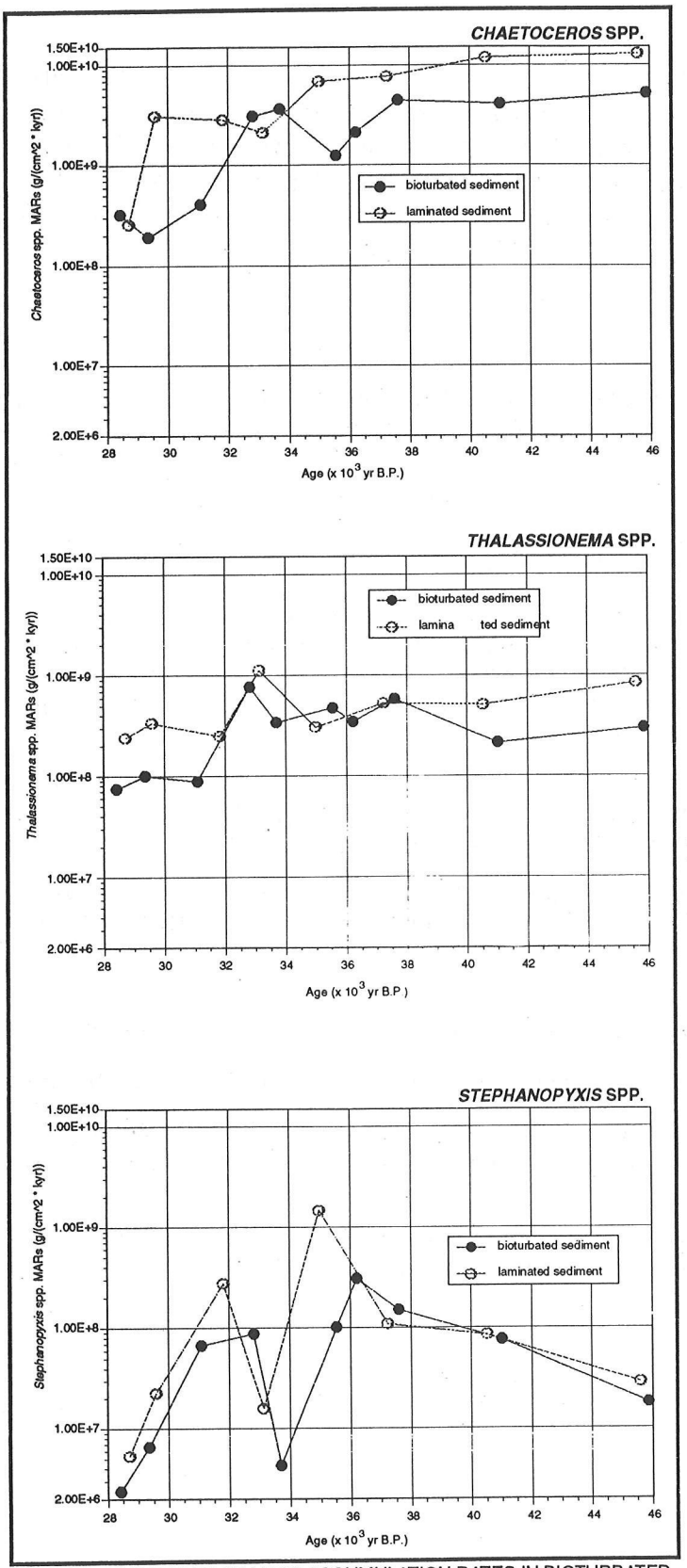

Figure 6. COMPARISON OF MASS ACCUMULATION RATES IN BIOTURBATED AND LAMINATED DEPOSITS FOR *CHAETOCEROS* spp., *THALASSIONEMA* spp., AND *STEPHANOPYXIS* spp. FOR ODP SITE 893A

Higher MARs in most laminated samples are probably the result of better preservation in the absence of bioturbation.

for *Thalassionema* spp. remain relatively constant from 46,000 to 28,000 years ago, while MARs for *Chaetoceros* spp. decrease (Figure 7). This suggests a decrease in upwelling-related diatom productivity relative to non-upwelling-related diatom productivity approaching the onset of glacial Stage 2. Although this decrease in diatom flux may be an artifact of localized productivity and changing sea level at Santa Barbara Basin preceding the OIS-3/OIS-2 transition, it coincides with the termination of laminated deposits on the continental slope off central and northern California (Anderson *et al* 1989; Gardner *et al* 1992; Hemphill-Haley and Gardner 1994).

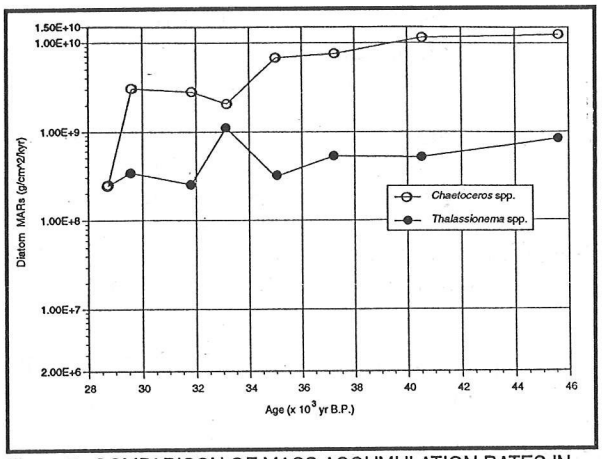

Figure 7. COMPARISON OF MASS ACCUMULATION RATES IN LAMINATED SAMPLES ONLY FOR *CHAETOCEROS* spp. AND *THALASSIONEMA* spp. FOR ODP SITE 893A

Acknowledgments

Discussions with J. Gardner, W. Dean, C. Lange, and C. Sancetta benefited the study. Thanks to P. Dartnell for providing geochemical data and reviewing the manuscript. This study was funded by the U.S. Geological Survey "Correlation of the Marine and Terrestrial Records of Climate" (CMTR) project, which is part of the Global History and Climate Change Program.

References

Anderson, R.Y., J.V. Gardner, E. Hemphill-Haley. 1989. Variability of the late Pleistocene-early Holocene oxygen-minimum zone off northern California. Pages 75-84 in *Aspects of Climate Variability in the Pacific and Western Americas*. D.H. Peterson, editor. American Geophysical Union, Washington, DC.

Gardner, J.V., W.E. Dean, R. Kayen. 1992. *USGS Cruise F2-92, Central and Southern California Margin.* U.S. Geological Survey Open-File Report 92-342, 354 pp.

Gardner, J.V., L.E. Heusser, P.J. Quinterno, S.M. Stone, J.A. Barron, R.Z. Poore. 1988. Clear Lake record vs. the adjacent marine record: A correlation of their past 20,000 years of paleoclimatic and paleoceanographic responses. Pages 171-182 in *Late Quaternary Climate, Tectonism, and Lake Sedimentation in Clear Lake, Northern California Coast Ranges*. J.D. Simms, editor. Special Paper 214, Geological Society of America, Boulder, CO.

Hemphill-Haley, E. 1993. *Distribution and Taxonomy of Late Quaternary Diatoms from Gravity Cores L13-81-G117, L13-81-G138, L13-81-G145, and TT197-G330, Northern California Continental Slope.* U.S. Geological Survey Open-File Report 93-340, 108 pp.

Hemphill-Haley, E., and J.V. Gardner. 1994. Revised ages for laminated-sediment intervals and a Holocene-marker diatom from the northern California continental slope. *Quaternary Research* 41:131-135.

Hemphill-Haley, E., J.V. Gardner, P. Dartnell. In review. Diatom and geochemical evidence for variability in coastal upwelling off northern California during Oxygen-Isotope Stage 3. *Marine Geology.*

Huyer, A. 1983. Coastal upwelling in the California Current system. *Progress in Oceanography* 12:259-284.

Kennett, J.P., J.G. Baldauf, *et al.* 1994. Site 893. Pages 15-81 in *Proceedings of the Ocean Drilling Program, Initial Reports*, Vol. 146 (Pt. 2). G.K. Westbrook, B. Carson, R.J.H. Musgrave, editors. Ocean Drilling Program, College Station, TX.

Reimers, C.E., C.B. Lange, M. Tabak, J.M. Bernhard. 1990. Seasonal spillover and varve formation in the Santa Barbara Basin, California. *Limnology and Oceanography* 35(7):1577-1585.

Neogene through Pleistocene Paleoclimate of the Great Salt Lake Region, Northeastern Great Basin, USA

Thomas E. Moutoux and Owen K. Davis

Introduction

In a cooperative agreement between Amoco Production Company and the University of Arizona Geosciences Department, extensive data and resources associated with 15 deep wells drilled in the Great Salt Lake are currently on loan at the University of Arizona. Seismic data, electric and lithologic logs, cuttings and previously-prepared pollen slides will eventually permit a thorough study of both the tectonic and climatic history of the Great Salt Lake region. The preliminary study presented here concentrates on the Late Tertiary and Pleistocene climatic reconstruction of the eastern Great Basin through examination of fossil pollen. To date, pollen has been counted from five of the wells: Carrington Island "H", Bridge "L", South Rozel "J", Indian Cove "I", and East Gunnison "P" (Figure 1). Both the South Rozel and Bridge counts are tentatively believed to represent about 7 million years of record.

Previously, climatic reconstructions of this duration in the Great Basin required piecing together paleoclimatic information from multiple sites. Invariably, this introduces the problems of stratigraphic correlation and paleo-site compatibility. A few studies in and around the Great Basin offer coherent, if not continuous, paleoclimatic records; however, these span only the last about 3 million years. These studies include Tulelake (Adam *et al* 1989), Searles Lake (Smith 1984), and the INEL core from southern Idaho reported on by Thompson (1991) in his thorough paper on Pleistocene environments and climates in the western United States.

Site Information

The Great Salt Lake is in the northeastern portion of the Great Basin Province. Currently the lake partially fills a structural half graben. The Wasatch Range to the east expresses the faulted side of this half graben, and the subsequent basin is filled with more than 12,000 feet of sediment in some locations. The surface of the lake is about 4,200 feet above sea level. Precipitation is brought into the area predominantly through large frontal systems during the winter. Annual precipitation totals are generally 12 to 16 inches (300 to 400 mm). Mean annual temperature is about 10 to 11 degrees Celsius.

In: C.M. Isaacs and V.L. Tharp, Editors. 1995. *Proceedings of the Eleventh Annual Pacific Climate (PACLIM) Workshop, April 19-22, 1994.* Interagency Ecological Program, Technical Report 40. California Department of Water Resources.

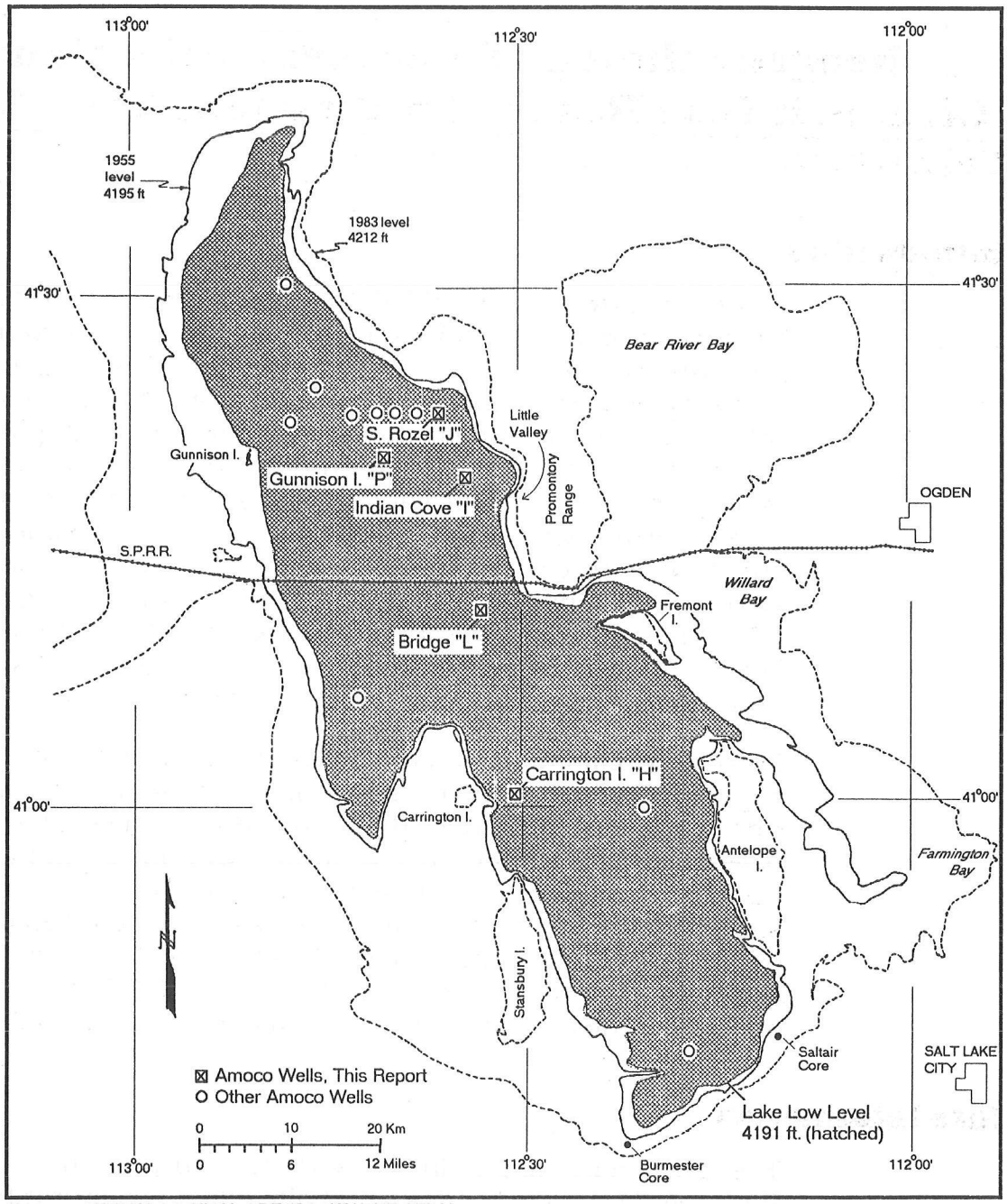

Figure 1. STUDY LOCATION, GREAT SALT LAKE, UTAH

Due to the large elevational variation in the region, there is an equally large variation in regional plant communities. The basin floor surrounding the lake is characterized by shadescale steppe, which predominantly consists of members of the Chenopodiaceae including shadescale (*Sarcobatus*) and saltbush (*Atriplex*). Sagebrush (*Artemisia*) and grasses are also widely present. At slightly higher elevations, *Artemisia* becomes more dominant, creating the sagebrush steppe. At still higher elevations, pinyon-juniper and oak woodlands are present. These woodlands consist dominantly of pinyon pine (*Pinus edulis*) and juniper (*Juniperus*), and oak

(*Quercus*) and maple (*Acer*), respectively. In the higher mountains such as the Wasatch, these woodlands give way to forests consisting mainly of lodgepole pine (*Pinus contorta*), white fir (*Abies concolor*), douglas fir (*Pseudotsuga menziesii*), and aspen (*Populus tremuloides*). In the highest forested area, spruce (*Picea engelmannii*), limber pine (*Pinus flexilis*), and bristlecone pine (*Pinus longaeva*) dominate.

Palynology

Pollen slides were prepared by Amoco using cuttings gathered at 10- to 30-foot intervals from the individual wells. Pollen was obtained from undisclosed quantities of sediment representing a 30-foot interval. Slides were made at about every 100 feet for 12 of the 15 wells. Of the five wells counted to date, only the South Rozel and Bridge wells have been counted to near their bases (about 6,800 and 12,100 feet, respectively). The Indian Cove well is the deepest, penetrating over 12,400 feet of sediment; however, high pollen deterioration percentages at about 5,000 feet have led us to temporarily cease counting. Pollen from the East Gunnison and Carrington Island wells have been counted to 3,700 and 2,730 feet, respectively. Pollen counts consist of 300 upland pollen types whenever possible. Aquatic and riparian pollen, as well as other palynomorphs such as spores and dinoflagellates, are recorded but kept outside the sum. The upland pollen types make up the "sum", which serves as the divisor for all percentages.

The pollen percentage diagrams created for the five wells are remarkably similar, suggesting that a region signal is being reflected. Only the two longest pollen records are shown here (Figure 2). The two diagrams are plotted with pollen percentage verses depth in feet and have in no way been altered to reflect variations in sedimentation rate. For the sake of clarity, the regional pollen trends are discussed relative to the Bridge well depths.

Very significant pollen percentage changes can be seen in the Bridge well. From the base of the well to about 10,800 feet, *Pinus* and *Sarcobatus* dominate the count, with *Pinus* averaging around 20 to 40% and *Sarcobatus* hovering at about 20%. Chenopodiaceae-*Amaranthus* (Cheno-Ams), *Artemisia* and *Ephedra* (joint-fir, Mormon tea) occur at 5 to 10%. Interestingly, Compositae pollen is present at this depth interval, though not in high percentages. Between about 10,800 and 8,700 feet, the Cheno-Ams, *Artemisia*, and Compositae disappear almost completely. *Pinus* reaches nearly 80% before it again begins to drop off, giving way to a relative increase in *Sarcobatus*, reaching over 40%. Pollen percentages from these first two intervals do not match the modern vegetation now in the area(Davis, in press). At about 8,700, the Cheno-Ams, *Artemisia*, and Compositae return, and the *Sarcobatus* and *Ephedra* begin to taper off. Between 8,700 feet and 4,000 feet, *Pinus*, *Sarcobatus*, and *Ephedra* all continue to decline. *Artemisia* reaches a high of about 30% at about 7,000 feet but again falls off and tends to fluctuate around 20%. Cheno-Ams

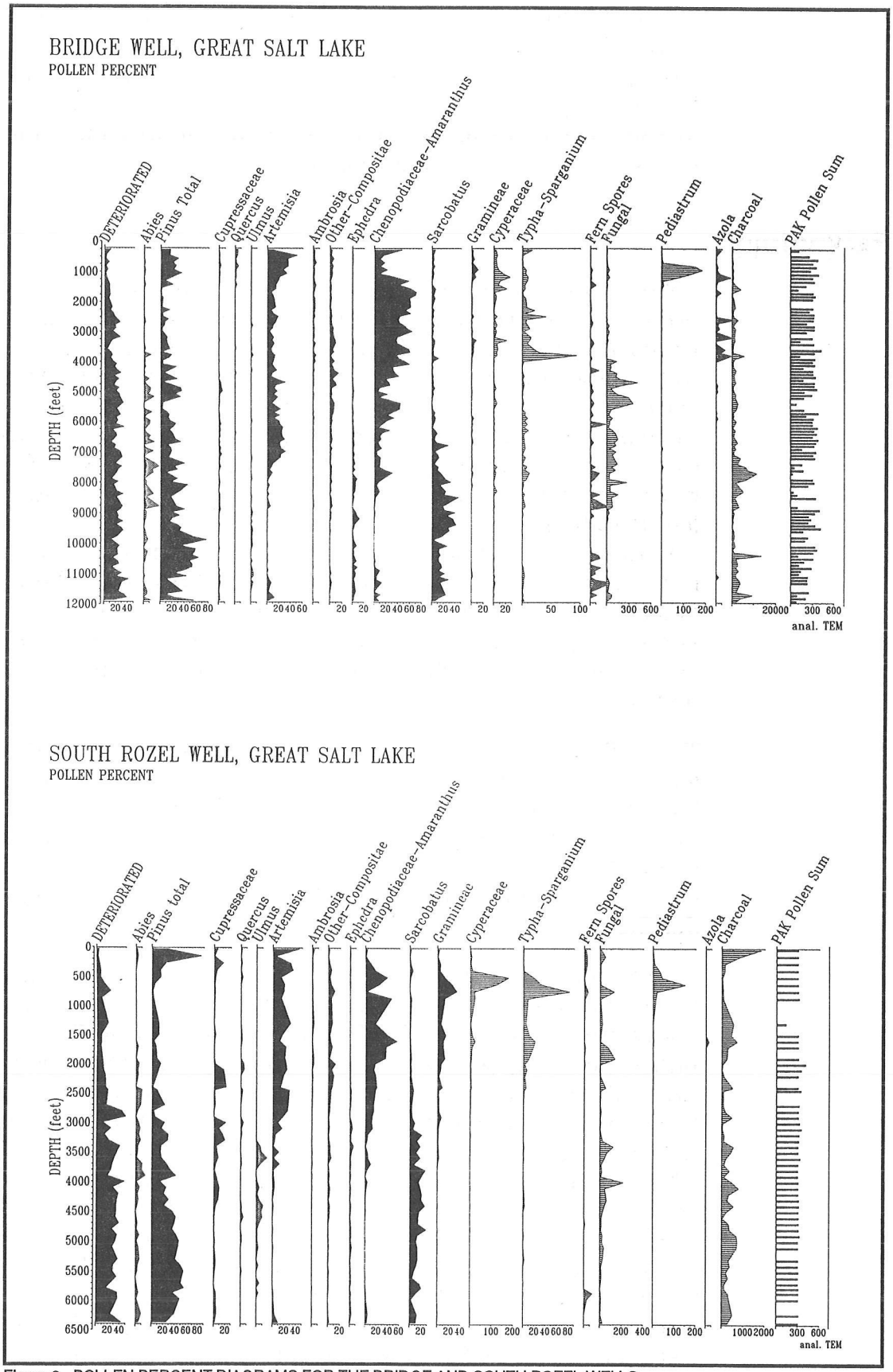

Figure 2. POLLEN PERCENT DIAGRAMS FOR THE BRIDGE AND SOUTH ROZEL WELLS

Upland pollen types have solid black curves. Other palynomorphs outside the sum have horizontally striped curves. Hatched areas represent 5X exaggeration of the original curve.

and Compositae both increase, with Cheno-Ams increasing to over 40% and Compositae reaching its high at about 12%. Pollen percentages during this interval most closely resemble that of a shadescale steppe and periodically a sagebrush steppe (Davis, in press). The interval between about 4,000 and 1,500 feet shows a continued increase in Cheno-Am pollen, attaining a maximum of over 60%. *Pinus* continues its general decreasing trend, reaching an all-time low of about 3% at 1,500 feet. Again, pollen percentages from this interval most closely reflect those from a shadescale steppe, but with even higher Cheno-Am percentages and lower *Pinus* percentages, suggesting an even warmer and drier environment than the modern shadescale steppe. The interval from 1,500 feet to the top is characterized by a strong increase in *Pinus* and *Artemisia* and a rapid decrease in Cheno-Ams. These changes, along with increases in *Quercus*, Cupressaceae, and Graminae, suggest that the paleo-lake was often surrounded by sagebrush steppe and pygmy woodland during this interval (Davis, in press).

Chronology and Correlation

The chronology and correlations used in this preliminary stage of the study are tentative. Currently, only two units within the Indian Cove well and one within East Gunnison can be positively assigned an absolute age. The two units in Indian Cove are both ash layers. The ashes were recently chemically analyzed and compared to regional ashes of known ages. This "fingerprinting" resulted in the match of the lower ash (2,630 feet) with the Huckleberry Ridge Tuff and the upper ash (1,460 feet) with the Lava Creek "B" Ash (William P. Nash, written communication, September 20, 1994). The Huckleberry Ridge Tuff and Lava Creek "B" Ash are assigned ages of 2.01 and 0.61 million years ago, respectively (Christiansen 1979). The dated unit in East Gunnison is a basalt with a thickness of about 200 feet. Although the basalt has actually been K/Ar-dated from material taken from a neighboring well, the seismic signature of this impressive unit is so strong that there is no mistaking the correlation. The K/Ar date on the basalt is about 3.1 ma, which makes it a likely correlative of the surficially exposed Rozel Basalt.

Correlation of these dated units to the other wells is accomplished primarily through comparison of the pollen percentage diagrams, and subsequently fine-tuned through alignment of ash layers. Sediments from each of the five wells were thoroughly examined for ash, both welded and loose shards. This search resulted in location of occasional, but not common ash layers. At this time, having few ash layers is beneficial to the study in that it allows for simpler correlations between ash units. Frequent ash layers would only add confusion in the absence of a more accurate correlation technique. Future chemical analysis and finger printing of all the ashes found in the well sediments should eventually allow for better correlations and absolute age dating. The Rozel Basalt found in the East Gunnison well is tentatively recognized in the Indian

Cove well as a thick Basaltic conglomerate. No other correlations with this basalt can be confidently made. Huckleberry Ridge Tuff, Lava Creek "B" Ash, and Rozel Basalt correlations can be seen as dashed lines on Figures 3 and 4.

Climatic Reconstruction

All quantitative climatic reconstructions were made through comparison with contemporary pollen samples. A database of pollen percentages consisting of 1,367 western United States surface samples has been compiled by Dr. O.K. Davis and used here as a source for possible modern analogs (Davis, in press). A computer program designed by Davis utilizes the square cord distance dissimilarity function in searching out these analogs. The program compares pollen percentages from every modern sample in the database to those of the target fossil pollen sample. In all, 28 common pollen types are compared for each sample. A modern sample is considered an analog if a dissimilarity value of 0.15 or lower is calculated. A value of 0.15 implies that two samples are five times more likely to be the same than different.

Associated with each surface sample is climatic information consisting of estimated mean annual temperature and precipitation. Once all modern analogs are determined for a fossil sample, the climatic information associated with each modern analog is summed and averaged. This permits mean annual values with error bars to be calculated.

Modern analogs were found for every fossil sample counted in the Indian Cove and Carrington Island wells, and all but two samples near the base of East Gunnison had matches. It is now believed that none of these three wells represents much more than 5 million years of record (see Figures 3 and 4). Interestingly, both the South Rozel and Bridge wells, which are believed to contain over 12 million years of record, can only be climatically reconstructed back to about 7.0 to 7.5 ma. Beyond this age, only two samples from each well produced any modern analogs, and these occur near the base of the wells (samples not shown in Figures 3 and 4). In both wells, modern analogs cease to be found when the Cheno-Ams, *Artemisia*, and Compositae are virtually absent and the pollen spectrum is dominated by *Pinus*, *Sarcobatus*, and *Ephedra*. This analog gap may be the result of holes in the modern surface sample database, it may be related to preferential deterioration of certain pollen types, or perhaps the fossil pollen accurately represents a vegetation assemblage that simply does not exist at the present.

The climatic reconstructions of all five wells are presented in Figures 3 and 4. Climatic correlation among the wells is not very tight, which must be partly attributed to uncertainties involved in the current time/stratigraphic correlation of the wells. Despite these uncertainties, a few features illustrated in the reconstructions are worth mentioning. The most notable is the apparently sudden change to a cooler and moister

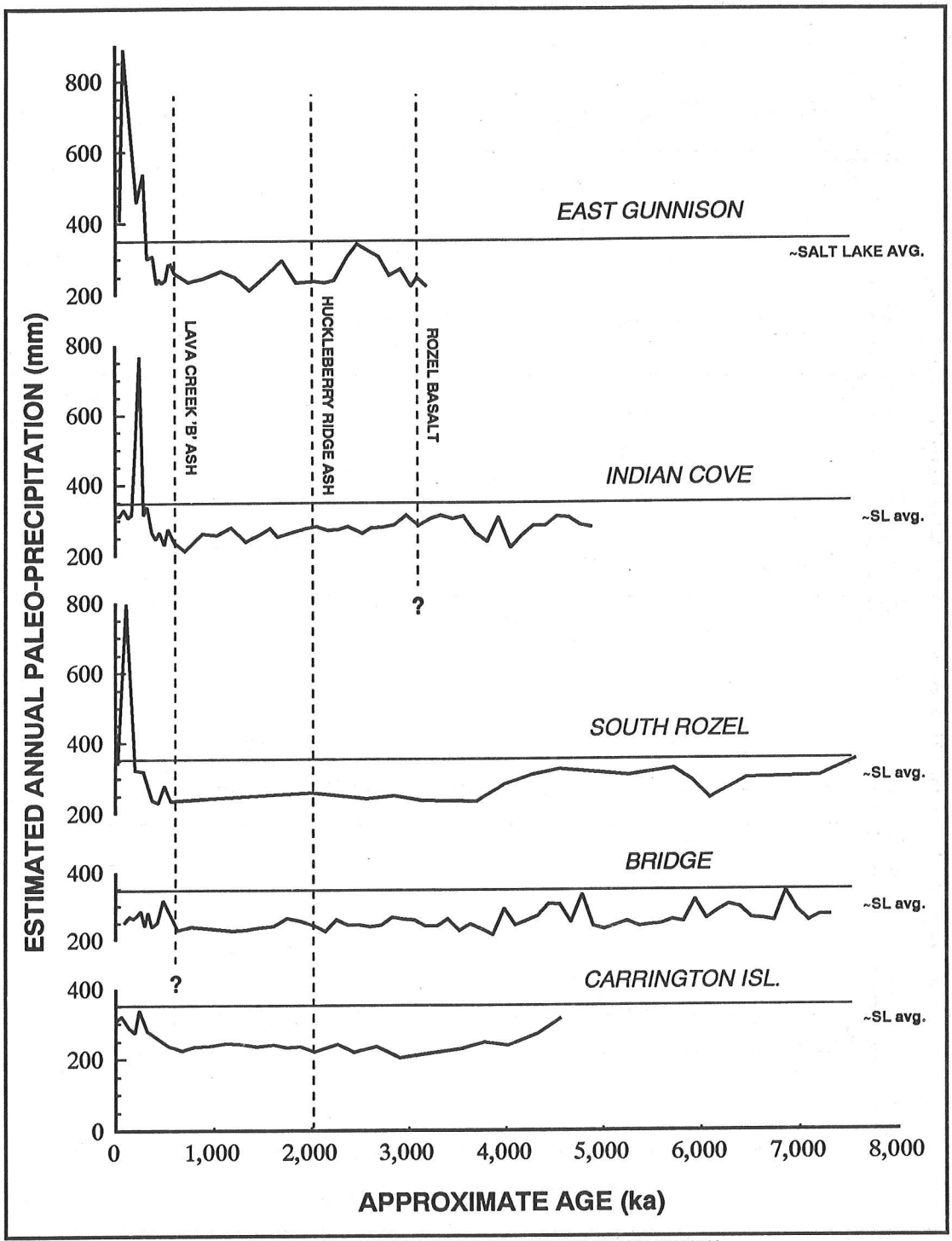

Figure 3. PALEO-PRECIPITATION RECONSTRUCTION FOR THE GREAT SALT LAKE REGION
Approximate positions of the Rozel Basalt, Huckleberry Ridge Ash, and Lava Creek "B" Ash are shown with vertical dashed lines.

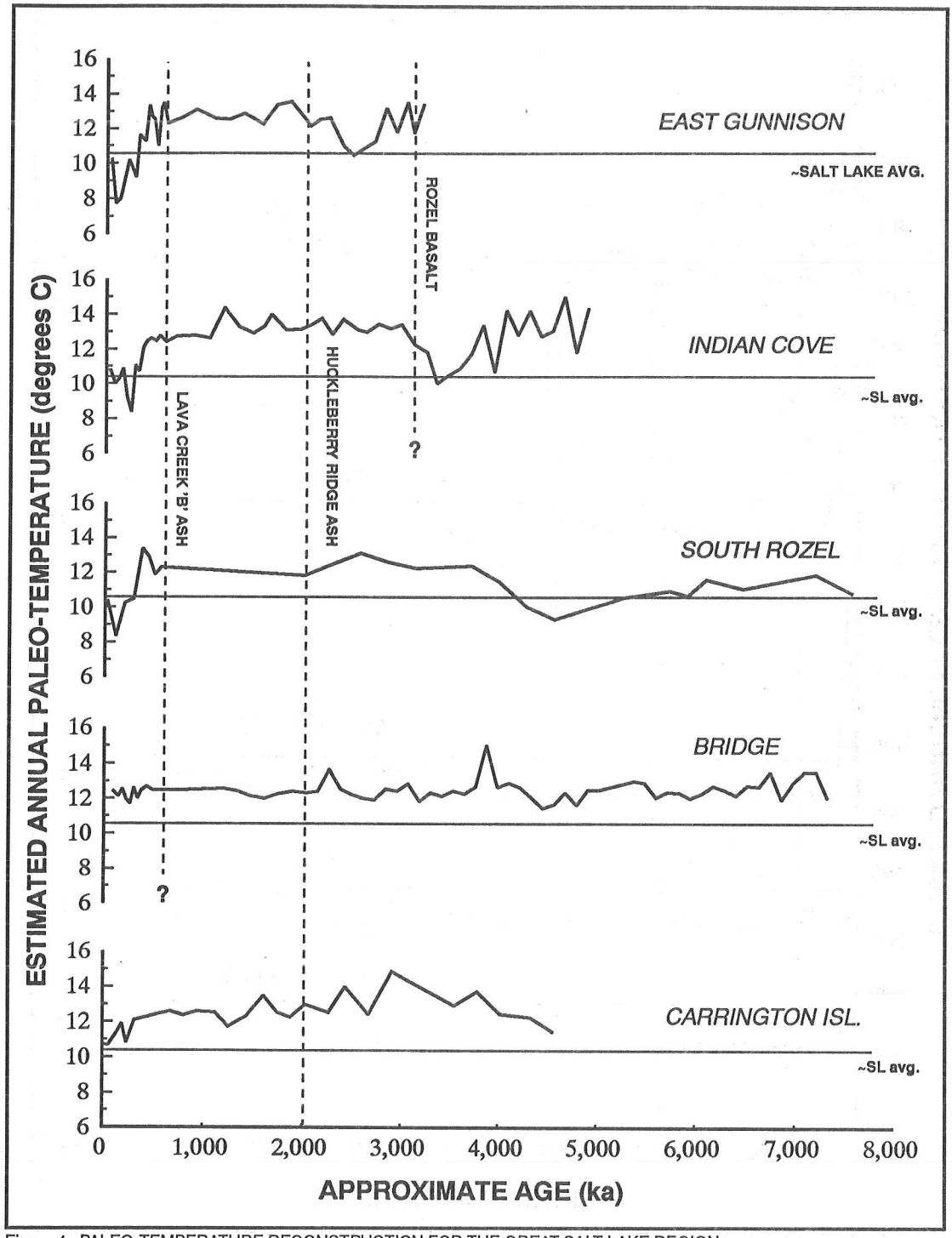

Figure 4. PALEO-TEMPERATURE RECONSTRUCTION FOR THE GREAT SALT LAKE REGION
Approximate positions of the Rozel Basalt, Huckleberry Ridge Ash, and Lava Creek "B" Ash are shown with vertical dashed lines.

climate at about 700,000 years ago. All five wells register a change near this time, with the northern wells showing the largest fluctuations. If these northern wells accurately reflect the climate, mean annual temperature may have commonly been more than 2 degrees Celsius lower than at present, and precipitation may frequently have been double that of today. Before about 700,000 years ago, temperatures have generally been higher by 1 to 3 degrees, and precipitation has been lower than today by 50 to 100 mm. Although there appears to be no overall trend to the temperature, there does seem to be a slight trend toward decreasing precipitation since the late Miocene (~7.5 million years ago).

Acknowledgments

We thank Amoco Production Company for eagerness in loaning us the materials necessary to make this study work and the National Science Foundation for monetary contributions. We also give special thanks to Dr. William Nash for the timely ash dates.

References

Adam, D.P., A.M. Sarna-Wojcicki, H.J. Rieck, J.P. Bradbury, W.E. Dean, R.M. Forester. 1989. Tulelake, California: The last three million years. *Palaeogeography, Palaeoclimatology, Palaeoecology*, 72:89-103

Christiansen, R.L. 1979. Cooling units and composite sheets in relation to caldera structure. Pages 29-42 in *Ash Flow Tuffs*. C.E. Chapman and W.E. Elston, editors. GSA Special Paper 180.

Davis, O.K. (in press). Climate and vegetation patterns in surface samples from arid western USA: Application to Holocene climatic reconstructions. *Palynology*.

Smith, G.I. 1984. Paleohydrologic regimes in the southwestern Great Basin, 0-3.2 my ago, compared with other long records of "global" climate. *Quaternary Research* 22:1-17.

Thompson, R.S. 1991. Pliocene environments and climates in the western United States. *Quaternary Science Reviews* 10:115-132.

A 139-Year Dendroclimatic Cycle, Cultural/Environmental History, Sunspots, and Longer-Term Cycles

Thor Karlstrom

Introduction

Higher resolution time-stratigraphic records suggest correlation of lower frequency paleoclimatic events with Milankovitch obliquity/precessional cycles and of higher frequency events with the evidently resonance-related Pettersson maximum tidal force (MTF) model (Karlstrom 1961). Subsequently published records, mainly pollen (Hevly and Karlstrom 1974), seemingly confirm that atmospheric resonances may have modulated past climatic changes in phase with average MTF cycles of 1668, 1112, and 556 years, as calculated in anomalistic years from planetary movements by Stacey (1963, 1967). Stacey accepts Pettersson's (1914) dating of AD 1433 (517 YBP) for the last major perihelian spring tide based solely on calculations of moon- and earth-orbital relations to the sun. Use of AD 1433 as an origin for the tidal resonance model seemingly continues to provide a best fit for the timing of cyclical patterns in the presented paleoclimate time series.

Dating basal contacts (point boundaries) in Southwest alluvium produces temporal clustering seemingly in phase with the doubling of the 556-year Phase Cycle or its 2/1 (278-year) resonance (Hevly and Karlstrom 1974; Karlstrom 1988). This result, however, is unconfirmed by spectral analyses of Colorado Plateau dendroclimatic records that clearly define only 1- to 2-year cycles (Dean 1988). This could result either from tree-ring standardization procedures that eliminate longer-term trends or from difficulties in applying spectral analyses to detrended composite records characterized by:

- Relatively short cross-dated segments that further limit lower-frequency analysis.
- Interrupted high-frequency cyclical patterns that episodically change sign through a transition point, suggesting nonlinear response to an external forcing function (chaos theory).
- Varying amounts of distorting noise (nonclimatic effects on tree growth).

Moreover, spectral analytical results statistically define dominant cycle lengths (not their timing) and are sensitive to differing levels of smoothing

In: C.M. Isaacs and V.L. Tharp, Editors. 1995. *Proceedings of the Eleventh Annual Pacific Climate (PACLIM) Workshop, April 19-22, 1994.* Interagency Ecological Program, Technical Report 40. California Department of Water Resources.

and positioning that can mask real cycles and generate spurious ones (aliasing). Use of half-cycle smoothing positioned on cycle turning points thus should provide a more direct and critical test of the resonance model, since the model imposes severe constraints on both timing and cycle length and permits concurrent testing of longer- and shorter-term harmonics.

Half-Cycle Analysis of Southwest Dendroclimatic Records

As shown in Figures 1-10, preliminary half-cycle analyses of Southwest dendroclimatic records from California to New Mexico and Coloradoproduce common intervals of generally warmer/drier climate alternating with intervals of cooler/wetter climate that are most strongly in phase with the doubling of the 278-year subphase cycle, or the 4/1 (139-year) resonance of the 556-year phase cycle. Higher frequency resonance patterns vary from record to record, evidently reflecting differing response functions, variable timing of nonlinear phase reversals, and differing amounts and distribution of distorting noise.

Trend correlation coefficients of the 139-year cycle range from 0.75 to 1.0, or within the upper part of the correlation range (<0.6->0.9) of tree-ring/climate calibrations. This suggests that the cycle is real, regionally robust, and evidently related to changing atmospheric patterns and dynamics. Continued half-cycle analysis of other dendroclimatic records may define diagnostic regional patterns as well as differing local responses, thus advancing understanding of climatic/biologic processes.

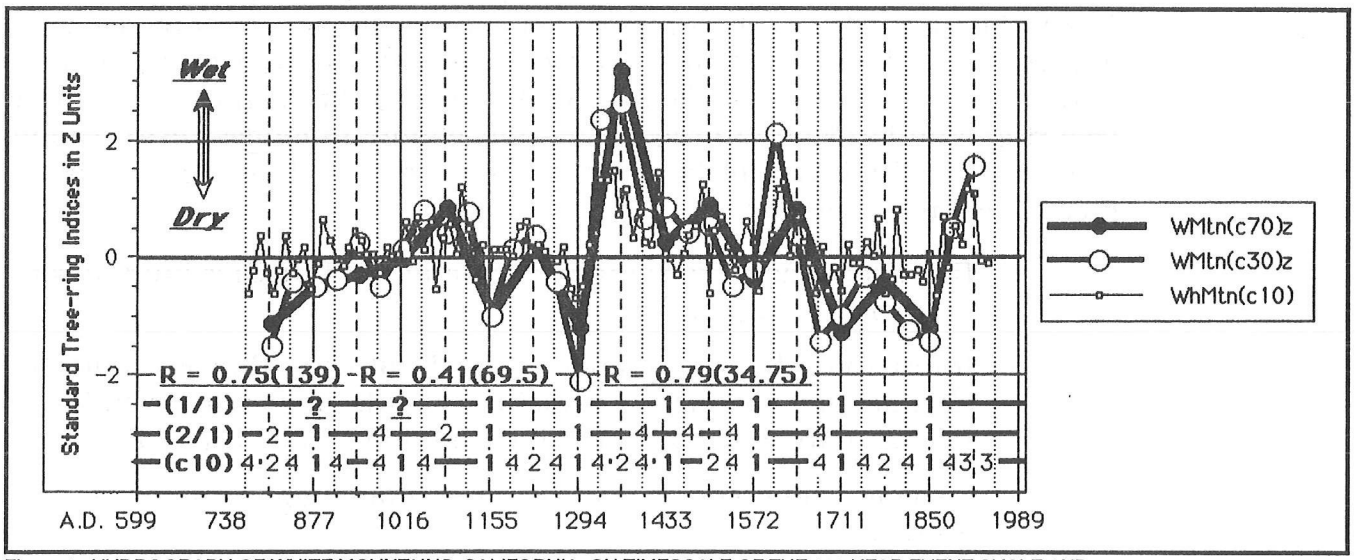

Figure 1. HYDROGRAPH OF WHITE MOUNTAINS, CALIFORNIA, ON TIMESCALE OF THE 139-YEAR EVENT CYCLE AND ITS 2/1 (69.5-YEAR) AND 4/1 (34.75-YEAR) RESONANCES

Half-cycle and near-half-cycle smoothing positioned on cycle turning points; conversion to Z units after smoothing. Decadal indices from Station 12 (Fritts 1967). Trend correlations suggest a fairly strong precipitation response to the 139-year event cycle and a stronger response to its 4/1 (34.75-year) resonance (Bruckner cycle).

Refined analysis requires use of annual indices that permit the most precise half-cycle smoothing (Figures 6-9). Near half-cycle smoothing using 10-year and 20-year smoothed indices (Figures 1-5) does not appear to significantly affect analytical results of the longer-term trends, but it does limit analyses to those cycles with wave lengths of more than 20 and 40 years, respectively.

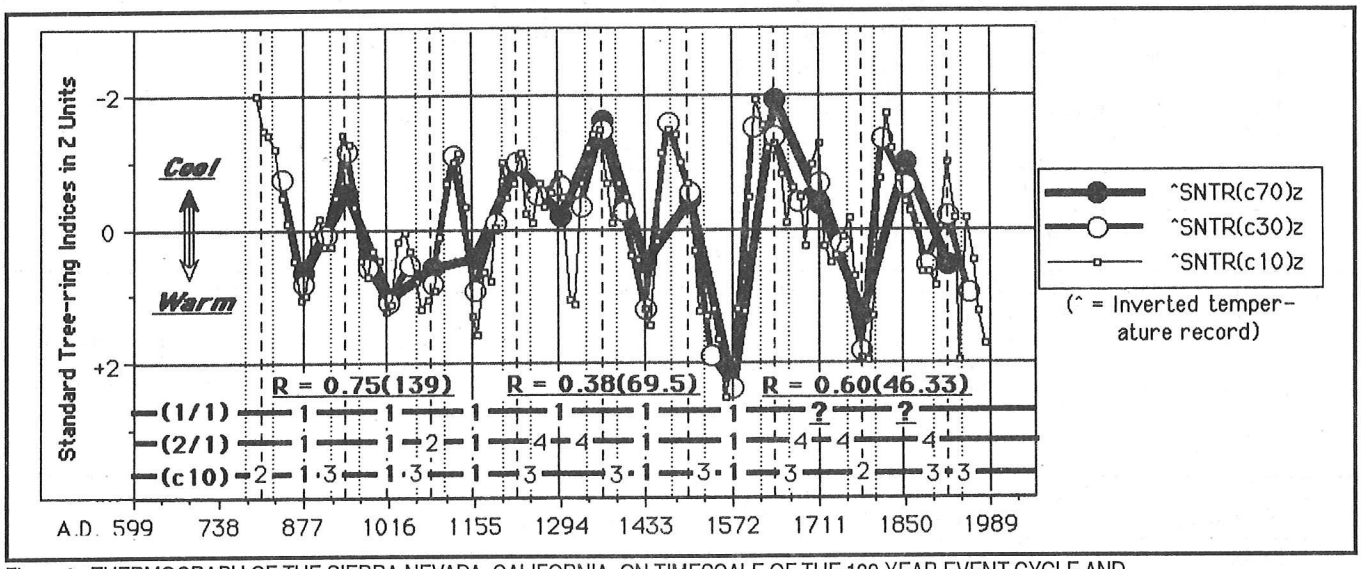

Figure 2. THERMOGRAPH OF THE SIERRA NEVADA, CALIFORNIA, ON TIMESCALE OF THE 139-YEAR EVENT CYCLE AND ITS 2/1 (69.5-YEAR) AND 3/1 (46.33-YEAR) RESONANCES

Half-cycle and near-half-cycle smoothing positioned on cycle turning points; conversion to Z units after smoothing. Upper timberline tree-ring 10-year indices from Scuderi (1987). Trend correlations suggest a fairly strong temperature response to the 139-year event cycle. In higher frequencies there is a stronger tendency to respond to the 3/1 than to the 2/1 resonance. Contrast with Figure 1.

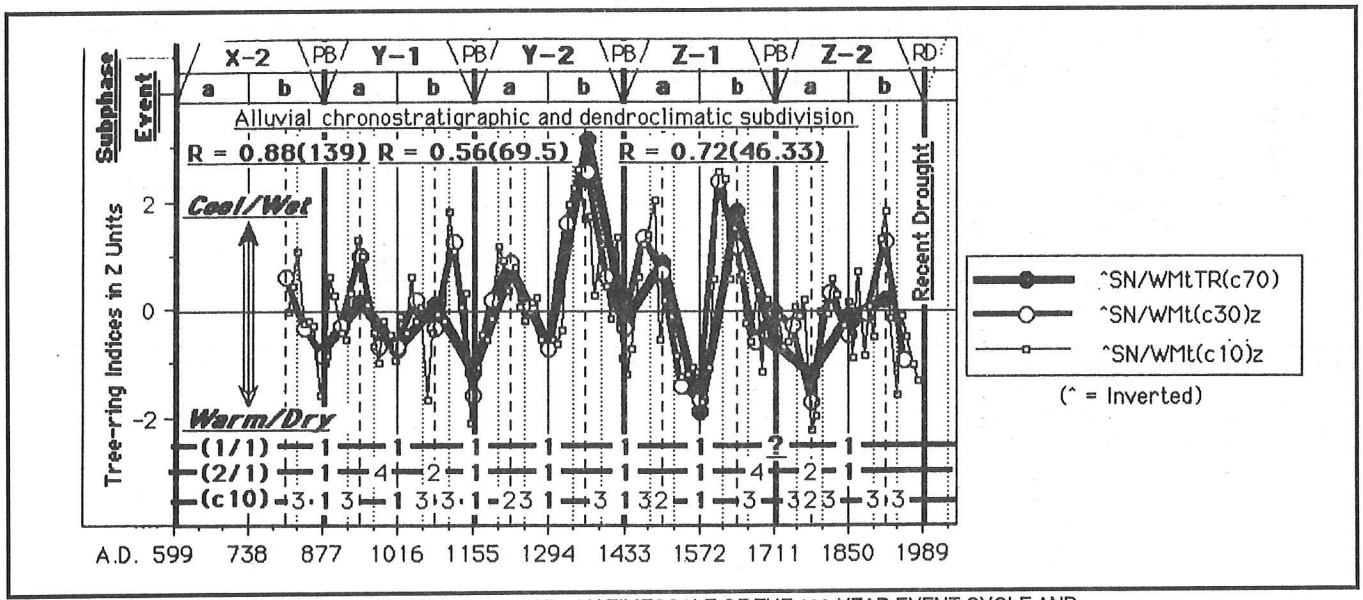

Figure 3. HYDROTHERMOGRAPH OF CENTRAL CALIFORNIA ON TIMESCALE OF THE 139-YEAR EVENT CYCLE AND ITS 2/1 (69.5-YEAR) AND 3/1 (46.33-YEAR) RESONANCES

Constructed by combining hydrograph of White Mountains (Figure 1) with inverted thermograph of the Sierra Nevada (Figure 2). The combined precipitation/temperature record improves correlation with the 139-year event cycle and emphasizes higher frequency response to the 3/1 resonance. The sign inversion in Z-2a evidently results from an unusually deep temperature trough at the half-cycle position centered AD 1780. The chronostratigraphic subdivision is after Karlstrom (1988). PB = Point Boundary (clustering of alluvial basal-contact dates).

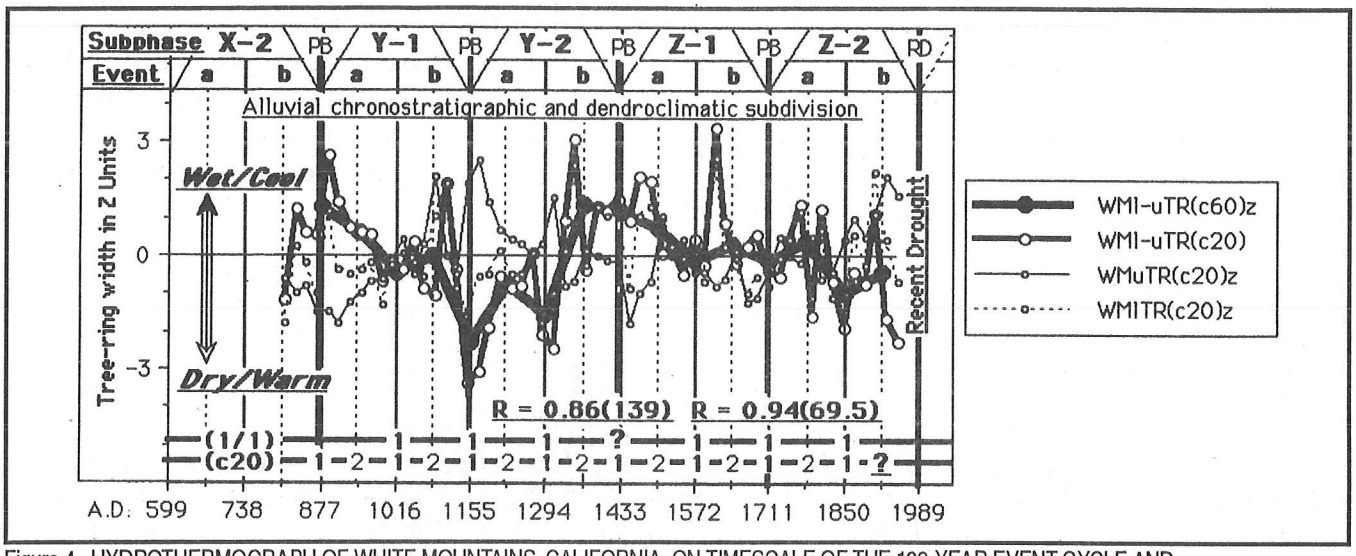

Figure 4. HYDROTHERMOGRAPH OF WHITE MOUNTAINS, CALIFORNIA, ON TIMESCALE OF THE 139-YEAR EVENT CYCLE AND ITS 2/1 (69.5-YEAR) RESONANCE

Curve constructed by combining the lower timberline (precipitation) record with the upper timberline (temperature) record, which is inverted to satisfy parallelism with the paleoclimatic equation. The 20-year tree-ring indices are from LaMarche (1974). The chronostratigraphic subdivisions are from Karlstrom (1988). PB = Point Boundary (clustering of basal-contact dates). As in Figure 3, combination of precipitation and inverted temperature curves improves correlation with the 139-year event cycle but, in contrast, also suggests a strong in-phase relationship with the 2/1 (69.5-year) resonance rather than with the 3/1 (46.33-year) resonance.

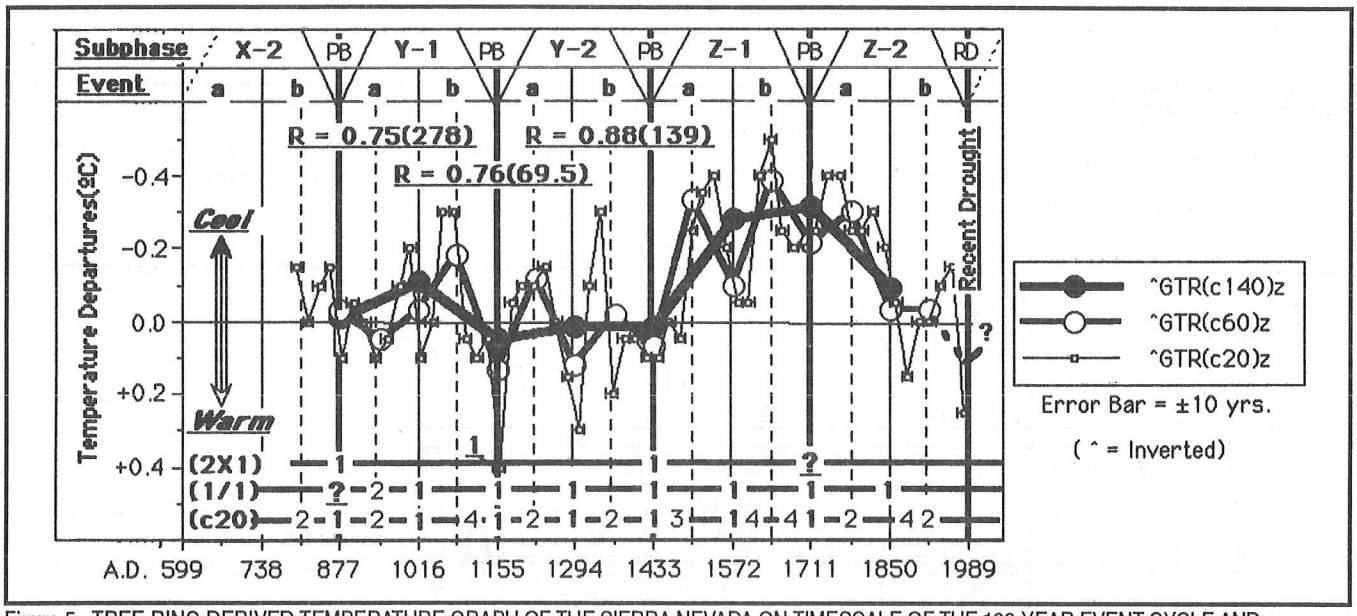

Figure 5. TREE-RING-DERIVED TEMPERATURE GRAPH OF THE SIERRA NEVADA ON TIMESCALE OF THE 139-YEAR EVENT CYCLE AND ITS 2/1 (69.5-YEAR) RESONANCE

Half-cycle smoothing and chronostratigraphic subdivision as before. Curve replotted at 20-year intervals from Graumlich (1992). Strongest correlations are with the 139-year event cycle and its 2/1 (69.5-year) resonance. Compare with Figures 1, 2, and 4.

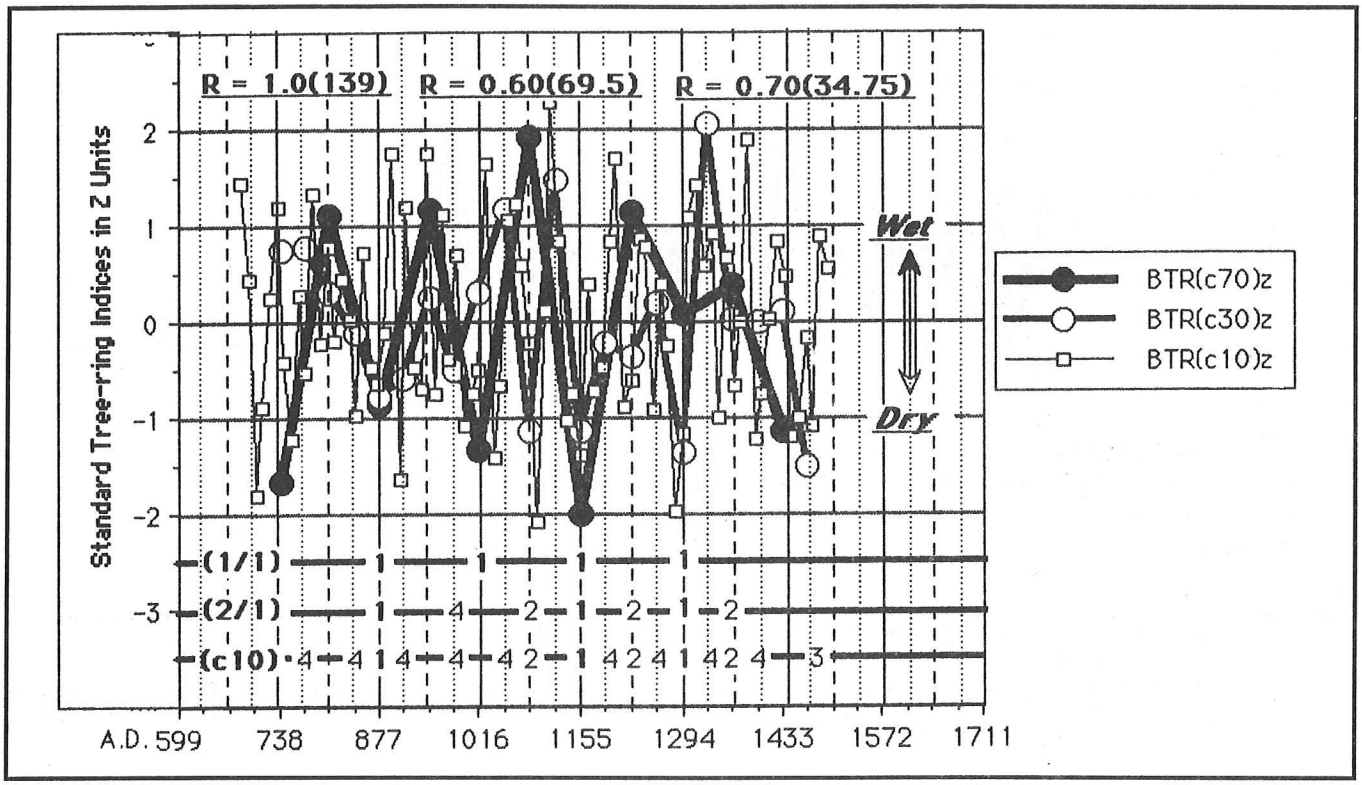

Figure 6. HYDROGRAPH OF SOUTHERN COLORADO PLATEAUS ON TIMESCALE OF THE 139-YEAR EVENT CYCLE AND ITS 2/1 (69.5-YEAR) AND 4/1 (34.75-YEAR) RESONANCES

Half-cycle smoothing as before. Seventeen station 10-year indices from Berry (1982). Very strong precipitation response to the event cycle; lesser but significant response to the 4/1 (34.75-year) resonance (Bruckner cycle).

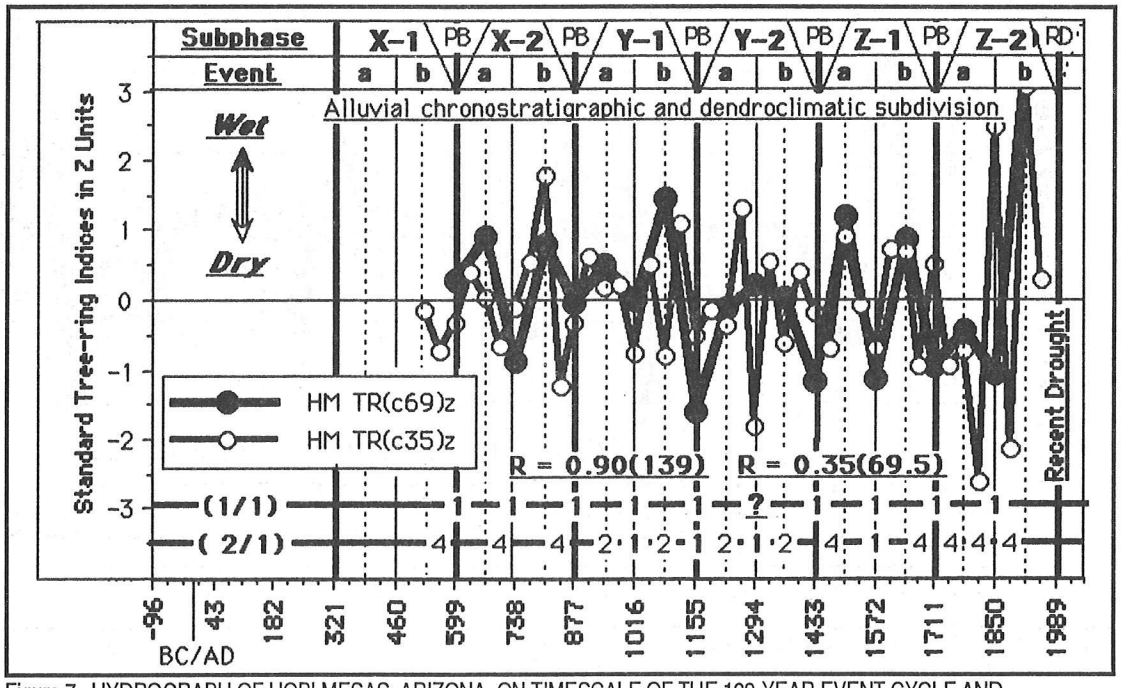

Figure 7. HYDROGRAPH OF HOPI MESAS, ARIZONA, ON TIMESCALE OF THE 139-YEAR EVENT CYCLE AND ITS 2/1 (69.5-YEAR) RESONANCE

Half-cycle smoothing and chronostratigraphic subdivision as before. Annual tree-ring indices from Dean and Robinson (1978). Very strong response to the event cycle; weak or insignificant response to the 2/1 resonance.

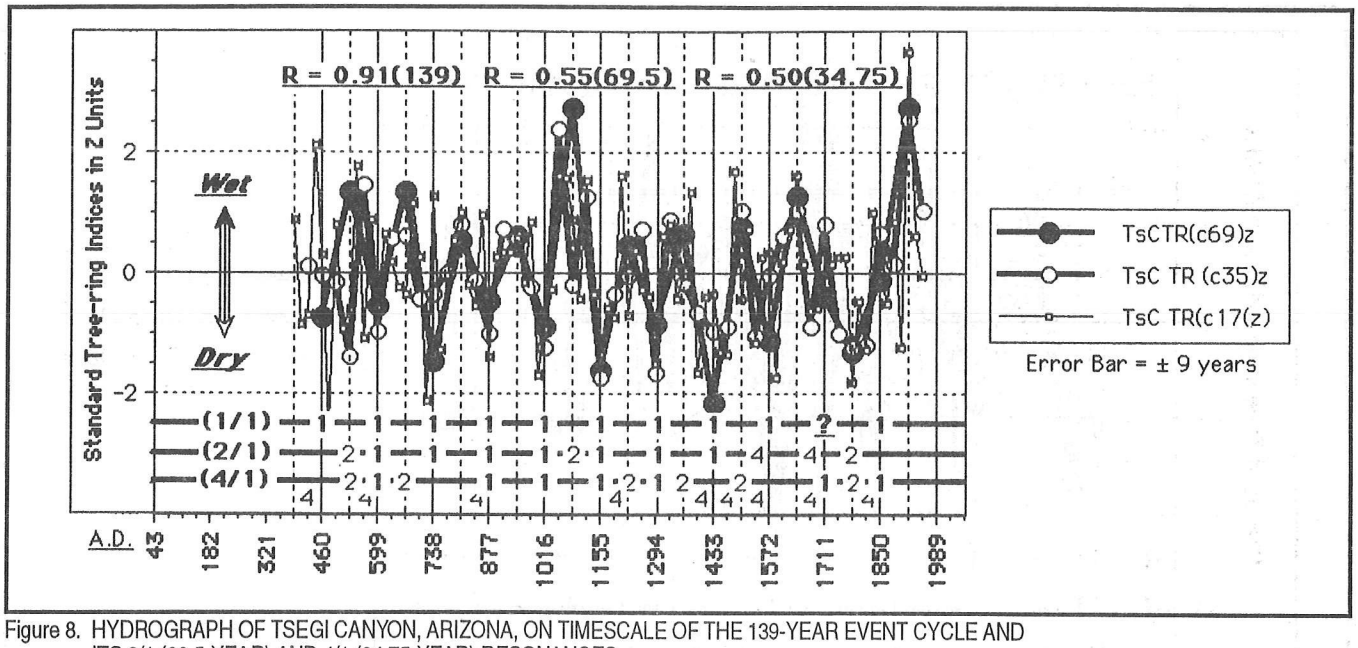

Figure 8. HYDROGRAPH OF TSEGI CANYON, ARIZONA, ON TIMESCALE OF THE 139-YEAR EVENT CYCLE AND ITS 2/1 (69.5-YEAR) AND 4/1 (34.75-YEAR) RESONANCES

Half-cycle smoothing same as before. Annual tree-ring indices from Dean and Robinson (1978). Very strong response to the event cycle; weak or insignificant response to the higher frequency half-resonances. The sign inversion between AD 1711 and 1850 appears to result from an unusually deep dry interval at the half-cycle position (AD 1780) or contemporaneous with the deep temperature high in one of the Sierra Nevada records (Figure 2), but not evident in the other (Figure 5)..

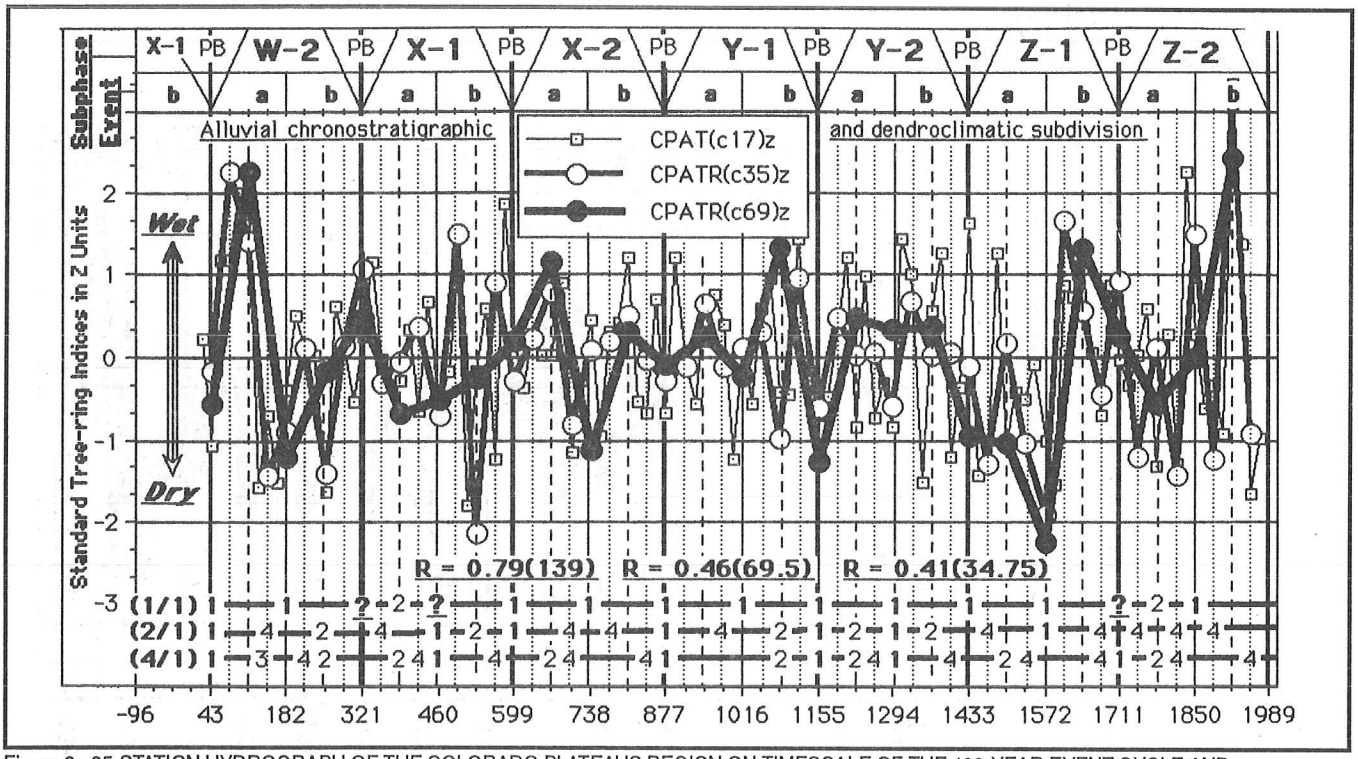

Figure 9. 25-STATION HYDROGRAPH OF THE COLORADO PLATEAUS REGION ON TIMESCALE OF THE 139-YEAR EVENT CYCLE AND ITS 2/1 (69.5-YEAR) AND 4/1 (34.75-YEAR) RESONANCES

Half-cycle smoothing and chronostratigraphic subdivision same as before. Annual indices from Dean and Robinson (1978). Though including many incomplete records, the regional composite retains a fairly strong response to the event cycle but weak or insignificant response to the higher frequency resonances.

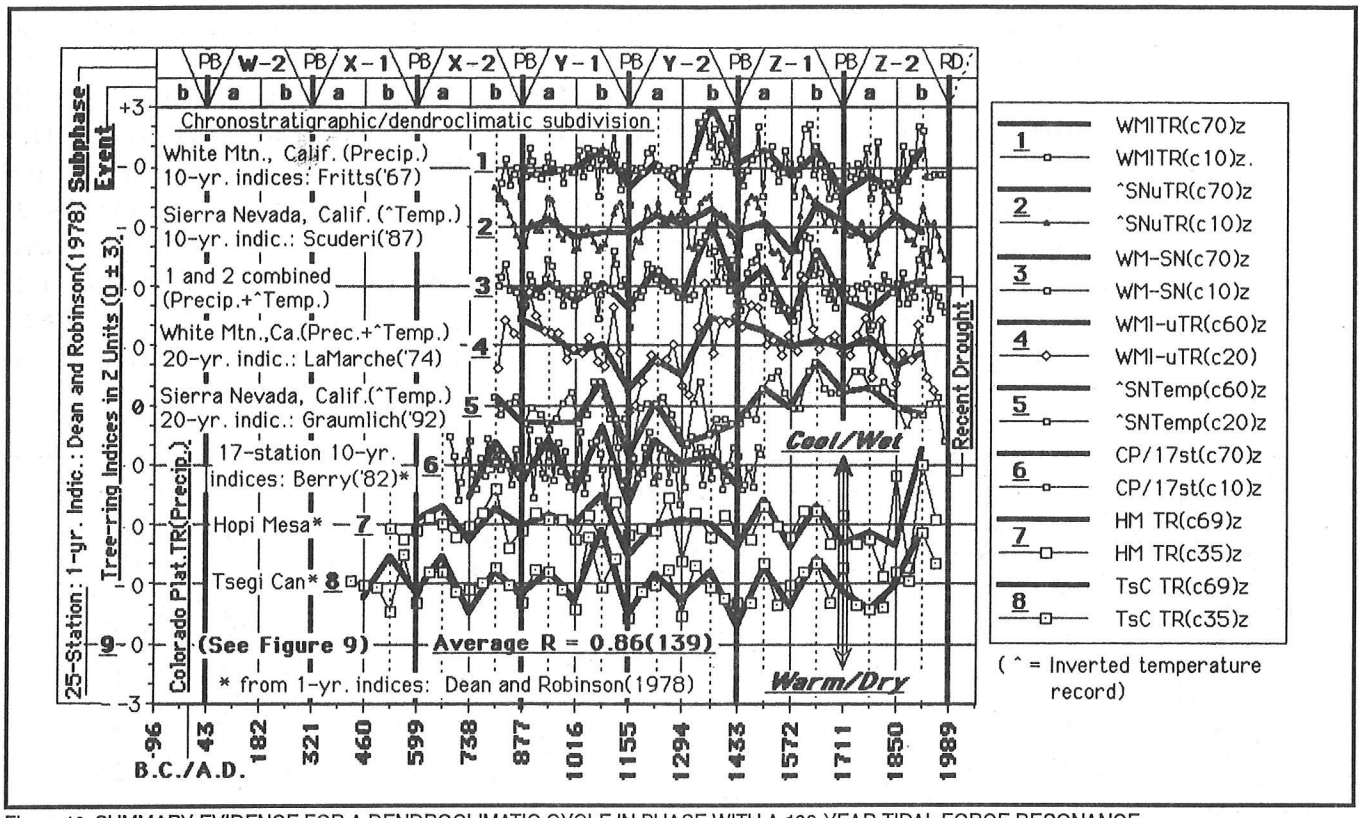

Figure 10. SUMMARY EVIDENCE FOR A DENDROCLIMATIC CYCLE IN PHASE WITH A 139-YEAR TIDAL FORCE RESONANCE

Trend correlations for local temperature and precipitation range from 0.75 to >0.90, or within the correlation range of tree-ring/climate calibrations. This suggests that the cycle is real and evidently related to changing atmospheric dynamics and patterns. Similar half-cycle analyses of other records may define differing regional patterns and responses, advancing understanding of climatic/biologic process.

Additional High-Resolution Records Suggesting Various Components of the Solar Insolation/Tidal Resonance Model

The 139-year resonance, herein called the *event cycle*, is but a higher-frequency component of the resonance model, as characterized by a series of longer- and shorter-term cycles ranging from years to thousands of years. Figures 11 to 29 provide additional examples of high-resolution records, many previously not analyzed for the presence of secondary cycles, which appear to record various harmonic components of the solar insolation/tidal resonance model.

Egyptian Cultural/Environmental Events

Egypt provides one of the longest historically chronicled records of political and environmental change (Hoffman 1979; James 1979). Economic and, by implication, political fortunes were intimately tied to the annual flooding of the Nile River. Series of extremely low and extremely high floods could have seriously affected the economic base and, thus, political stability. Resonance analysis of the Egyptian record suggests the strongest correlation between dynastic subdivision and the 139-year event cycle (Figure 11). Most dynastic changes took place during the dry

epicycles (presumably during intervals of falling and generally low flood levels), suggesting that environmental stress may have played a contributing role in dynastic succession. The three intermediate periods mark short intervals of extreme political unrest, with complete loss of central administrative control and (including in the last two periods) split local control shared with foreign invaders. Reasons for these intervals of rapidly changing political fortunes remain enigmatic and speculative, but they probably reflect a mix of internal and external social factors combined with the possibility of occasional higher destabilizing floods, since all of the intermediate periods are centered on wet epicycles and essentially begin and end in dry epicycles of the 139-year event cycle.

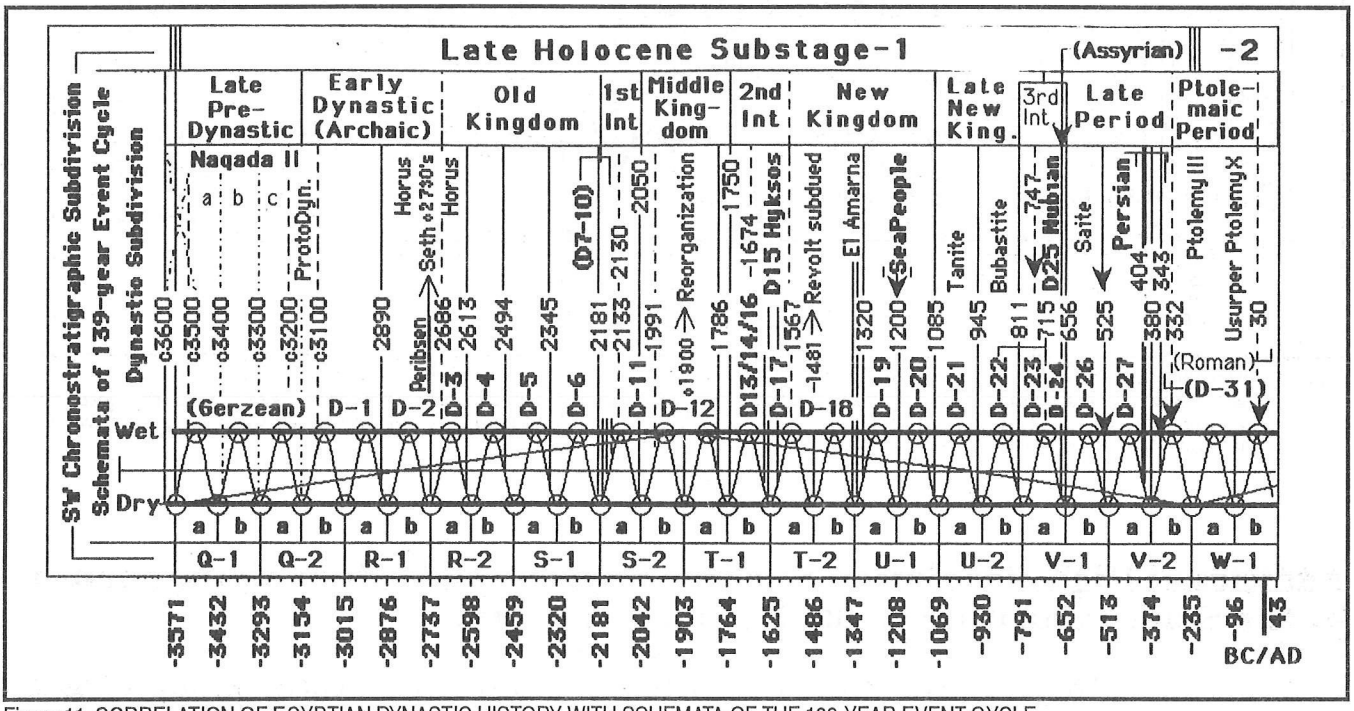

Figure 11. CORRELATION OF EGYPTIAN DYNASTIC HISTORY WITH SCHEMATA OF THE 139-YEAR EVENT CYCLE

Reconstruction of dynastic record primarily after James (1979), who notes that dating is approximate and increasingly so toward the beginning of the record. Most dated boundaries (solid lines) fall within the dry epicycles and the remaining few (dashed lines) fall within the wet epicycles, indicating that environmental stress (lower Nile levels?) may have contributed to dynastic succession. See Figure 27 for extended correlation of the Egyptian/Nubian record with longer-term climatic trends.

Sunspot/Climate Correlations

Intense climatic research has focused on correlation of climate with solar change as indirectly indexed by the sunspot cycle of about 11.1 years and by its double Hale magnetic cycle of about 22.2 years. Correlation has been attempted both with sunspot number and sunspot cycle-length.

One of the strongest correlations suggesting cause-and-effect relationships between solar activity and climate is provided by Friss-Christiansen and Lassen (1992), who correlate sunspot cycle-length with Northern Hemisphere average temperature and with the Iceland temperature curve of Bergthorsen (1969). In Figure 12, I extend the Iceland temperature

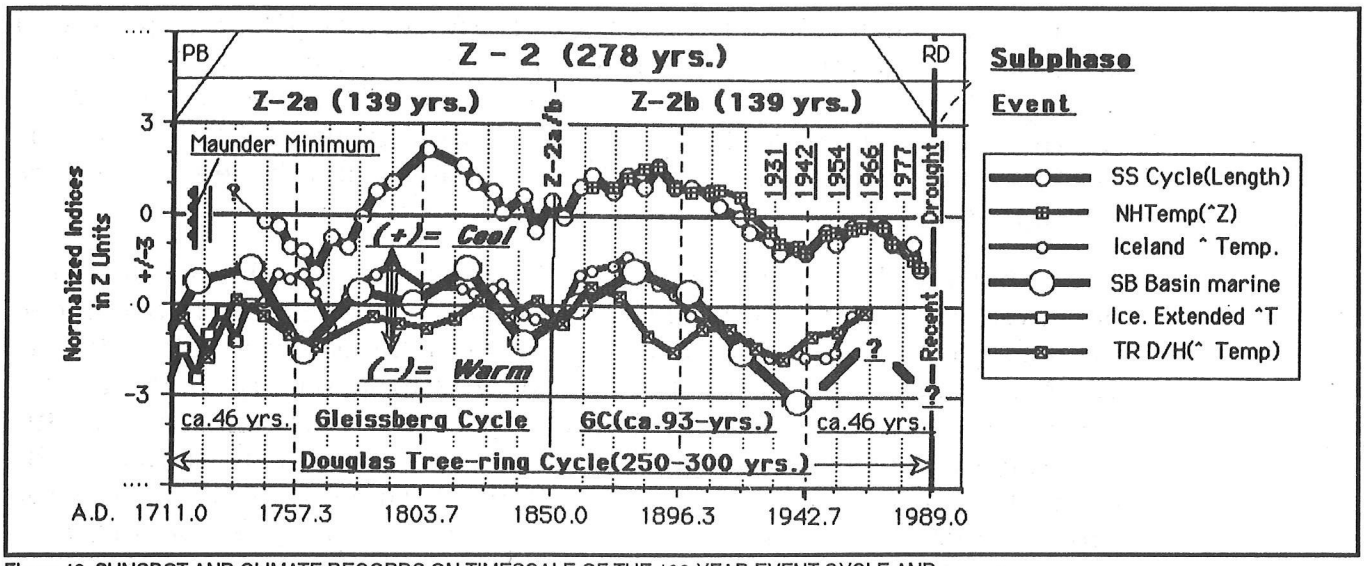

Figure 12. SUNSPOT AND CLIMATE RECORDS ON TIMESCALE OF THE 139-YEAR EVENT CYCLE AND ITS 3/1 (46.3-YEAR) AND 12/1 (11.5-YEAR) RESONANCES

Sunspot, hemispheric temperature, and Iceland indices to 1745 from Friis-Christiansen and Lassan (1991); extension of Iceland temperature record by indices from Bergthorssen (1969). Santa Barbara marine indices from Pandolfi *et al* (1980); tree-ring-dated isotope indices from Epstein and Yapp (1976). Sunspots and collated climatic records appear to be related to the tidal resonance model through in-phase relationships with the about 46-year resonance and its double Gleissberg sunspot cycle (see Figures 14 and 15). Some tendency for sunspot length and higher-resolution climate records to oscillate in phase with the 11.5-year resonance.

curve to AD 1700 and add two proxy climate records (Figures 14 and 15) that also parallel the sunspot cycle-length curve as well as or better than the proxy Iceland temperature record. The sunspot-length and collated climatic records appear to be related to the tidal resonance model primarily through in-phase relationships with the about 46-year resonance and its double Gleissberg sunspot cycle. This, in turn, suggests some sort of relationship between solar activity and tidal resonances as dominated by lunar and solar perturbations of Earth's atmosphere. Researchers have estimated the Gleissberg cycle variously between 80 and 100 years in duration. Correlation with the tidal resonance model suggests its average length lies nearer 90 years.

Other researchers have sought correlation between climate and the sunspot cycle itself. Figure 13 is a graph of the solar-tide and sunspot curves used by Gribbin (1976) in support of his failed prediction of a 1982 major earthquake in the Los Angeles area. The prediction (Gribbin and Plagemann 1975) is based on the following linkages:

- Solar tides (due to perturbations of tidal planets Venus, Earth, and Jupiter) modulate the sunspot cycle,
- In turn affecting Earth's climate,
- In turn perturbing Earth's spin,
- In turn triggering earthquakes through resulting structural adjustment in Earth's crust.

Most scientists (Anderson and Okai 1975; Meeus 1975; and others) anticipated the failure of Gribbin and Plagemann's dire prediction. Among other criticisms, Anderson and Okai (1975) believe the sun/tide calculation is in error and that the planetary alignment of 1982 is not as tight as predictable for 1990 and, in either case, is insufficient to produce earthquakes.

The apparent failure of the solar tide/sunspot correlation does not necessarily impact traditional sunspot/climate correlation. I have added two tree-ring records to Figure 13, one from the Midwest (Michell *et al* 1979) and one from the Colorado Plateaus (this paper). Both records correlate well with the Hale double (magnetic) sunspot cycle. In his seminal analysis of weather cycles, Burroughs (1992) considers that the cyclical analysis by Michell *et al* (1979) of Midwest tree-ring records provides one of the best cases for a possible cause-and-effect relationship between solar activity and climate. Half-cycle analyses of annual indices of these tree-ring records (as well as of the sun/tide and sunspot curves) use turning points of a fundamental fifth harmonic of the tidal model that closely matches the timing and average length of the Hale double sunspot cycle. The strong cyclical pattern obtained by half-cycle smoothing of the Midwest record essentially replicates the results of Michell *et al* (1979), who used different analytical procedures.

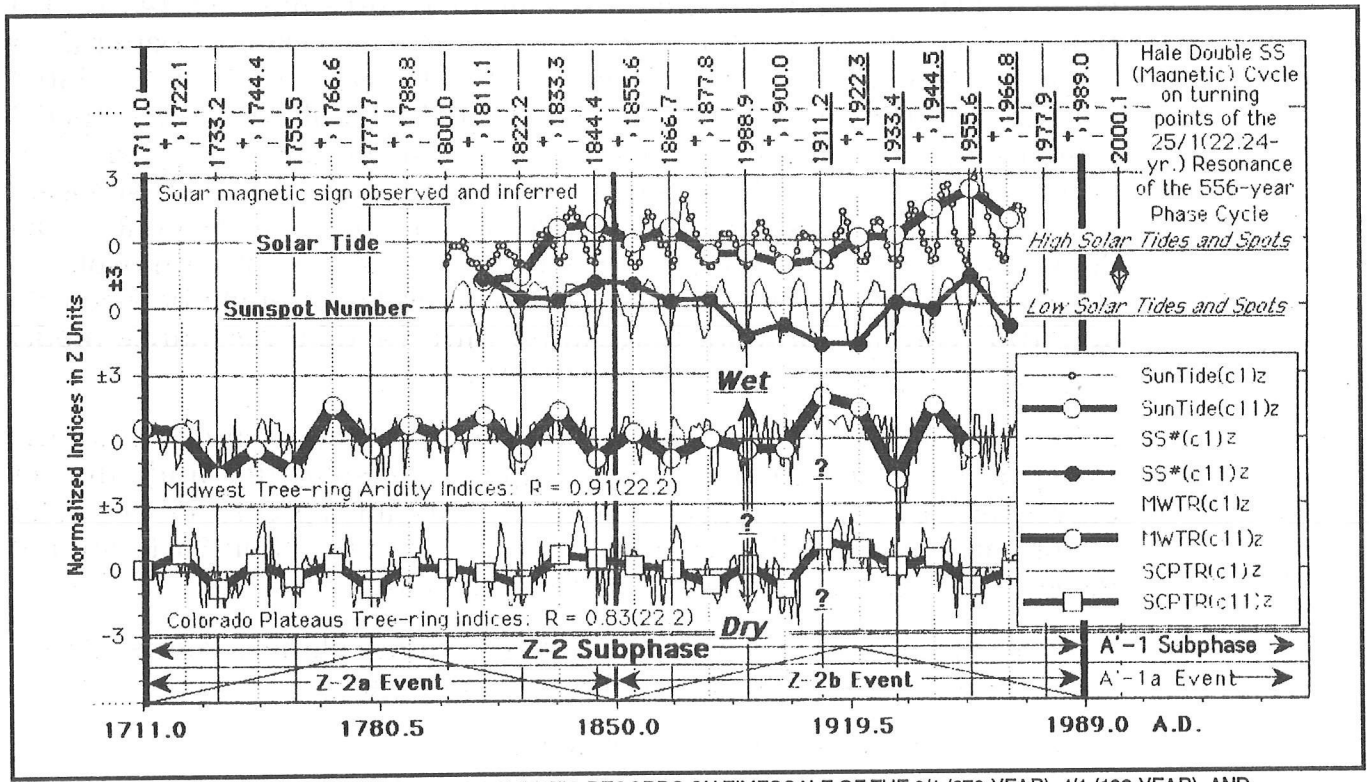

Figure 13. SOLAR TIDES, SUNSPOTS, AND DENDROCLIMATIC RECORDS ON TIMESCALE OF THE 2/1 (278-YEAR), 4/1 (139-YEAR), AND 25/1 (22.24-YEAR) RESONANCES OF THE 556-YEAR PHASE CYCLE

Annual indices of sunspots and solar tides from Wood in Gribbin (1976); Midwest tree-ring indices from Michell *et al* (1979) in Burroughs (1992); Colorado Plateaus tree-ring indices from Dean and Robinson (1978). Half-cycle smoothing on turning points of the 25/1 (22.24-year) resonance that is in phase with the average Hale double sunspot (magnetic) cycle. This, in turn, seemingly integrates solar/earth tidal phases with terrestrial climate through solar magnetic change (+ solar magnetism = generally increased Earth rainfall).

Though more complacent, the smoothed Colorado Plateaus tree-ring curve shows similarities, including the short interval of phase reversals near the beginning of the century. The comparably smoothed sunspot curve does not show the same pattern of secondary trends, but it does suggest correlation with the 139-year event cycle in that lower sunspot numbers occur in the middle and higher sunspot numbers occur near the beginning and end of the cycle. These higher- and lower-frequency correlations seemingly integrate solar/tidal phases with terrestrial climate through solar magnetic change (with positive solar magnetism equating with generally increased Earth precipitation).

Uncertainties remain concerning the physical linkages between solar magnetism, tidal resonances, and climate. Equally critical, the Hale cycle has been observed only since the beginning of this century, and projection of the same magnetic alternation between successive sunspot cycles into the past or the future remains speculative.

Lower Frequency Components of the Solar Insolation/Tidal Resonance Model

In Figures 14-29, I provide additional high-resolution climate records that are seemingly in phase with longer-term components of the solar insolation/tidal resonance model. Procedures for analyzing time stratigraphy and pollen time series remain the same as discussed in Karlstrom (1961), Ray and Karlstrom (1968), Karlstrom (1969), Hevly and Karlstrom (1974), and Euler *et al* (1979).

Figures 14-16 include a California tree-ring isotope, a California marine, and a Swedish pollen time series that seem to be primarily in phase with the 278-year subphase cycle.

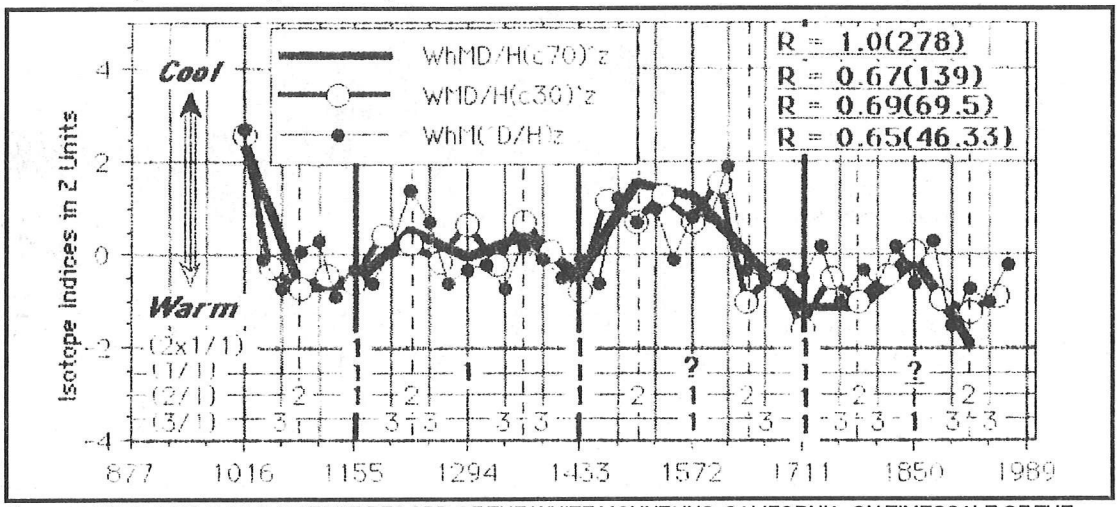

Figure 14. TREE-RING-DATED ISOTOPE RECORD OF THE WHITE MOUNTAINS, CALIFORNIA, ON TIMESCALE OF THE 139-YEAR EVENT CYCLE AND ITS 2/1 (69.5-YEAR) AND 3/1 (46.33-YEAR) RESONANCES

Centered 10-year isotope (D/H) temperature indices from Epstein and Yapp (1976).Taken as a whole, the record shows a strong tendency to oscillate in phase with the 278-year subphase cycle but weak or insignificant tendencies with the event cycle and its 2/1 (69.5-year) and 3/1 (46.33-year) resonances. Note, however, some apparent systematics in the complex resonance pattern. Between AD 1150 and 1433 (subphase Y-2), the secondary trends are apparently dominated by the event cycle, between AD 1433 and 1711 (subphase Z-1) by its 2/1 resonance, and between AD 1711 and the present (subphase Z-2) by its 3/1 resonance (see Figure 12). It remains unclear how much of the complexity results from distorting noise, from nonlinear response, or from selective local tree response to in- and out-phasing of superposed atmospheric resonances. Note similarities with the California marine record (Figure 15).

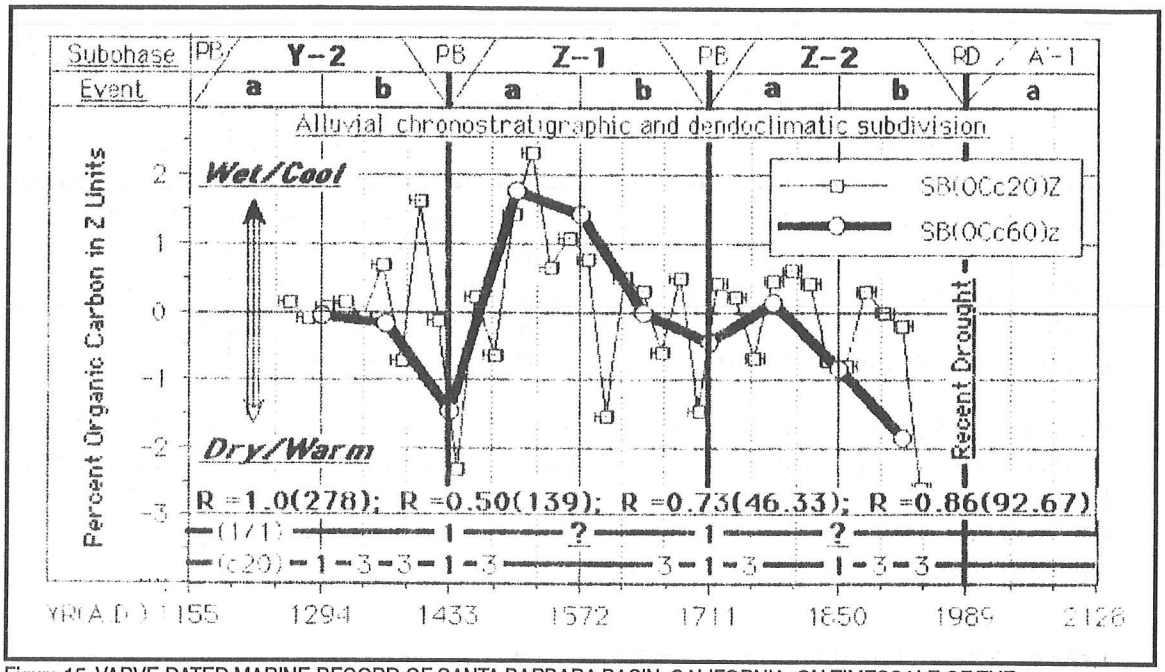

Figure 15. VARVE-DATED MARINE RECORD OF SANTA BARBARA BASIN, CALIFORNIA, ON TIMESCALE OF THE 139-YEAR EVENT CYCLE AND ITS 3/1 (46.33-YEAR) RESONANCE

Indices from Pandolfi *et al* (1980), replotted at 20-year intervals. Original indices collated with a Japanese tree-ring record that includes a cycle of 273 20 years (18/0) and 271 11 years (D/H). As shown, a similar-length marine cycle is in phase with the 278-year subphase cycle, suggesting that greater amounts of organic carbon were supplied during major Southwest wet (depositional) intervals. Record shows a tendency to oscillate in phase with the about 46-year resonance and a stronger tendency with its double (about 93-year) Gleissberg cycle (Figure 12).

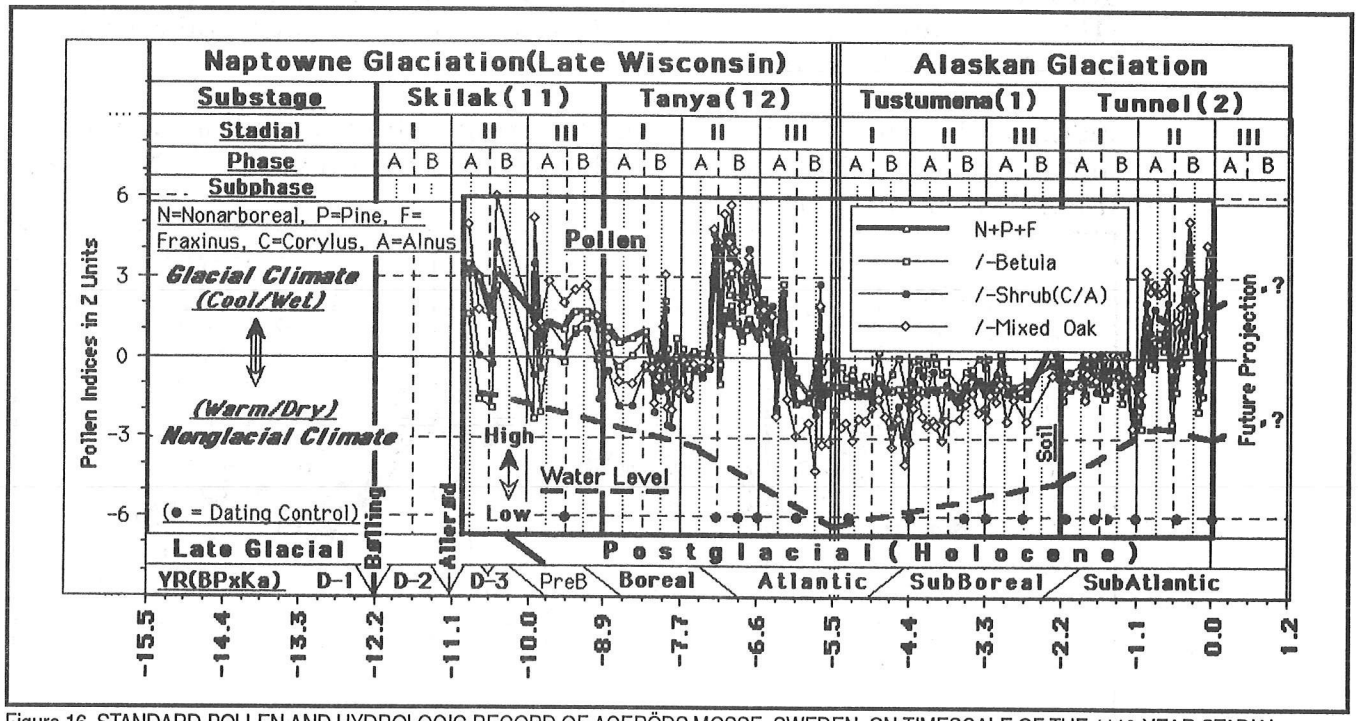

Figure 16. STANDARD POLLEN AND HYDROLOGIC RECORD OF AGERÖDS MOSSE, SWEDEN, ON TIMESCALE OF THE 1112-YEAR STADIAL CYCLE AND ITS 2/1 (556-YEAR) PHASE AND 4/1 (278-YEAR) SUBPHASE RESONANCES

Pollen and relative hydrologic indices after Nilsson (1964a,b). The Alaska glacial (point boundary) classification and its cyclical subdivisions (Karlstrom 1961; upper 5 rows) are correlated with the transition-boundary classification of Europe (lower 2 rows). Strong tendency to oscillate in phase with the 278-year subphase resonance. The record suggests that the late-Atlantic marks a drier and the warmest interval in Postglacial time (Karlstrom 1956; Figures 18, 21, 23, 24). Nilsson's chronology is based on a minor conversion (x1.03) of conventional 14/C dates (half life of 5568 years). For comparability with other 14/C-dated records, the above Agaröds Mosse chronology is also derived by using conventional 14/C results.

Figures 17 and 18 include a California and an Alaska pollen time series that seem to be primarily in phase with the 556-year phase cycle.

Figures 19-22 include two marine time series (from Equatorial Pacific and the Antarctic), a dated hydrologic/pollen record from Utah, and an Arizona pollen time series that seem to be primarily in phase with the 1112-year stadial cycle.

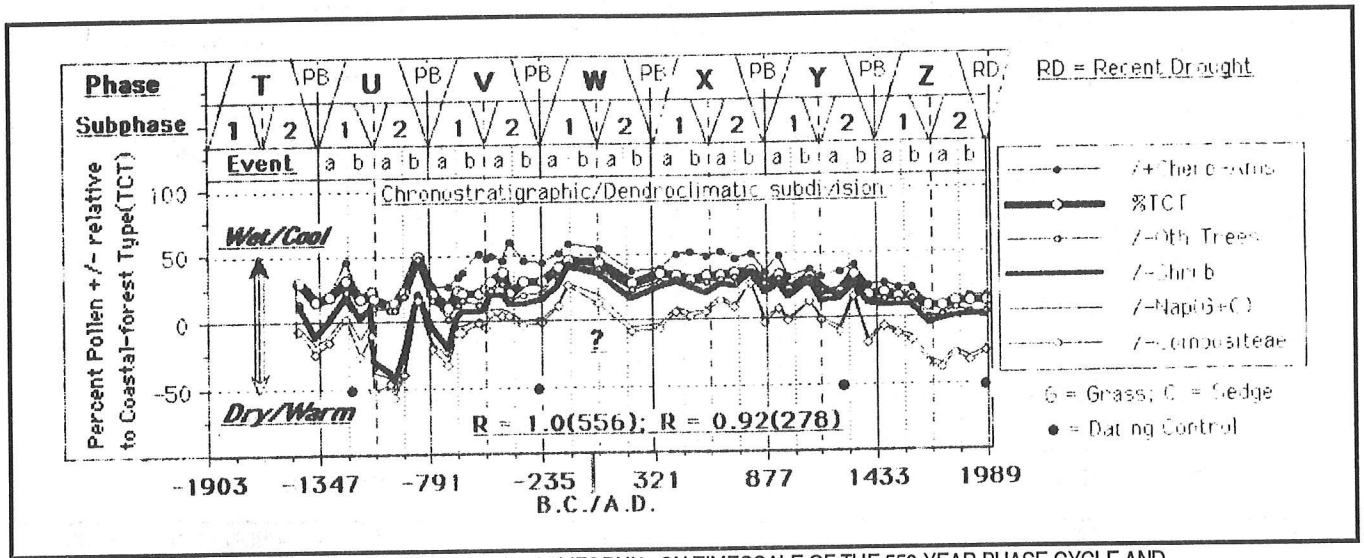

Figure 17. BIOCLIMATIC HISTORY OF PEARSON'S POND, CALIFORNIA, ON TIMESCALE OF THE 556-YEAR PHASE CYCLE AND ITS 2/1 (278-YEAR) SUBPHASE AND 4/1 (139-YEAR) EVENT RESONANCES

Dated pollen indices from Adam (1975). Chronostratigraphic subdivision after Hevly and Karlstrom (1974), Karlstrom (1988). PB = point boundary (clustering of basal-contact dates). Strongest tendency to oscillate in phase with the phase cycle and its 2/1 subphase resonance; weaker tendency with the event cycle.

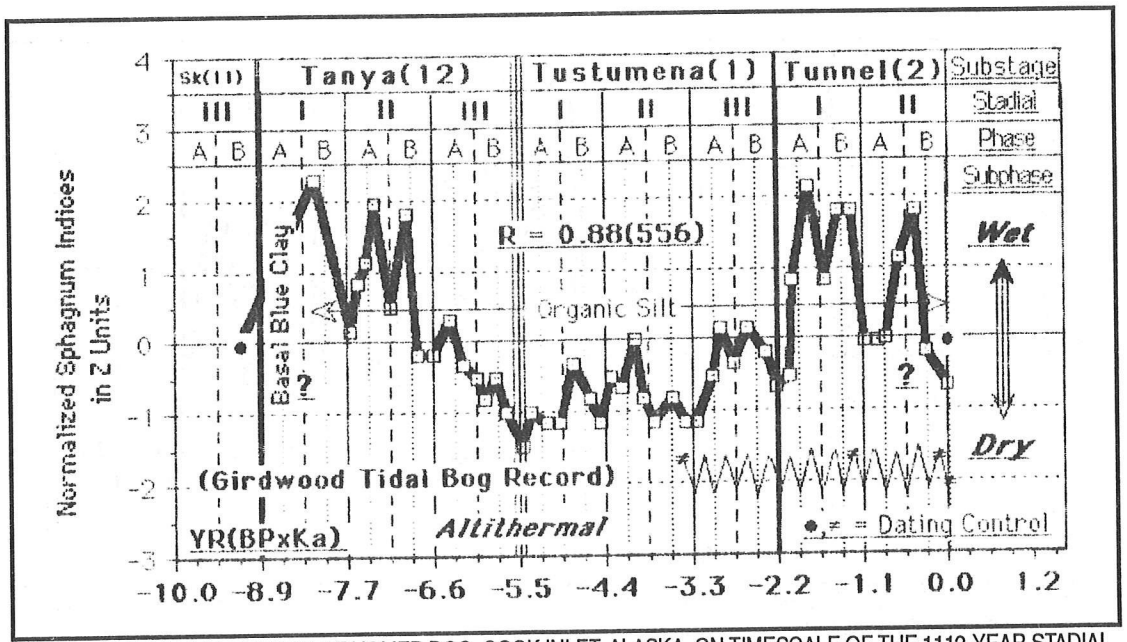

Figure 18. BIOCLIMATIC RECORD OF HOMER BOG, COOK INLET, ALASKA, ON TIMESCALE OF THE 1112-YEAR STADIAL CYCLE AND ITS 2/1 (556-YEAR) PHASE CYCLE AND 4/1 (278-YEAR) SUBPHASE RESONANCE

Pollen indices of Huesser (1965) time-calibrated by basal date listed in Karlstrom (1964). The higher-frequency Girdwood Bog record is schematically plotted as interpreted climatically in Karlstrom (1961). Because of lesser sensitivity, Homer Bog shows the strongest tendency to oscillate in phase with the 556-year phase cycle and positions the driest Postglacial interval contemporaneous with that in the late-Atlantic of northern Europe (Figure 16).

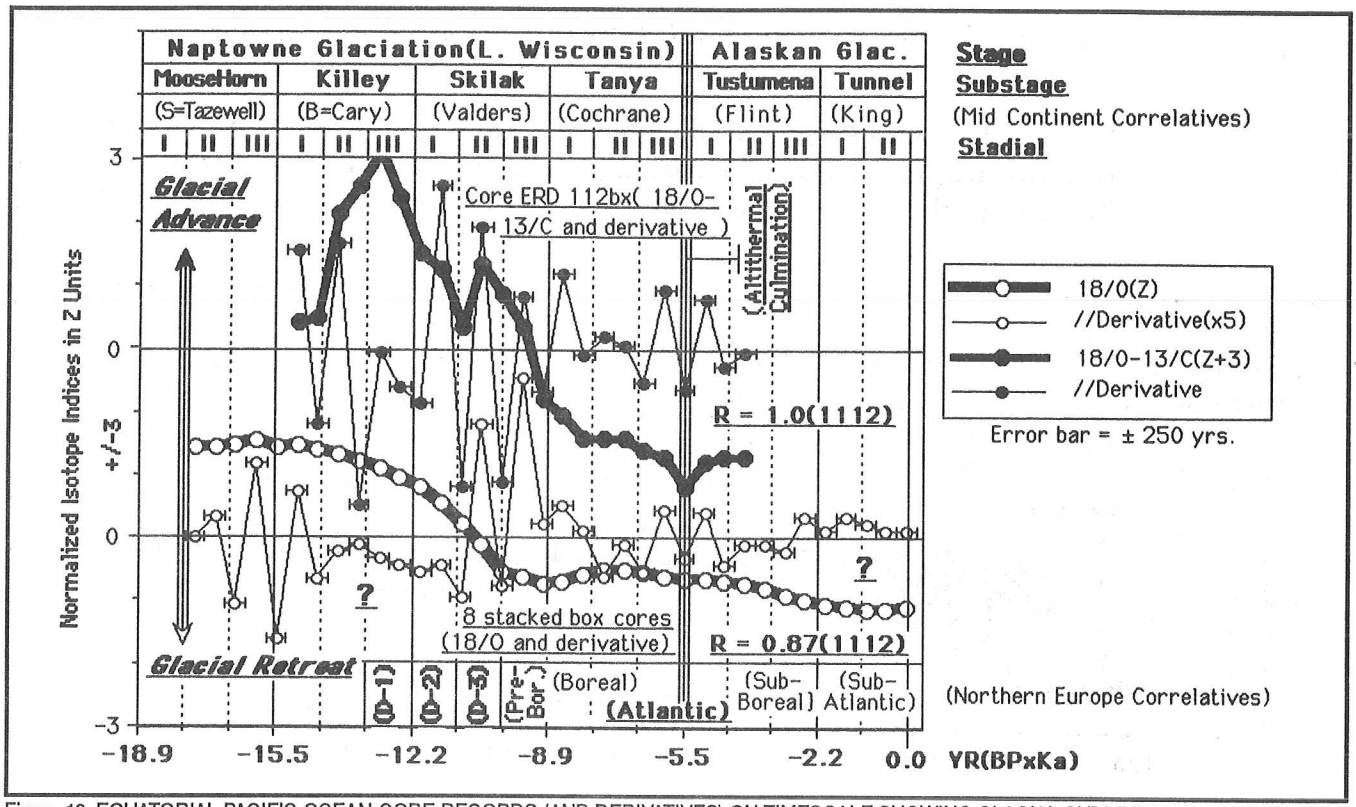

Figure 19. EQUATORIAL PACIFIC OCEAN-CORE RECORDS (AND DERIVATIVES) ON TIMESCALE SHOWING GLACIAL SUBDIVISIONS ON TURNING POINTS OF THE 3336-YEAR SUBSTAGE CYCLE AND ITS 3/1 (1112-YEAR) STADIAL RESONANCE

Centered 500-year-interval isotope indices from Berger *et al* (1987). Alaska glacial chronology and correlations after Karlstrom (1961, 1976b). Lower row = classic Scandinavian bioclimatic (pollen) subdivision of Late Glacial and Postglacial time (Figure 16). The derivatives suggest that secondary trends of glacial melting (18/0) and surface water temperature (13/C) were strongly in phase with the stadial cycle during the last 18000 years. D-1 to 3 = Dryas glacial advances.

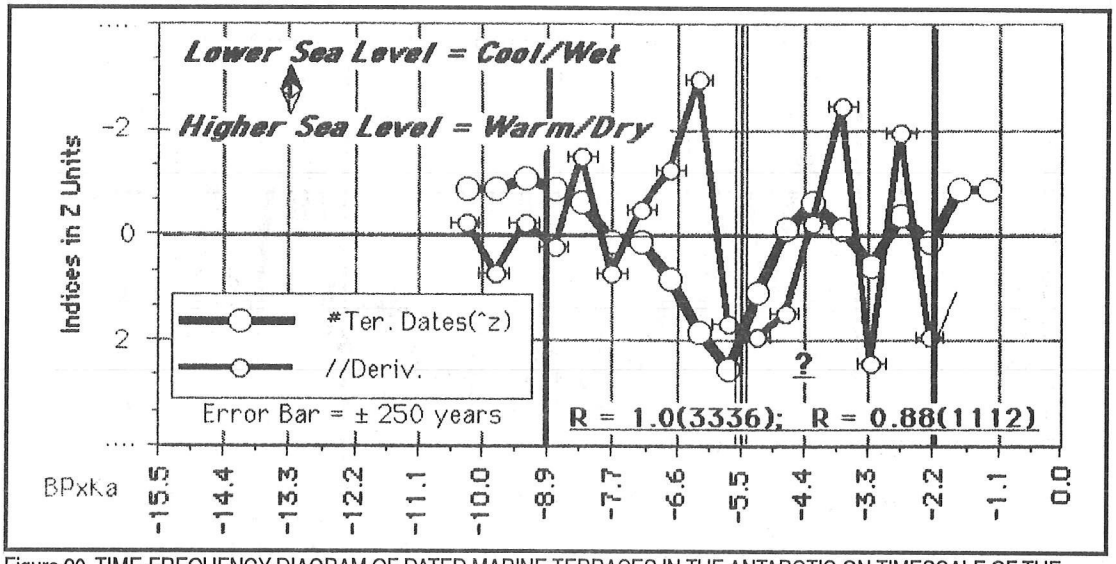

Figure 20. TIME-FREQUENCY DIAGRAM OF DATED MARINE TERRACES IN THE ANTARCTIC ON TIMESCALE OF THE 1112-YEAR STADIAL CYCLE

Centered 500-year indices from Berkman (1992). N=88. Clustering of dates suggests a high sea level stand during the culmination of the Northern Hemisphere Altithermal. Derivative amplification suggests a strong tendency for secondary sea levels to oscillate in phase with the 1112-year stadial cycle. Correlations with terrestrial records suggest glacioeustatic controls.

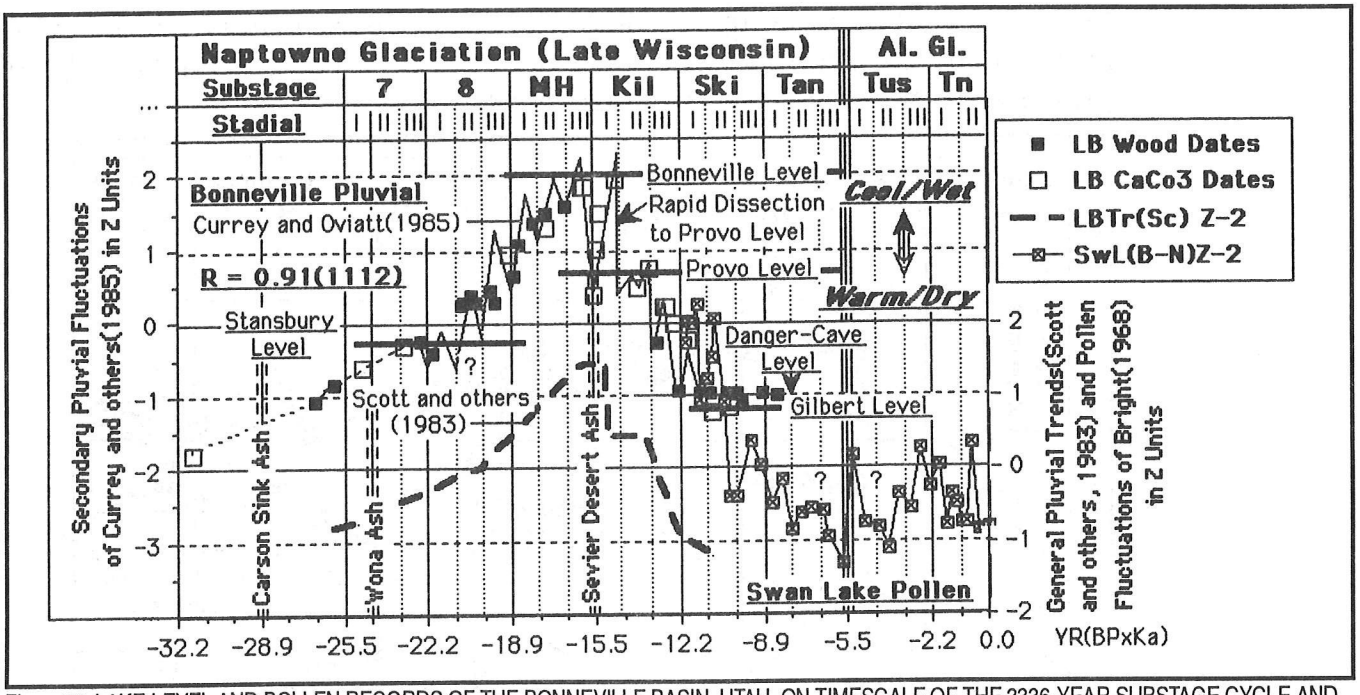

Figure 21. LAKE-LEVEL AND POLLEN RECORDS OF THE BONNEVILLE BASIN, UTAH, ON TIMESCALE OF THE 3336-YEAR SUBSTAGE CYCLE AND ITS 3/1 (1112-YEAR) STADIAL RESONANCE

Clustering of dated littoral- and shallow-water samples strongly suggests secondary lake-level changes between 22000 and 11000 YBP in phase with the 1112-year stadial cycle. The pollen record evidently extends the same resonance pattern to the present (Hevly and Karlstrom 1974). Recorded volcanic eruptions apparently occurred during interstadial (lower water/drought) epochs.

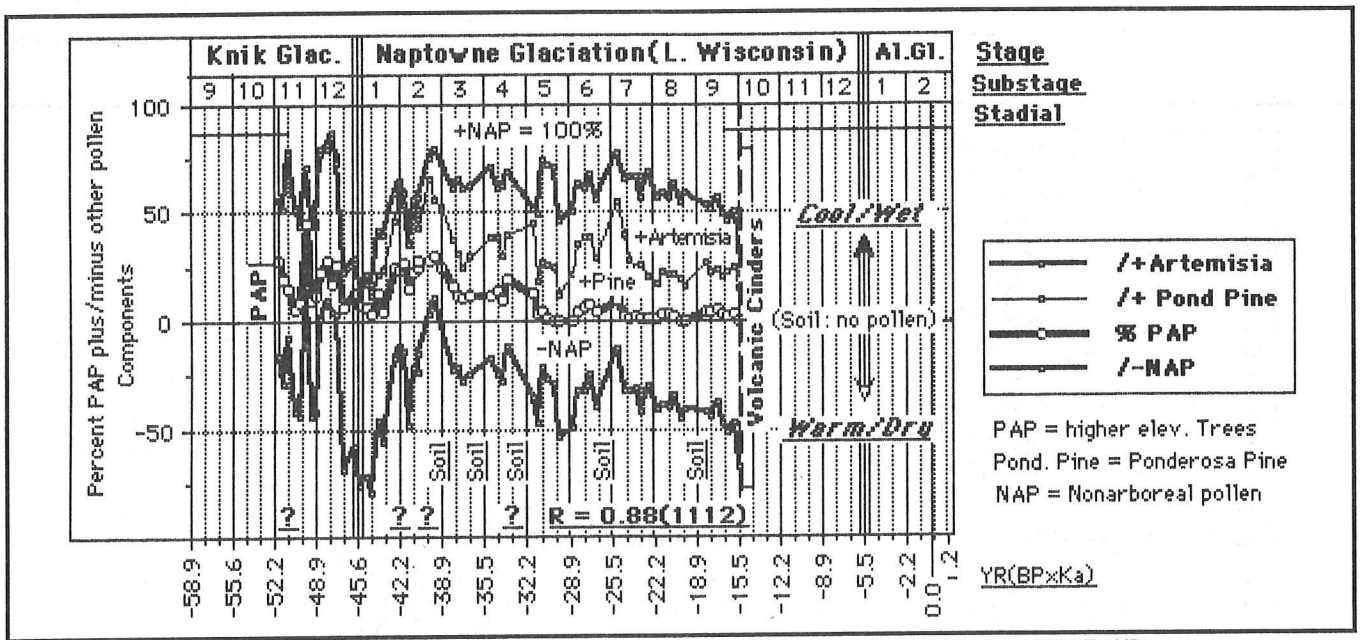

Figure 22. BIOCLIMATIC RECORD OF WALKER LAKE, ARIZONA, ON TIMESCALE OF THE 3336-YEAR SUBSTAGE CYCLE AND ITS 3/1 (1112-YEAR) STADIAL RESONANCE

Pollen indices from Berry as time-calibrated in Karlstrom (1976b). Strong tendency for the record to oscillate in phase with the stadial cycle. Several of the inter-substage epochs are marked by soils (oxidized zones with no pollen) suggesting lower water levels and subaerial exposure. The covering volcanic cinders date contemporaneous with the Sevier Desert Ash of the Lake Bonneville Basin to the north (Figure 21).

Figures 23-26 include three pollen time series (from Canada and Spain) and a Tunisian ground water time series that seem to be primarily in phase with the 3336-year substage cycle.

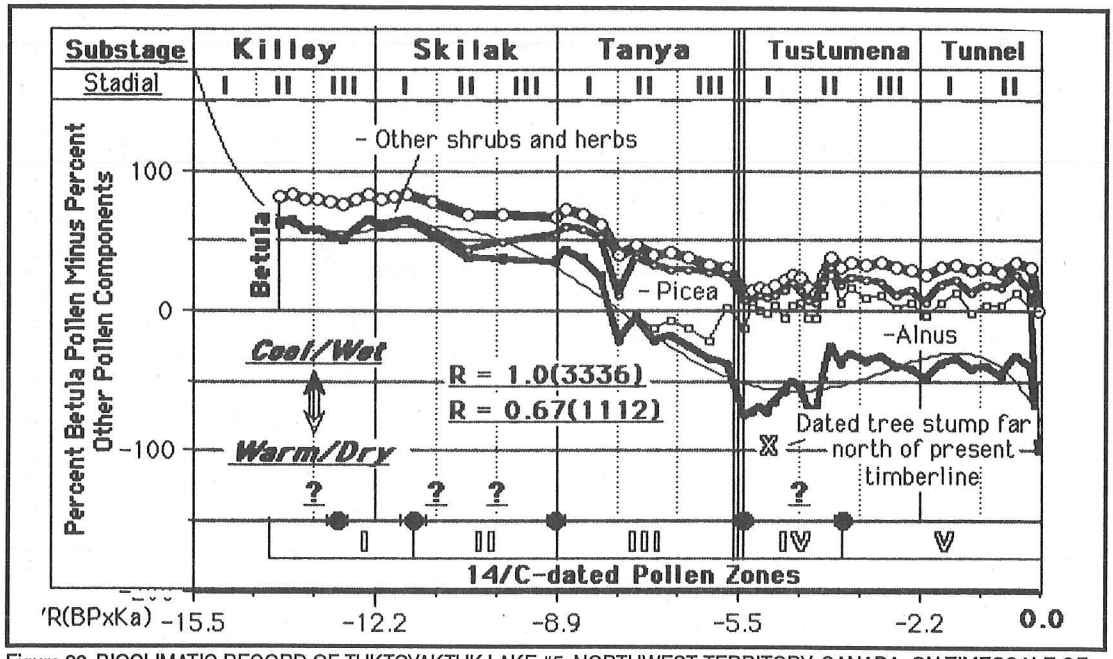

Figure 23. BIOCLIMATIC RECORD OF TUKTOYAKTUK LAKE #5, NORTHWEST TERRITORY, CANADA, ON TIMESCALE OF THE 3336-YEAR SUBSTAGE CYCLE AND ITS 3/1 (1112-YEAR) STADIAL RESONANCE

Pollen indices from Richie and Hare (1971). This high-latitude record (N70°) suggests warmest/driest climate and most northerly expansion of timberline between 5000 and 6000 years ago, or contemporaneous with Altithermal culmination, as dated in the Southwest and elsewhere (Figures 16, 18, 19, 20, 21). Strong tendency to oscillate in phase with the substage cycle; weaker tendency with the stadial cycle.

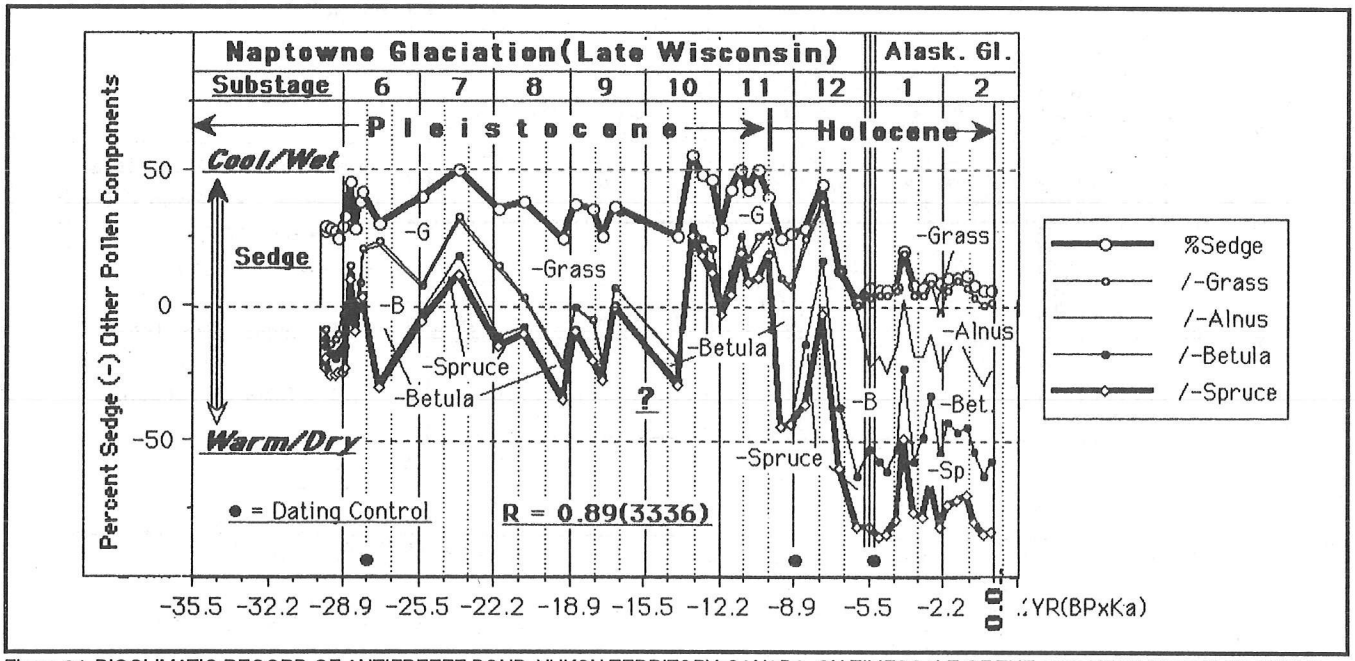

Figure 24. BIOCLIMATIC RECORD OF ANTIFREEZE POND, YUKON TERRITORY, CANADA, ON TIMESCALE OF THE 3336-YEAR SUBSTAGE CYCLE AND ITS 3/1 (1112-YEAR) STADIAL RESONANCE

Pollen indices from Rampton (1970). Alaska glacial classification and cyclical subdivision from Karlstrom (1961). Trend analysis suggests a strong response to the substage cycle and, where the sampling interval is sufficiently close, to the stadial cycle.

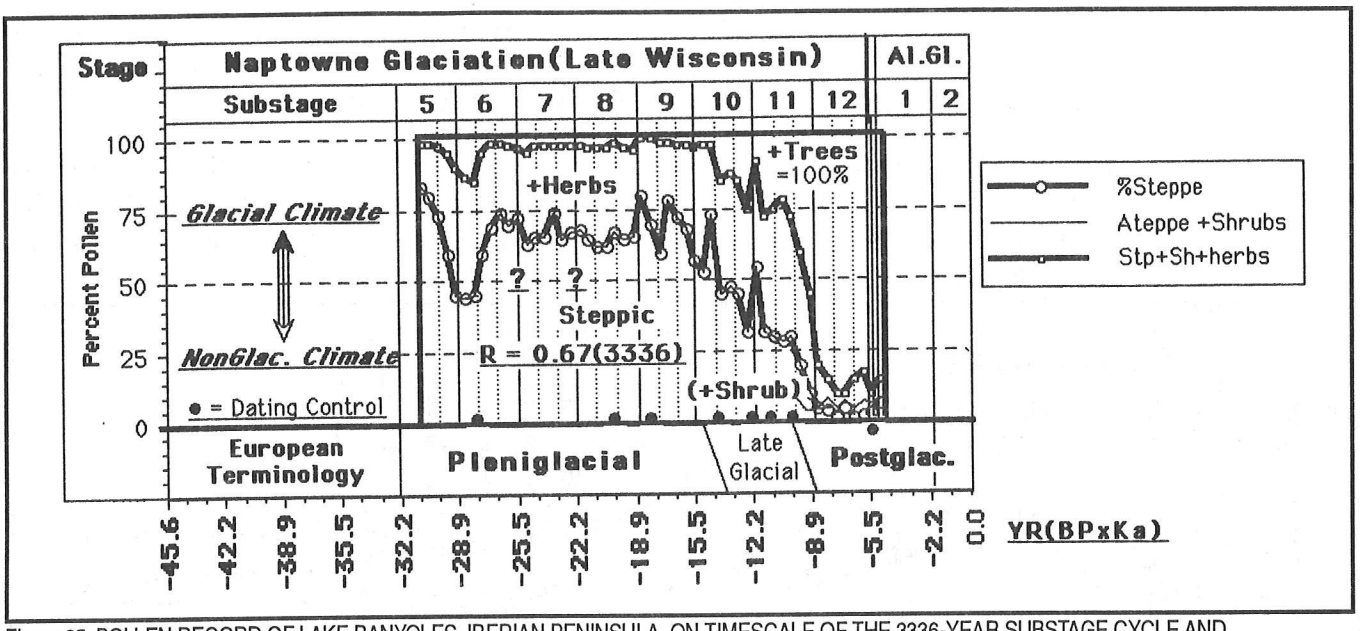

Figure 25. POLLEN RECORD OF LAKE BANYOLES, IBERIAN PENINSULA, ON TIMESCALE OF THE 3336-YEAR SUBSTAGE CYCLE AND ITS 3/1 (1112-YEAR) STADIAL RESONANCE

Pollen indices replotted at 500-year intervals from Figure 4B in Perez-Obriol and Juliá (1994). Dating control by U/Th and radiocarbon. Alaska glacial classification and point-boundary cyclical subdivision (Karlstrom 1961; upper two rows) correlated with transition-boundary European classification (lower row). Fairly strong tendency for in-phase relationships with the substage cycle.

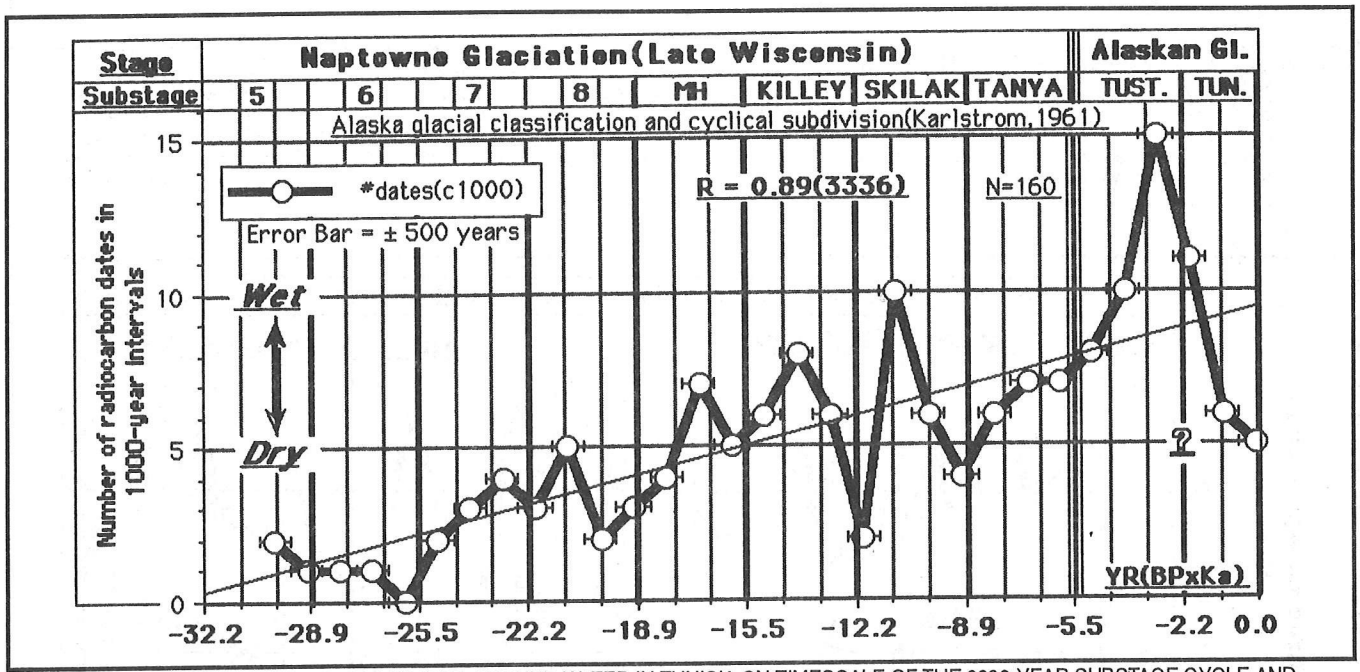

Figure 26. TIME-FREQUENCY DIAGRAM OF DATED GROUND WATER IN TUNISIA ON TIMESCALE OF THE 3336-YEAR SUBSTAGE CYCLE AND ITS 3/1 (1112-YEAR) STADIAL RESONANCE

Indices from Scharpenseel *et al* (1980). Wetter climate apparently reoccurred substantially in phase with the 3336-year substage cycle (Figure 27). Note the typical progressive decrease in number of dates with age.

Figure 27 includes dated Egyptian and Nubian cultural and environmental events, partly in phase with lower north latitude processional cycles and partly with the 3336-year substage cycle.

Figure 28 includes two marine isotope chronologies (from the Equatorial Pacific and Equatorial Atlantic oceans) that are fine-tuned to the 65°N latitude insolation curve and considered to provide standard global records of the Ice Ages.

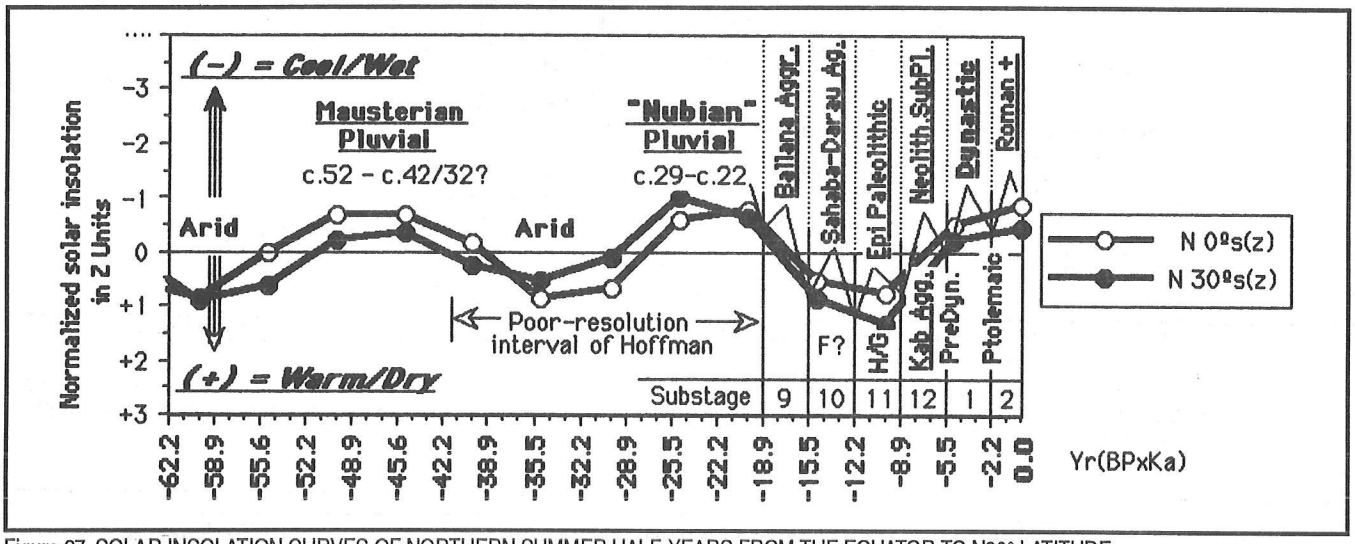

Figure 27. SOLAR INSOLATION CURVES OF NORTHERN SUMMER HALF-YEARS FROM THE EQUATOR TO N30° LATITUDE

The 3336-year substage cycle is schematically superposed on the insolation trends. Dated Nubian and Egyptian cultural/environmental events are positioned as summarized in Hoffman (1979). More recent dating of Nubian pluvials c29-22 and c9-6/3 (Neolithic subpluvial and Dynastic in age) is after Pachur and Hoelzman (1991), and appears to confirm the correlation between generally wetter climate and precessional solar-insolation minima north of the Equator. Secondary hydrologic and cultural events apparently are in phase with the 3336-year substage cycle. F? = possible earliest farming during the Sahaba Darau Aggradation interval (substage 10). H/G = temporary return to hunting and gathering strategies during the ensuing drier Epi Paleolithic interval (substage 11). See Figure 11 for historical subdivision of Dynastic time.

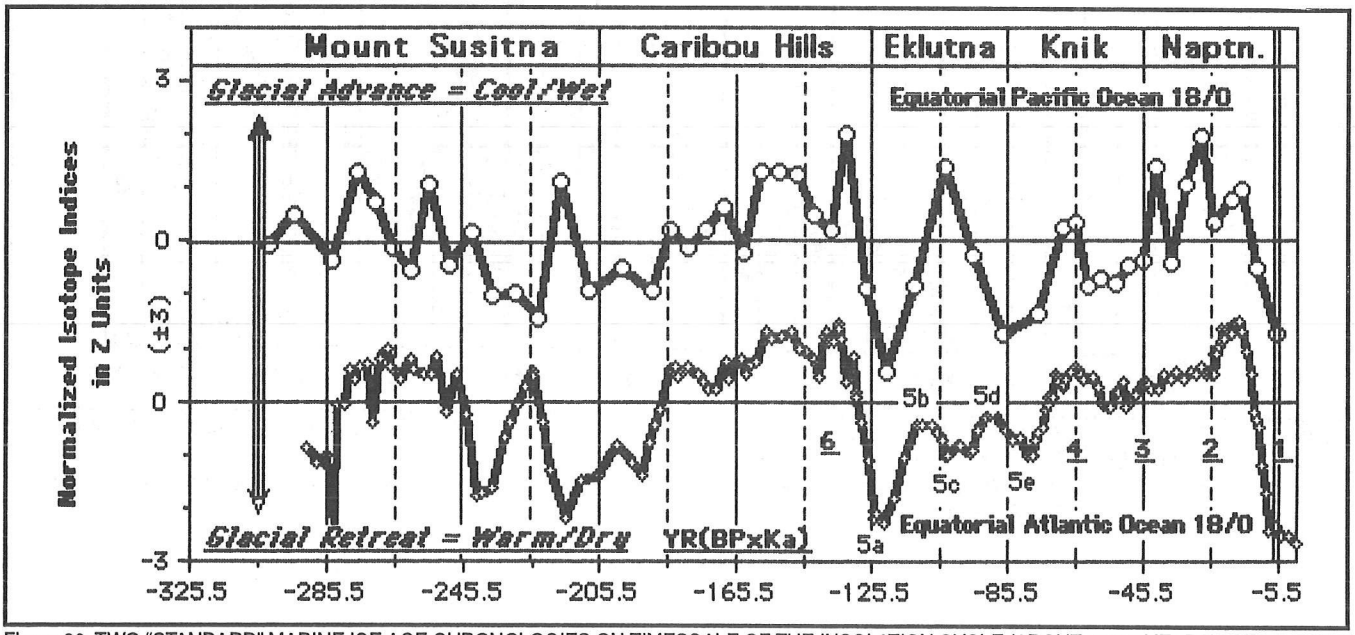

Figure 28. TWO "STANDARD" MARINE ICE AGE CHRONOLOGIES ON TIMESCALE OF THE INSOLATION CYCLE (ABOUT 40000 YEARS) AND ITS 2/1 (ABOUT 20000 YEARS) RESONANCE ASSUMING A RESPONSE LAG OF ABOUT 4500 YEARS (Karlstrom 1961)

Equatorial Pacific record from Chuey *et al* (1987); the Equatorial Atlantic record from Martinson *et al* (1987). Both are fine-tuned to the Milankovitch climatic model assuming corresponding response lags. The curves differ mainly in (1) out-of-phase relationships about 225000 YBP, and (2) relative glacial amplitudes of the last 125000 years, suggesting either heterogeneities in the global record or difficulties with dating procedures and sample mixing. Note the tendency for near in-phase oscillations with the obliquity 2/1 (about 20000-year) resonance.

Figure 29 shows the latitudinal insolation curves that progressively change from the dominant obliquity cycle at the poles to the dominant precessional cycle at the Equator. Since the isolation curves are based on summer half-years, precessional trends north of the Equator are 180 degrees out of phase with those south of the Equator. Six selected high-resolution terrestrial-climate time series are referenced as to type and source and in the figure are positioned according to latitude. These dated records seem to parallel the local latitudinal insolation trends more closely than the records at other latitudes, suggesting direct latitudinal insolation control of climate. Particularly significant is the apparent 180-degree phase reversal across the Equator, as represented by the Afar and Egyptian/Nubian records to the north and the East Africa records immediately south of the Equator, just those relations expected from local Precessional-insolation control. The Antarctic (Vostock) ice-core record of temperature and CO_2 strikingly parallels Obliquity/Precessional cycle trends in the South 60°-90° Latitude belt, the precessional elements of which are also 180 degrees out of phase with those in the Northern Hemisphere and with the associated K/Ar-dated North American glacial record of Richmond (1976). TheNorth 37°Latitude Devils Hole isotope/ temperature record of Winograd *et al* (1992) also parallels Richmond's glacial chronology (glaciations 6-8) and the corresponding insolation

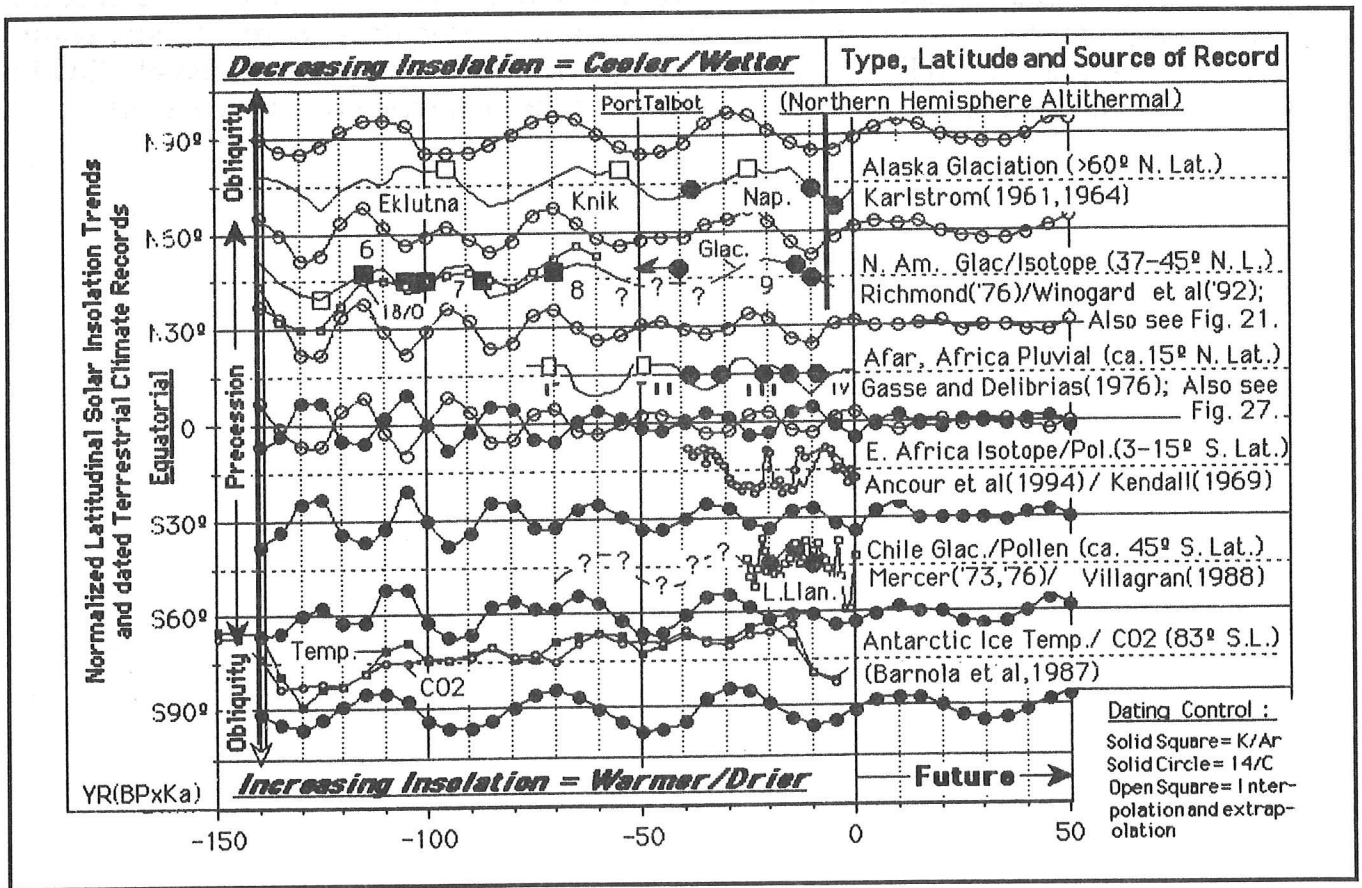

Figure 29. LATITUDINAL INSOLATION CONTROL OF TERRESTRIAL CLIMATIC RECORDS

These dated records seemingly parallel more closely the local latitudinal insolation trends than the records at other latitudes. If these climate records are representative of their respective latitudinal belts, the conventional concept of inter-hemispheric climatic synchrony must be reassessed as a basis for Ice Age correlations and resulting global paleoclimatic reconstructions (Karlstrom 1961). See also Crowley and Kim (1994).

trends in the North 30°-60° Latitude belt. Cause-and-effect relationships are apparently satisfied by a consistent response lag (0-5000 years) between the modulating latitudinal insolation trends and the independently dated climate changes. Precessional elements of the Milankovitch model are also invoked by Crowley and Kim (1994) to accommodate the recent coral dating of about 130,000 years ago for a major high-sea-level stand and for the contemporaneous high-temperature interval in the Devils Hole isotope record. Additional long, high-resolution terrestrial records (particularly in the upper north latitudes and the middle south latitudes) are required for more critical testing of the Obliquity/Precessional insolation model and for direct assessment of the latitudinal representativeness of the selected time series.

Natural Fluctuations of Atmospheric Greenhouse Gases

The striking correlation in the Antarctic ice-core record between isotope temperature and CO2 contributes to the current greenhouse gas controversy by providing direct evidence of large, natural, temperature-related fluctuations in atmospheric CO2. Coupled with recent evidence of declining greenhouse gas components in the atmosphere following culmination of a drought (warmer/drier) interval about 1990, as predicted by the resonance model (Figures 1-10; Karlstrom 1976a), this strongly suggests that current climate modeling requires modification to accommodate higher as well as lower frequency, natural (nonanthropogenic) climate fluctuations in future projections of atmospheric greenhouse gases.

References

Adam, D.P. 1975. A late Holocene pollen record from Pearson's Pond, Weeks Creek Landslide, San Francisco Peninsula, California. *U.S. Geological Survey Jour. Research* 3:721-731.

Ancour, A.M., C. Hillaire-Marchel, R. Bonnefille. 1994. Late Quaternary biomass changes from ^{13}C measurements in a highland peat bog from equatorial Africa (Barundi). *Quat Research* 41:225-233. See also Bonnefille,

Anderson, D.R., and E. Okai. 1975. On the planetary theory of sunspots. *Nature* 253:511-513.

Barnola, J.M., D. Raymond, Y.S. Korotkevich, C. Lorius. 1987. Vostock ice core provides 160,000 year record of atmospheric CO_2. *Nature* 329:408-414. Also Jouzel *et al. Nature* 329-403.

Berger, W.H., J.S. Killingley, E. Vincent. 1987. Time scale of the Wisconsin/Holocene transition: Oxygen isotope record of the western Equatorial Pacific. *Quat. Research* 28:295-306.

Bergthorsen, P. 1969. An estimate of drift ice and temperature in Iceland in 1000 years. *Jour. of Jökull* 19:94-101.

Berry, M.S. 1982. *Time/Space and Transition in Anasazi Prehistory*. University of Utah Press, Salt Lake City. 147 pp.

Bright, R.C. 1968. Pollen and seed stratigraphy of Swan Lake, southeastern Idaho: Its relationship to regional history. *Jour Idaho State Univ Mus Tebiwa 9.*

Burroughs, W.J. 1992. *Weather Cycles: Real or Imaginary?* Cambridge University Press, Cambridge. 201 pp.

Chuey, J.M., D.K. Rea, N.G. Pisias. 1987. Late Pleistocene paleoclimatology of the central Equatorial Pacific: A quantitative record of eolian and carbonate deposition. *Quat. Research* 38:323-339.

Crowley, T.J., and K.Y. Kim. 1994. Milankovitch forcing of the last interglacial sea level. *Science* 265:1566-1567.

Currey, D.R., and C.G. Oviat. 1985. Durations, average rates and probable causes of Lake Bonneville expansions, stillstands, and contractions during the last deep-lake cycle, 32,000 to 100,000 years ago. Pages 9-14 in P.A. Kay and H.F. Diaz, eds. *Problems of and Prospects for Predicting Great Salt Lake Levels.* Papers from a conference held in Salt Lake City, March 24-25, 1985.

Dean, J.S. 1988. Dendroclimatology and paleoenvironmental reconstruction on the Colorado Plateaus. Pages 119-167 in The Anasazi in a Changing Environment. G. Gummerman, editor. School of American Research Advanced Seminar Book. Cambridge University Press, Cambridge.

Dean, J.S., and W.J. Robinson. 1978. Expanded tree-ring chronologies for the southwest United States. *Chronology Series III, Laboratory of Tree-Ring Research.* Univ. of Arizona, Tucson. 58 pp.

Epstein, S., and C.I. Yapp. 1976. Climatic implications of the D/H ratio of hydrogen in C/H groups in tree cellulose. *Earth Planet. Sci. Letters* 30:252-266.

Euler, R.C., G.J. Gumerman, T.N.V. Karlstrom, J.S. Dean, R.H. Hevly, 1979. The Colorado plateaus: Cultural dynamics and paleoenvironment. *Science* 205:1089-1101.

Friis-Christiansen, E., and K. Lassen. 1991. Length of solar cycle: An indicator of solar activity closely associated with climate. *Science* 254:698-700.

Fritts, H.C. 1967. Tree-ring analysis (dendroclimatology). Pages 1008-1026 in *The Encyclopedia of Atmospheric Sciences and Astrogeology.* R.W. Fairbridge, Editor. Reinhold. New York.

Gasse, F., and G. Delibrias. 1976. Les Lacs de L'afar Central (Ethiopie et F.F.A.I.). Pages 529-575 in Shoji Horie, editor. *Paleolimnology of Lake Biwa and the Japanese Pleistocene* 4.

Graumlich, L.J. 1992. A 1000-year record of climatic variability in the Sierra Nevada, California: Handout, Am Quat Assoc, 12th Biennial Meeting. August 24-26, University of California, Davis.

Gribbin, J.R. 1976. *Forecasts, Famines and Freezes.* Walker and Company, New York.

Gribbin, J.R., and S.H. Plagemann. 1975. *The Jupiter Effect.* Vintage Books, Random House, New York.

Heusser, C.J. 1965. A Pleistocene phytogeographical sketch of the Pacific Northwest and Alaska. Pages 469-483 in *The Quaternary of the United States.* H.E. Wright Jr and D.J. Frey, editors. Princeton Univ. Press, Princeton, New Jersey.

Hevly, R.H., and T.N.V. Karlstrom. 1974. Southwest paleoclimatic and continental correlations. Pages 257-295 in *Geology of Northern Arizona with Notes on Archaeology and Paleoclimate.* T.N.V. Karlstrom et al, editors. Geol. Soc. of America Field Guide 1, Rocky Mountain Meeting, Flagstaff, Arizona.

Hoffman, M.A. 1979. *Egypt Before the Pharaohs.* Alfred F. Knopf, New York. 391 pp.

James, T.G.H. 1979. *Introduction to Ancient Egypt.* Farrar Straus Giroux, New York, in association with British Museum Publication Limited, London. 286 pp.

Karlstrom, T.N.V. 1956. The problem of the Cochrane in late Pleistocene chronology. *U.S. Geological Survey Bulletin* 1021J:303-331.

Karlstrom, T.N.V. 1961. The glacial history of Alaska: Its bearing on paleoclimatic theory. *Annals New York Academy of Science* 95 Article 1:290-340.

Karlstrom, T.N.V. 1964. *Quaternary Geology of the Kenai Lowland and Glacial History of the Cook Inlet Region, Alaska.* U.S. Geological Survey Professional Paper 443. 69 pp.

Karlstrom, T.N.V. 1969. Geological investigation of the Kodiak Island Refugium. Pages 19-54 in G.N.V. Karlstrom and G.E. Ball, editors. *The Kodiak Island Refugium: Its Geology, Flora, Fauna and History.* The Boreal Institute, University of Alberta by Ryerson Press, Toronto. 262 pp.

Karlstrom, T.N.V. 1976a. Stratigraphy and paleoclimate of the Black Mesa basin. *U.S. Geological Survey Circular* 778:18-22.

Karlstrom, T.N.V. 1976b. Quaternary and upper Tertiary time-stratigraphy of the Colorado Plateaus, continental correlations and some paleoclimatic implications. Pages 275-282 in *Quaternary Stratigraphy of North America.* W.C. Mahaney, editor. Hutchinson and Ross, Stroudsburg, PA.

Karlstrom, T.N.V. 1988. Alluvial chronology and hydrologic change of Black Mesa and nearby regions. Pages 45-91 in *The Anasazi in a Changing Environment.* G.J. Gummerman, editor. School of American Research Advance Seminar Book. Cambridge University Press, London.

Kendall, R.L. 1969. An ecological history of the Lake Victoria Basin. *Ecological Monographs* 39:121-176.

Lamarche, V.C. Jr. 1974. Paleoclimatic inferences from long tree-ring records. *Science* 183:1043-1048.

Martinson, D.G., N.G. Pisias, J.D. Hays, J. Imbrie, T.C. Moore Jr., N.J. Shackleton. 1987. Age dating and the orbital theory of the Ice Ages: Development of a high-resolution 0 to 300,000-year chronostratigraphy. *Quat. Research* 27:1-29.

Meeus, J. 1975. Comments on the Jupiter effect. *Icarus* 26:257-270.

Mercer, J.H. 1976. Glacial history of southernmost South America. *Quat Research* 6:125-166.

Mercer, J.H., and C.A. Laugenie. 1973. Glaciers in Chile ended a major readvance about 36,000 years ago; some global comparisons. *Science* 183:1017-1019.

Nilsson, T. 1969a. Standardpollen diagramme und ^{14}C datierungen aus dem Agaröds Mosse im mittieren Schonen. *Lunds Universitets Ärskrift N.F.* Avd. 2. Bd 59, Nr 7: 1-52 Häkan Ohissons Boktryckeri, Lund.

Nilsson, T. 1969b. Enwicklungsgeschichtliche studien im Ageröds Mosse, Schonen. *Lunds Universitets Arsshift N.F.* Avd. 2. Bd 59. Nr 8:1-34 Häkan Ohlssons Boktryckeri, Lund.

Pachur, H.-J. and P. Hoelzman. 1991. Paleoclimatic implications of late Quaternary lacustrine sediments in western Nubia, Sudan. *Quat. Research* 36:257-278.

Pandolfi, L.J., E.K. Kalil, P.R. Doose, L.H. Levine, L.M. Libby. 1980. Climate periods in trees and a sea sediment core. *Radiocarbon* 22:740-745.

Perez-Obriol, R., and R. Juliá 1994. Climatic change on the Iberian Peninsula recorded in a 30,000-year pollen record from Lake Banyoles. *Quat. Research* 41:91-98.

Pettersson, O. 1914. Climatic variations in historic and prehistoric time. *Svenska Hydrogr Biol Komm Skriftern* 5.

Rampton, V. 1970. *Late Quaternary Vegetation and Climatic History of the Snag-Klutlan Area, Southwestern Yukon Territory, Canada.* Geol. Soc. America Bull. 81.

Ray, L.L., and T.N.V. Karlstrom. 1968. Theoretical concepts in time-stratigraphic subdivision of glacial deposits. Pages 115-119 in *Means of Correlation of Quaternary Successions.* R.B. Morrison and H.E. Wright, Jr., editors. University of Utah Press, Salt Lake City.

Richie, J.R., and F.K. Hare. 1971. Arctic tree line. *Quat. Research* 1:331-342.

Richmond, G.M. 1976. Pleistocene stratigraphy and chronology in the mountains of western Wyoming. Pages 353-379 in W.C. Mahaney, editor. *Quaternary Stratigraphy of North America.* Dowdon, Hutchison and Ross Inc., Stroudsburg, PA.

Scharpenseel, H.W., H. Zakosek, U. Neue, H. Schiffmann. 1980. Search for pedogenic phases during the younger Pleistocene and Holocene (Soltanien and Rharbien) of Tunisia. *Radiocarbon* 22:879-884.

Scott, E.W., W.D. McCoy, R.R. Shroba, and M. Rubin. 1983. Reinterpretation of the exposed record of the last two cycles of Lake Bonneville, western United States. *Quat Research* 20:261-285.

Scuderi, L.A. 1987. Glacial variations in the Sierra Nevada, California, as related to a 1200-year tree-ring chronology. *Quat. Research* 27:220-231. (Also 1990. *Quat. Research* 34:67-85).

Stacey, C. 1963. Cyclical measures: Some tidal aspects concerning equinoctial years. *Annals New York Academy of Science* 105, Article 7:421-460.

Stacey, C. 1967. Earth motions and time and astronomic cycles. Pages 335-340 and 999-1003 in *The Encyclopedia of Atmospheric Sciences and Astrogeology.* R. Fairbridge, editor. Reinhold Publishing, New York.

Villagrán, C. 1988. Late Quaternary vegetation of southern Isla Grande de Chloe, Chile. *Quat Research* 29:294-306.

Winogard, I. J., T.B. Coplen, J.M. Landwehr, A.C. Riggs, K. R. Ludwig, B. J. Szabo, P. T. Kolesar, K. M. Revesz. 1992. Continuous 500,000-year climate record from vein calcite in Devils Hole, Nevada. *Science* 258:255-260.

Climatology of the Seasonal Precipitation Maximum in the Western United States

Cary J. Mock

ABSTRACT: The western United States is characterized by heterogeneous patterns of seasonal precipitation regimes due to the hierarchy of climatic controls that operate at different spatial scales. A climatology of intermonthly precipitation changes, using data from more than 4,000 stations including high-elevation sites, illustrate how different climatic controls explain the spatial distribution of the seasonal precipitation maximum. These results indicate that smaller-scale climatic controls must be considered along with larger-scale ones to explain patterns of spatial climate heterogeneity over mountainous areas. The results also offer important implications for scholars interested in assessing spatial climatic variations of the western United States at different timescales.

Introduction

Precipitation of the western United States varies spatially because of numerous smaller-scale climatic controls embedded within larger-scale controls, primarily as a result of the rugged physiography in the region (Bryson and Hare 1974; Hirschboeck 1991). The distribution of the seasonal precipitation maximum exhibits complex patterns, with different seasonal maxima intermixed in some areas (Pyke 1972; Tang and Reiter 1984). Several scholars have examined spatial variations of precipitation over the region and assessed the climatic controls responsible for these variations (*eg*, Tang and Reiter 1984). These studies were able to infer how larger-scale climatic controls explain spatial precipitation variation; however, their surface data networks were too sparse to examine smaller-scale climatic controls. Their data networks also included few high-elevation sites; that is problematic for interpreting spatial precipitation variations in the western United States.

This study presents a precipitation climatology of the western United States and adjacent Canada and Mexico, using a spatially dense network of stations to detect spatial variations at both large and small scales. The study area includes the states west of the Mississippi River to cover a diverse range of spatial climatic scales and controls. Data consist of averaged modern climatic normals of monthly precipitation from more than 4,000 stations (Figure 1).

Precipitation data came from four sources: World WeatherDisc Associates (1990), Atmospheric Environmental Service (1982) of Canada, Willmott *et al* (1981), and the Soil Conservation Service (1988). The Soil Conservation Service network contains data from high-elevation stations, which are useful for delineating smaller-scale climatic features in mountainous

In: C.M. Isaacs and V.L. Tharp, Editors. 1995. *Proceedings of the Eleventh Annual Pacific Climate (PACLIM) Workshop, April 19-22, 1994.* Interagency Ecological Program, Technical Report 40. California Department of Water Resources.

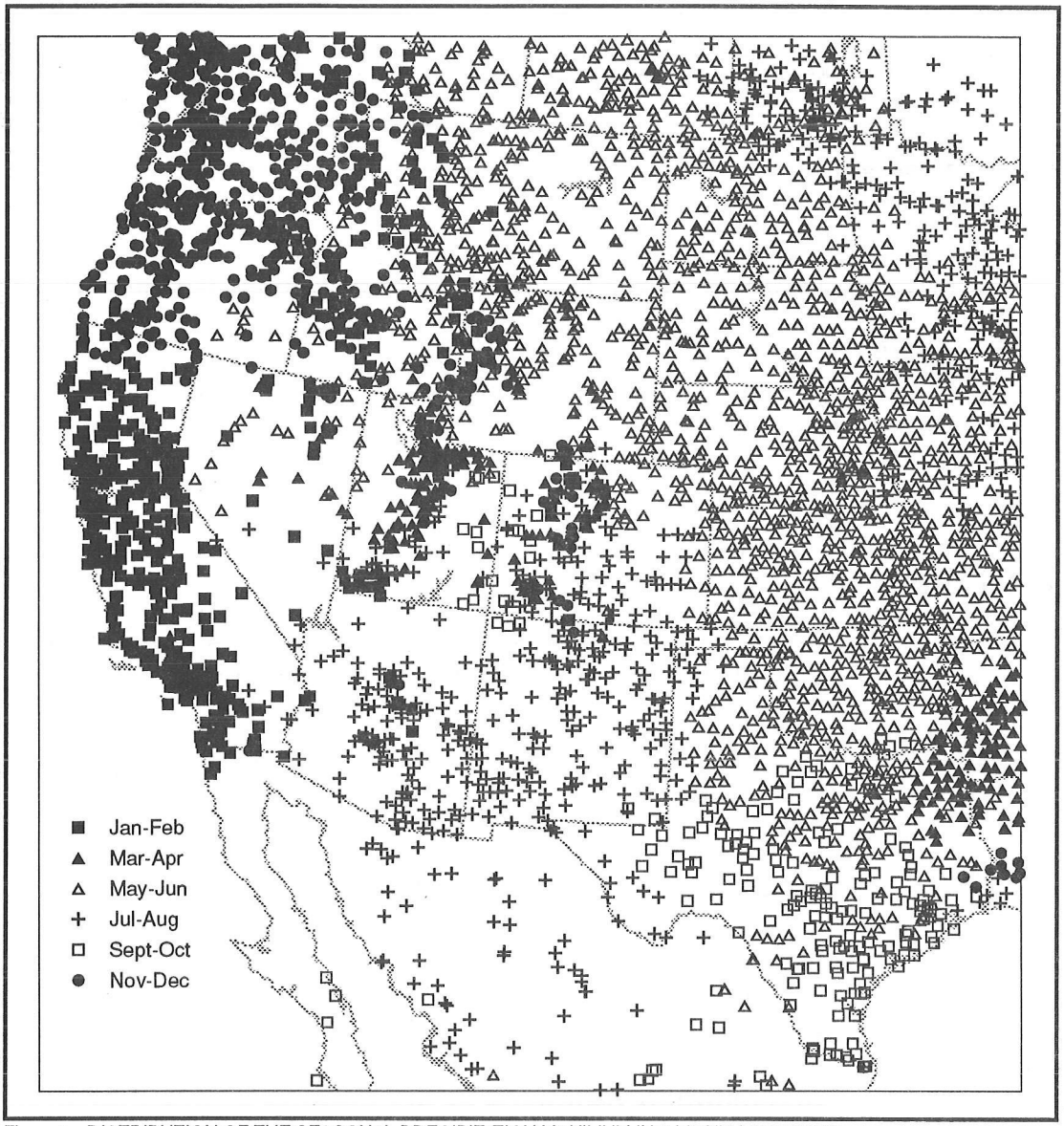

Figure 1. DISTRIBUTION OF THE SEASONAL PRECIPITATION MAXIMUM IN 2-MONTH SEASONS

terrain. Monthly precipitation data from World WeatherDisc and Atmospheric Environmental Service are 1951-1980 normals; that period represents a useful climatic normal because it excludes the widespread droughts of the 1930s and 1980s, which may present misleading representations of climatic normals (Mock 1991). Some of the climatic normals of periods from the datasets by Willmott *et al* (1981) and the Soil Conservation Service vary due to the data being relatively scarce and discontinuous, particularly for the latter dataset. The shorter records, however, span at least 10 years and are not believed to be a severe constraint when combined with longer networks of climatic data for delineating smaller-scale precipitation variations.

Seasonal Precipitation Maximum Regimes

In anticipation of the seasonal analyses of the hierarchy of different spatial climatic controls on precipitation variations, a map indicating regimes of the seasonal precipitation maximum was generated. This map was constructed by mapping the time of year of the precipitation maximum for each station in 2-month seasons (Figure 1). This classification provided a clear analysis of different precipitation regimes as they relate to different climatic controls. The map shows both large-scale and small-scale patterns. Some homogeneous areas are evident. These are the November/December and January/February regimes of the Pacific coast; the May/June regime over most of the Great Plains; the July/August regime over Arizona, southeastern California, New Mexico, and northwestern Mexico; the November/December and March/April regimes in east Texas; and the September/October regime in southeastern Texas and southern Baja California.

Spatial heterogeneity of seasonal precipitation regimes, however, is clearly evident over the mountainous areas. A small region of a September/October regime over southwestern Colorado and southeastern Utah is evident, but other areas in Utah, western Colorado, southeastern Oregon, and Nevada show a mixture of precipitation regimes. Spatial heterogeneity is also evident in western Montana and eastern Idaho, but there it involves a less complex mixture of regimes than for the Utah/Colorado region to the south.

Construction of Intermonthly Precipitation Maps

To examine the climatic controls that cause patterns of spatial heterogeneity of the seasonal precipitation maximum, the author constructed intermonthly maps for selected seasons. Each map summarizes intermonthly trends for 2 months simultaneously for a particular season, showing the relative changing areal extent of precipitation variations. Maps were constructed with symbols indicating the sign of intermonthly trends for each station. For example, a symbol in the analysis of intermonthly trends for summer precipitation could indicate decreased precipitation from June to July as well as from July to August. The months summarized in this paper are December/January (winter), March/April (spring), July/August (summer), and September/October (fall).

December/January Intermonthly Precipitation Trends

The summary of December/January trends shows a number of distinctive patterns at both larger and smaller scales (Figure 2). Large-scale controls include the southward progression of the jet stream (Pyke 1972). This migration explains precipitation increases in December and decreases in January (*DecI, JanD*) for parts of Washington and Oregon and

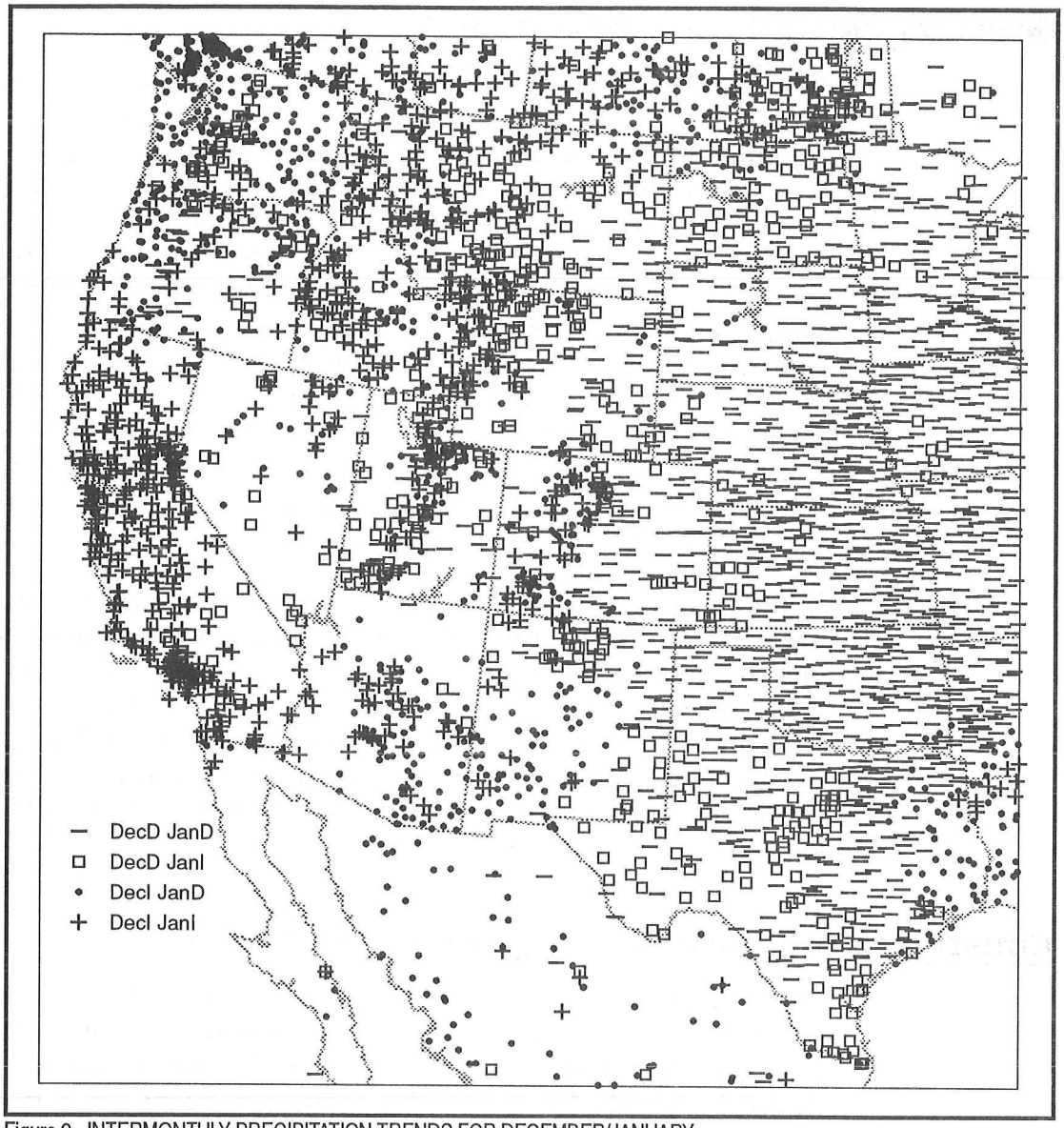

Figure 2. INTERMONTHLY PRECIPITATION TRENDS FOR DECEMBER/JANUARY

increases in both December and January (*DecI, JanI*) for most of California. The establishment of the PNA (Pacific North American teleconnection) pattern explains December decreases and January decreases (*DecD, JanD*) over most of the Great Plains as northwesterly flow is more frequent. It also explains precipitation increases over southern Canada and the northern Great Plains from increased leeside cyclogenesis in Alberta (Whittaker and Horn 1982).

Smaller-scale climatic controls explain why some areas show patterns of heterogeneity in the precipitation changes. Low-elevation pathways explain the distribution of precipitation increases for both December and January (*DecI, JanI*) for the Snake River Plain, western Wyoming, and upper Colorado River Valley, as Pacific air is advected inland (Bryson and Hare 1974). Conversely, because of their high elevation, some sites in the northern Cascades experience decreases of precipitation for both Decem-

ber and January (*DecD, JanD*), because they are less exposed to moisture sources and situations for orographic precipitation enhancement. Some stations in the American Southwest show precipitation increases in December and decreases in January (*DecI, JanD*). The increases in December correspond to what Tang and Reiter (1984) termed as the "Plateau Monsoon of Winter." They suggested that although the plateau is generally dry during winter, some axes of precipitation enhancement occur in the Great Basin and Colorado, between the Great Basin and Four Corner highs. Some high-elevation sites are more susceptible to receiving precipitation from strong mid-level westerly and southwesterly flow than are broad interior valleys, which would experience dry, rainshadow-like conditions. Convergence zones may explain localized areas of intermonthly precipitation variation in Washington and Oregon. Similarly, cyclogenesis in the southern Rockies and Gulf of Mexico, as well as their influences on the spatial distribution of the low-level jet, explain precipitation variation for locations in eastern Texas.

March/April Intermonthly Precipitation Trends

Precipitation trends for March/April also exhibit both large- and small-scale variations. The Great Plains show a homogeneous response of precipitation increases for March and April (*MarI, AprI*) (Figure 3). Although several climatic controls influence precipitation in the Great Plains, most of them involve the same large-scale pattern of increased troughing into the western United States that cause leeside cyclogenesis in the Rocky Mountains (Whittaker and Horn 1982). Southern Texas shows a region of precipitation decreases for March as a result of frequent occurrences of this troughing pattern. Increases in April are due to the increased moisture advected from the Gulf of Mexico.

Most of Washington, Oregon, California, the Snake River Plain, western Wyoming, and western Mexico exhibit precipitation decreases for both months (*MarD, AprD*) due to a strengthened and expanded Pacific subtropical high, and a weakened Aleutian low. However, some locations in Oregon and Washington have increases for March and decreases for April. The causal mechanisms are still not clear, but they likely involve topographic influences, increased convective activity at lower elevations, and/or some aspect of precipitation recycling (Pyke 1972). An area of March increases and April decreases (*MarI, AprD*) in Arizona and the Four Corners region represent the influence from Great Basin cyclogenesis and the subtropical jet stream.

Stations in the mountainous regions of Utah, Colorado, Arizona, Nevada, and New Mexico illustrate a pattern of spatial heterogeneity. Some stations west of the Continental Divide in Colorado exhibit more of a wet Great Plains-type regime as a result of topographic gaps and south- or east-facing slopes. Some low-elevation stations in Utah, Nevada, and Arizona lie in the rainshadow of moist air masses from the Gulf of California and the Pacific Ocean, thus indicating precipitation decreases

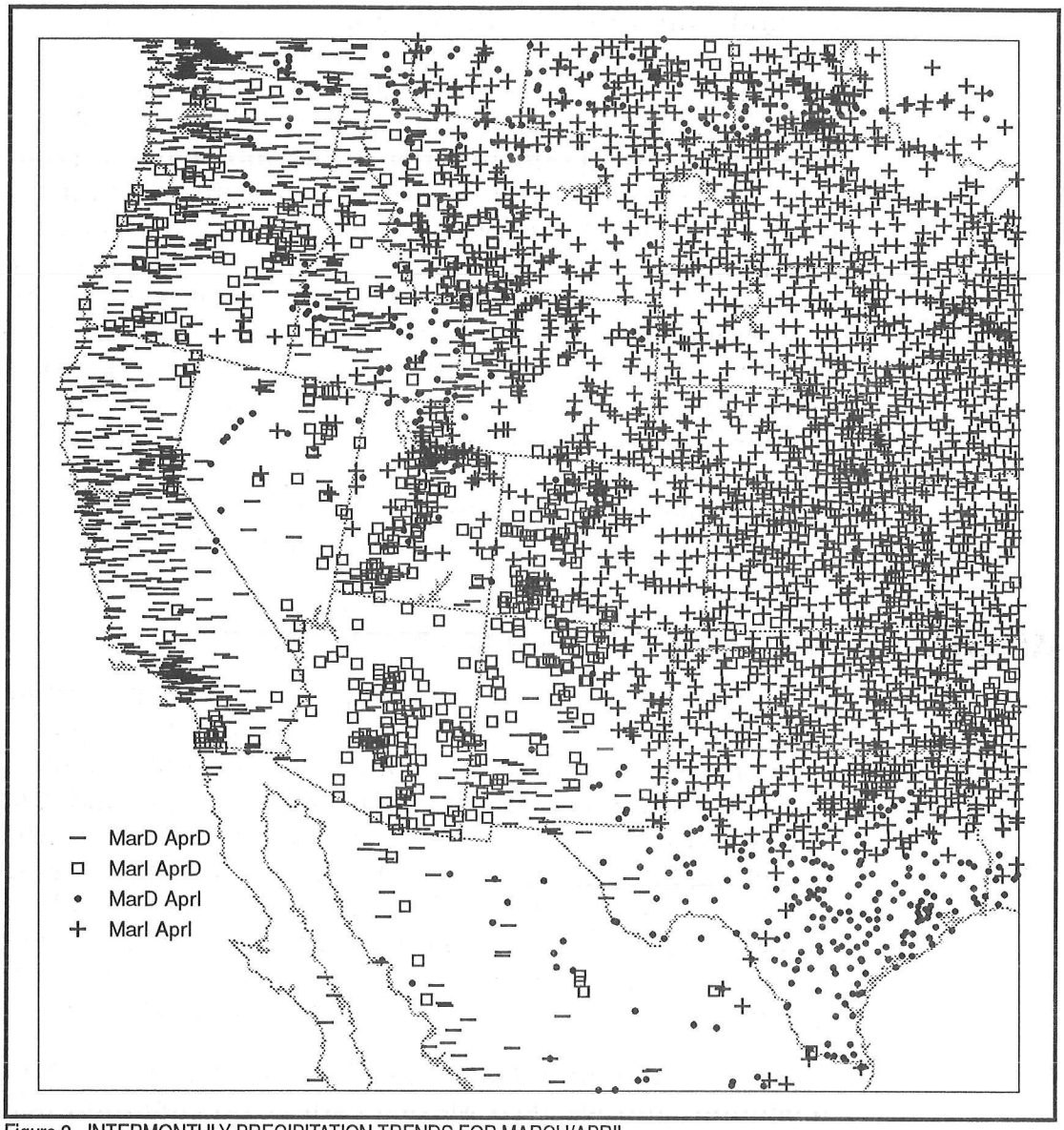

Figure 3. INTERMONTHLY PRECIPITATION TRENDS FOR MARCH/APRIL

for both March and April. The assessments of climatic controls on precipitation for the Four Corners states, the Great Basin, and parts of the Pacific Northwest are site-specific for many cases.

July/August Intermonthly Precipitation Trends

The map of July/August intermonthly trends shows that precipitation decreases in northern Great Plains are fairly homogeneous (*JulD, AugD*), with August precipitation increases to the north and east (*JulD, Augl*) responding to Alberta lows and high thunderstorm frequency respectively (Figure 4). However, conditions in the Great Plains are still relatively wet during summer, largely due to the formation of mesoscale convective systems (Hirschboeck 1991). An upper-level subtropical ridge, which explains the summer monsoon in the American Southwest (Carleton 1987), does not cause a homogeneous distribution of precipitation de-

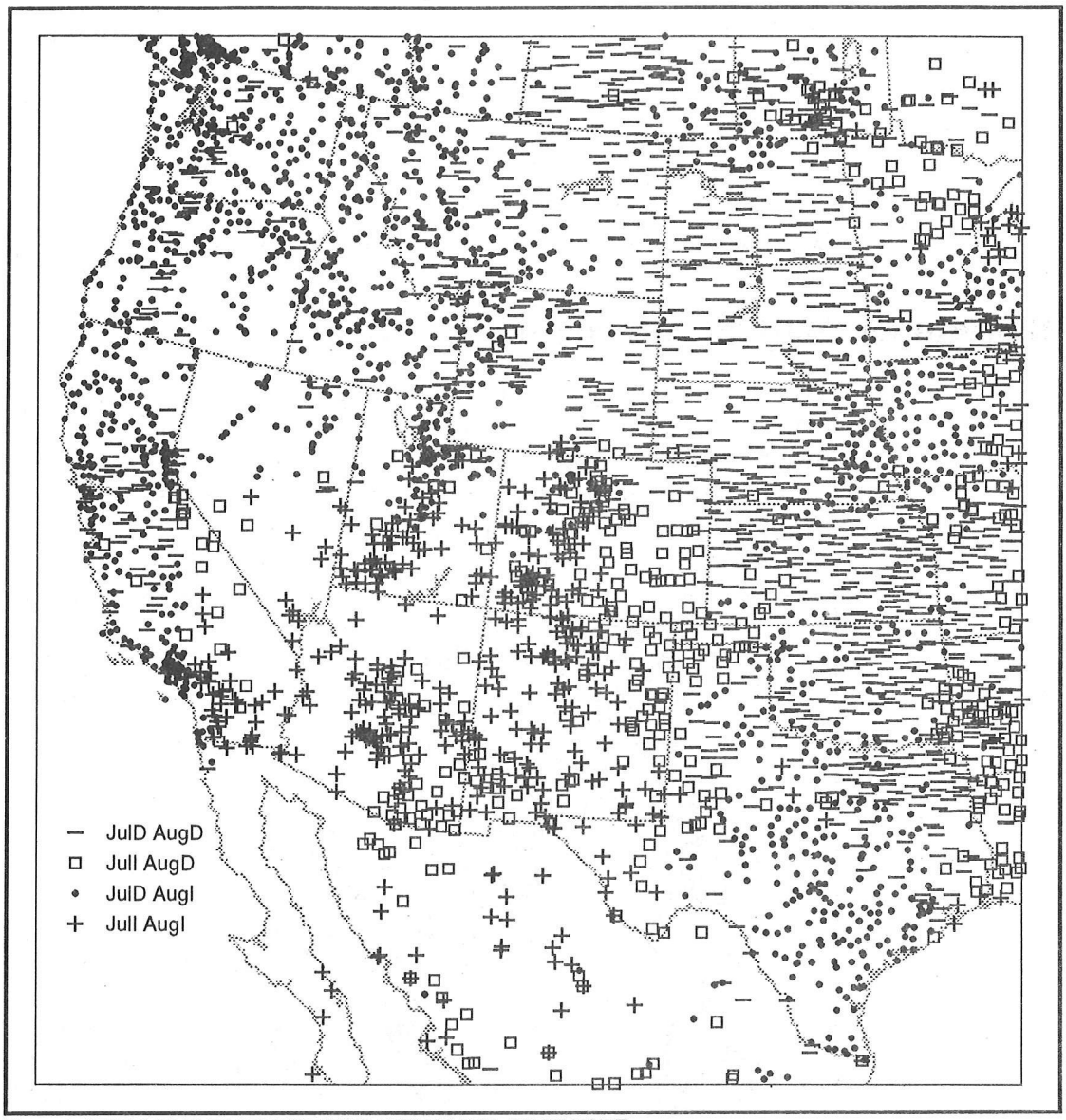

Figure 4. INTERMONTHLY PRECIPITATION TRENDS FOR JULY/AUGUST

creases in the southern Great Plains because of effects from the tropical upper-tropospheric trough and tropical storms from the east in August. A westward shift of the summer monsoon is apparent, with July increases and August decreases (*JulI, AugD*) over the southern Plains, and increases for both months (*JulI, AugI*) for much of the Southwest, consistent with implications by Tang and Reiter (1984). Stations that deviate from the westward shift have their climatic regimes controlled by topography.

Most stations in the Pacific Northwest experience July decreases due to the strong Pacific subtropical high and August increases due to a relatively higher frequency of upper-level disturbances as compared with July (*JulD, AugI*). However, the Cascades and some high-elevation areas in Idaho and Montana show precipitation decreases for both July and August. As compared with surface frontal systems, upper-level disturbances usually

bring relatively more precipitation to lower elevations than to higher ones (Schermerhorn 1967). The upward motion in upper-level disturbances relates with vorticity aspects that do not deal with orographic aspects. A peculiar area of July increases and August decreases (*JulI, AugD*) is evident along the eastern Sierra Nevada. The August decreases are the result of lower-level divergence, which is indirectly related to topographic influences and the thermal trough (Hill 1993).

September/October Intermonthly Trends

The map for September/October (Figure 5) illustrates stations with precipitation increases for both September and October (*SepI, OctI*) over most of the Pacific states and interior Pacific Northwest. The increases reflect the influence from mid-latitude cyclones originating in the Gulf of Alaska. Topography plays an important role on the spatial extent, with the Snake River Plain, Cascade Range, and Sierra Nevada having the

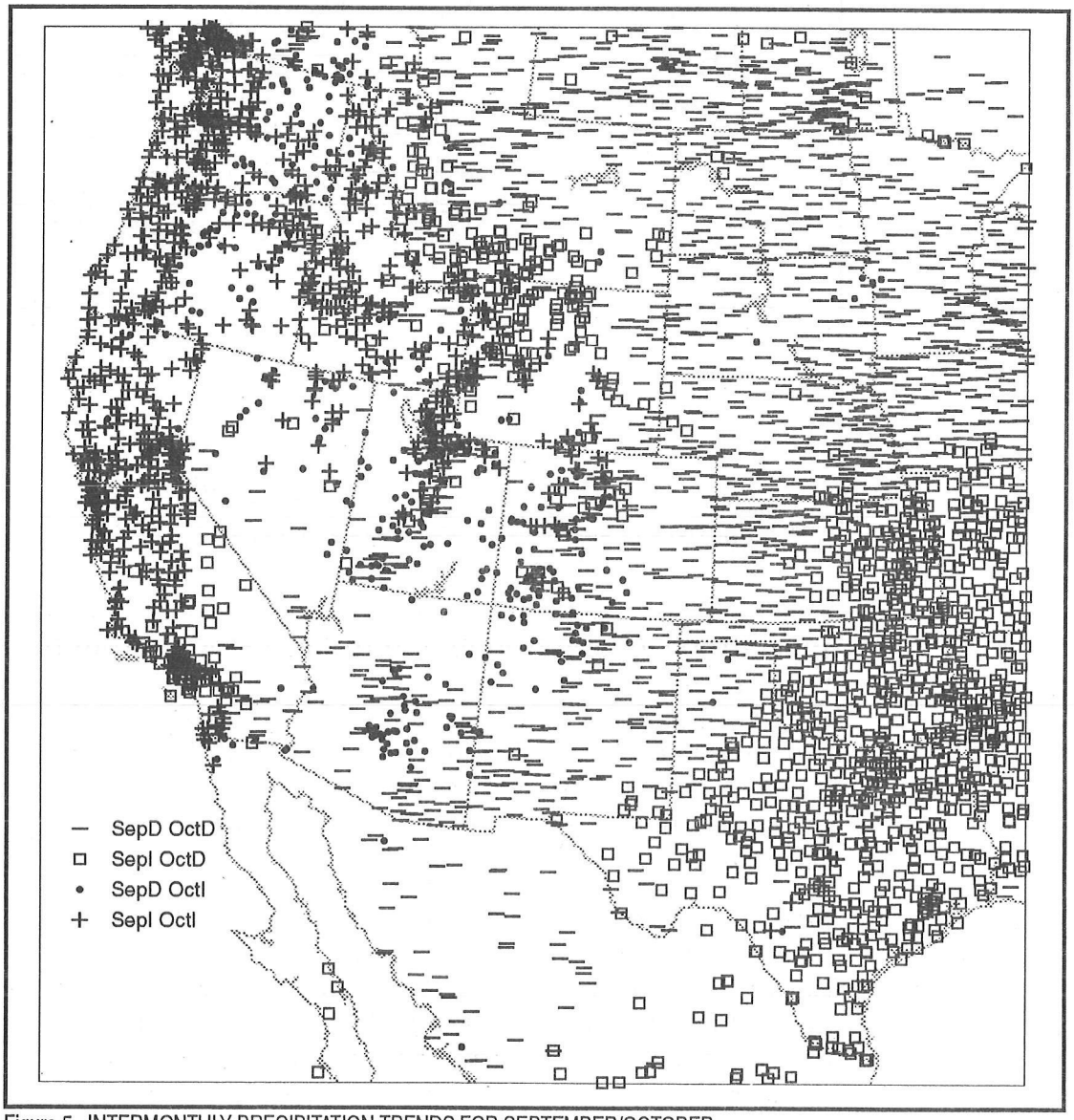

Figure 5. INTERMONTHLY PRECIPITATION TRENDS FOR SEPTEMBER/OCTOBER.

largest increases (Bryson and Hare 1974). Some large increases for both months are also located over the Wasatch Range in northern Utah, in northern Nevada, and in western Colorado, but they may reflect the influence of cutoff lows (Hirschboeck 1991). Some stations with precipitation increases for September and precipitation decreases for October (*SepI, OctD*) scattered over Nevada, Utah, and Colorado also reflect the influence of cutoff lows. Locations with precipitation increases for September and decreases for October in Baja California and the southeastern Great Plains indicate the effects from easterly disturbances and tropical storms. Most stations over the American Southwest exhibit precipitation decreases for both months (*SepD, OctD*) in Arizona, New Mexico, northwestern Mexico, and southeastern California, illustrating the final dissipation of the summer monsoon (Tang and Reiter 1984). Similar decreases are also evident throughout the northern and central Great Plains due to modified Pacific airstreams penetrating far inland (Bryson and Hare 1974). These airstreams reduce convective activity, limit the spatial extent of the low-level jet, and reduce the frequency of mesoscale convective systems.

Conclusions

Climatological analyses of intermonthly precipitation trends for four seasons clearly illustrates that a number of climatic controls interact with one another to jointly explain spatial climate variation. Intermonthly maps show that larger-scale climatic controls, such as the polar jet stream, the Pacific subtropical high, and the subtropical ridge, play important roles on spatial variation of climate in the region. They do not, however, explain all the patterns in some mountainous areas where smaller-scale climatic controls are the rule rather than the exception. Smaller-scale climatic controls, such as physiography and the thermal trough, also play important roles in explaining spatial precipitation variation. For example, these smaller-scale controls explain why some stations in the mountainous areas of Utah and Colorado have winter precipitation maxima while other nearby stations have spring and summer maxima.

Results from this study provide several applications regarding research on climatic change for the western United States. A knowledge of precipitation responses at a variety of spatial scales to particular large-scale circulation patterns can improve spatial resolution for forecasting seasonal precipitation anomalies (*eg*, from ENSO events), parameterization of general circulation models, and refinement of lateral boundary conditions for high-resolution mesoscale models. Such an understanding can also aid in analyses of floods (Hirschboeck 1991) and late-Quaternary paleoclimates (Mock 1994) in the region. Improvement of spatial and temporal records of high-elevation sites will aid in future analyses of the hierarchy of climatic controls and the heterogeneous precipitation responses that characterize the climate of the western United States.

References

Atmospheric Environmental Service. 1982. *Canadian Climate Normals. Volume 1, Precipitation.* Environment Canada, Ottawa, Canada, 602 pp.

Bryson, R.A., and F. K. Hare. 1974. The climates of North America. Pages 1-47 in *Climates of North America, World Survey of Climatology Vol. 11.* R.A. Bryson and F.K. Hare, editors. Elsevier, New York.

Carleton, A.M. 1987. Summer circulation climate of the American Southwest, 1945-1984. *Annals of the Associations of American Geographers* 77:619-634.

Hill, C.D. 1993. Forecast problems in the Western Region of the National Weather Service: An overview. *Weather and Forecasting* 8:158-165.

Hirschboeck, K.K. 1991. Climate and floods. Pages 67-88 in *National Water Summary 1988-89 — Floods and Droughts: Hydrologic Perspectives on Water Issues.* U.S. Geological Survey Water-Supply Paper 2375, Denver, Colorado.

Mock, C.J. 1991. Drought and precipitation fluctuations in the Great Plains during the late nineteenth century. *Great Plains Research* 1:26-57.

Mock, C.J. 1994. Synoptic climatological aspects of late-Quaternary paleoclimates of the western United States. Pages 124-128 in *Preprints, Sixth Conference on Climate Variations,* American Meteorological Society, Boston.

Pyke, C.B. 1972. *Some meteorological aspects of the seasonal distribution of precipitation in the western United States and Baja California.* University of California Water Resources Center, Contribution No. 139, 204 pp.

Schermerhorn, V.P. 1967. Relations between topography and annual precipitation in western Oregon and Washington. *Water Resources Research* 3:707-711.

Soil Conservation Service. 1988. Snow Survey and Water Supply Products Reference. West National Technical Center, Portland, Oregon, 132 pp.

Tang, M., and E.R. Reiter. 1984. Plateau monsoons of the Northern Hemisphere: a comparison between North America and Tibet. *Monthly Weather Review* 112:617-637.

Whittaker, L.M., and L.H. Horn. 1982. *Atlas of Northern Hemisphere Extratropical Cyclone Activity, 1958-1977.* University of Wisconsin Press, Madison, Wisconsin, 65 pp.

Willmott, C.J., J.R. Mather, and C.M. Rowe. 1981. Average monthly and annual surface air temperature and precipitation for the world. Part 2. The Western Hemisphere. *Publications in Climatology* 34:1-378.

World WeatherDisc Associates. 1990. World WeatherDisc CD-ROM. World WeatherDisc Associates, Inc., Seattle, Washington.

Some Effects of Earth's Surface on Winter Jet Stream Positions in the Northern Hemisphere and Rainfall Patterns in Northern and Central California

Stephen H. Holets

ABSTRACT: Pacific Gas and Electric Company developed an analog model for predicting total rainfall in its Sierra Nevada watersheds 1 to 2 months in advance. The rainfall outlook model is based on the empirical technique of matching monthly average polar-front jet stream positions in the eastern and central regions of the North Pacific with historical jet stream positions. A knowledge of the mean position of the jet stream and probable contributing factors to its configuration are important for this modeling effort.

This report shows that the mean wintertime polar-front jet stream structure consists of three long waves. Prominent ridges in the jet stream flow occur near the longitudes of India, eastern Pacific/west coast of North America, and eastern Atlantic/British Isles; prominent troughs occur near the longitudes of the Middle East, western Pacific, and western Atlantic/east coast of North America. The ridges mainly occur just upstream of major mountain ranges, and the troughs in the jet stream flow mainly occur near regions of warm sea-surface temperatures. The mean jet stream pattern is plotted on a physical map of the world, revealing some of the effects the Himalayas and Tibetan Plateau region apparently have on deflecting the upper-air flow in that area. These observations support current theory that mountain ranges and land and ocean thermal contrasts play important roles in the climatological three planetary wave pattern. Synoptic-scale transient eddies may play a dominant role in some regions, such as the central and eastern portions of the North Pacific and North Atlantic.

One of the climatological ridges occurs along the west coast of North America. The mean position of this quasi-stationary ridge is 44°N latitude and 130°W longitude or in the eastern Pacific, just off the central Oregon coast. The position of the jet stream at this location appears to be the main reason most Pacific storms pass to the north of California. Sustained rainfall in northern and central California occurs only when the storm track is displaced southward of this climatological position.

Introduction

Optimal hydroelectric planning and scheduling begin with an accurate prediction of the potential water resource availability. The National Weather Service provides monthly rainfall outlooks that are only slightly more accurate than chance and are very general in nature because they cover the entire continental United States. Since useful long-range rainfall outlooks have not been available in the past, PG&E has relied on median rainfall for predicting water runoff and hydroelectric generation, even though the use of a median (or moderate rainfall) prediction may be an oversimplification.

To improve rainfall outlooks and ultimately enhance hydro resource planning, PG&E's Research and Development Department has sponsored development of a model for specifically predicting regional monthly wintertime rainfall patterns in its watersheds in the Sierra Nevada. The

In: C.M. Isaacs and V.L. Tharp, Editors. 1995. *Proceedings of the Eleventh Annual Pacific Climate (PACLIM) Workshop, April 19-22, 1994.* Interagency Ecological Program, Technical Report 40. California Department of Water Resources.

resulting monthly rainfall outlook model is based on the empirical techniques of matching monthly average jet stream positions in the eastern and central regions of the North Pacific with historical jet stream positions. In the case of each selected analog, occurrences within the light, moderate, or heavy rainfall categories for the following month are noted. Probability-like distributions are then established from these historical rainfall totals for use in predicting future monthly rainfall at selected watershed sites. Model results for the 1992-93 and 1993-94 winters were much more accurate than chance, suggesting that model methods are tapping into a predictable weather process.

In modeling efforts, it is important to understand the characteristics of the parameters used in the models. This is especially true in long-range analog modeling, because some subjective decisions are sometimes necessary in making the rainfall outlooks. In the case of the PG&E model, which uses jet stream parameters, one important feature is the mean state of the wintertime polar-front jet. Mean positions of the jet stream in the Northern Hemisphere are presented in this report, along with probable factors contributing to its configuration. In addition, rainfall patterns in northern and central California will be related to mean jet locations in the eastern region of the North Pacific and west coast of North America.

Jet Stream Data

Jet stream mean and variability parameters are used in the long-range analog model because of the strong relationship between rainfall and jet stream positions. When the jet is over California, the state is usually "wet"; when it is to the north or south, the state is usually "dry".

The wintertime polar-front jet is a zone of strong winds, meandering in ever-changing wave patterns in the Northern Hemisphere. This area coincides with the Polar Front, or the region of maximum horizontal temperature gradients between cold polar air to the north and warm subtropical air to the south, as shown in Figure 1. The jet core is typically in the vicinity of the 250-millibar level, or about 9500 meters above the ground with the Polar Front zone sloping upward to the north. On the average, the polar-front jet axis lies directly above the Polar Front with a projection of the jet on the frontal surface intersecting at about 5580 meters on 500-mb upper-air weather maps. For this research project, PG&E had historical weather maps for the 500mb surface dating back to 1947; the period of available 250-mb surface maps was much shorter. As a result, 500-mb maps were used in all analyses.

Latitude positions of the wintertime 5580-meter contour on 500-mb charts were manually calculated as the locations of the polar-front jet above the ground. A quick comparison between 250-mb and 500-mb jet locations suggests that, in most cases, this is an excellent approximation, especially over the oceans. These jet data were calculated from afternoon (0000Z) 500-mb maps for every 10 degrees longitude from November to

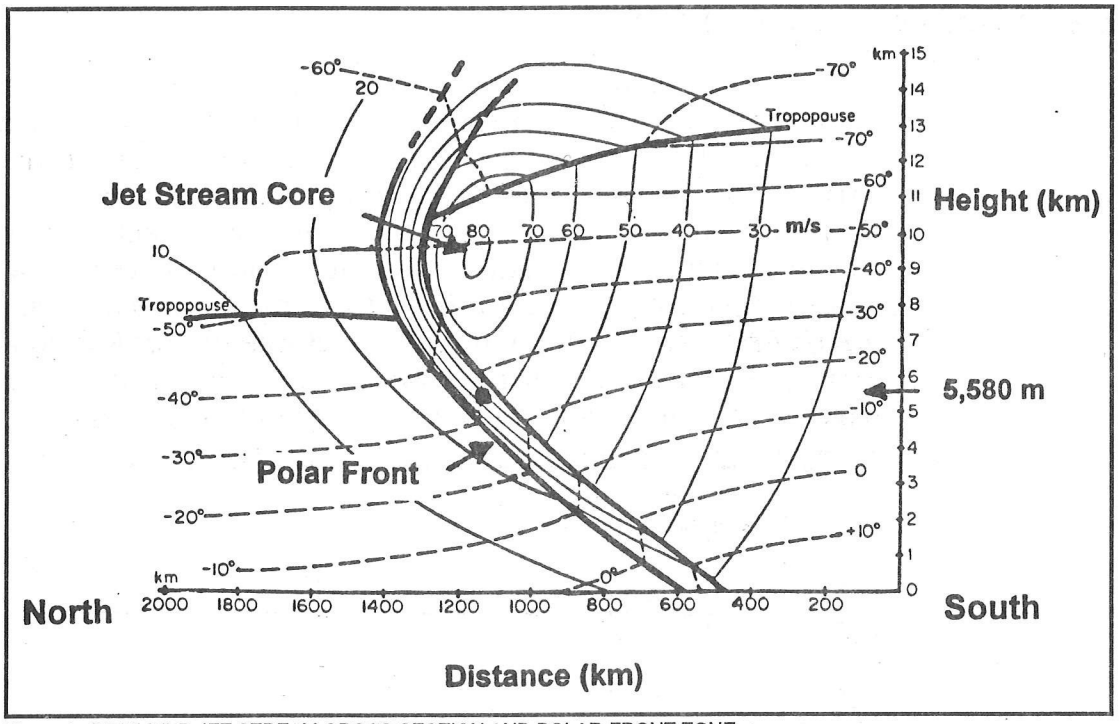

Figure 1. IDEALIZED JET STREAM CROSS SECTION AND POLAR-FRONT ZONE
The jet stream core intersects the Polar Front at about 5580 meters.
SOURCE: Palmén and Newton 1969.

April. When the 5,580-meter contour crossed a longitude at two or more locations, the highest latitude was used for discontinuous cases such as "cutoff lows", and the lowest value was used for continuous, unbroken contours. The reason for neglecting "cutoff lows" is that once the cutoff occurs, the flow is no longer part of the jet stream.

Two monthly jet stream databases were developed. One database contains jet stream positions for 1960 to 1994, which covers the mid-latitude region of the western Pacific (150°E longitude) to the mid-North American continent (90°W longitude) or one-third of the Northern Hemisphere. Jet stream positions for this database were computed from 500-mb maps every third day (10 maps per month), instead of every day (about 30 maps per month). Computing positions for every day or every other day was too labor intensive, and continuity in weather patterns was lost when every fourth day was chosen. Validity of estimating jet stream positions with a sample size of 10 instead of 30 was tested for several historical monthly periods. Mean monthly jet stream positions from 10 maps (every third day) were within $\pm 1°$, $\pm 1.5°$, and $\pm 2°$ latitude of values computed from 30 maps (every day) 80%, 90%, and 95% of the time, respectively. Thus, jet stream latitudes computed from 500-mb maps 3 days apart give an excellent approximation of mean monthly polar-front jet position over the ground.

The second jet stream database covers 1989 to 1994 and latitude positions at every 10 degrees longitude around the Northern Hemisphere. These jet positions were calculated once a day from afternoon (0000Z) 500-mb weather maps.

Mean Jet Stream Patterns

The 30-year mean monthly positions of the jet stream from the western Pacific to the mid-North American continent for November through April, 1961 to 1990, are shown in Figure 2. A dramatic seasonal shift in jet stream locations occurs at all longitudes except in the eastern Pacific. The jet is much farther north in the western Pacific, central Pacific, and western North American continent during November and April. These data suggest that ***mean wintertime polar-front jet stream patterns, useful for long-range rainfall predictions, lock into place in December and continue through March***. As a result, the mean wintertime jet stream was determined with only December through March data.

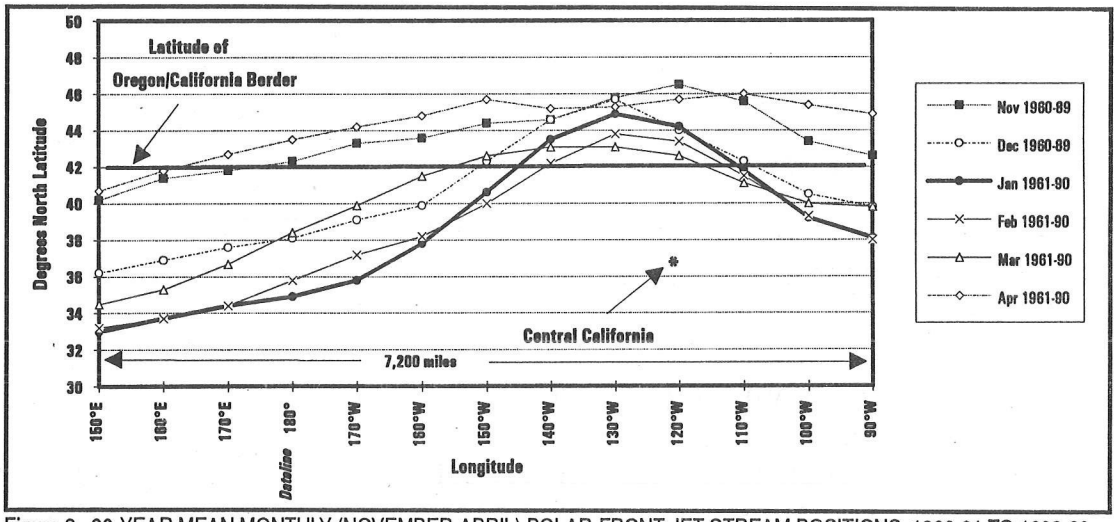

Figure 2. 30-YEAR MEAN MONTHLY (NOVEMBER-APRIL) POLAR-FRONT JET STREAM POSITIONS, 1960-61 TO 1989-90

Mean wintertime (December-March) jet stream positions for the 5-year period 1989 to 1994 are shown in Figure 3. Regions of low yearly wintertime jet stream variability are from 80°E (India) to 180° (central Pacific) and 100°W (central North America) to 50°W (central Atlantic). ***The eastern Pacific Ocean and eastern Atlantic Ocean to the Middle East are the regions of high variability.***

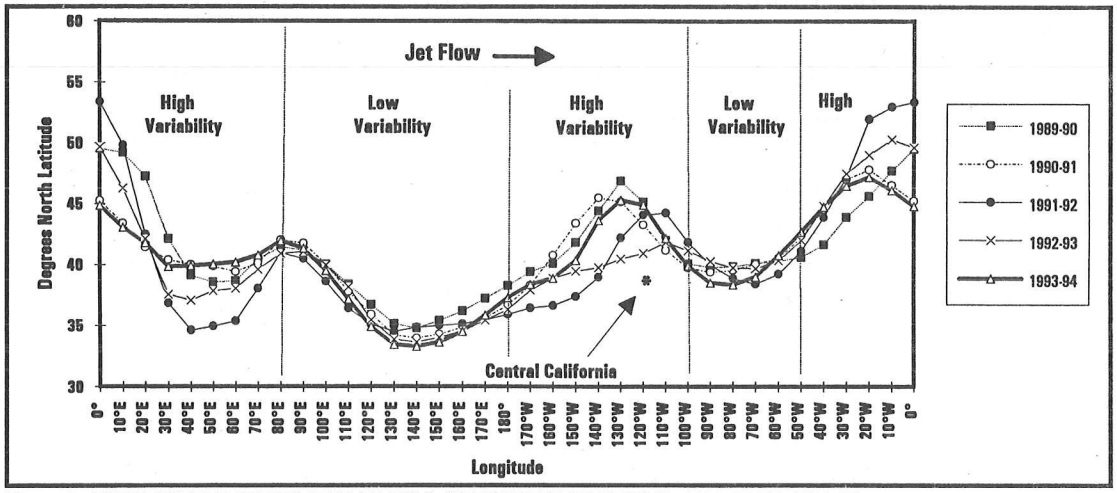

Figure 3. MEAN WINTER (DECEMBER-MARCH) JET STREAM POSITIONS, 1989-90 TO 1993-94

The mean wintertime jet stream structure in the Northern Hemisphere for the 5-year period is shown in Figure 4. ***This structure consists of three long waves***. Prominent ridge axes occur at 80°-90°E (India), 120°-130°W (eastern Pacific/west coast of North America), and 0°-10°W (eastern Atlantic/British Isles). A step-like pattern occurs in ridge axes (41°N to 44°N to 49°N from left to right in Figure 4). Prominent trough axes occur at 40°-60°E (Middle East), 130°-140°E (western Pacific), and 70°-90°W (western Atlantic/east coast of North America). Trough axes latitudes are 38°N, 34°N, and 39°N, respectively.

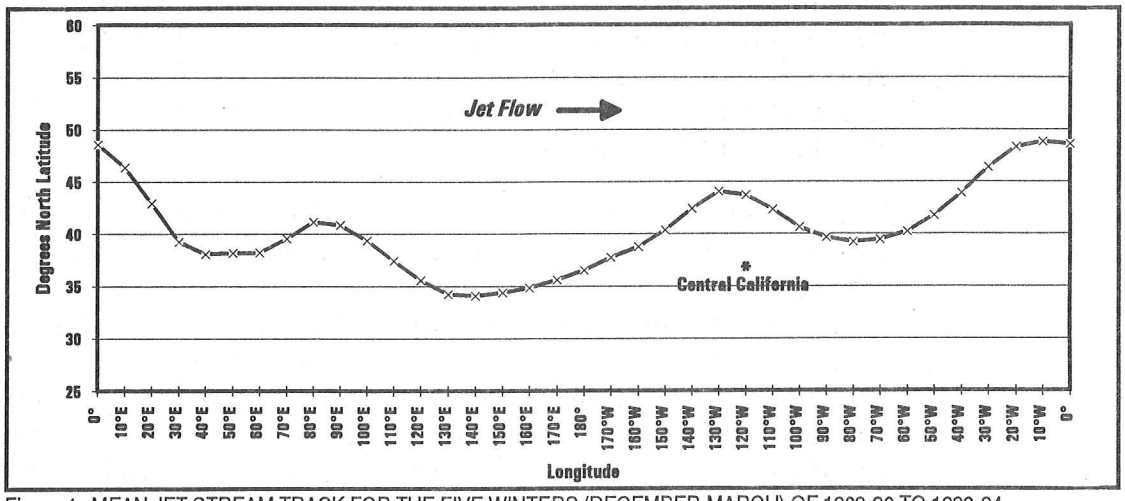

Figure 4. MEAN JET STREAM TRACK FOR THE FIVE WINTERS (DECEMBER-MARCH) OF 1989-90 TO 1993-94

The mean jet stream pattern in Figure 4 is only for a 5-year period. How representative is this configuration to the long-term mean? Figure 5 shows a comparison of 5-year and 30-year mean jet stream positions from the western Pacific to the mid-North American continent. For at least this third of the Northern Hemisphere, the 5-year positions are representative of the long-term mean.

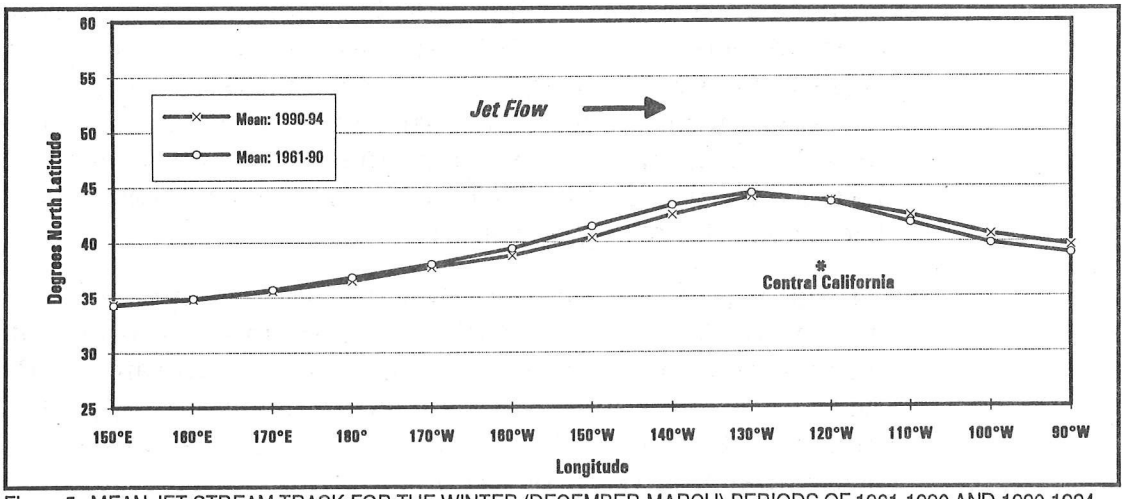

Figure 5. MEAN JET STREAM TRACK FOR THE WINTER (DECEMBER-MARCH) PERIODS OF 1961-1990 AND 1990-1994

It is important to emphasize here that the jet stream positions represent locations of the jet stream axis and do not address wind speed in the jet. The maximum average wintertime speed (120 knots) occurs over Japan (140°E longitude); the next highest speed (100 knots) occurs over the Middle East (50°E longitude). Average speed of the jet over eastern North America (80°W longitude) is 80 knots.

Discussion

Normally, four or five long waves are evident on daily 500-mb weather maps. The *exact* three long-wave pattern as shown in Figure 4 probably never exists on *daily* maps. It is merely a statistical averaging result of the fact that long-wave troughs and ridges have a tendency to remain fixed at certain locations.

This raises the question: "Why do daily troughs and ridges of the jet stream stagnate in these areas?" Wallace (1983) and Broccoli and Manabe (1992) suggest that deflection of air as it encounters mountain ranges is a primary factor in determining the longitudes of the quasi-stationary long-wave ridges. Conservation of potential vorticity of flow over the mountains would cause vertical shrinking of the air column. Eastward-moving air would turn to the south as it flowed up the terrain, thus creating a ridge near the mountain and a trough downstream. Some factors concerning mountains that may affect standing wave formation are: the width of the mountains (Bolin 1950), the latitude of the mountains (Frenzen 1955), and the location on west coasts of continents (Palmén and Newton 1969; Rossby 1973). The extent, orientation, and almost equal spacing of the high mountain ranges in the Northern Hemisphere are other probable factors.

Early studies by Sutcliffe (1951), Smagorinsky (1953), and Rossby (1973) suggest that thermal effects of land and ocean play an important role in standing wave formation. Besides mountains and possibly land and ocean effects, Rossby (1973) suggests that the strength of the westerlies is important in forming the long-wave pattern. Grotjahn (1993) presents several arguments for transient eddy (short-wave winter storms) forcing as a factor in the long-wave formation. Some lows merge, leading to a larger low. Also, lows migrate to higher latitudes as they travel away from the areas of storm generation.

Grotjahn (1993) concludes that the three long-wave pattern is probably a combination of many of these factors, but that orographic and thermal forcing functions dominate. Positions of mountains and oceans in relation to the three long-wave structure basically supports this conclusion in many areas of the Northern Hemisphere, as shown in Figure 6. Ridges occur just upstream of major mountain ranges, and troughs in the jet stream mainly occur near regions of warm sea-surface temperatures.

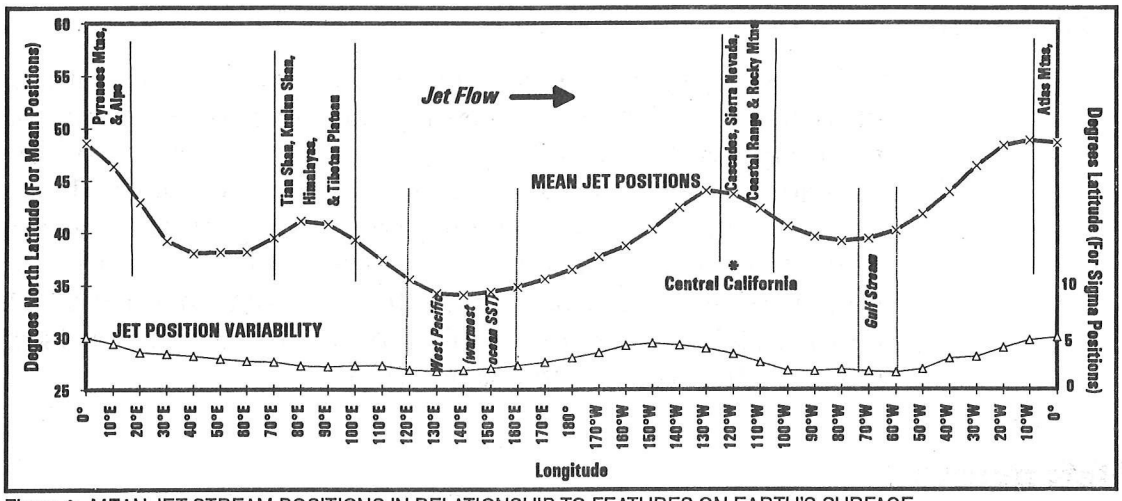

Figure 6. MEAN JET STREAM POSITIONS IN RELATIONSHIP TO FEATURES ON EARTH'S SURFACE

The mean jet stream pattern, plotted on a physical map of the Earth in Figure 7, reveals some of the effects the Himalayas and Tibetan Plateau region apparently have on deflecting the upper-air flow in that area. The jet stream ridge nearly follows the terrain outline of the Tien Shan Mountains.

Orographic and thermal forcing probably dominate in some of the low year-to-year jet stream variability regions of the Northern Hemisphere, such as the Himalayas and Tibetan Plateau region and warm sea-surface temperature regions of the western tropical Pacific and Gulf Stream in the western Atlantic (Figure 3). The Himalayas and Tibetan Plateau are imposing barriers to any westerly winds. Sea-surface temperatures in the western tropical Pacific and Gulf Stream regions probably vary little from winter to winter.

It is difficult, however, to conclude that these orographic and sea-surface temperature forcings are important in some regions of high year-to-year wintertime jet stream variability, such as the portions of the ridges in the central and eastern regions of the North Pacific and North Atlantic. The mountain ranges on the western North American continent would affect the flow of westerly winds only a few hundred kilometers upstream in the eastern Pacific. The Coast Ranges, Cascades, Sierra Nevada, and Rocky Mountains consist of a continuous north-south barrier to eastward-moving flow. In addition, there is probably not enough variation in the mean wintertime sea-surface temperature pattern across the North Pacific and North Atlantic to cause a northward deflection of the flow. Consequently, the eastward progression of transient eddies may be an important factor in these regions because storm systems typically migrate to higher latitudes as they move across the oceans from west to east.

Conclusions

The mean polar-front jet stream pattern consists of a three long-wave pattern in the Northern Hemisphere. One of the climatological ridges in the mean jet flow occurs along the west coast of North America. The mean position of this quasi-stationary ridge is 44°N latitude and 130°W longitude, or in the eastern Pacific just off the central Oregon coast (Figure 5). The jet stream at this location appears to be the main reason most Pacific storms pass to the north of California. Sustained rainfall in northern and central California occurs only when the storm track is displaced southward of this climatological position.

References

Bolin, B. 1950. On the influence of the earth's orography on the westerlies. *Tellus* 2:184-195.

Broccoli, A.J., and S. Manabe. 1992. The effects of orography on midlatitude Northern Hemisphere dry climates. *J. Climate* 5:1181-1201.

Frenzen, P. 1955. Westerly flow past an obstacle in a rotating hemispherical shell. *Bull. Am. Meteorol. Soc.* 36:204-210.

Grotjahn, R. 1993. *Global Atmospheric Circulations.* Oxford University Press, New York. 430 pp.

Palmén, E., and C.W. Newton. 1969. *Atmospheric Circulation Systems: Their Structure and Physical Interpretation.* Academic Press, New York. 603 pp.

Rossby, C.G. 1973. The scientific basis of modern meteorology. Pages 502-529 in *Handbook of Meteorology.* F.A. Berry, E. Bollay, N.R. Beers, editors. McGraw-Hill, New York.

Smagorinsky, J. 1953. The dynamical influence of large-scale heat sources and sinks on the quasi-stationary mean motions of the atmosphere. *Quart. J. Roy. Meteorol. Soc.* 79:342-366.

Sutcliffe, R.C. 1951. Mean upper contour pattern of the Northern Hemisphere — The thermal-synoptic viewpoint. *Quart. J. Roy. Meteorol. Soc.* 77:435-440.

Wallace, J.M. 1983. The climatological mean stationary waves: Observational evidence. Pages 27-53 in *Large-Scale Dynamical Processes in the Atmosphere.* B.J. Hoskins and R.P. Pearce, editors. Academic Press, New York.

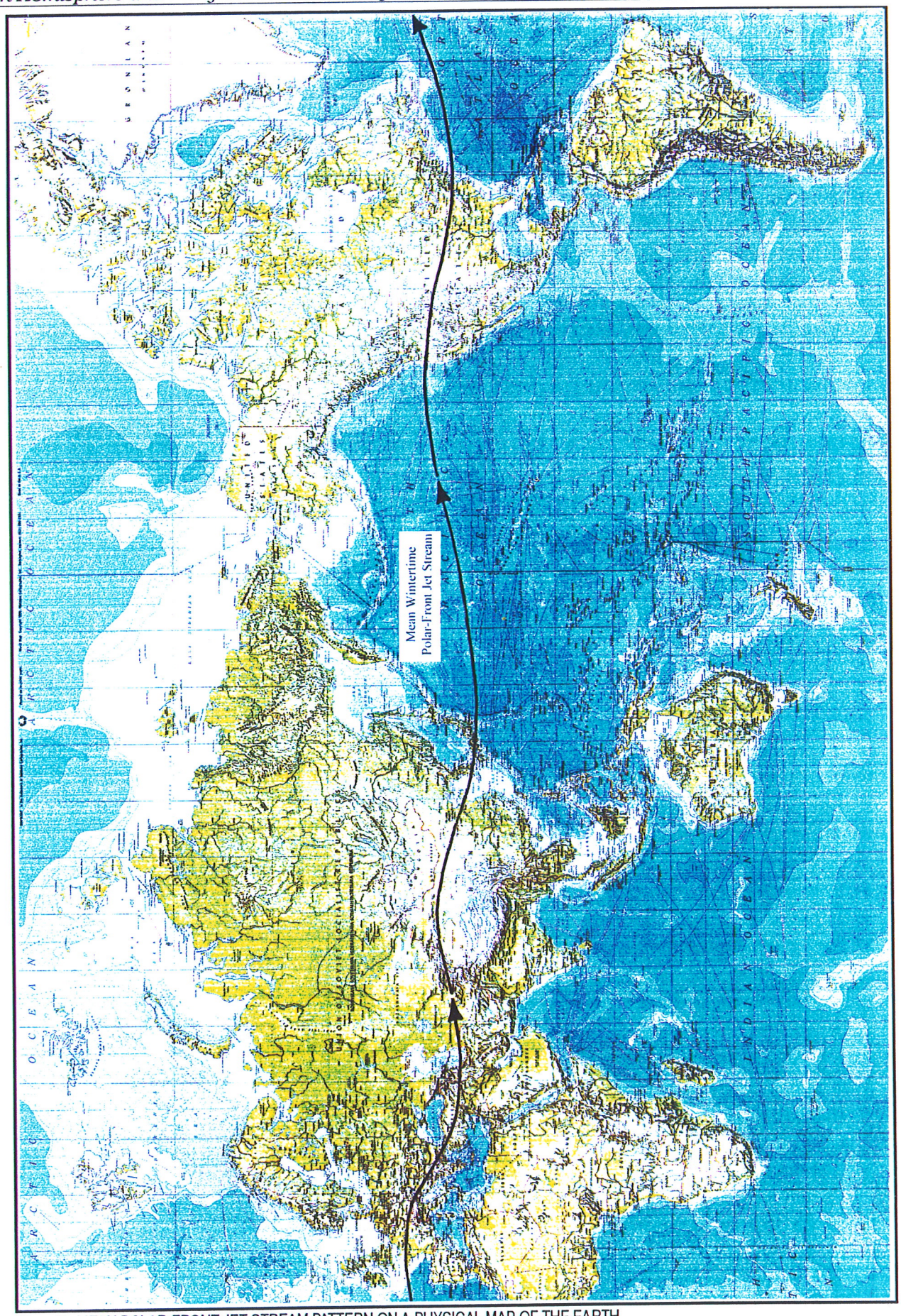

Figure 7. MEAN POLAR-FRONT JET STREAM PATTERN ON A PHYSICAL MAP OF THE EARTH

Drought should be based on relatively rare natural conditions. A reasonable threshold is that water year runoff (or predicted runoff) for a single year or a multiple set of years should be in the lower 10 percent of the historical range. The year 1994 would meet that criteria, although barely so, with the April 1 forecasts. The second part of a drought definition is reservoir storage. This should be less than 70 percent of average, I think.

There is nothing magic about 70 percent. If one wished to be more conservative, an argument could be made for 75 percent (and also for runoff to be in the lowest 15 percent). However, two dry years were required to reduce storage below 70 percent in 1988 (eventually to 14.8 million acre-feet and 68 percent of the current average 21.7 MAF for the 155 major in-state reservoirs on September 30 of that year) (Figure 1).

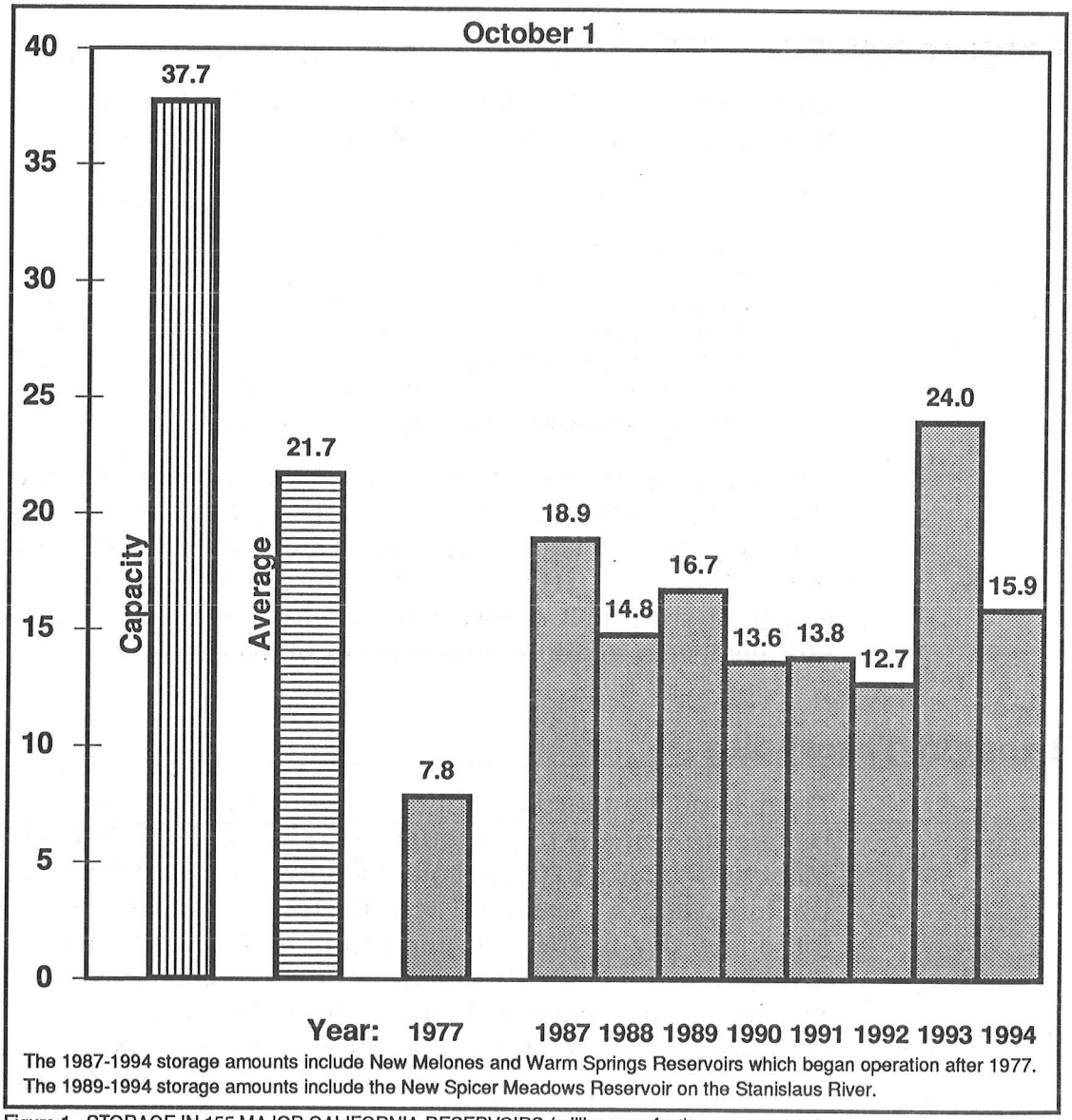

Figure 1. STORAGE IN 155 MAJOR CALIFORNIA RESERVOIRS (million acre-feet)

End of September storage in 1987 was 18.9 MAF, 87 percent of average and down about 9 MAF from April 1 storage. Storage in 1976 did drop below 70 percent — to 13.9 MAF or 64 percent — in one severe year.

April 1 reservoir storage now in 1994 stands at 24.2 MAF, 93 percent of average for the date, hardly alarming. Projected end of water year storage in 1994 is about 16 MAF, which would be 74 percent of average. This would leave water year ending storage just above the 70 percent threshold — not quite qualifying for drought status. Carryover storage from 1993 will soften the impact of low runoff this year, but concern about a possible second dry winter has placed California in an official "drought watch". The longer-term outlook for 1995 is precarious, dependent on increased precipitation next winter.

Water deliveries for State Water Project and Central Valley Project service areas are being curtailed in 1994, primarily because of the dryness of the year, but partly due to restrictions on winter and spring export from the Sacramento-San Joaquin Delta as a result of endangered species requirements. The State Water Project will deliver 50 percent of contractor amounts and the U.S. Bureau of Reclamation is delivering only 35 percent of Central Valley Project agricultural supplies (except that water rights and exchange agreement users get 75 percent) and 75 percent of urban supplies. Wildlife refugees will get 75 percent.

Addendum

Conditions remained drier than normal after April 1, 1994. The Sacramento River (Four River) Index turned out to be 7.8 MAF, the fourth driest of record and 42 percent of the 18.4 MAF average. Southern Sierra runoff into the San Joaquin and Tulare Lake basins was not quite as dry, ranking around the tenth driest of record, but was still less than half of average. Storage in the 155 major reservoirs on September 30, 1994, was 15.9 MAF, about 73 percent of average for the date. Figure 2 shows Sacramento River Index runoff for the current and recent years.

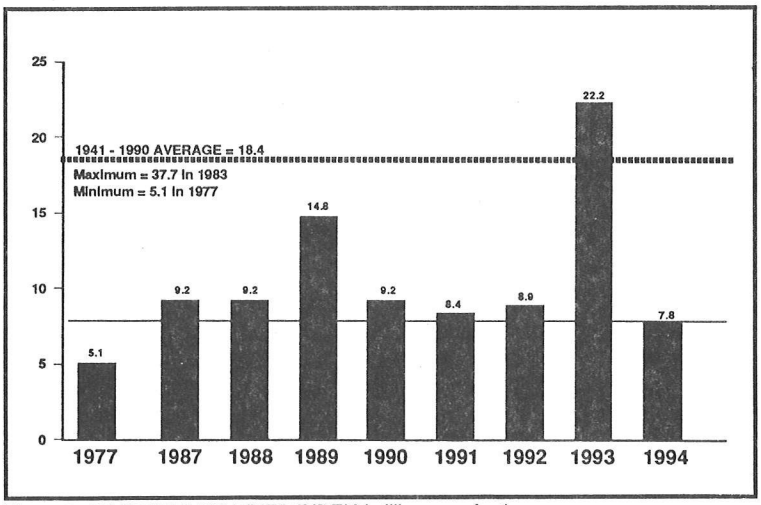

Figure 2. SACRAMENTO RIVER INDEX (million acre-feet).
The Sacramento River Index is the sum of unimpaired runoff from the Sacramento River at Bend Bridge, Feather River inflow to Lake Oroville, Yuba River at Smartville, and American River inflow to Folsom Lake.
The water year is October 1 through September 30.

Late Holocene Environmental Variability in the Upper San Francisco Estuary as Reconstructed from Tidal Marsh Sediments

Lisa E. Wells and Michelle Goman

ABSTRACT: Tidal marsh sediments collected from Browns Island in the lower Sacramento/San Joaquin Delta, California, are used to reconstruct environmental variability over the past 6.8 ka. Calibrated radiocarbon dates provide chronostratigraphic control. Trace metal analyses, grain-size variability, organic content, and macrofossils are used to define short- and long-term variations in relative salinity and inundation frequency. Aggradation began in subtidal fresh water conditions about 6.8 ka. Subtidal aggradation of clayey silts continued until about 6.3 ka, when conditions shifted toward a lower intertidal brackish marsh environment. By 5.1 ka, a brackish marsh plain had evolved, with surface water freshening after 4.1 ka. Conditions returned to brackish similar to the present after 2.3 ka. The uppermost part of the sediments (post-0.9 ka) have elevated trace metal contents probably related to modern contamination leaching downward into the sedimentary column. This initial coarse resolution sampling has also identified several short-period events: an extreme flood (about 0.5 ka) recognized by high mica content and overbank deposition of seeds from the pondweed *Potamogeton* and the foraminifera *Trochominna inflata*; several extreme droughts (about 3.0 ka) recognized by high trace metal contents (Cd and Pb) and high organic content; periods of increased tidal inundation (about 2.2 and 4.5 ka) recognized by high trace metal concentrations, low organic contents, and fossil indicators of inundation.

Introduction

The San Francisco Estuary is an inland arm of the ocean that floods the Sacramento, San Joaquin, and Santa Clara river valleys (Figure 1). The dominant source of fresh water into the estuary is the Central Valley of California, which drains 40% of the state via the Sacramento and San Joaquin rivers. The region has a Mediterranean climate with cool, wet winters and warm, dry summers. Most of the regional precipitation falls as snow in the Sierra Nevada such that discharge peaks in late spring when snow melts. Natural discharge variability is believed to have been quite high. In extreme flood years (*eg*, AD 1861/1862), the tidal range at the Golden Gate dropped to zero and the ocean was said to have been fresh 50 kilometers offshore at the Farallon Islands (Dana 1939). In extreme drought years (*eg*, AD 1841), tidal influence was felt as far upstream as the confluence of the Feather and Sacramento rivers, and brackish water penetrated well into the delta (Thompson 1957). Beginning in AD 1850, levee building, hydraulic gold mining, and channel dredging irreversibly changed the hydrologic balance of the estuary. Today, the discharge regime is highly muted as water is stored in reservoirs on nearly every river in the drainage basin. Since hydrologic monitoring did not begin until well after significant human modification had occurred, we must rely on geological proxy records to reconstruct the natural salinity and discharge variability of the system.

In: C.M. Isaacs and V.L. Tharp, Editors. 1995. *Proceedings of the Eleventh Annual Pacific Climate (PACLIM) Workshop, April 19-22, 1994.* Interagency Ecological Program, Technical Report 40. California Department of Water Resources.

Figure 1. MAP OF THE SAN FRANCISCO ESTUARY SHOWING CORE SITES (italicized) AND DISTRIBUTION OF PRESENT AND HISTORICAL WETLANDS.
Inset map shows limits of the Sacramento-San Joaquin drainage basin that would have naturally discharged through Carquinez Strait and the Golden Gate. (Base maps from Cohen and Laws 1990).

The Holocene estuary was created when the post-glacial rise of sea level allowed oceanic water to enter the Golden Gate sometime between 11 and 10 ka. Estuarine deposition began about 8.3 ka just inland of the Golden Gate, and by 6.8 ka sea level had risen into the Sacramento-San Joaquin Delta region (Atwater *et al* 1977). As sedimentation on mature tidal marsh plains tends to keep pace with the rate of sea level rise (Pethick 1981; Allen 1990; French and Spencer 1993), marsh plain sediments provide a thick and continuous record of environmental conditions for the last 7.0 ka. We have collected sediment cores from six marshes along the northern arm of the estuary to analyze the spatial characteristics of environmental change (Figure 1). Here we present our analysis of sediments from Browns Island, located downstream of the confluence of the Sacramento and San Joaquin rivers.

Environmental Setting

Browns Island, at the upstream end of Suisun Bay, is within the modern mixing zone between fresh water and salt water. Water chemistry varies both seasonally and interannually with the climatology of the watershed. Salinity drops to near zero values with the spring meltwater pulse and may stay low throughout the year during extreme flood years (*eg*, the 1983 El Niño year). During periods of drought (*eg*, 1976/1977), salinity increases in a sawtooth manner, peaking a little higher each subsequent drought year. Estuarine mixing is maintained by density differences between fresh and saline water rather than by tidal currents, and seasonal salinity stratification is largely controlled by the volume of freshwater inflow (Conomos 1979). The mixing zone moves upstream and downstream largely in response to the volume of freshwater flow; therefore, its location can be used as a proxy for freshwater discharge.

Within the mixing zone, flocculation of colloids is enhanced, and this results in a local turbidity maximum (Conomos and Peterson 1977; Burau *et al* 1994). Carquinez Strait is narrow, and tidal currents flush much of the sediment out into San Francisco Bay (Krone 1979, Burau *et al* 1994). Nonetheless, sedimentation rates in the quiet water adjacent to Carquinez Strait historically have yielded remarkably high sedimentation rates. Our comparison of maps from the mid-1800s with recent aerial photographs indicates local shoreline progradation of as much as 1.5 kilometer in the last 150 years. Since trace metals, especially Fe and Pb, are preferentially flocculated out of surface water at low salinity (*eg*, Boyle *et al* 1977; Bourg 1983; Duinker 1983), analysis of sediment trace metal contents can serve as a proxy for water salinity. The spatial relationship between trace metal concentration and salinity gradients in the San Francisco Estuary has been documented in both estuarine water (Flegal *et al* 1991) and in the distribution of trace metals in surface sediments (Peterson *et al* 1972; Ritson and Flegal 1994).

Interpretation of the trace metal records from tidal marsh sediment is complicated by the potential for diagenetic mobilization in the transition zone from oxidizing to reducing conditions (Zwolsman *et al* 1993). Once reducing conditions are stabilized in the saturated subsurface, there is probably little remobilization of trace metals (Bartlett and James 1993). Gleyed surface sediments (blue-gray) at Browns Island with rare brown mottling suggest that saturated and reducing conditions are maintained on the island. Even in the Netherlands, where redox reactions are well documented, trace metal profiles preserve extreme pollution events as discrete peaks (Zwolsman *et al* 1993), and we expect that short-period sedimentary events will also be recognizable in trace metal profiles.

Iron concentration in tidal sediments has also been related to the frequency of tidal inundation (Thomas and Varekamp 1991, Fletcher *et al* 1993). Long-term shifts in Fe content reflect the aggradation of the mud flat to a marsh plain (Fletcher *et al* 1993). These shifts in inundation frequency should also be reflected in changes in sedimentology (lower

organic content and higher silt content at lower elevations relative to mean sea level; Fletcher *et al* 1993; Pizzuto and Rogers 1992) and in plant-macrofossil distributions. Thus, the trace metal signature must be interpreted in light of other proxy information within the cores.

Plant distribution within the estuary is also stratified as a function of inundation frequency and salinity (Mall 1969; Josselyn 1983; Atwater *et al* 1979). The tidal marshes of the estuary can be subdivided into three broad categories: salt marsh, brackish marsh, and freshwater marsh. Salt marshes of San Francisco Bay are dominated by *Spartina foliosa* and *Salicornia virginica*; freshwater marshes of the Sacramento/San Joaquin Delta are dominated by *Scirpus californicus*, *Juncus* spp., *Carex* spp., *Salix lasiolepis*, and *Typha* spp. (Atwater *et al* 1979). *Phragmites communis* occurs most commonly in the loser, more brackish areas of the delta (J. West, personal communication). In the intermediate brackish marshes of Suisun Bay, San Pablo Bay, and Carquinez Strait, these plant species overlap, with the addition of a few plants restricted to the brackish environments, including *Scirpus robustus*, *Cordylanthus mollis*, and *Glaux maritima* (Atwater *et al* 1979). Seeds are well preserved within the section and are identifiable to the genus and occasionally species level. Thus, in conjunction with the other sedimentary characteristics of the cores, we use seed zonations as a proxy for regional salinity and tidal inundation variability through time.

Under modern conditions, Browns Island supports vegetation adapted to brackish water, notably *Scirpus acutus*, *Scirpus americanus*, *Typha angustifolia*, *Carex* sp., and *Distichlis spicata*. Exotic plants (*eg*, California fan palm, Japanese honeysuckle, and a species of acacia) were introduced around the turn of the century when a brothel was located at the western end of the island (Knight 1980). Other human modification of the island has been relatively minor — small levees were built around the island's edge, and linear mosquito ditches were cut across the island's surface. Neither of these has been maintained, and the island is one of the most pristine examples of brackish marsh in the San Francisco estuary.

Methods

We have collected piston core samples from two sites on the marsh plain at Browns Island. The first core site (BI-1992) is about 0.3 kilometer inland of the island's northern edge. The second core site (BI-1993) is more central, about 0.75 kilometer inland from the island's northern edge. BI-1992 cores extend to a depth of 780 centimeters; BI-1993 cores extend to 1060 centimeters. In addition, a monolith (roughly $125 * 10^3$ cm^3) of the surficial peats was excavated from the BI-1993 coring location.

The tidal marsh sediments are dominantly peat and clayey peat, with blue clayey silts at the base. Before being opened, cores were first

archived by x-ray (BI-1992 and BI-1993), gamma ray and magnetic susceptibility (BI-1993 only). After description of large macrofossils and soil characteristics, subsamples were taken for water content, organic content (by loss-on-ignition), grain-size analysis (silt:clay ratios), and trace metal content. A second sample was sieved, and the sand fraction, if present, was described.

We used a Perkin-Elmer model 3100 Atomic Absorption Spectrometer equipped with an HGA-600 Graphite Furnace for the analysis of trace metals in cored sediments. Subsamples for trace metal analyses (about 2 cc.) were taken at 10- or 50-cm intervals except for the section from 230 to 350 centimeters, where samples were taken every 1 centimeter. Bulk sediment samples were digested in a hot solution of 30% HNO_3 and 10% HCl for 45 minutes; after cooling, 1 mL of 30% H_2O_2 was added to the samples. The material was then filtered and the filtrate retained for analysis. According to Varekamp (1991), this is a heavy leach that will digest both organic matter and pedogenic pyrite but will not remove metals that are structurally bound within silicate minerals. Replicates were run for Fe samples from the 1992 core; the difference between the metal concentrations obtained from the replicate runs was about 1% of the total concentration.

Accelerator Mass Spectrometer radiocarbon ages on individual *Scirpus* seeds provide the chronostratigraphic control. Since peat deposits contain organic material with a variety of ages, it is important to date distinct peat components (Wells 1994; Nelson 1992; Belknap *et al* 1989). Dates on seeds from thin layers within the core yield the most consistent chronology; *ie,* rare stratigraphic reversals and nearly linear sedimentation rates (r^2=0.98). All radiocarbon dates discussed herein have been calibrated to the dendrochronological time scale (Stuiver and Reimer 1993).

Sedimentology

Sediments at Browns Island range from clayey silts to clayey peats (Figure 2). The sediments are saturated throughout the section. Water content ranges from 25% in the clayey silts to 90% in the peat layers. Sediment density ranges from 0.70 gm/cc in peat to 1.9 gm/cc in clayey silt. Sediment density increases rapidly within the upper few decimeters of the section and then remains relatively constant through zones of similar sediment composition (*ie,* within the peats or the silts). This implies that most of the compaction of the peat occurred shortly after burial. The high variability of organic content in the uppermost 50 centimeters reflects the low density of uncompacted plant materials. Roots, up to 1.5 centimeter in diameter, remain intact to depths of 30 centimeters. Below this depth, large roots have begun to collapse and decay, and by 50-cm depth all root debris has collapsed and flattened. There is also a strong correlation between organic content and clay content (r^2=82%). Both values peak between 300 and 600 centimeters and then drop off to

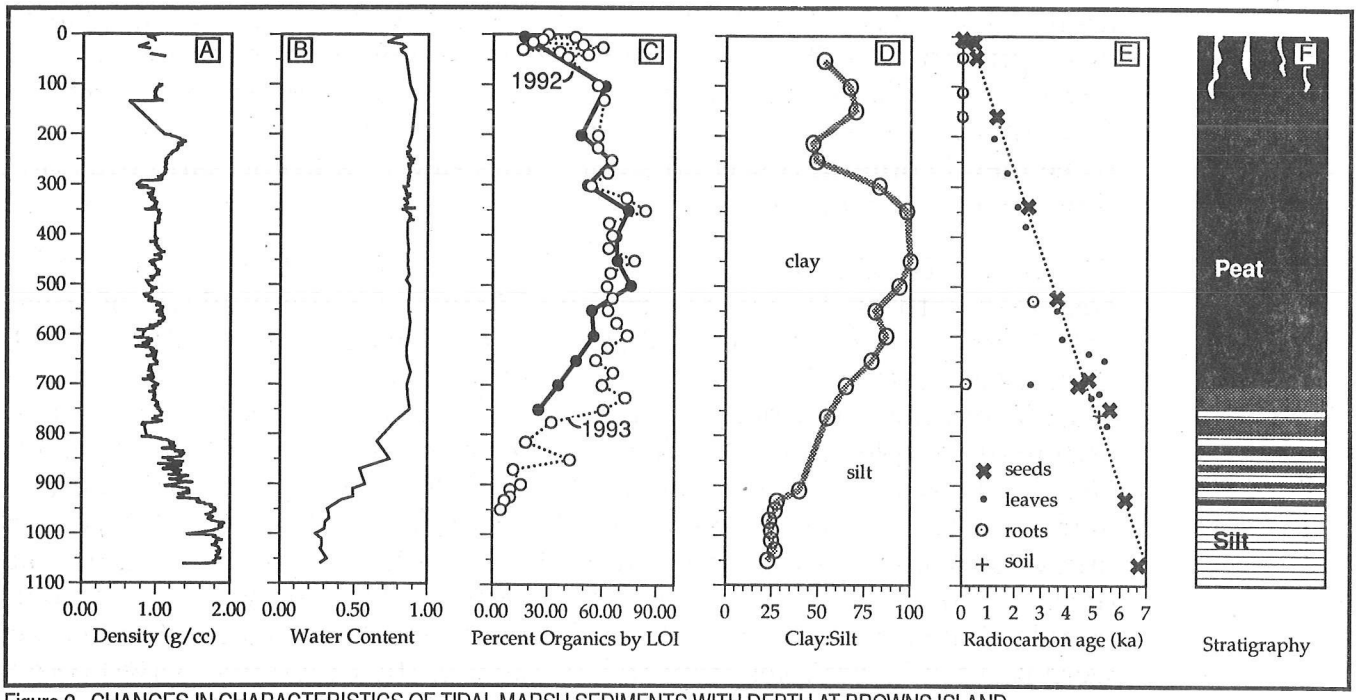

Figure 2. CHANGES IN CHARACTERISTICS OF TIDAL MARSH SEDIMENTS WITH DEPTH AT BROWNS ISLAND.
A. Density (g/cc) for core BI-1993. Upper 100 cm by traditional method, below 100 cm by gamma ray spectrometry.
B. Water content for core BI-1993.
C. Percent organics by loss-on-ignition.
D. Clay:silt ratios. Upper 7-meters core BI-1992; Lower 7 meters core BI-1993
E. Calibrated radiocarbon age from the various components with both cores.
F. Stratigraphy.

very low values at the base of the cores. The consistently low density and high water content suggest that little compaction has occurred and that changes in sediment composition reflect changes in the nature of sediment delivery to and accumulation on the marsh.

The resolution of the sedimentary record is constrained by the nature of marsh sedimentation and sediment diagenesis. X-radiographs of our cores show that fine-scale sedimentary laminations are often preserved and suggest that bioturbation is minimal. The fine-scale variations in the density log (Figure 2A) also reflect these changes in sediment composition and imply little vertical mixing or bioturbation of the detrital sediment. However, root penetration clearly introduces younger organic material to depths of perhaps as much as 1-2 meters. In the sediment monolith, roots are observed to penetrate through silt bands while leaving them largely intact. Stumpf (1983) also observed only minor bioturbation in tidal marshes in the eastern United States, and this is substantiated by recent work using the ^{137}Cs dating method (*eg*, Zwolsman *et al* 1993).

Since the bulk of organic material is autochonous root debris, increases in inorganic sediment content reflect increases in the allocthonous sediment supply. Thin silt layers occur sporadically throughout the peat section (*ie*, at 0.15, 0.45, 2.5, and 3 meters depth) and are most likely the deposits of overbank flood events. Extreme floods during 1983 and 1986 were observed to flush terrigenous sediment well into San Pablo Bay and out through the Golden Gate, and water turbidity increased markedly

during these floods. The discrete silt layers preserved in the core (1-2 millimeters thick) probably represent a single extreme-flood season or even a peak flood.

Trace Metals

There is a strong contrast in the trace metal concentrations between the upper and lower sections of the core (Figure 3). Above 600 centimeters, the correlation between organic content and trace metals is poor (r^2<40%); below this level the correlations are high (r^2=70-97%). The concentrations of Cd and Pb are positively correlated with organic concentration, while Fe is negatively correlated. Concentrations of Pb and Fe (0.408 and 44.66 mg/kg respectively) are high at the surface of the marsh. Lead drops to pre-modern levels by 1 meter depth (0.035 mg/kg), and Fe drops to pre-modern levels by 2 meters depth (20.76 mg/kg). Metal values generally remain low between 2 and 6 meters depth except for several discrete peaks in the concentrations of Cd and Pb. Between 6 and 8 meters, Pb and Cd concentrations increase but Fe values remain low; below 8 meters, Pb and Cd levels drop but Fe values increase.

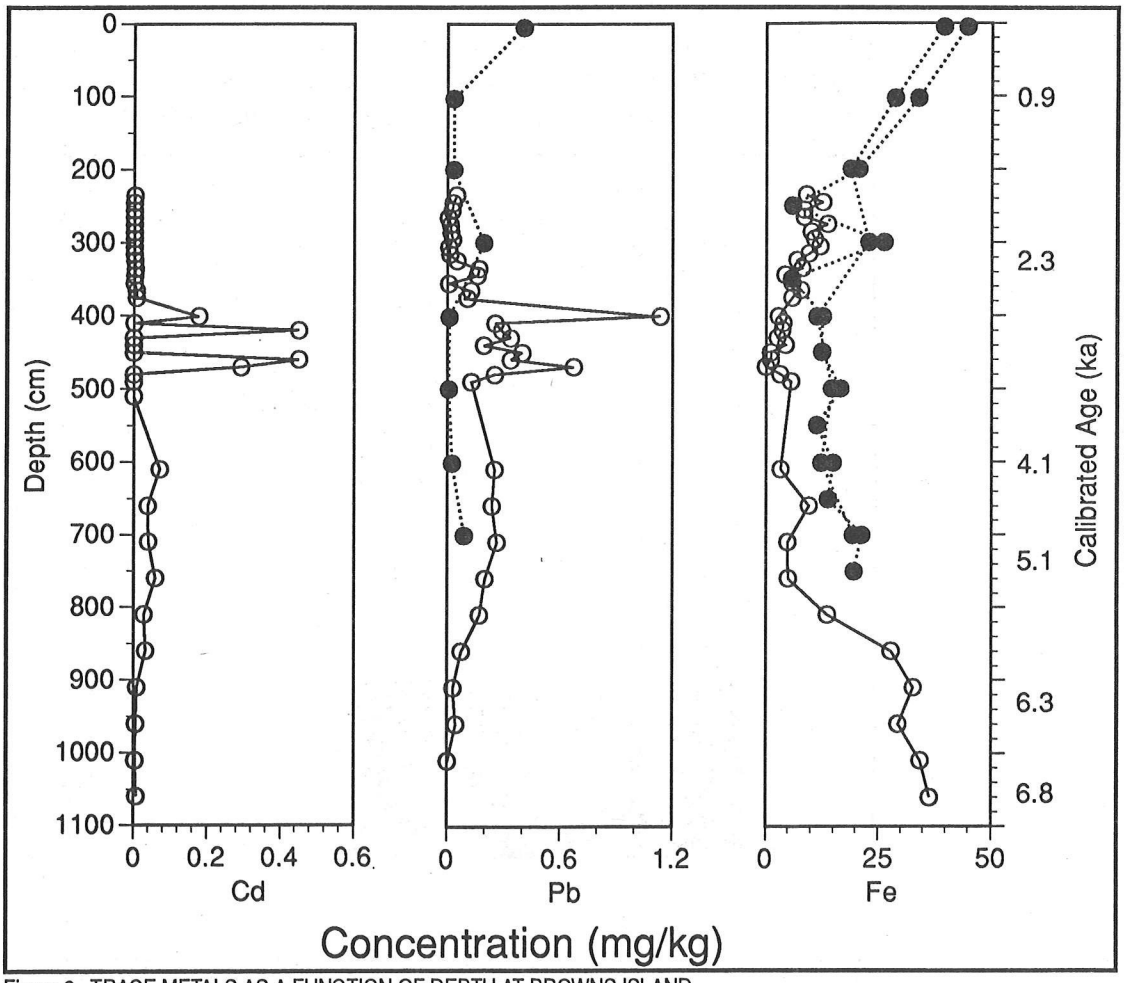

Figure 3. TRACE METALS AS A FUNCTION OF DEPTH AT BROWNS ISLAND.
Solid circles indicate values from core BI-1992; open circles indicate values from core BI-1993.
High resolution data (1-cm sampling intervals) between 200 and 400 cm depth in core BI-1993 have been averaged over decimeter for plotting here.

In addition to these long period trends, several discrete peaks are observed in the data. At 3 meters depth, Pb and Fe have small peaks; between 4 and 5 meters depth, there are several coincidental peaks in Pb and Cd; at 6.5 meters depth, Fe peaks; and at 7.6 meters depth, Cd peaks. In general, the more soluble elements (Cd and Pb) vary coincidentally but Fe behaves in an opposite fashion. As Cd is enriched in sea water, Cd peaks should reflect more saline inundation, and Pb, being transitional between Fe and Cd, should reflect moderate drought conditions.

Macrofossils

Stem, leaf, and root materials were described continuously throughout the cores and seeds were described at discrete intervals (Figure 4). Above 3.25 centimeters, the macrofossils are similar to the plants found on the island today; *Scirpus* seeds are common throughout this zone (BI-1992), *Scirpus americanus* roots are present to at least 0.5 meter depth (BI-1993) and *Distichlis* roots are present in the upper 20 centimeters. A few *Cyperaceae* seeds are also present in these uppermost sediments. Within a thin silt layer at 1 meter depth, seeds from the pondweed *Potamogeton* were found in BI-1992, and several foraminifera (*Trochomina inflata*) were found at this same depth in BI-1993. The presence of two species (*T. inflata* and *Potamogeton*) that live exclusively in the subtidal regions of the marsh within a discrete silt layer is indicative of a large overbank flood.

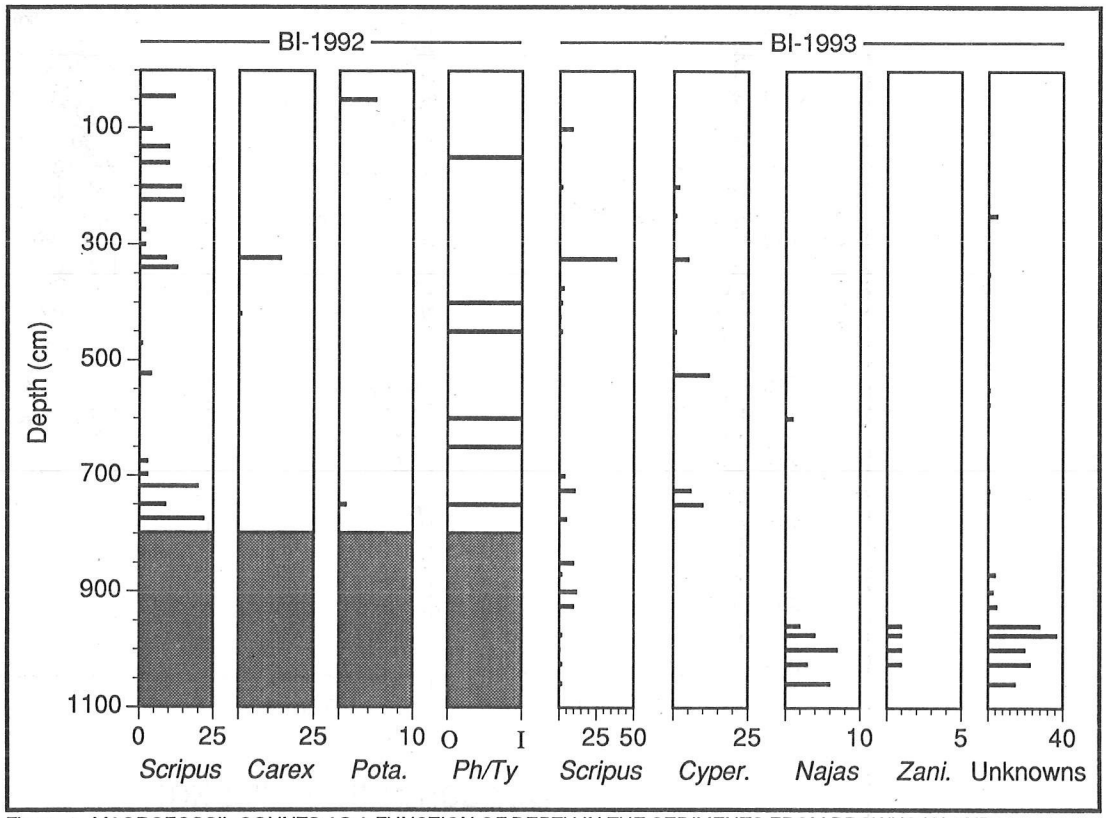

Figure 4. MACROFOSSIL COUNTS AS A FUNCTION OF DEPTH IN THE SEDIMENTS FROM BROWNS ISLAND.
Horizontal bars reflect the number of seeds counted in 1-cm-thick sediment layers for *Scirpus, Potamogeton, Cyperaceae, Najas,* and *Zanichellia.* The category Ph/Ty records the presence or absence (I/O) of stems from either *Phragmites* or *Typha* species.

At 3.0 and 3.5 meters depth, there is a small peak in frequency of *Scirpus* and *Cyperaceae* seeds. Between 3.5 and 7 meters depth, the frequency of all seeds decreases markedly, with only an occasional *Scirpus* or *Cyperaceae* seed present. However, stems and leaves fro *Typha/Phragmites* (we have not established a difference between the stem fragments of these two species) are common in this depth range. At 7 meters depth, the frequency of *Scirpus* seeds increases again and then drops off below 9.5 meters. Below 9.5 meters, seeds from *Najas* and *Zanichellia*, which do not occur on Browns Island today but are present farther upstream in the delta, become common. There is also an abundance of seeds from 21 unidentified species below 9.5 meters, suggesting that the regional diversity of plant life was high during this time.

Stratigraphic Interpretation and Environmental History

We subdivide the stratigraphy at Browns Island into six zones, numbered from the top (youngest) to bottom (oldest). Here we provide a stratigraphic interpretation of the deposits starting at the base of the section and working up.

The basal sediments of Zone 6 (9.5-10.6 m; 6.3-6.8 ka) are laminated clayey silts. The two identified seed types fro this level are submersed fresh to brackish water plants, *Najas* (water nymphs) and *Zanichellia* (horned pondweed). Many of the unidentified seed types in this section may be detrital seeds washed in from upstream and deposited with the detrital mud. The low levels of Cd and Pb suggest that the water tended toward fresh; the high Fe levels confirm the subtidal nature of deposition (Thomas and Varekamp 1991). We, therefore, interpret this zone to have been deposited on a fresh to slightly brackish subtidal mudflat with conditions similar to those upstream near Sacramento today.

Zone 5 (7.5-9.5 m; 5.1-6.3 ka) is a section of mud (clayey silt) interbedded with thin peat layers. The laminated structure of these sediments can be observed on the density logs (Figure 2A). The gradual increase in Cd and Pb through this zone suggest that the water was becoming more saline as sea level rose, and the decrease in Fe indicates a decrease in frequency of tidal inundation. This is confirmed by the increased frequency of *Scirpus* seeds, as *Scirpus* does not grow in subtidal conditions. Thin discrete peat layers within the muds probably result from plant colonization of the mudflats and their subsequent burial by subtidal mud. This stratigraphy indicates that the rates of sea level rise and sedimentation alternatively superseded each other such that incipient marshes formed and were subsequently drowned.

Zone 4 (6.0-7.5 m; 4.1-5.1 ka) sediments are peats with decreasing inorganic content with time. Cd levels are high in this zone, while Fe levels remain low. The frequency of *Scirpus* seeds decreases upward, and *Cyperaceae* seeds are present around 7 meters depth in the BI-1993 core. *Phragmites/Typha* leaf sheaths are present throughout. At 7.5 meters

depth, *Potamogeton* seeds are present in a layer that also has high Cd levels. The concurrence of *Potamogeton* with a trace metal indicator of high salinity suggests a rapid submergence and abrupt increase in relative sea level, perhaps resulting from a tectonic subsidence event. The apparent stratigraphic inversions indicated by radiocarbon dates from this zone may have resulted from local erosion and redeposition of marsh sediments. However, the submergence event was not sufficient to bury the peats in subtidal mud. The upper part of this zone is characterized by low-density peats that rapidly expand when the cores are cut open. We interpret Zone 4 to indicate deposition in a brackish tidal marsh with the possibility of tectonic subsidence occurring about 5 ka.

Zone 3 (3.25-6.0 m; 2.3-4.1 ka) sediments are clayey peats with very high organic content and only rare *Scirpus* or *Cyperaceae* seeds. Leaf sheaths of *Phragmites/Typha* are present throughout. We interpret the absence of seeds and high organic content to indicate deposition in a relatively freshwater tidal marsh. This is confirmed by the generally low metal concentrations in this zone. However, three discrete peaks i the Cd and Pb curves around 3 ka (401, 420, and 460 centimeters depth) indicate salinity intrusion and drought did occur during this time. It is interesting, however, that although the bulk sediment suggests lower mean salinity, the absence of laminations and silt bands suggests a lower frequency of extreme floods. Therefore, we interpret this to be a period when mean freshwater discharge was higher than modern while extreme drought was more common than extreme flood.

Zone 2 (1.0-3.25 m; 0.9-2.3 ka) sediments are peats with somewhat lower organic content than observed in Zone 3. The frequency of *Scirpus* seeds is higher here, especially in core BI-1992, and a few *Cyperaceae* seeds are present. The abundance of Scirpus and Cyperaceae seeds at the base of this zone may indicate a rather abrupt return to more brackish conditions at about 2.3 ka. At 3 meters depth (about 2.2 ka), there is a peak in concentrations of Pb and Fe. The increased inorganic content of the peat at this depth indicates either increased inundation frequency, decreased local organic production, or both. The coincidence of the peak in metals concentration with the decrease in organic content suggests there was an increase in inundation frequency most likely resulting from an increase in relative mean sea level.

Zone 1 (0-1.0 m; 0-0.9 ka) sediments are peats with elevated levels of Pb and Fe. Live roots are common in the upper 25 centimeters and probably extend throughout this section. The sediments have low densities and high water content. Atwater (1980) noted the presence of *Distichlis spicata* rhizomes to depths of about 1 meter, and we identified *Scirpus* seeds, *Scirpus americanus* roots, and *D. spicata* roots in this zone. A 1-centimeter-thick silty clay layer at 45 centimeters depth (0.5 ka) contains abundant sand-sized mica grains, seeds from the pondweed *Potamogeton*, and the agglutinated foraminifera *Trochominna inflata*. The detrital mica is most likely derived from the batholithic rocks of the Sierra

Nevada. In conjunction with seeds from a plant that grows exclusively in the open water of the marsh channels, this deposit indicates a large freshwater flood. A second thin silt band was observed at 15 centimeters depth (0.35 ka) in the BI-1993 monolith. Therefore, we interpret Zone 1 sediments to record conditions similar to those on Browns Island today: predominantly brackish water with occasional large-scale floods.

Summary and Conclusions

Peat sediments from Browns Island record paleoenvironmental conditions in the upper San Francisco Estuary during the later Holocene. By 6.8 ka, tidal waters had inundated the downstream end of the Sacramento/San Joaquin Delta, and subtidal deposition began in relatively fresh water. Intertidal marsh sedimentation was initiated by 5.1 ka, and the marsh plain aggraded in brackish water until 4.1 ka. Between 4.1 and 2.3 ka, local water freshened, indicating increased discharge from the Sacramento/San Joaquin drainage basin. After 2.3 ka, brackish conditions returned that continue to the present day. Enhanced trace metal concentrations at the surface result from modern metal contamination in the estuary.

stratigraphic data imply that shorter-period extreme events occurred throughout the later Holocene. The preservation of fine-scale laminations throughout much of the section indicates that these high-frequency events are common and well preserved. Examples of these short-period events are:

- Extreme flooding (*eg*, about 0.5 ka) recorded by thin silt layers with allocthonous fossil and terrigenous debris.
- Several extreme droughts (about 3.0 ka) recorded by a peak in Cd and Pb content during a period of relatively high organic deposition.
- Increased tidal inundation (about 2.2 and 4.5 ka) recorded by peaks in trace metals concentrations and relatively low organic content. These events may have resulted from catastrophic submergence during large earthquakes.

High-resolution sampling now in progress should allow us to resolve the relationships between changes in the long-term mean conditions described above and changes in the frequency of shorter-period extreme events. Preliminary data suggest extreme drought and salinity intrusion occurred even during periods when the mean freshwater discharge from the Sacramento/San Joaquin drainage basin was higher than modern values.

Acknowledgments

This research was supported by grants from the National Science Foundation (EAR-), Lawrence Livermore National Laboratories, and the University of California. The authors benefited from discussions with Karl Malamud Roam, Jay S. Noller, and Susan Kegley. Susan Kegley facilitated our use of the Atomic Absorption Spectrometer. Robert Kayan facilitated our use of the Gamma Ray and Magnetics Scans at the Marine Branch of the U.S. Geological Survey, Menlo Park. A longer version of this paper has been submitted to *Paleogeography, Paleoclimatology, Paleoecology.*

References

Allen, J.R.L. 1990. Constraints on measurement of sea-level movements from salt-marsh accretion rates. *Journal of Geological Society London* 147:5-7.

Atwater, B.F. 1980. *Attempts to Correlate Late Quaternary Climatic Records between San Francisco Bay, the Sacramento-San Joaquin Delta, and the Mokelumne River, California.* PhD Thesis, Newark, University of Delaware. 214 pp.

Atwater, B.F., S.G. Conard, J.N. Dowden, C.W. Hedel, R.L. MacDonald, W. Savage. 1979. History, landforms and vegetation of the estuary's tidal marshes. Pages 347-385 in *San Francisco Bay: The Urbanized Estuary.* T.J. Conomos, editor. Pacific Division, American Association for the Advancement of Science, California.

Atwater, B.F., C.W. Hedel, E.J. Helley. 1977. *Late Quaternary Depositional History, Holocene Sea-Level Changes and Vertical Crustal Movement, Southern San Francisco Bay, California.* U.S. Geological Survey, Professional Paper 1014.

Bartlett, R.J., and B.R. James. 1993. Redox chemistry of soils. *Advances in Agronomy* 50:151-208.

Belknap, D.F., R.C. Shipp, F. Stuckenrath, J.T. Kelley, H.W. Borns Jr. 1989. Holocene sea-level change in coastal Maine. Pages 85-105 in *Neotectonics of Maine.* W.A. Anderson and H.W. Borns, editors. Maine Geological Survey Bulletin 40.

Bourg, A.C.M. 1983. Role of fresh water/sea water mixing on trace-metal adsorption phenomena. Pages 245-263 in *Trace Metals in Sea Water.* C.S. Wong, E. Boyle, K.W. Bruland, J.D. Burton, E.D. Goldberg, editors. Plenum Press, New York.

Boyle, E.A., J.M. Edmond, E.R. Sholkovitz. 1977. The mechanism of iron removal in estuaries. *Geochimica et Cosmochimica Acta* 41:1313-1324.

Burau, J., S. Monismith, M. Stacey. 1994. Hydrodynamic transport and mixing processes in Suisun Bay. Page 59 in *Proceedings of the Pacific Division, American Association for the Advancement of Science,* 13, Part I.

Cohen, A.N., and J.M. Laws. 1990. *An Introduction to the Ecology of the San Francisco Estuary.* Save the Bay Foundation, for the San Francisco Estuary Project, San Francisco. 30 pp.

Conomos, T.J. 1979. Properties and circulation of San Francisco Bay waters. Pages 47-84 in *San Francisco Bay: The Urbanized Estuary.* T.J. Conomos, editor. Pacific Division, American Association for the Advancement of Science, California.

Conomos, T.J., and D.H. Peterson. 1977. Suspended particle transport and circulation in San Francisco Bay: An Overview. Pages 82-97 in *Estuarine Processes, Volume 2.* M. Wiley, editor. Academic Press, New York.

Dana, J. 1939. *The Sacramento: River of Gold.* Farrar and Rinehart, New York. 294 pp.

Duinker, J.C. 1983. Effects of particle size and density on the transport of metals to the ocean. Pages 245-263 in *Trace Metals in Sea Water.* C.S. Wong, E. Boyle, K.W. Bruland, J.D. Burton, and E.D. Goldberg, editors. Plenum Press, New York.

Flegal, A.R., G.J. Smith, G.A. Gill, S. Sañudo-Wilhelmy, L.C.D. Anderson. 1991. Dissolved trace element cycles in the San Francisco Estuary. *Marine Chemistry* 36:329-363.

Fletcher, C.H., J.E. Van Pelt, G.S. Brush, J. Sherman. 1993. Tidal wetland record of Holocene sea-level movements and climate history. *Paleogeography, Paleoclimatology, Paleoecology* 102:177-213.

French, J.R., and T. Spencer. 1993. Dynamics of sedimentation in a tide-dominated back-barrier salt marsh, Norfolk, UK. *Marine Geology* 110:315-331.

Josselyn, M. 1983. *The Ecology of San Francisco Bay Tidal Marshes: A Community Profile.* U.S. Fish and Wildlife Service FWS/OBS-83/23.

Knight, W. 1980. The story of Browns Island. *The Four Seasons* 6:3-10.

Krone, R.B. 1979. Sedimentation in the San Francisco Bay system. Pages 85-96 in *San Francisco Bay: The Urbanized Estuary.* T.J. Conomos, editor. Pacific Division, American Association for the Advancement of Science, California.

Mall, R.E. 1969. *Soil-Water Relationships of Waterfowl Food Plants in the Suisun Marsh of California.* Wildlife Bulletin 1. California Department of Fish and Game. 59 pp.

Nelson, A.R. 1992. Discordant 14C ages from buried tidal-marsh soils in the Cascadia subduction zone, southern Oregon coast. *Quaternary Research* 38:74-90.

Peterson, D.H., D.S. McCulloch, T.J. Conomos, P.R. Carlson. 1972. *Distribution of Lead and Copper in Surface Sediments in the San Francisco Bay Estuary, California.* U.S. Geological Survey Misc. Field Studies Map MF-323.

Pethick, J.S. 1981. Long-term accretion rates on tidal salt marshes. *Journal of Sedimentary Petrology* 51:571-577.

Pizzuto, J.E., and E.W. Rogers. 1992. The Holocene history and stratigraphy of palustrine and estuarine wetland deposits of central Delaware. *Journal of Coastal Research* 8:854-867.

Ritson, P.R., and A.R. Flegal. 1994. Contaminant lead cycling in San Francisco Bay: Lead Isotopic Analysis. Page 91 in *Proceedings of the Pacific Division, American Association for the Advancement of Science,* 13, Part I.

Stumpf, R.P. 1983. The processes of sedimentation on the surface of a salt marsh. *Estuarine and Coastal Shelf Science* 17:495-508.

Stuiver, M., and P.J. Reimer. 1993. Extended C-14 data base and revised CALIB 3.0 C-14 age calibration program. *Radiocarbon* 35:215-230.

Thomas, E., and J.C. Varekamp. 1991. Paleo-environmental analyses of marsh sequences (Clinton, Connecticut): Evidence for punctuated rise in relative sea level during the latest Holocene. *Journal of Coastal Research, Special Issue* 11:125-158.

Thompson, J. 1957. *The Settlement Geography of the Sacramento-San Joaquin Delta, California.* PhD Thesis, Stanford University, Stanford, CA. 551 pp.

Varekamp, J.C. 1991. Trace metal geochemistry and pollution history of mudflat and marsh sediments from the Connecticut coastline. *Journal of Coastal Research, Special Issue* 11:105-123.

Wells, L.E. 1994. Radiocarbon dating of tidal marsh deposits from the Sacramento/San Joaquin Delta. In *Quaternary Geochronology and Paleoseismology*. J.S. Noller, W.R. Lettis, and J.M. Sowers, editors (in preparation). Nuclear Regulatory Commission, Washington, DC.

Zwolsman, J.J.G., G.W. Berger, G.T.M. Van Eck. 1993. Sediment accumulation rates, historical input, postdepositional mobility and retention of major elements and trace-metals in salt marshes of the Scheldt estuary, SW Netherlands. *Marine Chemistry* 44:73-94.

Fijian Coral Reef Damage and Recovery from Cyclone Kina

Richard Casey, Annette Ciccateri, and Stewart J. Fallon

ABSTRACT: Early in 1993, Cyclone Kina struck the Fiji Islands, causing more than $100 million in property damage and damaging the coral environment as well. A few days after the cyclone, the most damaged reef was studied. The same reef had been studied 6 months before. This reef crest is dominated by *Acropora*. Comparison showed that 80-90% of the *Acropora* was torn from the outer reef and deposited in the inner lagoon. The larger foraminifer *Marginopora* had been reduced from a significant population to one living in-place specimen.

Coral transects at the airport and a site 15 kilometers east were run about every 6 months. Damage at the airport was greatest, probably because of a small submarine canyon that focused wave energy on the transect area. In both regions, a black band of algae developed, probably due to sediment covering the outer portion of the inner reef flat. This seemed to kill the benthic organisms and allowed the opportunistic algae to invade the area. It is estimated that it will take a few years to 30 years for the reef to recover to pre-Kina conditions.

Introduction

A visual survey of the major near-shore marine and terrestrial environments was conducted during June 1992. This was done as part of an initial study of Fijian environments in the initiation of a long-term global change survey. Of special importance to this study was a general survey of the coral environments off the Savusavu airport on Vanua Levu Island, Fiji (Figure 1).

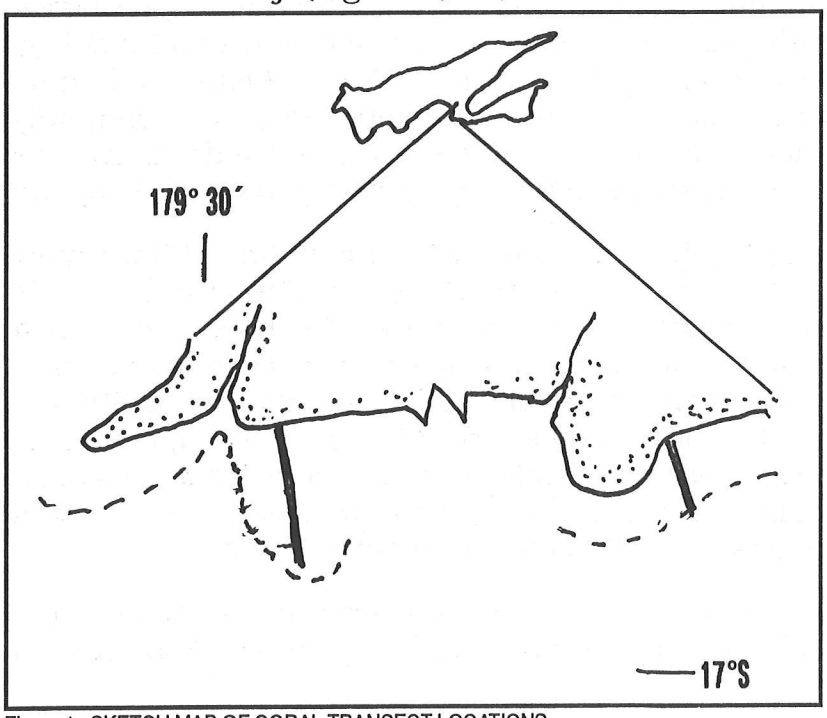

Figure 1. SKETCH MAP OF CORAL TRANSECT LOCATIONS

On January 3, 1993, Cyclone Kina hit Fiji. Our scientific party reached the Fijian Islands within a few days and altered our research plans to study damage done by the cyclone. Kina had caused more than $100 million in damage, including destroying up to 80% of the root crops and upsetting transportation throughout the islands. To date, our main concentration has been on coral damage and recovery.

In: C.M. Isaacs and V.L. Tharp, Editors. 1995. *Proceedings of the Eleventh Annual Pacific Climate (PACLIM) Workshop, April 19-22, 1994.* Interagency Ecological Program, Technical Report 40. California Department of Water Resources.

Procedures

Two reef areas (Figure 1) were selected for detailed research. The first was the Airport reef surveyed the previous summer; the second was a reef to the east of the airport about 15 kilometers by the Hibiscus Highway, just off the MuMu Resort.

Line transects were made off each area using the point intercept method. At the airport transect, observations were made at 20-cm intervals out to 45 meters offshore. At the MuMu transect, the 20-cm intervals were recorded for only the first 25 meters offshore. From that point, observations were made every meter to the reef crest.

At each point on the transect, we recorded the substrate and organisms found. We also made note of the condition of the reef surrounding the points. Reef terminology is shown in Figure 2.

The reef flat at the Airport transect extended about 500 meters offshore, compared to 300 meters offshore at the MuMu transect. The reef crest portions were each about 20 meters wide. The transects were performed at low tide with the aid of view boxes made of acrylic. Still and video photography were used for documentation and identification.

Transect Results

Figure 2 illustrates the main observations from the Airport transects. The inner reef flat corresponds to that portion of the reef flat that was documented at 20-cm intervals. The outer reef flat extends out to the reef crest, which is slightly elevated above the reef flat and dominated by *Acropora*. Before the damage by Kina (August 29 on Figure 2), *Marginopora* (larger foraminiferans containing symbiotic algae and commonly referred to as puca shells) was common and well represented in each zone of the reef. The outer reef displayed a healthy, mature growth of *Acropora*.

In January 1993 (Figure 2), the most obvious result of Kina at the airport was the destruction of about 80% of the *Acropora*. The 70-meter-wide band of *Acropora* stands near the reef crest appeared to have been planed off. *Acropora* hash from the outer reef appears to have been spread onto the reef flat, filling depressions on the flat. This hash did not exhibit the characteristic bleached color of old reef rubble; most still appeared to have the color of living *Acropora*. Therefore, we concluded that this hash was very recently broken off living stands. In some cases, the *Acropora* hash may have traveled some 400 meters over the reef flat.

SCUBA work on the seaward slope documented some *Acropora* hash and one large displaced table coral that scratched the seaward slope as it fell (Figure 3).

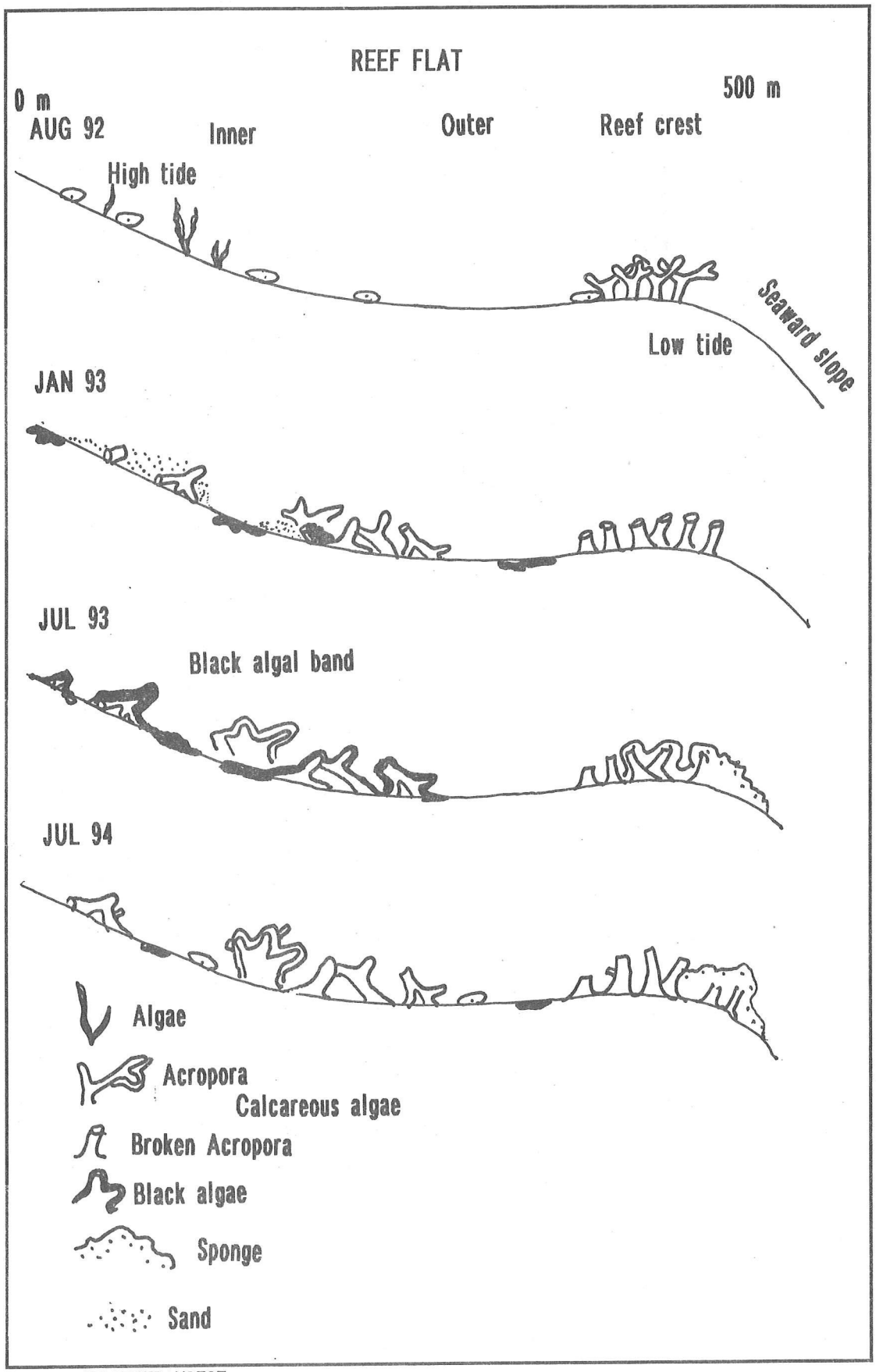

Figure 2. AIRPORT TRANSECT

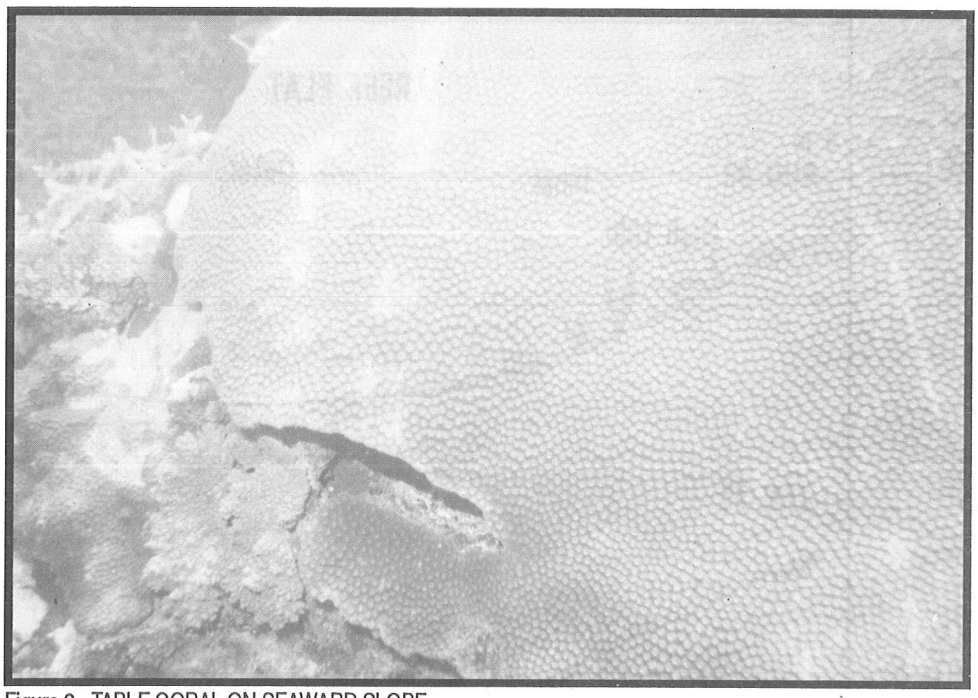

Figure 3. TABLE CORAL ON SEAWARD SLOPE

The inner reef flat also contained sediment of silt to sand sizes. These sediments were deposited in the deeper pockets, sometimes covering the small algae and seagrass beds of the area.

During this transect, only one living *Marginopora* foram was observed; evidently the others were washed away by intense wave action during the cyclone. There also appeared to be a significant amount of dead sea urchins, many of which had broken and/or missing spines. The population of brittle stars and blue sea stars seemed unaffected by the storm, owing perhaps to their ability to hide in the crevices and holes in the reef flat.

A week after the Airport transect, we performed the MuMu transect. This reef appeared to be less damaged than the reef at the airport. There was significantly less *Acropora* hash in the reef flat crevices, and the stands of living, healthy *Acropora* did not appear planed off, as did those at the airport. Only a few *Acropora* stands appeared to have had tips broken off by the storm. Populations of *Marginopora* were prevalent throughout the entire reef flat, and other fragile organisms such as alga and several species of sponge survived the storm and were found along the entire transect. Figure 4 shows a detailed view.

By July 1993 at the airport, the outer portion of the inner reef flat was covered by black encrusting algae to the degree that we referred to this as a black algal band. This black algal band appears to have covered a

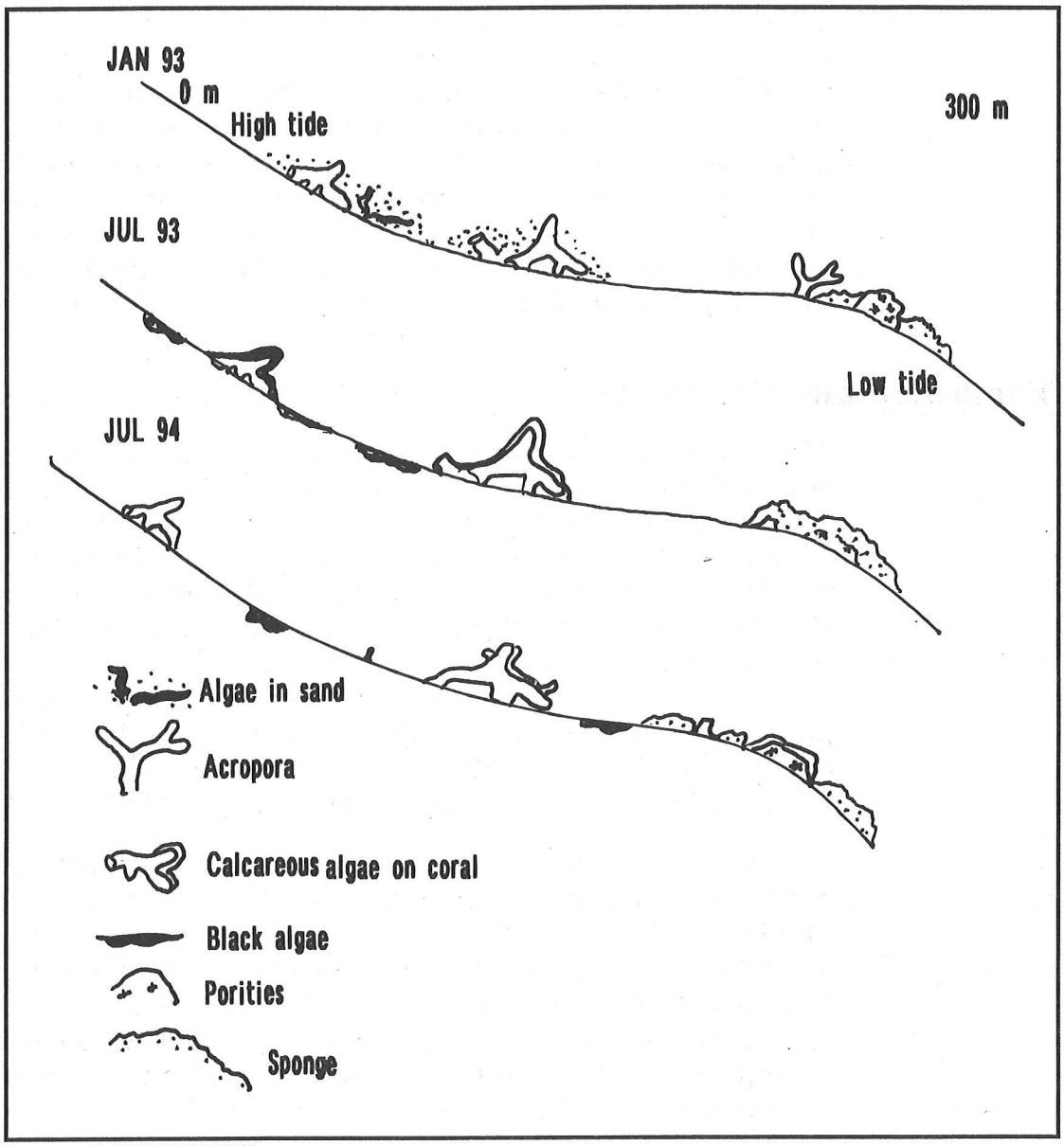

Figure 4. MU MU TRANSECT

10-meter-wide patch about 80 meters from the shore. The band appears to have covered some of the broken *Acropora* stands. In the mid-reef region, the cyclone rubble, including *Acropora* hash, was mainly encrusted with pink calcareous algae, which was starting to form a hard ground. A thick, mainly brown sponge covered the cyclone-cropped *Acropora* stands. This sponge coverage encompassed about 70% of the total outer reef area.

At MuMu there was no significant change in July 1993 from the transect in January. The only similarity to the airport reef was that a band of black encrusting algae also covered a 10-meter-wide patch of *Acropora* that had been broken off by the storm. This patch was about 70 meters from the shore.

During a transect performed at the airport in July 1994, the black algal band on the inner reef appeared to have broken up, leaving only small patches. Small corals (*Acropora, Pocillipora*) appeared to be recruiting in the open areas. The brown sponge cover on the outer reef was considerably reduced, with small corals recruiting on dead *Acropora* regions previously covered. Throughout the reef flat area, juvenile *Acropora* and *Pocillipora* were growing from the bases of corraline calcareous algae, exposed fossil reef, and dead in place corals. *Marginopora* also appeared to be returning to the reef flat area, as well as the urchin populations.

Discussion and Conclusion

We believe the considerable destruction to the coral reefs was not due only to Cyclone Kina, but to a combination of the cyclone and effects of the 3-year El Niño leading up to and surpassing the cyclone. The Weekly Climate Bulletin of January 12, 1994, states, "the warm episode conditions that have persisted in the tropical Pacific during the last three years showed signs of weakening in December [1993]." We have been aware of this El Niño and noted at least some coral bleaching on each of our trips to Fiji. The coral damage we observed then was the result of a one-two punch. The first was the weakening of the coral by the long El Niño due to the pond of warm water in the western tropical Pacific. The second was this specific cyclone and other storms spawned by the El Niño conditions.

The only record of a similar event we could find affecting Fiji was the cyclone of February 1965 (Cooper 1965). This cyclone also followed the El Niño if 1962 and 1963. Cooper mentions severe coral damage but mainly reports general conditions such as the types of dead fish. Both cyclones (1965 and 1993) developed in the western tropical Pacific and approached Fiji from the northwest. The 1965 cyclone passed by islands at longitude 170°E, and the 1993 cyclone entered the waters between the two main islands, Viti Levu to the south and Vanua Levu to the north.

After the 1993 cyclone, the Airport and MuMu regions studied exhibited differences in wave damage, with the most severe damage at the airport. The most probable reason for this difference is that just west of the Airport transect is a small submarine canyon cut by a stream. This depression concentrated wave energy in this section of reef. Although there is a stream west of MuMu, it has not cut a submarine canyon and, thus, there is no enhancement of wave energy.

The black bands of algae at each transect may also be influenced by the streams. Sediment brought in by rain associated with the cyclone was deposited in the outer portion of the inner reef flat at both sites. This sediment cover killed the benthic organisms, allowing the opportunistic black algae to invade the area after the sediment was removed by wave action.

From visual observation, the transects could have been located anywhere. The same general zonations occur throughout the surrounding area, despite local patchiness.

The reef has not continued its pre-Kina conditions in a year and a half. Since the last cyclone was in 1965, it seems likely that the reef will return to pre-Kina conditions sometime within a few to 30 years. However, sources suggest that the El Niño-like conditions appear to be developing in the equatorial Pacific as this is being written.

Reference

Cooper, M.J. 1965. Destruction of marine flora and fauna in Fiji caused by the hurricane of February 1965. *Pacific Sciences* 20:137-141.

Scientific Statistics and Graphics on the Macintosh

Stanley L. Grotch

ABSTRACT: The personal computer has become commonplace on the desk of most scientists. As hardware costs have plummeted, software capabilities have expanded enormously, permitting the scientist to examine extremely large datasets in novel ways. Advances in networking now permit rapid transfer of large datasets, which can often be used unchanged from one machine to the next. In spite of these significant advances, many scientists still use their personal computers only for word processing or e-mail, or as "dumb terminals". Many are simply unaware of the richness of software now available to statistically analyze and display scientific data in highly innovative ways. This paper presents several examples drawn from actual climate data analysis that illustrate some novel and practical features of several widely-used software packages for Macintosh computers.

Introduction

In many organizations, scientists have ready access to more than one computer, often both a work station (*eg*, SUN, HP, SGI) and a Macintosh or other personal computer. The scientist commonly uses the work station for "number crunching" and data analysis, and the Macintosh is relegated to word processing or serves as a "dumb terminal" to a mainframe computer. In an informal poll, I found that few of my colleagues used their Macintoshes for either statistical analysis or graphical data display.

This state of affairs is particularly unfortunate because over the last few years both the computational capability and, even more so, the software availability for the Macintosh have become quite formidable. In some instances, powerful tools are now available for the Macintosh that may not exist or may be far too costly for the so-called "high end" work stations. Many scientists are unaware of the wealth of extremely useful, off-the-shelf Macintosh software that already exists for scientific graphical and statistical analysis.

This paper is a personal view, illustrating several software packages that have proved valuable in my own work in analysis and display of climatic datasets. It is not meant to be an all-inclusive enumeration, nor is it to be taken as an endorsement of these products as the best of their class. Rather, extensive use has proven these few packages to be generally capable of satisfying my particular needs for statistical analysis and graphical data display. I focus on some of the more novel features found to be of value.

The discussion is divided into three sections, the first two illustrating Macintosh software for statistical data analysis and for graphical data display. The final section summarizes the work and offers some comments regarding the future.

In: C.M. Isaacs and V.L. Tharp, Editors. 1995. *Proceedings of the Eleventh Annual Pacific Climate (PACLIM) Workshop, April 19-22, 1994.* Interagency Ecological Program, Technical Report 40. California Department of Water Resources.

Statistical Analysis Software for the Macintosh

A number of general-purpose statistical software packages are now available for the Macintosh. For a detailed review intercomparing their capabilities, see Best and Morganstein (1991). Reviews frequently appearing in popular journals such as *MacWorld* are of great benefit in keeping abreast of developments. In my own work, two statistical packages have been of particular value: Data Desk and StatView.

No single package seems to offer all the features one needs. Each has its strengths and weaknesses. This is both good and bad for the scientist — good in that feature duplication is minimized, but bad in that multiple packages must be purchased and subsequently mastered. This latter point, the continual intellectual demand placed on the scientist, has largely contributed to the lack of personal computer use. The scientist feels so overwhelmed with day-to-day responsibility that "makes us rather bear those ills we have, than fly to others that we know not of". This is particularly so with the more sophisticated software packages, which require frequent use to maintain the necessary skill for effective operation.

Both Data Desk and StatView provide the user with an arsenal of the most important statistical analysis tools: standard summary statistics (means, variances, non-parametrics, *etc*), inference testing (equivalence of means), correlation, regression, analysis of variance. Data Desk, particularly, provides excellent instruction manuals, and both have competent telephone technical support. With networking becoming commonplace, both programs will readily accept data matrices generated on other computers in a range of formats. Tab-delimited ASCII matrices are easily read without user intervention.

The two packages differ, however, in their basic philosophy regarding graphical data display. Data Desk is far more interactive, but produces cruder graphics. On the other hand, although StatView is typically slower, it can generate truly presentation-quality graphics. To achieve speed and high interactivity, Data Desk has few (or no) controls for user-determined plot limits, grid lines, fonts, annotation, *etc*, features nicely implemented in StatView. On the other hand, Data Desk can generate and rapidly rotate 3-dimensional point clouds, a feature still not implemented in StatView.

One of the most useful and innovative features implemented in Data Desk (but not in StatView) is the concept known as "linked plots". Here, any points highlighted in one display are correspondingly highlighted in all others. As an illustration of the power of this technique, consider a problem commonly encountered in data analysis. We want to compare two datasets and spatially locate those points that show the greatest similarities and the greatest differences.

Assume we have available on a common grid observations of precipitation from two sources. A histogram of the gridpoint differences in precipitation is displayed in Figure 1, top panel. If a binary indicator of land (=0) or water (=1) is available at every gridpoint, a second plot showing the continental land masses can readily be produced (Figure 1, lower panel). To generate the lower display, all grid points are first plotted as a scatter plot, yielding a simple rectangular grid. The land grid points are then selected using the land/water index, and instantly only the land grid points are highlighted. Note that in the static displays presented here, several *extremely important* distinguishing features present with a TV monitor are absent: color, intensity, and temporal on/off flashing. The color and shape chosen to differentiate a given group of points is maintained in all displayed plots.

To select a region of the histogram (here the lower tail), the user merely touches the vertical bars of the histogram with a program tool, and the

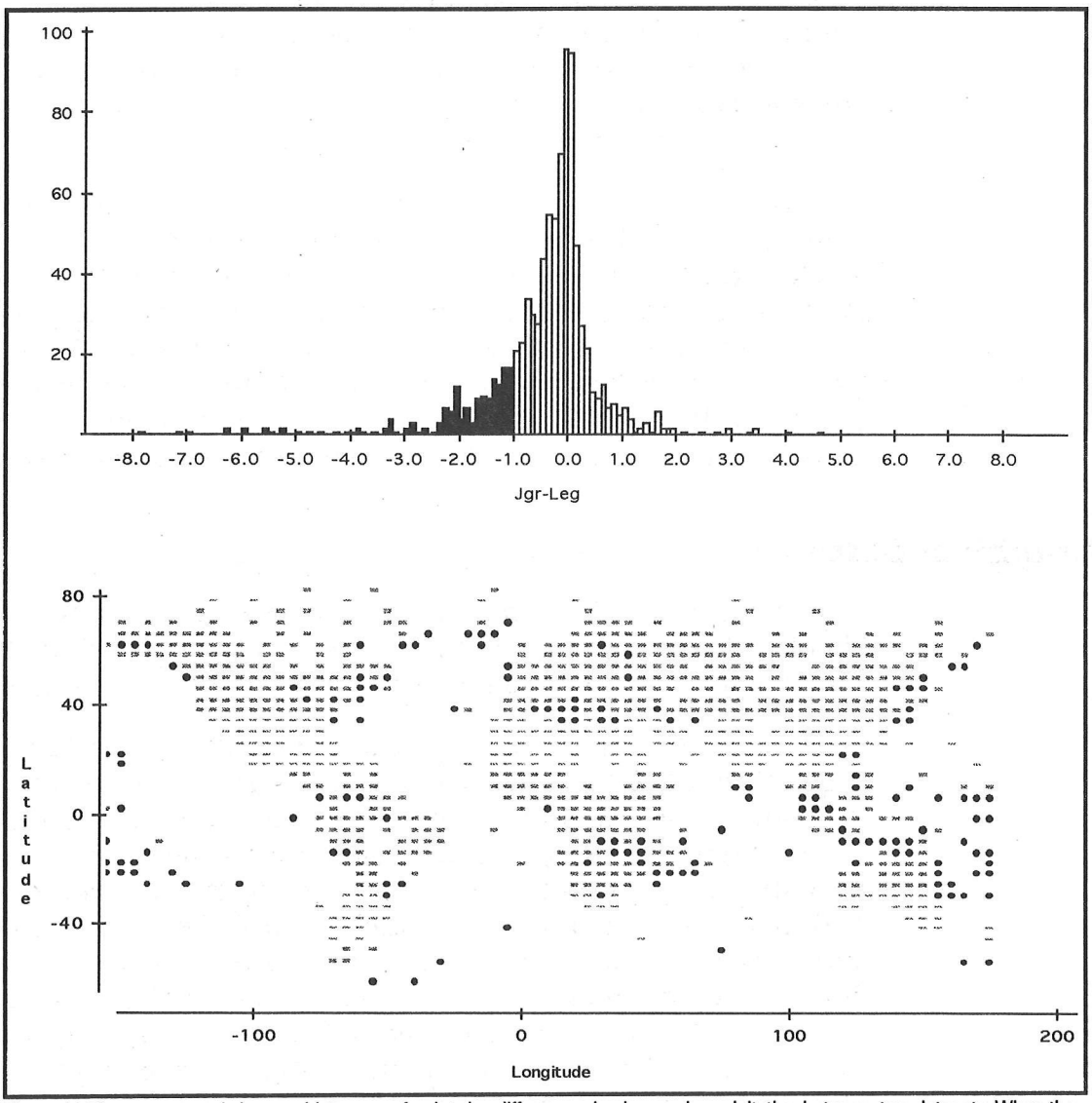

Figure 1. The upper panel shows a histogram of pointwise differences in observed precipitation between two datasets. When the lower tail of the histogram is selected in Data Desk, it darkens. Simultaneously, points corresponding to these maximal differences glow on a world map indicating where these differences arise.

selected bars instantly darken on the histogram display. Simultaneously, those grid points captured in the highlighted ranges also glow on the lower map. These map-selected points can be preserved using color and/or shape, or the user can choose another set of ranges in the histogram and the initial selection will disappear. To spatially locate and differentiate the three regions (lower tail, upper tail, and central region [best agreement]), each grouping is chosen, in turn, on the histogram. As relevant points are automatically selected on the lower map, they can be differentiated using different colors and/or shapes. The remarkable interactivity of this process must be experienced to be fully appreciated.

Linked plots also function in the opposite direction. If, for example, one wanted to determine what the histogram of differences was for only the tropical region, the same tool would be moved along the latitudinal axis of the lower map, capturing the desired range of latitudes (Figure 2, lower panel). At the same moment, a sub-histogram would darken (Figure 2, upper panel), showing the histogram relevant to only the selected points. Similarly, if the histogram for a specific area such as the continent of Africa was required, another tool (a lasso) would be used to encircle the appropriate area on the map, and again the captured points would yield a darkened sub-histogram.

Additionally, any selected points are automatically highlighted on *all other* displays shown on the screen using the same colors and symbols. In the example here, if data for, say, temperature *vs.* cloudiness at these gridpoints were available, when the African points were selected with the lasso tool, these points would also glow on the temperature/cloudiness plot. The extraordinary potential of this technique for interactively analyzing multivariate datasets has not been exploited by most scientists, largely due to ignorance of the existence of such tools for the Macintosh.

Graphical Software

I have found three software packages of particular value for scientific data display: Kaleidagraph, Delta Graph, and Spyglass Transform and Dicer. Once again, each package has virtues and disadvantages.

Many excellent software packages exist for producing the "bread and butter" plots of the scientist: 2-dimensional scatter and line plots. Any "recommended" choice among these is particularly subjective. In my own experience, Kaleidagraph has proven particularly easy to use and versatile in permitting considerable control in the embellishment of 2-dimensional graphics. In Kaleidagraph, the user has considerable latitude over setting axis limits, axis direction, the appearance of grid lines, fonts, symbols, colors, arrows, lines, background color. These can be quickly and interactively added, changed, and moved. While such capabilities might seem superfluous, in scientific graphics these capabilities are essential to produce both esthetically pleasing and scientifically informative graphics.

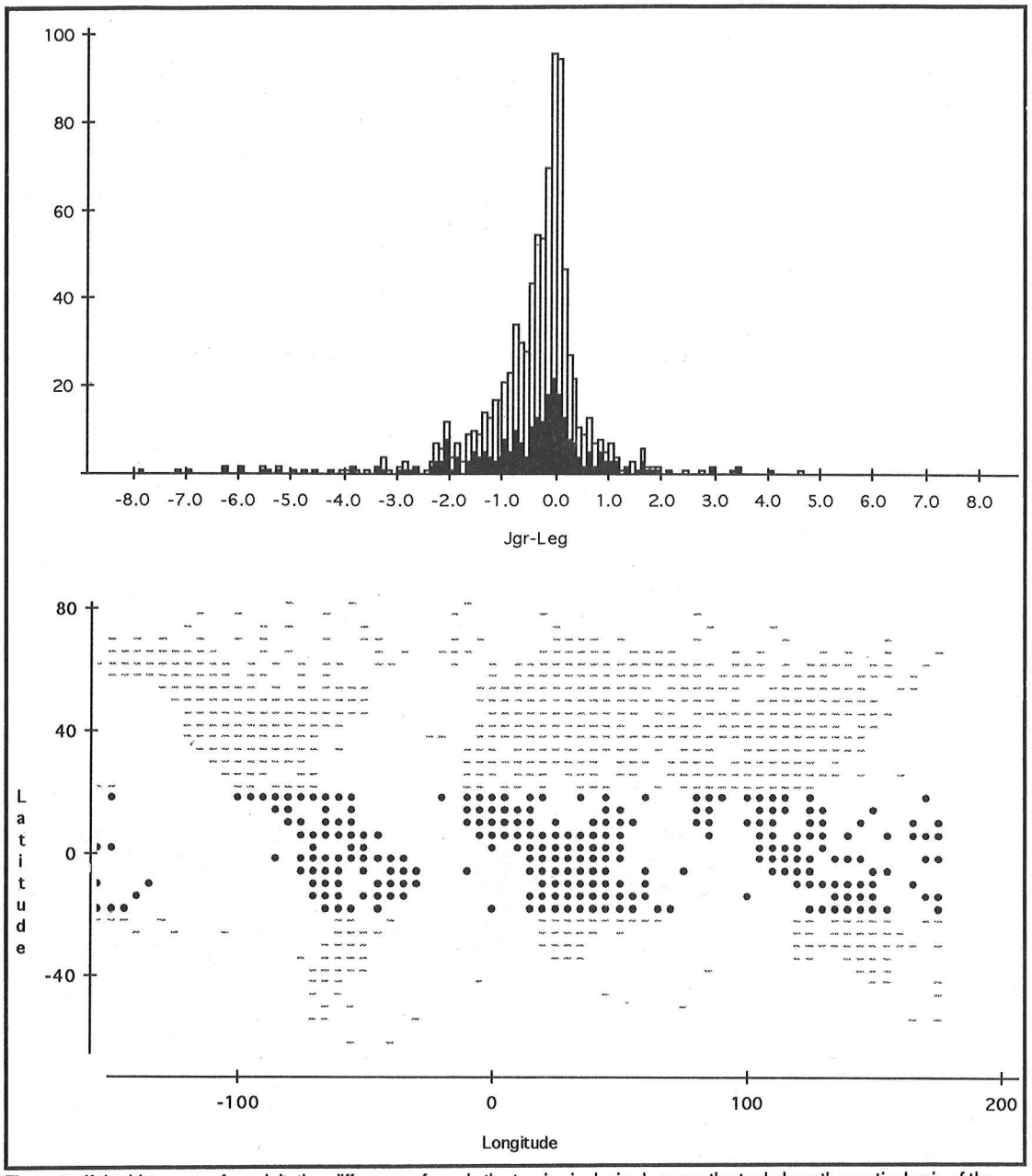

Figure 2. If the histogram of precipitation differences for only the tropics is desired, move the tool along the vertical axis of the lower map until the desired latitudinal range is captured. As the tool is moved, chosen points glow in the map display. Simultaneously, a darkened sub-histogram is outlined in the upper histogram, showing the distribution for only the tropical gridpoints.

As might be expected, the number of software packages which can produce truly effective 3-dimensional scientific plots is much less than for 2-dimensional. Kaleidagraph has no 3D plotting capability. Data Desk, Delta Graph and Spyglass all have 3D capabilities, but each has important advantages and limitations.

Data Desk can display point clouds in space, and it is highly interactive in rapidly rotating these points to produce a realistic 3D effect. (The linked plot feature described above also functions with the 3D plots). However, although the 3D effect using parallax motion is visually

excellent on the screen, the result is often disappointing when produced as a hard copy. Delta Graph and Spyglass, on the other hand, are both too slow to produce motion interactively, but both do generate presentation-quality 3D graphics.

The Spyglass suite of software (Transform, View, Plot, and Dicer) is perhaps the most innovative and most impressive in its capability for scientific data display. Although the software has virtually no numerical statistical capability, the packages are remarkable in their ability to produce both 2- and 3-dimensional false color images and animations. Several illustrative examples are presented using Spyglass Transform and Dicer. However, much of the visual impact and differentiation produced by using color is lost in the figures presented here.

Transform is the primary false color plotting package of the Spyglass suite. Any data matrix, say a meteorological field, expressed as a function of latitude and longitude, is quickly rendered in either two or three dimensions using color to code the magnitude of the variable presented. A broad range of built-in color mappings is available, and these can be quickly changed in an interactive manner. Continental outlines, vector, and contour overlays can be added to any 2-dimensional display. Figure 3 shows the temperature distribution predicted by a global GCM. The subtle gradations in the color original are lost in this reproduction.

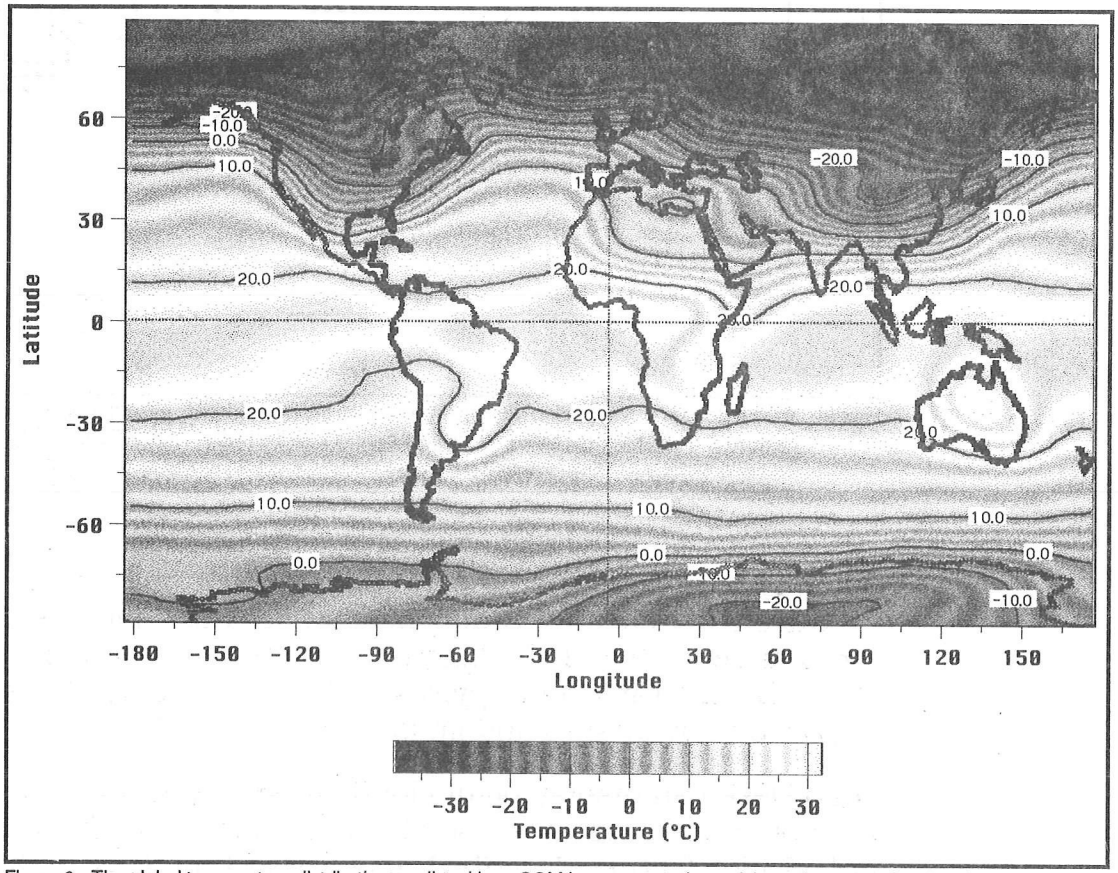

Figure 3 The global temperature distribution predicted by a GCM is represented as a false color map using Spyglass Transform. To produce this display, the underlying colored map is overlaid with a contour map (also generated with Transform) and continental outlines (obtained from another source).

With Spyglass Transform these same data can also be quickly rendered as a wiremesh surface in three dimensions, as shown in Figure 4. Transform permits the user to interactively change viewpoint and the aspect ratio used as well as the color mapping selected. To better permit spatial orientation in these displays, the continental areas can also be directly shaded on the data surface. Once again, the importance of color in such displays cannot be ignored. Once a satisfactory 2D or 3D plot is generated, the user may save all the instructions as a macro to facilitate reproducing similarly-scaled plots for intercomparison of datasets or for generating animations.

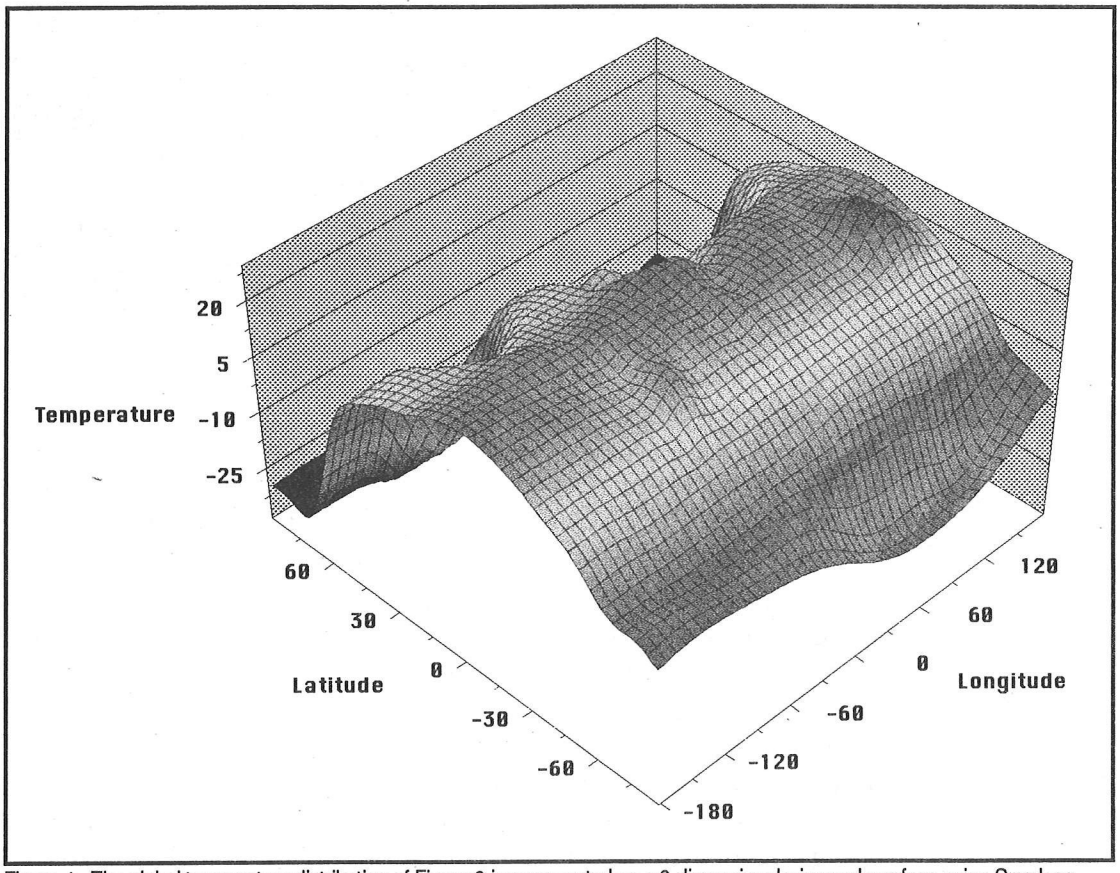

Figure 4 The global temperature distribution of Figure 3 is represented as a 3-dimensional wiremesh surface using Spyglass Transform. The user can interactively change many features of the plot, including user viewpoint, aspect ratio, axis scaling and labeling, and colors.

For many years the Macintosh has been the computer of choice for work in the graphic arts. Capabilities in this area are impressive. The ability to "cut and paste" graphics from disparate sources are of considerable value in scientific graphics. No longer does the scientist have to generate all the components of each graphic in a single program.

For example, in Figure 5 a 3D wiremesh rendition of the temperature data of Figures 3 and 4 from Spyglass Transform is merged seamlessly with a world map using Adobe Photoshop. The 2D map of Figure 3 could just as easily be inserted in this lower plane. With the many tools provided in graphics programs, the user can quickly resize and overlay

different plots and add textual and arrow annotations. To enhance the printed output, colors can be altered interactively, and brightness and contrast can be changed quickly. For presentations on the printed page or as view graphs, these capabilities can change a dull plot into one far more visually appealing and informative.

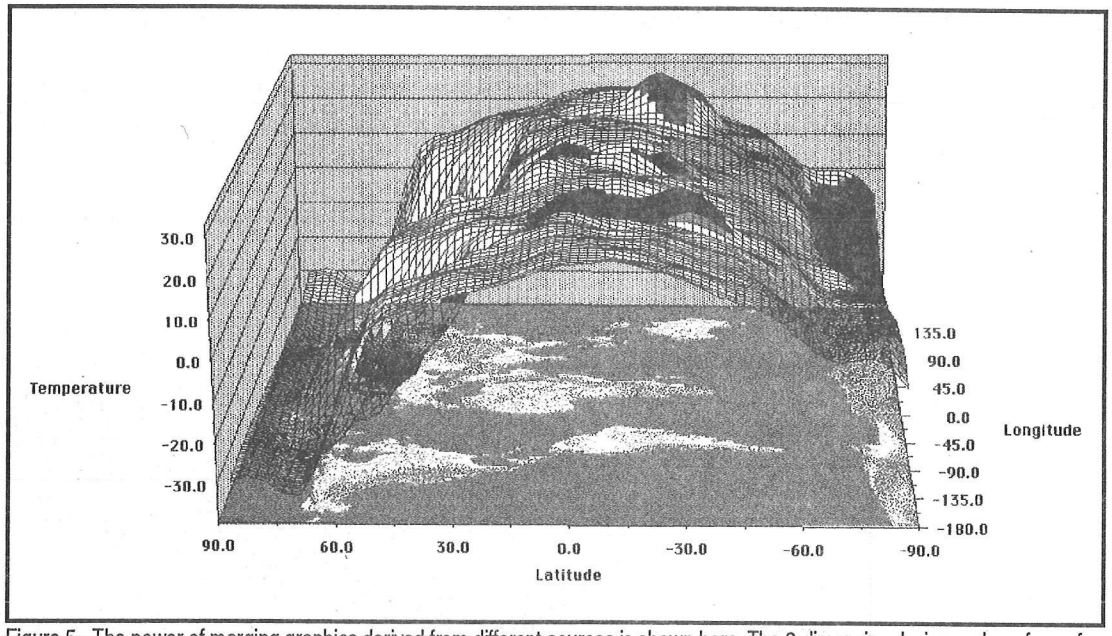

Figure 5. The power of merging graphics derived from different sources is shown here. The 3-dimensional wiremesh surface of global temperature is generated using Spyglass Transform. The lower world map, showing topography, was obtained from the Macldas group at Wisconsin via Internet. The two graphics were seamlessly merged using Adobe Photoshop. To obtain better spatial location, the continents may be shaded in the upper surface as well, using other capabilities in Transform.

Dicer is probably the most novel of the suite of Spyglass programs. As the name implies, Dicer permits the user to consider 3-dimensional data as a solid piece of food through which slices or blocks can be cut out and the results displayed using a variety of user-specified color tables. Figure 6 shows monthly average climatologies for 850-mb temperature. The horizontal cut planes show the January and July temperature distributions. Vertical cuts in the remaining planes show the corresponding temporal-spatial distributions. After selection, the user can quickly move or delete any of these slices.

Blocks can also be interactively cut out of the dataset or isosurfaces can be produced, highlighting other aspects of the data. In Dicer, the user can generate a series of parallel slices to produce very effective animations. For example, in the example of Figure 6, the user can easily produce 12 horizontal slices to obtain a 2D animation of monthly climatology. These frames can be converted readily to Apple's Quick Time system, permitting easy viewing on virtually any Macintosh.

The range of features and the degree of interactivity incorporated into this software is remarkable. These capabilities are particularly valuable in the geophysical sciences, where highly dimensional data are common.

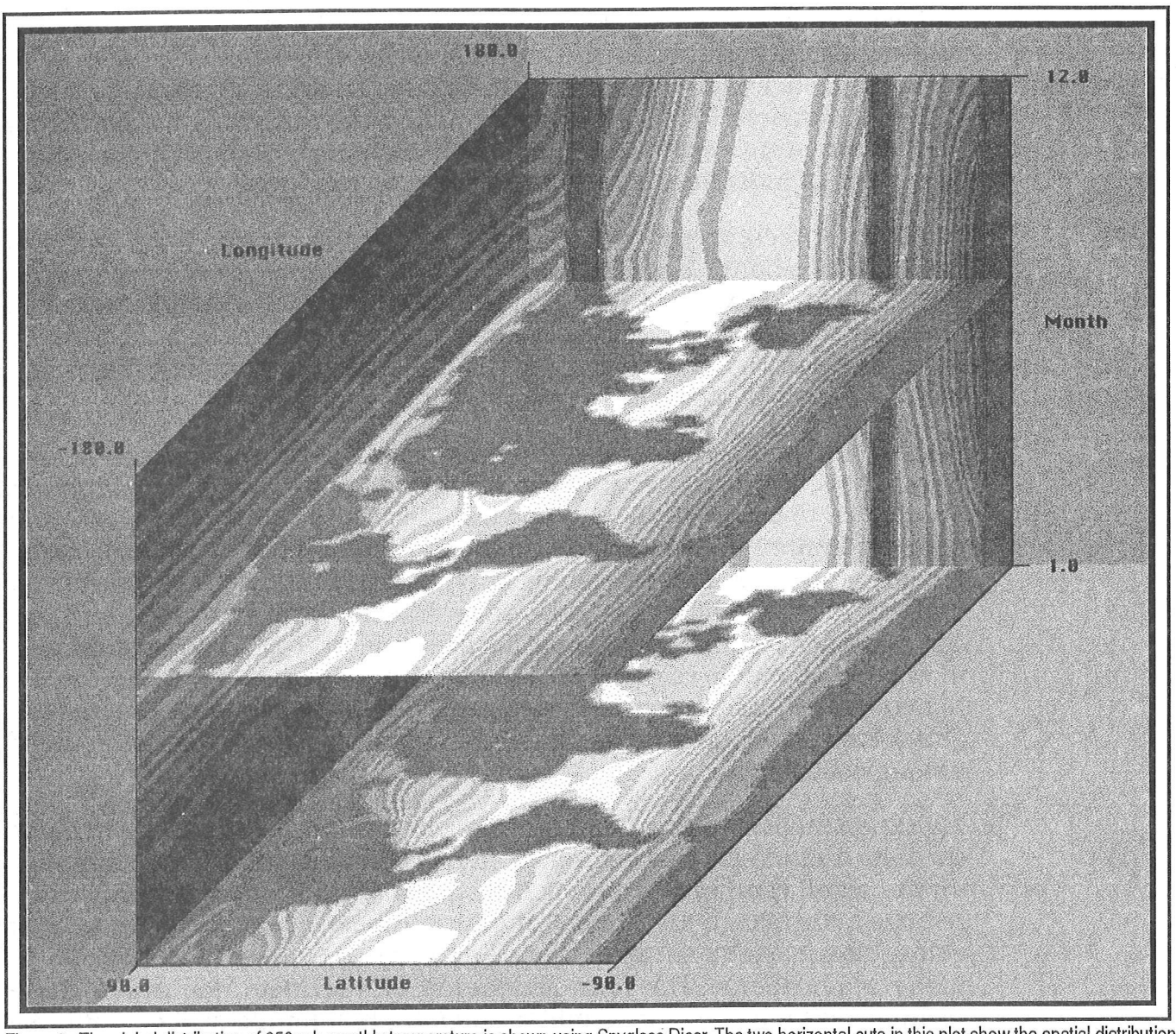

Figure 6, The global distribution of 850-mb monthly temperature is shown using Spyglass Dicer. The two horizontal cuts in this plot show the spatial distribution of the January and July average climatologies. Dicer permits cuts to be made interactively along any of the axes, as well as obliquely through the data. Thus, one can examine 2-dimensional views through the 3-dimensional dataset. Blocks and isosurfaces through the data can also be represented. The effects are particularly useful when displayed in color.

Conclusions

There can be little doubt that scientific data analysis is undergoing explosive growth. Hardware advances on all fronts permit examination of datasets undreamed of a few years ago. Intense competition among software vendors has proven an extraordinary blessing to the scientist. The constant improvements in capabilities and ease of operation during the last few years are truly remarkable.

Software enhancements are likely to continue at a rapid pace. One area of practical importance to the scientist is the development of scripts or macros to facilitate reproducing the same analyses or displays using different datasets. This will be of particular importance in intercomparing and contrasting results and in producing animations of data where hundreds of individual frames must often be produced.

Infusion of techniques from the field of graphic arts and the world of multimedia should exert considerable influence in scientific graphics. With software such as Adobe Photoshop, it becomes a simple matter to interactively overlay bits and pieces of plots obtained from entirely different sources to produce considerably enhanced products. The application of such procedures is now in its infancy.

Animation (or, more generally, multimedia) is another major growth area in graphics. Until very recently, scientists had to have help from graphics specialists to produce effective movies. This was typically very costly and severely limited the number of animations attempted. It also restricted experimentation. This situation is changing rapidly. Desktop movie-making by the scientist is now quite feasible with packages such as Spyglass. Movie editing software for merging, titling, adding sound, *etc*, is becoming much easier to master and much more available for the Macintosh. Finally, standard movie-playing software, such as Apple's QuickTime, will greatly facilitate the process of sharing animations among colleagues.

My experience has shown that many scientists still are unwilling to make the time and intellectual commitment needed to master these techniques on the small computer. There is little question that many techniques do require a significant investment of time and near-constant usage to be of value. Some, such as animations, may be unnecessary diversions in many applications. The next generation of scientists, for whom these technologies may be more familiar and less threatening, will no doubt be more receptive to their use. I believe these new technologies can provide the scientist with enormously powerful tools in the area broadly characterized as scientific data analysis.

Acknowledgment

This work was performed under the auspices of the U.S. Department of Energy by the Lawrence Livermore National Laboratory under Contract No. W-7405-Eng-48.

References

Best, A.M., and D. Morganstein. 1991. Statistics Programs Designed for the Macintosh: Data Desk, Exstatix, Fastat, JMP, Statview II, and Super Anova. *American Statistician*. 45(4), 318-333

Software Sources

Data Desk: Data Description, Inc., P.O. Box 4555, Ithica, NY (607/257-1000).

DeltaGraph: DeltaPoint, Inc., 2 Harris Court, Monterey, CA 93940 (408/648-4000).

Kaleidagraph: Synergy Software, 2457 Perkiomen Avenue, Reading, PA 19606 (215/779-0522).

Spyglass: Spyglass, Inc., P.O. Box 6388, Champaign, IL 61826 (217/355-6000).

StatView: Abacus Concepts, Inc. , 1984 Bonita Avenue, Berkeley, CA (510/540-1949).

Appendix A
AGENDA

Eleventh Annual Pacific Climate (PACLIM) Workshop
April 19-22, 1994

AGENDA

Eleventh Annual Pacific Climate Workshop
Asilomar Conference Center, Pacific Grove, California
April 19-22, 1994

Meal Schedule
Breakfast 7:30-9:00 am
Lunch 12:00-1:00 pm
Dinner 6:00-7:00 pm

Tuesday Evening, April 19, 1994
Moderator: Walt Dean

7:00-7:20 Welcome and Announcements

7:20-7:40 *Scientific Statistics and Graphics on the MacIntosh*
Stanley L. Grotch, Lawrence Livermore National Laboratory, Livermore, CA

7:40-8:00 *Intervention Analysis: A Time Series Method for Detecting Interdecadal Regime Shifts*
Robert C. Francis and Steven R. Hare, School of Fisheries, Seattle, WA

8:00-8:20 *Coral Reef Destruction in Fiji Due to Hurricane Kina*
Richard Casey, Annette Ciccateri, Stewart Fallon, Antonette Gutierrez, Patrick Earley, Becky Kamps, and Paul Kotol, Ocean Research Institute, San Diego, CA

8:20-8:40 Brief Poster Introductions (1 minute each) by Poster Presenters

8:45 — Social

Wednesday Morning, April 20, 1994
Invited Talks, High Resolution Paleoclimate Records
Moderators: Robert Dunbar and Caroline Isaacs

8:30-9:10 *Natural Archives of Interannual Climate Variability*
Malcolm Hughes, Tree-Ring Laboratory, University of Arizona, Tucson, AZ

9:10-9:50 *Patterns and Causes of High Paleoenvironmental Variability in Southern South America:* Late-Glacial versus Late Holocene
Vera Markgraf, Regina A. Figge, Ray Kenny, and James W.C. White, University of Colorado, Boulder, CO

9:50-10:30 *Inter-Decadal Climate Variability in the Southern Hemisphere: Evidence from Tasmanian Tree Rings over the Past Three Millennia*
Edward R. Cook, Brendan M. Buckley, and Rosanne D. D'Arrigo, Lamont-Doherty Earth Observatory, Palisades, NY

10:30-11:00 Break

11:00-11:20 *The Southern Oscillation Reconstructed from Corals in the West Pacific Warm Pool*
Julia Cole, INSTAAR, University of Colorado, Boulder, CO

11:30-12:00 *Eastern Pacific Corals Monitor Long-Term History of ENSO and ITCZ Rainfall*
Robert Dunbar and Bradley Linsley, Rice University, Houston, TX

Wednesday Afternoon, April 20, 1994
Invited Talks, High Resolution Paleoclimate Records (continued)
Moderators: Robert Dunbar and Caroline Isaacs

1:30-2:10 *Reconstruction of Global Climate of the Past 2000 Years from Varved-Anaerobic Sediments of the Eastern Pacific Oceans*
Timothy R. Baumgartner, Scripps Institution of Oceanography, La Jolla, CA

2:10-2:50 *An Overview of Decadal to Century Time Scale Variability in the Climate System*
Thomas Stocker, Physics Institute, University of Bern, Switzerland

2:50-3:20 Break

3:20-4:00 *Determining the Role of Linear and Nonlinear Interactions in Records of Climate Change: Possible Solar Influences in Annual to Century-Scale Records*
Terri Hagelberg and Julie Cole, University of Rhode Island, Narragansett, RI

4:00-4:40 *Volcanoes and Global Change: Probable Short-Term and Possible Long-Term Links*
David K. Rea and Libby M. Prueher, University of Michigan, Ann Arbor, MI

Wednesday Evening, April 20, 1994
Invited Talks

7:30-8:10 *Chaos and Climate Fluctuations*
H. Bruce Stewart, Brookhaven National Laboratory, Upton, NY

8:10-8:30 *The Birth of a New University: CSU Monterey Bay*
Steven Arvizu, Interim Provost, California State University, Monterey Bay

8:30— Social

Thursday Morning, April 21, 1994
Moderator: Dan Cayan

8:30-8:50 *Streamflow Patterns in Panama and Chile Associated with the Extreme Phases of the* Southern Oscillation
Thomas C. Piechota, John A. Dracup, E.B. Browne, T.A. McMahon, and F.H.S. Chiew, University of California, Los Angeles, CA

8:50-9:10 *Variability of West Coast Marine Fog: Large-Scale Development and Prediction*
M.K. Filonezuk and D.R. Cayan, Scripps Institution of Oceanography, La Jolla, CA

9:10-9:30 *Hydrologic Response Unit Delineation for the Tuolumne and Merced River Basins, Yosemite National Park, California*
Jan W. van Wagtendonk and Michael Dettinger, Yosemite Field Station, El Portal, CA

9:30-10:00 Break

10:00-10:20 *Climatic Controls and the Spatial Distribution of Summer Precipitation Seasonality in the Western United States*
Cary J. Mock, University of Oregon, Eugene, OR

10:20-10:40 *Atmospheric Forcing of Recent Trends toward Early Snowmelt Runoff in California*
Michael D. Dettinger and Daniel R. Cayan, U.S. Geological Survey, San Diego, CA

11:00-11:20 *Some Effects of the Earth's Surface on Wintertime Jet Stream Positions in the Northern Hemisphere and Rainfall Patterns along the West Coast*
Stephen Holets, Pacific Gas & Electric Company, San Francisco, CA

11:20-11:40 *Remote-Sensed Ecosystems and Climate Variability*
Susan Ustin, University of California, Davis, CA

11:40-12:00 *Radiolarian Flux in the Santa Barbara Basin as an Index of Climate Variability*
Amy Weinheimer and D.R. Cayan, Scripps Institution of Oceanography, La Jolla, CA

Thursday Afternoon, April 21, 1994
Moderator: Dave Peterson

1:50-2:10 *Centennial-Scale Stratigraphies of Organic Carbon and Carbonate from Santa Barbara Basin ODP Site 893*
James V. Gardner and Peter Dartnell, U.S. Geological Survey, Menlo Park, CA

2:10-2:30 *A 5000-Year High-Resolution Oxygen and Carbon Isotopic Record of Paleo-Streamflow in San Francisco Bay Estuary*
B. Lynn Ingram, James C. Ingle, and Mark E. Conrad, University of California, Berkeley, CA

2:30-2:50 *Variations in Freshwater Inflow to the San Francisco Estuary as Reconstructed from Tidal Marsh Sediments*
Lisa E. Wells and Michelle Goman, University of California, Berkeley, CA

2:50-3:10 *A Change in the California Current*
John McGowan, Scripps Institution of Oceanography, La Jolla, CA

Thursday Evening, April 21, 1994
Invited Talk

7:30-8:10 *Climate, One Year at a Time: A Retrospective*
Roger Y. Anderson, The University of New Mexico, Albuquerque, NM

8:50— Social

Friday Morning, April 22, 1994
Moderator: Platt Bradbury

8:30-8:50 *Chronology of Eolian Deposition in the Gran Desierto, Sonora, Mexico*
Donald Gautier, Stephen Stokes, Thomas S. Ahlbrandt, and Christopher J. Schenk, U.S. Geological Survey, Denver, CO

8:50-9:10 *Has the California Drought Returned?*
Maurice Roos, California Department of Water Resources, Sacramento, CA

9:10-9:30 *Internal Consistency of Low-Frequency Tree-Growth Variations in the Northern Great Plains*
David M. Meko, University of Arizona, Tucson, AZ

9:30-9:40 *The California Snow Survey Program — Climate Variability and Water Resources*
Frank Gehrke, California Department of Water Resources, Sacramento, CA

9:40-10:10 Break

10:10-10:20 *Northeastern Pacific Temperature Changes: High Resolution Records from Coastal Trees*
Gregory C. Wiles, Rosanne D. D'Arrigo, and Gordon C. Jacoby, Lamont-Doherty Earth Observatory, Palisades, NY

10:20-10:40 *A Coral Isotope Record of Rossby Wave Transmission in the Indonesian Passage*
Michael D. Moore, Lisa E. Wells, and Richard G. Fairbanks, University of California, Berkeley, CA

10:40-11:00 *Paleoseasonality of Southeast Asia: High Resolution Isotope Records from Fossil Corals on Sumba Island, Indonesiaa*
Daniel P. Schrag and Michael D. Moore, Princeton University, Princeton, NJ

11:00-11:20 *Neogene through Pleistocene Paleoclimate of the Great Salt Lake Region, Northeastern Great Basin, USA*
Thomas E. Moutoux and Owen K. Davis, University of Arizona, Tucson, AZ

Appendix B

POSTER PRESENTATIONS

Eleventh Annual Pacific Climate (PACLIM) Workshop
April 19-22, 1994

POSTER PRESENTATIONS

Eleventh Annual Pacific Climate Workshop
Asilomar Conference Center, Pacific Grove, California
April 19-22, 1994

Middle and Upper Pleistocene Climate Records from the Upper Klamath Basin, California and Oregon
David Adam, U.S. Geological Survey, Menlo Park, CA

Modern Hydrology and Climatology of the Amargosa River near Tecopa, California
Diana Elder Anderson, Robert C. Balling, Jr., and Stephen G. Wells, University of California, Riverside, CA

Holocene History and Paleoclimatic Implications of Lodgepole Pine (Pinus contorta va. murrayana) in the Sierra Nevada, California
R. Scott Anderson, Northern Arizona University, Flagstaff, AZ

A 1500-Year, Semi-Decadal Record of Climate Change in Elk Lake, Minnesota: The Impact of Solar and Seasonal Climate Variability on Lacustrine Varves
J.P. Bradbury, W.E. Dean, and R.Y. Anderson, U.S. Geological Survey, Denver, CO

Interannual Variability in Heat Content over the North Pacific Basin
Daniel R. Cayan, W.B. White, A.J. Miller, and J.M. Oberhuber, Scripps Institution of Oceanography, La Jolla, CA

Effect of Variable Water-Input Rates on Outflow Water Chemistry in an Alpine Microcatchment Experiment, Loch Vale Watershed, Colorado
David W. Clow, U.S. Geological Survey, Denver, CO

Spatial and Temporal Patterns of Spectral and Time Domain Parameters of Modern Temperature Records
Rachael G. Craig and Leila Shiozawa, Kent State University, Kent, OH

Mathematical Decomposition of Organic Carbon in Marine Sediments
Peter Dartnell and James V. Gardner, U.S. Geological Survey, Menlo Park, CA

Glacial to Holocene Contrasts in Organic Matter Preservation on the California Continental Margin
Walter E. Dean and James V. Gardner, U.S. Geological Survey, Denver, CO, and Menlo Park, CA

Reconstruction of Aridity for the Sierra de la Laguna, Baja California Sur, Mexico
Sara Diaz, Laura Arriaga, Cesar Salinas, and Daniel Lluch, Centro de Investigaciones Biologicas del Noroeste, La Paz, Mexico

Evidence for Large, Rapid Changes in Atmospheric CO2 from Carbon Isotopes in a Peat Core from Harberton, Argentina
Regina A. Figge, James W.C. White, Philippe Ciais, Ray Kenny, and Vera Markgraf, University of Colorado, Boulder, CO

Diatom Evidence for High Productivity and Upwelling in the California Current during Late Oxygen-Isotope Stage 3
Eileen Hemphill-Haley, U.S. Geological Survey, Eugene, OR

Coastal Southern California Paleoclimates during the Last 150 ka: Pollen Data from ODP Site 893A, Santa Barbara Basin
Linda E. Heusser, Lamont-Doherty Earth Observatory, Palisades, NY

Simulations of Surface Current Trajectories Illustrate the Extremes of Recent Climate Interannual Variability in Eastern North Pacific Circulation 1946-1993
Jim Ingraham, National Oceanographic and Atmospheric Administration, Seattle, WA

Southwest Dendroclimatic Records and a 140-Year Resonance Cycle
Thor Karlstrom, Seattle, WA

More News about Seasonal Resolution of Laminated Sediments in Santa Barbara Basin (Re: Diatoms)
Carina B. Lange and Arndt Schimmelmann,
Scripps Institution of Oceanography, La Jolla, CA

Long-Term Changes in Winter Synoptic Circulation Patterns: Evidence from Recent Changes in Alpine Timberlines in the Western United States
Kenneth L. Petersen, Westinghouse Hanford Company, Richland, WA

A Spatial-Temporal Analysis of Marine Winds in the California Coastal Region
Larry Riddle and Daniel R. Cayan, Scripps Institution of Oceanography, La Jolla, CA

Another Way to View Time
Gary D. Sharp, CIRIOS, Monterey, CA

A Late Pleistocene-Early Holocene Pollen Record from San Miguel Island, California: Preliminary Results
G. James West and Jon M. Erlandson, U.S. Bureau of Reclamation, Sacramento, CA

Appendix C
ATTENDEES

Eleventh Annual Pacific Climate (PACLIM) Workshop
April 19-22, 1994

Eleventh Annual Pacific Climate Workshop Attendees
Asilomar Conference Center, Pacific Grove, California
April 19-22, 1994

David Adam
U.S. Geological Survey - MS 915
345 Middlefield Road
Menlo Park, CA 94025
415/329-4970
Fax 415/329-4975
dadam@mojave.wr.usgs.gov

Diana Anderson
University of California, Riverside
Department of Earth Sciences
Riverside, CA 92521
909/787-2194
Fax 909/787-4324
amargosa@ucrac1.ucr.edu

R. Scott Anderson
Environmental Sciences
Box 5694, North Arizona University
Flagstaff, AZ 86011
602/523-5821
Fax 602/523-7290
sa@nauvax.ucc.nau.edu

Roger Y. Anderson
University of New Mexico
Dept. of Earth & Planetary Sciences
Albuquerque, NM 87131
505/277-1639
Fax 505/277-8843
ryand@triton.unm.edu

Lisa Ramirez Bader
U.S. Geological Survey
Box 25046, MS 939, DFC
Denver, CO 80225
303/236-5547
Fax 303/236-0459
lbader@sedproc.cr.usgs.gov

Kenneth Baltz
NOAA Marine Fisheries Science Center
Tiburon Laboratory
3150 Paradise Drive
Tiburon, CA 94920
415/435-3149
Fax 415/435-3675

Harold P. Batchelder
University of California, Davis
Division of Environmental Studies
Davis, CA 95616-8576
916/752-2332
Fax 916/752-3350
hpbatchelder@ucdavis.edu

Timothy Baumgartner
Scripps Institution of Oceanography
University of California, San Diego
Marine Life Research Group
9500 Gilman Drive, Dept. 0227
La Jolla, CA 92093-0227
619/534-2171
Fax 619/534-7641
trbaumgartner@ucsd.edu
tbaumgar@cicese.mx

J. Platt Bradbury
U.S. Geological Survey
Box 25046, DFC, MS 919
Denver, CO 80225
303/236-5666
Fax 303/236-5690
bradbury@greenwood.cr.usgs.gov

Randy Brown
California Department of Water Resources
Environmental Services Office
3251 S Street
Sacramento, CA 95816-7017
916/227-7531
Fax 916/227-7554
rbrown@eso.water.gov

Richard Casey
University of San Diego
Ocean Research International
650 Loring Street
San Diego, CA 92109
619/483-6507

Daniel Cayan
Scripps Institution of Oceanography
University of California, San Diego
9500 Gilman Drive, Dept. 0224
La Jolla, CA 92093-0224
619/534-4507
Fax 619/534-8561
cayan@seaaira.ucsd.edu

Annette Ciccateri
University of San Diego
Ocean Research International
650 Loring Street
San Diego, CA 92109
619/483-6507

David W. Clow
U.S. Geological Survey
Box 25046, MS 415, DFC
Denver, CO 80225
303/236-4882 Extension 294
dwclow@dcolka.cr.usgs.gov

Julia Cole
INSTAAR, Campus Box 450
University of Colorado
Boulder, CO 80309
303/492-0595
Fax 303/492-6388
coleje@spot.colorado.edu

Edward R. Cook
Lamont-Doherty Earth Observatory
Tree Ring Laboratory
Palisades, NY 10964
914/365-8618
Fax 914/365-3046
drdendro@lamont.ldeo.columbia.edu

Richard G. Craig
Kent State University
Department of Geology
Kent, OH 44240
216/672-7987
Fax 216/672-7949
rcraig@gilbert.kent.edu

Ernest P. Daghir
National Weather Service
660 Price Avenue
Redwood City, CA 94063
415/364-2422
Fax 415/364-2599

Peter Dartnell
U.S. Geological Survey
345 Middlefield Road, MS 999
Menlo Park, CA 94025
415/354-3086
Fax 415/354-3224
pete@octopus.wr.usgs.gov

Walter E. Dean
U.S. Geological Survey
Box 25046, MS 939, DFC
Denver, CO 80225
303/236-5760
Fax 303/236-0459
dean@sedproc.cr.usgs.gov

Michael Dettinger
U.S. Geological Survey
5735 Kearny Villa Road, Suite O
San Diego, CA 92123-1135
619/637-6845
Fax 619/637-9201
mddettin@s101pcasnd.wr.usgs.gov

Sara Díaz
Centro de Investigaciones
Biológicas del Noroeste
Km 1. Carr San Juan de la Costa
Apdo Postal 128 La Paz 23000
BCS México
112/5-36-33
Fax 112/5-53-43

Paul Doose
Southern California Edison
Environmental Affairs
2244 Walnut Grove Avenue
Rosemead, CA 91770
818/302-4096

Kathleen Dorsey
Kinetic Laboratories, Inc.
370 Washington Street
Santa Cruz, CA 95060
408/457-3950
Fax 408/426-0405

John Dracup
University of California, Los Angeles
3066 Engineering I
Civil & Environmental Engineering Department
Los Angeles, CA 90024-1593
310/825-2176
Fax 310/206-7245
dracup@seas.ucla.edu

Robert B. Dunbar
Rice University
Department of Geology
P.O. Box 1892F
Houston, TX 77251
713/527-4883

Stewart Fallon
University of San Diego
3994 Morrell Street
San Diego, CA 92109
619/272-4085

Regina A. Figge
INSTAAR
University of Colorado at Boulder
Campus Box 450
Boulder, CO 80309
303/492-6072
Fax 303/492-6388
figge_r@cubldr.colorado.edu

Maria K. Filonczuk
Scripps Institution of Oceanography
3140 Midway Drive - A310
San Diego, CA 92110
619/225-1357
maria@sundog.ucsd.edu

Richard Forester
U.S. Geological Survey
Box 25046, MS 919, DFC
Denver, CO 80225
303/236-5656
Fax 303/236-5690
forester@rcolka.cr.usgs.gov

Dianne Fox
U.S. Geological Survey
Box 25046, MS 939, DFC
Denver, CO 80225
303/236-1647
Fax 303/236-0459
dfox@sedproc.cr.usgs.gov

Robert C. Francis
University of Washington
School of Fisheries WH-10
Seattle, WA 98195
206/543-7345
Fax 206-685-7471
rfrancis@fish.washington.edu

James V. Gardner
U.S. Geological Survey
345 Middlefield Road, MS-999
Menlo Park, CA 94025
415/354-3087
Fax 415/354-3191
jim@octopus.wr.usgs.gov

Donald Gautier
U.S. Geological Survey
Box 25046, MS 939, DFC
Denver, CO 80225
303/236-5740
Fax 303/236-8822
gautier@bpgsvr.cr.usgs.gov

Frank Gehrke
California Department of Water Resources
P.O. Box 942836
Sacramento, CA 94236-0001
916/653-8255
Fax 916/653-8272
gridley@snow.water.ca.gov

Stanley L. Grotch
Lawrence Livermore National Laboratory
7000 East Avenue
Livermore, California 94550
510/423-6741
Fax 510/422-5844

Terri King Hagelberg
University of Rhode Island
Graduate School of Oceanography
Narragansett, RI 02882
401/792-6662
Fax 401/792-6709
terrih@gsosun1.gso.uri.edu

Eileen Hemphill-Haley
U.S. Geological Survey
c/o 1272 Geological Sciences
University of Oregon
Eugene, OR 97403-1272
503/346-4582
Fax 503/346-4692
email: eileen@octopus.wr.usgs.gov

Linda Heusser
Clinton Road
Tuxedo, NY 10987
914/351-5290
Fax 914/351-5290
heusser@ACFcluster.nyu.edu

Stephen H. Holets
Pacific Gas & Electric Co.
77 Beale Street, Room 1651, MC B16A
P.O. Box 770000
San Francisco, CA 94177
Phone 415/973-4530 — Fax 415/957-9348
shh2@gcd_ms@gbu_gts_sfgo

Malcolm Hughes
University of Arizona
Laboratory of Tree-Ring Research
Building 58
Tucson, AZ 85721
602/621-6470
Fax 602/621-8229
mhughes@ccit.arizona.edu

Jim Ingraham
NOAA
Alaska Fisheries Science Center
7600 Sand Point Way NE
BIN C15700, Building 4
Seattle, WA 98115-0070
206/526-4241
Fax jingram@refm.noaa.gov

Lynn Ingram
University of California, Berkeley
Department of Geology & Geophysics
Berkeley, CA 94720
510/642-2575
Fax 510/643-9980
ingram@violet.berkeley,edu

Caroline Isaacs
U.S. Geological Survey
345 Middlefield Road, MS 999
Menlo Park, CA 94025
415/354-3014
Fax 415/354-3191
caroline@octopus.wr.usgs.gov

Alan D. Jassby
University of California, Davis
Division of Environmental Studies
Davis, CA 95616
916/752-3438
adjassby@ucdavis.edu

Johanna Jurgens
University of Arizona
Department of Geosciences
Tucson, AZ 85721
602/792-2336 (home)
Fax 602/621-2672

John Kahrs
U.S. Geological Survey
345 Middlefield Road, MS 999
Menlo Park, CA 94025
415/354-3221
jhahrs@octopus.wr.usgs.gov

Thor Karlstrom
U.S. Geological Survey (Ret)
4811 Brace Point Drive
Seattle, WA 98136
206/935-7087

Yvonne Katzenstein
University of California, Riverside
Department of Earth Sciences
Riverside, CA 92521-0423
909/787-2194
Fax 909/787-4324

Charles David Keeling
Scripps Institution of Oceanography
0220, University of California, San Diego
La Jolla, CA 92093-0220
619/534-4230
Fax 619/534-0784
cdkeeling@ucsd.edu

Joanie Kleypas
NCAR
P.O. Box 3000
Boulder, CO 80307-3000
303/497-1637
Fax 303/497-1400
kleypas@ncar.ucar.edu

Carina Lange
Scripps Institution of Oceanography
Geological Resources Division
9500 Gilman Drive
La Jolla, CA 92093-0215
619/534-4605
Fax 619/534-0784
clange@ucsd.edu

John Laurmann
3372 Martin Road
Carmel, CA 93923-8230
408/625-6696

Chin-I Lin
Pacific Gas & Electric Company
R&D Department
3400 Crow Canyon Road
San Ramon, CA 94583
510/866-5396
Fax 510/866-5318

Ana MacKay
U.S. Geological Survey
1675 West Anklam Road
Tucson, AZ 85745
602/670-6821
Fax 602/670-6806
ammackay@rcamnl.wr.usgs.gov

Vera Markgraf
INSTAAR
University of Colorado
Boulder, CO 80309-0450
Phone 303/492-5117
Fax 303/492-6388
markgraf@spot.colorado.edu

John A McGowan
Scripps Institution of Oceanography
0228, University of California, San Diego
La Jolla, CA 92093-0228
619/534-2074
Fax 619/534-6500

Dave Meko
University of Arizona
Laboratory of Tree-Ring Research
Tucson, AZ 85721
602/621-3457
Fax 602/621-8229
dmeko@ccit.arizona.edu

Ted Melis
University of Arizona
4500 West Speedway Road
Tucson, AZ 85745
602/670-6821
Fax 602/670-6806

Cary J. Mock
Department of Geology and Geography
University of Massachusetts
Amherst, MA 01003
413/545-2286
Fax 413/545-1200

Michael Moore
University of California, Berkeley
Museum of Paleontology
Berkeley, CA 94720
510/526-3225
Fax 510/524-7241

Thomas E. Moutoux
Department of Geosciences
Gould-Simpson Building
University of Arizona
Tucson, AZ 85721
602/621-7953
Fax 602/621-2672

Tom Murphree
Dept of Meteorology, MR-Me
Naval Postgraduate School
Monterey, CA 93943-5000
408/656-2723
Fax 408/656-3061
murphree@lady.met.nps.navy.mil

Elise Pendall
University of Arizona
Department of Geosciences
Tucson, AZ 85721
602/743-7792
elisep@ccit.arizona.edu

Kenneth L. Petersen
Westinghouse Hanford Co.
P.O. Box 1970, MS H4-14
Richland, WA 99352
509/376-9765
Fax 509/376-4081

David H. Peterson
U.S. Geological Survey
345 Middlefield Road, MS 496
Menlo Park, CA 94025
415/354-3366
Fax 415/354-3363

Thomas C. Piechota
University of California, Los Angeles
Civil and Environmental Engineering Department
3066 Engineering I
Los Angeles, CA 90024-1593
310-206-8612
Fax 310/206-7245
piechota@seas.ucla.edu

David Piper
U.S. Geological Survey
345 Middlefield Road, MS 902
Menlo Park, CA 94025
415/329-5187
Fax 415/329-5110
dzpiper@mojave.wr.usgs.gov

Paula Quinterno
U.S. Geological Survey
345 Middlefield Road, MS 999
Menlo Park, CA 94025
415/354-3201
Fax 415/354-3191
paula@octopus.wr.usgs.gov

David K. Rea
Department of Geological Sciences
University of Michigan
1006 C.C. Little Building
Ann Arbor, MI 48109-1063
313/936-0521
Fax 313/763-4690
david.rea@umich.edu

Kelly Redmond
Western Regional Climate Center
Desert Research Institute
P.O. Box 60220
Reno, NV 89506-0220
702/677-3139
Fax 702/677-3157
krwrcc@nimbus.sage.unr.edu

Larry Riddle
Scripps Institution of Oceanography
0224, University of California, San Diego
La Jolla, CA 92093-0224
619/534-1869
Fax 619/534-8561
riddle@kidlat.ucsd.edu

Maurice Roos
CA Dept of Water Resources
1416 Ninth Street
P.O. Box 942836
Sacramento, CA 94236-0001
916/653-8366
Fax 916/653-8272

Connie Sancetta
National Science Foundation
4201 Wilson Boulevard, Room 725
Arlington, VA 22203
703/306/1586
Fax 703/306-0390
csancett@nsf.gov

Arndt Schimmelmann
Department of Geological Sciences
Geology 129, Indiana University
1005 East 10th Street
Bloomington, IN 47405-1403
812/855-7645
Fax 812/855-7961
aschimme@indiana.edu

Gary Sharp
Center for Climate/Ocean Resources Study
780 Harrison Road
Salinas, CA 93907
408/449-9212
Fax 408/647-4225
gsharp@igc.apc,org

H. Bruce Stewart
Brookhaven National Laboratory
Building 490-D
Upton, NY 11973
516/282-4179
Fax 516/282-5047
bstewart@bnl.gov

Thomas F. Stocker
Climate and Environmental Physics
Physics Institute, University of Bern
Sidlerstrasse 5
3012 Bern, Switzerland
+41 31 631 44 64
Fax +41 31 631 44 05
stocker@phil.unibe.ch

Robert Swanson
Climatological Consulting Corporation
1216 Babel Lane
510/676-2228

Sus Tabata
Institute of Ocean Sciences
P.O. Box 6000
9860 West Saanich Road
Sidney, BC, Canada V8L 4B2
604/363-6573
Fax 604/363-6746
tangerine@ios.bc.ca

Susan Ustin
University of California, Davis
Davis, CA 95616
916/752-0621
Fax 916/752-5262
slustin@ucdavis.edu

John Vaccaro
U.S. Geological Survey
1201 Pacific Avenue, Suite 600
Tacoma, WA 98402
206/593-6510
Fax 206/593-6514
jvaccaro@fs01dwatcm.wr.usgs.gov

Jan W. van Wagtendonk
National Biological Survey
Yosemite Field Station
El Portal, CA 95318
209/372-0465
Fax 209/372-0569
jan%yose@cerl.cecer.army.mil

Mike Wangler
University of California, Riverside
Department of Earth Sciences
Riverside, CA 92521-0423
909/787-3434 (message)
Fax 909/787-4324
mwangler@ucrac1.ucr.edu

John B. Weeks
U.S. Geological Survey
P.O. Box 25046, MS 412, DFC
Lakewood, CO 80225-0046
303/236-5021
Fax 303/236-5034

Amy Weinheimer
Scripps Institution of Oceanography
University of California, San Diego
La Jolla, CA 92093-0220
Phone 619/534-2049
weinheim@weather.ucsd.edu

Lisa Wells
University of California
Department of Geography
501 Earth Sciences Building
Berkeley, CA 94702
510/642-1281
Fax 510/647-3370
lwells@garnet.berkeley.edu

Stephen G. Wells
University of California, Riverside
Department of Earth Sciences - 036
Riverside, CA 92521-0423
909/787-4367
Fax 909/787-4324
wells@ucrac1.ucr.edu

G. James West
U.S. Bureau of Reclamation
3429 Oyster Bay
Davis, CA 95616
916/978-4542
Fax 916/978-5284

Gregory C. Wiles
Tree Ring Laboratory
Lamont-Doherty Earth Observatory
Palisades, NY 10964
914/365-8517
Fax 914/365-3046
druidgw@lamont.1deo.columbia.edu

Memorie Yasuda
Scripps Instution of Oceanography
University of California, San Diego
9500 Gilman Drive, 0215
La Jolla, CA 92093-0215
619/534-6510
Fax 619/534-0784
myasuda@sdcc3.ucsd.edu

James R. Young
Southern California Edison
P.O. Box 800
2244 Walnut Grove Avenue
Rosemead, CA 91770
818/302-9191
Fax 818/302-9730
youngjr@sce.com